Doctoral Dissertation

Charged Lepton Flavor Violation Process $\mu^- e^- \to e^- e^-$ in Muonic Atoms

Yuichi UESAKA

Graduate School of Science,
Osaka University

February 2018

Abstract

Lepton flavors are well-conserved quantities in the standard model (SM) of particle physics. While lepton flavor violation (LFV) is forbidden in the frame of the SM, theories beyond the SM naturally predict LFV. Neutrino flavor oscillation is one example of LFV processes, which requires non-zero neutrino masses. Charged lepton flavor violating (CLFV) processes are expected to provide important signals on physics beyond the SM.

$\mu^- e^- \to e^- e^-$ decay in a muonic atom is proposed as a new CLFV process by Koike *et al.* This process has several advantages: cleaner experimental signal because the sum of energies of two electrons is fixed value around muon mass due to two-body decay, sensitivity for both contact and photonic CLFV interactions, and strong enhancement of transition probability due to nuclear Coulomb attraction.

In this thesis, we have analyzed quantitatively the $\mu^- e^- \to e^- e^-$ decay in a muonic atom. We formulated the transition rate in terms of multipole expansion of the CLFV interactions and partial wave expansion of lepton wave functions. The muon and electron wave functions of the previous analysis are improved by solving Dirac equation with Coulomb interaction of the finite nuclear charge distributions. As a result, we found very interesting role of improved lepton wave functions, which depends very much on the CLFV mechanism: the transition probability enhanced (suppressed) for the contact (photonic) process. The effect is significant for heavier atoms, where the obtained decay rate for contact process is about one order of magnitude larger than the previous estimation for ^{208}Pb, while that for photonic process is about four times smaller. By using the improved lepton wave functions, the difference among CLFV interaction shows up in the observables of the $\mu^- e^- \to e^- e^-$ process. We conclude that the atomic number dependence of the decay rate and the energy-angular distribution of emitted electrons are useful tools to distinguish between contact and photonic interactions. Furthermore, we have studied the asymmetry of an emitted electron from polarized muon. The obtained asymmetry is sufficiently large and we found it can be used to explore the chiral structure of the CLFV interaction.

Acknowledgments

I would like to express my sincere gratitude to my supervisor, Professor M. Asakawa for providing me this precious study opportunity as a Ph.D student in his laboratory.

I especially would like to express my deepest appreciation to my supervisor, Professor T. Sato for his elaborated guidance, considerable encouragement and invaluable discussion that make my research of great achievement and my study life unforgettable.

I am very grateful to my collaborators, J. Sato, M. Yamanaka, and Y. Kuno, for their valuable cooperation in our discussion.

I am also very grateful to past and present members of our laboratory for enabling me to have a productive courage life.

Finally I would like to extend my indebtedness to my parents for their support, understanding, and encouragement throughout my school life.

Contents

Chapter 1

Introduction

Three types of charged leptons are currently known: electron (e), muon (μ) and tau lepton (τ). They are the charged lepton of the first generation, second generation, and third generation, respectively. Neutrinos of each generation are electron neutrino (ν_e), muon neutrino (ν_μ), and tau neutrino (ν_τ). The properties of the three charged leptons are very similar except their masses. The mass of an electron is about 0.511 MeV while the mass of muon and tau lepton are about 106 MeV and about 1777 MeV, respectively. Origin of three generation is deep problem in particle physics to be answered.

Three lepton numbers, electron number (L_e), muon number (L_μ), tau number (L_τ), are defined for each flavor shown in Table 1.1. The process where any lepton numbers do not conserve is called Lepton Flavor Violating (LFV) process.

Table 1.1: Lepton flavor numbers assigned to each standard model (SM) particles. Conventionally, particles have a positive number while anti-particles have a negative number. All lepton flavor numbers of quarks are zero.

	e^-	ν_e	μ^-	ν_μ	τ^-	ν_τ	e^+	$\overline{\nu}_e$	μ^+	$\overline{\nu}_\mu$	τ^+	$\overline{\nu}_\tau$
L_e	+1	+1	0	0	0	0	−1	−1	0	0	0	0
L_μ	0	0	+1	+1	0	0	0	0	−1	−1	0	0
L_τ	0	0	0	0	+1	+1	0	0	0	0	−1	−1

As an example, for the Michel decay of a muon,

$$\mu^+ \to e^+ \nu_e \overline{\nu}_\mu, \tag{1.1}$$

where both electron number L_e and muon number L_μ conserve. On the other hand, following process, where the muon decays into an electron and a photon, is a LFV process because L_e and L_μ do not conserve.

$$\mu^+ \to e^+ \gamma. \tag{1.2}$$

LFV in the charged lepton sector is called Charged Lepton Flavor Violation (CLFV). Currently, no CLFV processes were observed yet.

The history of CLFV search began with the discovery of the second lepton, muons. Muons were discovered from cosmic rays by Neddermeyer and Anderson in 1937 [1]. The mass was accidentally close to the mass of Yukawa's predicted meson (pion), so it was considered to be a particle that mediates the nuclear strong interaction at that time. However, in 1947, Conversi *et al.* found that the particles discovered by Neddermeyer *et al.* did not interact strongly [2], and in the same year Powell *et al.* discovered true Yukawa mesons [3]. The recognition of the new lepton with the same properties as electron except for mass can be considered to be the beginning of flavor physics.

Since the muon has the same quantum number as the electron except for its mass, it was expected at that time that a muon can decay into an electron with single photon emission, $\mu \to e\gamma$. This reaction is not

prohibited from the conservation law of energy, momentum and angular momentum. A search for $\mu \to e\gamma$ using cosmic rays was performed by Hincks and Pontecorvo in 1947 [4], which is the first CLFV searches. It was concluded that the branching ratio was less than 10%.

After the discovery of parity violation, in 1958, Feynman and Gell-Mann proposed charged vector bosons which mediates the weak interaction [5]. However, if such bosons exist, the branching ratio of $\mu^+ \to e^+\gamma$ decay is expected to be about 10^{-4}, which is inconsistent with the limit $\mathrm{Br}(\mu^+ \to e^+\gamma) < 2 \times 10^{-5}$ from CLFV experiments at the time [6]. This discrepancy was solved by distinguishing between two neutrinos [7, 8], electron and muon neutrino. The existence of muon neutrino was confirmed directly by Brookhaven by Danby *et al.* in 1962 [9]. Then, the lepton flavor was introduced, and the concept that each lepton flavor (electron number L_e and muon number L_μ) conserves independently was born.

In 1967, the SM of electroweak interaction was formulated by Weinberg and Salam. This model is based on the SU(2) × U(1) gauge theory proposed by Glashow in 1961 [10]. The SM is the connection of the BEH mechanism, which was proposed in 1964 by Englert, Brout, and Higgs [11, 12, 13], with the model of Glashow. The renormalizability of this theory was shown in 1971 by 't Hooft and Veltman [14, 15, 16]. In addition, since it was consistent with most experimental results, it can be said that the SM is a very successful theory at least on the currently accessible energy scale.

In the SU(2) × U(1) gauge theory with only one Higgs doublet and massless neutrinos, the conservation law of the lepton flavor numbers will automatically appear only from the gauge invariance and the renormalizability of Lagrangian. That is, CLFV processes are forbidden in the framework of the SM, and this is a natural explanation for the fact that any CLFV processes have not been observed at present time.

However, in the solar neutrino and atmospheric neutrino, an interesting phenomenon where neutrinos oscillate between different flavors (neutrino oscillation) was observed at the end of the 1990's. The neutrino mixing suggests that flavor of charged leptons may not be strictly conserved. An example is the exotic muon decay into an electron and a photon $\mu \to e\gamma$. This process would be caused by the neutrino oscillation $\nu_\mu \to \nu_e$ in the intermediate state, as shown in Fig. 1.1. However, when evaluating the branching ratio $\mathrm{Br}(\mu \to e\gamma)$, it is extremely small, which shows that it is impossible to be detected at least with modern observation accuracy: [17, 18, 19]

$$\begin{aligned} Br(\mu \to e\gamma) =& \frac{\text{Decay width of } \mu \to e\gamma}{\text{Total decay width of a muon}} \\ \simeq& \frac{3\alpha_{em}}{32\pi} \left| \sum_{i=2,3} U^*_{\mu i} U_{ei} \frac{\delta m^2_{i1}}{m^2_W} \right|^2 \simeq 10^{-54}, \end{aligned} \tag{1.3}$$

where m_W is a mass of charged weak boson, $U_{\alpha i}$ is an element of Pontecorvo-Maki-Nakagawa-Sakata (PMNS) matrix, and $\delta m^2_{ij} = m^2_i - m^2_j$ indicates a mass square difference of neutrinos.

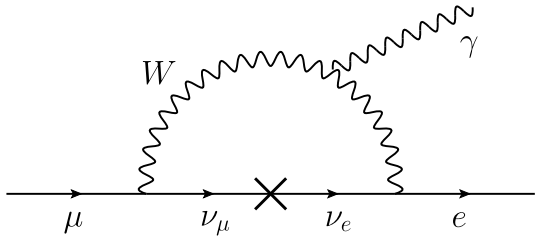

Figure 1.1: Feynman diagram of $\mu \to e\gamma$ induced by mixing of an intermediate neutrino.

Thus, in the SM, very accurate conservation of flavor in any charged lepton reactions is guaranteed. However, when trying to build a model that extends the SM, there are several sources that cause CLFV, and the existence of CLFV is actually predicted in many theories. As one of promising examples predicting observable CLFV effects, let us consider the supersymmetry model (SUSY). In SUSY, the interaction at high energy scale, such as the mass scale of the right-handed neutrino or the unified scale, can be the origin of

CLFV. Here, the rare decay search of a muon is an indirect probe of the high energy scale. In SUSY with a seesaw model, the Yukawa coupling of Higgs doublets, lepton doublets, and right handed neutrinos can cause large flavor mixing in slepton sector [20, 21, 22]. As a result, the branching ratio of CLFV decay can be as large as the current upper limit value. Supported by such theoretical predictions, the expectation that the CLFV process will be observed in the near future is increasing today.

Also, in general, rare process searches can be a clue for undiscovered particles even if they are heavy. For example, the CLFV branching ratio due to Fermi interaction is scaled by factor $(m_W/m_X)^4$, where m_X is the mass of unknown heavy particle. According to this argument, it is possible to observe m_X up to $\mathcal{O}(100)$ TeV in the current accuracy of CLFV searches for the exotic muon decay. It would be very difficult to see such heavy particles directly using current particle accelerators, and it can be said that the rare decay searches are very useful for searching for new particles.

At present, CLFV processes of muons are the most actively studied among CLFV searches. This is because muons can be produced in large quantities by a high intensity proton accelerator, so it is rather easy to obtain high statistics, and the lifetime of a muon is relatively long and measurement with very high precision can be performed. Many search experiments search for CLFV processes including a muon such as $\mu^+ \to e^+\gamma$, $\mu^+ \to e^+e^+e^-$, μ^--e^- conversion process in muonic atom, muonium-antimuonium conversion process, and so on have been done until today. The upper limit is being reduced by a factor of about two digits every 10 years, and a dramatic development of experimental technology have been made. The current upper limits on the CLFV branching ratio of a muonic rare process are in the order of 10^{-12} to 10^{-13}.

Many CLFV processes have been discussed and searched so far, as summarized in Chapter 2. Each of the processes has different advantages as a prove of CLFV. For example, $\mu^+ \to e^+\gamma$ has the best sensitivity to dipole CLFV operators, while $\mu^+ \to e^+e^+e^-$ and μ^--e^- conversion are also sensitive to four-Fermi CLFV operators $\bar{e}\mu\bar{e}e$ and $\bar{e}\mu\bar{q}q$, respectively. To understand the complete structure of CLFV interaction, many different CLFV processes should be studied.

The exotic decay process of the muonic atom $\mu^-e^- \to e^-e^-$ was proposed by Koike *et al.* [23] as a new possibility to search for Charged Lepton Flavor Violation (CLFV). It is a CLFV process where CLFV interaction between a muon and an electron bound in nuclei emit an pair of electrons. There are three major advantages of focusing on this process.

First, this process may be sensitive not only to the photonic interaction $\mu \to e\gamma$ but also to the Fermi interaction as seen in $\mu^+ \to e^+e^+e^-$. This indicates that we can investigate the more complete structure of the new physics in studying the $\mu^-e^- \to e^-e^-$ process.

Second, this process can be regarded as a two-body decay with a good approximation. The total energy of emitted electrons is about the mass of a muon. Therefore, the experimental signal is expected to be very clear.

Third, it is possible to raise the branching ratio by choosing muonic atoms with a large atomic number Z. For comparison, let us consider a similar CLFV reaction $\mu^+e^- \to e^+e^-$ in a muonium, which is a binding system of an anti-muon and an electron. Since the overlap of the wave functions of an anti-muon and an electron is small, this transition probability is also expected to be considerably small. While, in a muonic atom with a large atomic number, nuclei will attract leptons inside, so that the overlap between a 1s muon and 1s electrons can be increased. It is expected that the transition rate is enhanced by the factor $(Z-1)^3$. For example, if lead of $Z = 82$ is used, a reaction rate of about 5×10^5 times that of muonium can be obtained. However, as muons in muonic atoms decay not only by Michel decay but also by muon capture by nuclei, generally the lifetime of muonic atoms decreases as Z increases. It has been experimentally measured that the lifetime $\tilde{\tau}_\mu$ of muonic atoms is 2.2 μs for hydrogen and about 80 ns for lead. However, as described above, the reaction rate increases exceeding the decrease of the lifetime $\tilde{\tau}_\mu$ as Z increases. Therefore, by increasing Z, it is expected that the branching ratio of the CLFV decay $\mathrm{Br}(\mu^-e^- \to e^-e^-) = \tilde{\tau}_\mu \Gamma(\mu^-e^- \to e^-e^-)$ will also increase qualitatively.

The search for $\mu^-e^- \to e^-e^-$ is proposed in the COMET Phase-I experiment at J-PARC, Japan [24]. This new process could be essential to identify the scenario of new physics via the addition of sterile neutrinos at near future experiments [25].

As is well known, the effects of the Coulomb interaction are significant for the ordinary decay of bound muons in heavy nuclei [26, 27, 28]. Since the quantitative evaluation of the decay process is needed in order

to disentangle the mechanism of CLFV interaction, it is important to update the estimations of Ref. [23] by taking into account the effects of the Coulomb interactions for the relativistic leptons. The importance of the Coulomb distortion for the $\mu^- - e^-$ conversion process in a muonic atom has been reported in Refs. [29, 30, 31]. For the $\mu^- - e^-$ conversion process where the nucleus stays intact, it is sufficient to consider the s-wave muon and electron states. For $\mu^- e^- \to e^- e^-$ decay of muonic atom, on the other hand, two electrons with the energy of approximately one half of the muon mass are emitted in the final state. The angular momentum of each electron is not limited in this process. A formalism of the $\mu^- e^- \to e^- e^-$ decay with the partial wave expansion of leptons is necessary, as has been common in the nuclear beta decay and muon capture reactions [32].

In this thesis, we aim to quantitatively evaluate the decay rate and shed light on the property of the $\mu^- e^- \to e^- e^-$ process. Important effects in quantitative treatment are listed below.

1. Relativistic effects of bound leptons.
2. Distortion of scattering electrons.
3. Finite volume of nuclear charge distribution.

We perform analysis of $\mu^- e^- \to e^- e^-$ in muonic atom using Dirac lepton wave functions with a nuclear Coulomb interaction of finite nuclear charge distribution and show their importance. We study how the use of improved lepton wave function modifies the decay rate and we study possible observable which have a capability to distinguish CLFV operators. Furthermore, we show that the muon polarization can be an useful tool to distinguish the chiral structure of CLFV interaction.

The structure of this thesis is as follows: We review charged lepton flavor violation in Chapter 2 in order to understand the position of the $\mu^- e^- \to e^- e^-$process in a muonic atom. In Chapter 3, we introduce the effective Lagrangian which describe the $\mu^- e^- \to e^- e^-$ process to achieve model-independent analysis. Chapter 4 shows the analytic formula for the transition probability, which includes above improvement. The formulation shown in Chapter 4 is based on our papers [33, 34]. The study for the polarized muon is shown in Chapter 5. The numerical results are shown and discussed in Chapter 6. Finally, we summarize in Chapter 7.

Chapter 2

Search for CLFV

We summarize current status of experiments to search for the CLFV [35, 36, 37, 38, 39, 40, 41, 42, 43, 44]. Here, we do not discuss exotic processes which include lepton number violation (e.g. μ^--e^+ conversion), baryon number violation (e.g. $\tau^- \to \mu^-\pi^- p$), or $\Delta L_i \geq 2$ (e.g. muonium-antimuonium oscillation).

2.1 Muon Decay

Experiments on muon rare decay provide us strong restrictions on new physics using high intensity muon beam. The current upper limits of LFV are summarized in Table 2.1. Here we focus three decay modes: $\mu \to e\gamma$, $\mu \to eee$, and μ-e conversion.

Table 2.1: Current status of searches for muon rare decays which violate lepton flavor numbers. The second column shows current upper limit for the branching ratio. The branching ratios of the fourth line and below is normalized to the muon capture rate by the nucleus.

Mode	Current upper bound	C.L.	Experiment	Year	Reference
$\mu^+ \to e^+\gamma$	4.2×10^{-13}	90%	MEG	2016	[45]
$\mu^+ \to e^+e^+e^-$	1.0×10^{-12}	90%	SINDRUM	1988	[46]
$\mu^-\mathrm{Ti} \to e^-\mathrm{Ti}$	6.1×10^{-13}	90%	SINDRUM II	1998	[47]
$\mu^-\mathrm{Au} \to e^-\mathrm{Au}$	7×10^{-13}	90%	SINDRUM II	2006	[48]
$\mu^-\mathrm{Pb} \to e^-\mathrm{Pb}$	4.6×10^{-11}	90%	SINDRUM II	1996	[49]

2.1.1 $\mu \to e\gamma$

The most easily conceived process of muonic CLFV may be $\mu \to e\gamma$. Since there are only two particles in the final state, an electron and a photon are emitted back-to-back and each of their energies is equal to half of the muon mass ($E_e = E_\gamma \simeq 52.8$MeV) neglecting electron mass at the rest frame of initial muon. In order to make effective use of this property, it is important to stop muons in a material. Therefore positive muons must be used because negative muons form muonic atoms in the material, which ruins the advantage of two-body kinematics. The searches for $\mu \to e\gamma$ have a long history of 60 years. The first experiment was performed by Hincks and Pontecorvo [4] at Chalk River. They used cosmic ray muons stopped in a lead absorber and measured the coincidence of two Geiger-Müller counters. As the result, they concluded "that each decay electron is not accompanied by a photon of about 50 MeV".

Conventionally, the effective field theory is used to analyze rare processes model-independently. In the approach, the effective interactions are formed by assuming the same gauge and Lorentz symmetry as the SM. The dimension of the effective operators is not limited, but since higher-dimension operators would be

more suppressed by the scale of new physics, it is reasonable to consider only small-dimension operators. The effective interaction Lagrangian describing $\mu \to e\gamma$ is given as

$$\mathcal{L}_{\mu\to e\gamma} = -\frac{4G_F}{\sqrt{2}} m_\mu [A_R \bar{e}\sigma^{\mu\nu} P_R \mu + A_L \bar{e}\sigma^{\mu\nu} P_L \mu] F_{\mu\nu} + [H.c.], \tag{2.1}$$

where $A_{R/L}$ are dimensionless coupling constants. Using Eq. (2.1), we can represent the differential branching ratio of $\mu^+ \to e^+\gamma$ with polarized muon as [50]

$$\frac{dBr\left(\mu^+ \to e^+\gamma\right)}{d\cos\theta_e} = 192\pi^2 \left[|A_R|^2 \left(1 - P\cos\theta_e\right) + |A_L|^2 \left(1 + P\cos\theta_e\right) \right]. \tag{2.2}$$

Here P is the magnitude of the muon spin polarization and θ_e is the angle between the muon polarization and the momentum of an emitted positron. The total branching ratio is

$$Br\left(\mu^+ \to e^+\gamma\right) = 384\pi^2 \left(|A_L|^2 + |A_R|^2 \right). \tag{2.3}$$

Two major backgrounds for $\mu^+ \to e^+\gamma$ searches can be considered. One of them is a radiative muon decay (RMD), $\mu^+ \to e^+\nu_\mu\overline{\nu}_e\gamma$, with neutrinos carrying small energies. The branching ratio for RMD is 1.4% for $E_\gamma > 10$MeV. Of course, this would not be background if the detector had infinite energy resolution. Therefore it is important to understand the kinematics of RMD to reduce contribution of background. The differential decay rate has been calculated as a function of E_e, E_γ, and the angle between an electron and a photon, $\theta_{e\gamma}$, in Ref. [51, 52]. Within approximations: $E_e \approx m_\mu/2$, $E_\gamma \approx m_\mu/2$, and $\theta_{e\gamma} \approx 1$ to consider the case that neutrinos carry off small amount of energy, the differential decay rate is given as

$$\begin{aligned} &d\Gamma\left(\mu^+ \to e^+\nu_\mu\overline{\nu}_e\gamma\right) \\ \simeq &\frac{G_F^2 m_\mu^5 \alpha_{em}}{3\times 2^8\pi^4} \left[(1-x)^2(1 - P\cos\theta_e) + \left(4(1-x)(1-y) - \frac{1}{2}z^2 \right)\left(1 + P\cos\theta_e\right) \right] dxdydzd\cos\theta_e, \end{aligned} \tag{2.4}$$

where $x = 2E_e/m_\mu \approx 1$, $y = 2E_\gamma/m_\mu \approx 1$, and $z = \pi - \theta_{e\gamma} \approx 0$. Suppose δx, δy, and δz are half-width of signal region for x, y, and z, respectively, the branching rate for RMD which could mimic the signal is [53]

$$dBr\left(\mu^+ \to e^+\nu_\mu\overline{\nu}_e\gamma\right) = \frac{\alpha_{em}}{16\pi} \left[J_1 \left(1 - P\cos\theta_e\right) + J_2 \left(1 + P\cos\theta_e\right) \right] d\cos\theta_e. \tag{2.5}$$

Here there are two cases of the formula of J_1 and J_2, depending on δz:

$$J_1 = \left(\delta x\right)^4 \left(\delta y\right)^4, \tag{2.6}$$

$$J_2 = \frac{8}{3} \left(\delta x\right)^3 \left(\delta y\right)^3, \tag{2.7}$$

for $\delta z > 2\sqrt{\delta x \delta y}$, and

$$J_1 = \frac{8}{3} \left(\delta x\right)^3 \left(\delta y\right) \left(\frac{\delta z}{2}\right)^2 - 2\left(\delta x\right)^2 \left(\frac{\delta z}{2}\right)^4 + \frac{1}{3}\frac{1}{\left(\delta y\right)^2} \left(\frac{\delta z}{2}\right)^8, \tag{2.8}$$

$$J_2 = 8\left(\delta x\right)^2 \left(\delta y\right)^2 \left(\frac{\delta z}{2}\right)^2 - 8\left(\delta x\right)\left(\delta y\right) \left(\frac{\delta z}{2}\right)^4 + \frac{8}{3}\left(\frac{\delta z}{2}\right)^6, \tag{2.9}$$

for $\delta z \leq 2\sqrt{\delta x \delta y}$. In practice, the resolution of positron energy is typically better than that of photon energy, so that $\delta x < \delta y$. Moreover the angular resolution δz is worse than $2\sqrt{\delta x \delta y}$. Thus Eqs. (2.6) and (2.7) should be usually used for J_1 and J_2, and in most cases, J_2 is much larger than J_1.

The other background is accidental detection of a positron from Michel decay and a photon from various sources. The sources of such high energy photons are expected to be RMD, annihilation in flight positron ($e^+e^- \to \gamma\gamma$), and scattering off a nucleus ($eN \to eN\gamma$). As time resolution of detector gets better, this kind of background is expected to be reduced. This background is more important because prompt RMD background is only about 10% of accidental one for modern experiments.

The strongest limit of $\mu^+ \to e^+\gamma$ has been given by MEG experiment: $Br\left(\mu^+ \to e^+\gamma\right) < 4.2\times 10^{-13}$ [45]. The next MEGII experiment is also scheduled in 2018 and expected to reach a sensitivity of 6×10^{-14} with three years [54].

2.1.2 $\mu \to eee$

The second simplest CLFV process is $\mu \to eee$. Since this is three-body decay, each energy of final electrons is not fixed but their total energy is m_μ in the rest frame of initial muon. As is $\mu^+ \to e^+\gamma$, it is also favored to use positive muon for making use of the kinematical advantage: $\mu^+ \to e^+e^+e^-$.

In this searches, the signal is two positrons and one electron where their total energy is the mass of muon and their total momentum is zero. The final particles are well constrained by kinematics. However many of the similar problems as $\mu^+ \to e^+\gamma$ searches also exist in $\mu^+ \to e^+e^+e^-$ searches. Moreover the energy range of signal positrons overlaps with that of positrons emitted from ordinary decay of muons.

In the effective Lagrangian approach introduced in the review of $\mu \to e\gamma$, the effective Lagrangian is written down as

$$\mathcal{L}_{CLFV} = \mathcal{L}_{\mu\to e\gamma} + \mathcal{L}_{\text{contact}}, \tag{2.10}$$

$$\begin{aligned}\mathcal{L}_{\text{contact}} =& -\frac{4G_F}{\sqrt{2}}[g_1(\overline{e}P_R\mu)(\overline{e}P_Re) + g_2(\overline{e}P_L\mu)(\overline{e}P_Le) \\ &+ g_3(\overline{e}\gamma_\mu P_R\mu)(\overline{e}\gamma^\mu P_Re) + g_4(\overline{e}\gamma_\mu P_L\mu)(\overline{e}\gamma^\mu P_Le) \\ &+ g_5(\overline{e}\gamma_\mu P_R\mu)(\overline{e}\gamma^\mu P_Le) + g_6(\overline{e}\gamma_\mu P_L\mu)(\overline{e}\gamma^\mu P_Re)] + [H.c.],\end{aligned} \tag{2.11}$$

where g_is $(i = 1, 2, \cdots, 6)$ are coupling constants. Here the photonic part, $\mathcal{L}_{\mu\to e\gamma}$, is given in Eq. (2.1). Using this Lagrangian, we can write the total branching ratio as [50]

$$\begin{aligned}Br\left(\mu^+ \to e^+e^+e^-\right) =& \frac{1}{8}\left(G_{12} + 16G_{34} + 8G_{56}\right) + 128\pi\alpha_{em}\left[\ln\left(\frac{m_\mu^2}{m_e^2}\right) - \frac{11}{4}\right]\left(|A_R|^2 + |A_L|^2\right) \\ &+ 8\sqrt{4\pi\alpha_{em}}\text{Re}\left[2A_Rg_4^* + 2A_Lg_3^* + A_Rg_6^* + A_Lg_5^*\right].\end{aligned} \tag{2.12}$$

Here we have used the following notation:

$$G_{ij} = |g_i|^2 + |g_j|^2, \qquad G'_{ij} = \text{Re}\left[g_i^*g_j\right]. \tag{2.13}$$

More detailed information, such as a differential decay rate, is also given in Ref. [50]. In case that only the photonic interaction contributes, the model-independent ratio of $Br\left(\mu^+ \to e^+e^+e^-\right)$ to $Br\left(\mu^+ \to e^+\gamma\right)$ is expected to be

$$\frac{Br\left(\mu^+ \to e^+e^+e^-\right)}{Br\left(\mu^+ \to e^+\gamma\right)} \simeq \frac{\alpha_{em}}{3\pi}\left[\ln\left(\frac{m_\mu^2}{m_e^2}\right) - \frac{11}{4}\right] \simeq 0.006. \tag{2.14}$$

Now there are two major backgrounds again. For a search for $\mu^+ \to e^+e^+e^-$, a serious physics background is $\mu^+ \to e^+e^+e^-\nu_\mu\overline{\nu}_e$ where the neutrinos have small energy. The other is an accidental coincidence of a positron from Michel decay with a pair of e^+e^- from another source. The examples of e^+e^- pair sources are Bhabha scattering of positrons and splitting of virtual photon from RMD. The e^+e^- pair from photon splitting can be reduced by eliminating the pair whose invariant mass is small. However this reduction makes lower sensitivity for the some specific models where the photonic interaction dominates.

The current limit of $\mu^+ \to e^+e^+e^-$ is given by the SINDRUM experiment in 1988, but for nearly 20 years, there is no searches for $\mu^+ \to e^+e^+e^-$ process at all. Mu3e experiment at the Paul Scherrer Institut in Switzerland is planned for the near future. The experiment aims to the sensitivity of 10^{-16} [55].

2.1.3 μ-e Conversion in a Muonic Atom

The previous two CLFV searches of $\mu^+ \to e^+\gamma$ and $\mu^+ \to e^+e^+e^-$ are performed by using positive muons because negative muons would be trapped by a nucleus. Another promising CLFV search is μ^--e^- conversion in a muonic atom.

In general, an unstable particle can decay into more than or equal to two other particles because of four-momentum conservation. However, if the recoil energy of heavy particle can be neglected, the particle

is allowed to decay into one lighter particle, effectively, such as $\mu \to e$. If such CLFV decay mode happens, the detection would be simple and clear because the signal is only one high-energy electron. The system of a muonic atom actually enables us to archive the situation.

A nucleus is much heavier than the muon mass. Nuclear degrees of freedom is not necessary treated explicitly but it can be included as a potential for lepton as long as we consider processes where the nucleus keeps unchanged. Therefore a muon is allowed to convert into an electron in a muonic atom kinematically, freed from spacial momentum conservation. This process is called as μ^--e^- conversion in a muonic atom.

So far, we have mentioned only the coherent transition, where the state of the nucleus does not change before and after the μ^--e^- conversion. You can generally consider both of a ground state and an excited state as final state of the nucleus. However, in usual case, the transition from a ground state to a ground state is dominant because the rate of the coherent transition is enhanced by a factor approximately equal to square of the number of participating nucleons. Actually, the rates including transition to exited states have been calculated by shell-model approximation and random phase approximation [56, 57]. According to these results, the transition rates to excited states are small. Recently, future searches for spin-dependent incoherent processes was discussed in Ref. [58].

This CLFV search is said to be sensitive for two kinds of interactions. One is photonic interaction given in Eq. (2.1), which generates one-photon-exchange process between a muon and a nucleus, as shown by Fig. 2.1-(a). The other is non-photonic interaction, which is described by four-Fermi interaction among two leptons and two quarks, as shown by Fig. 2.1-(b). The general Lagrangian of the non-photonic interaction at quark level is given as

$$\begin{aligned}\mathcal{L}_{4-\mathrm{Fermi}} = -\frac{G_F}{\sqrt{2}} \sum_{q=u,d,s} \Big[&(g_{LS}\overline{e}_L\mu_R + g_{RS}\overline{e}_R\mu_L)\,\overline{q}q + (g_{LP}\overline{e}_L\mu_R + g_{RP}\overline{e}_R\mu_L)\,\overline{q}\gamma_5 q \\ &+ (g_{LV}\overline{e}_L\gamma^\mu\mu_L + g_{RV}\overline{e}_R\gamma^\mu\mu_R)\,\overline{q}\gamma_\mu q + (g_{LA}\overline{e}_L\gamma^\mu\mu_L + g_{RA}\overline{e}_R\gamma^\mu\mu_R)\,\overline{q}\gamma_\mu\gamma_5 q \\ &+ \frac{1}{2}(g_{LT}\overline{e}_L\sigma^{\mu\nu}\mu_R + g_{RT}\overline{e}_R\sigma^{\mu\nu}\mu_L)\,\overline{q}\sigma_{\mu\nu}q + [H.c.]\Big], \end{aligned} \tag{2.15}$$

where g_{LX} and g_{RX} are dimensionless coupling constants for the left-handed and right-handed electron, respectively, and $X = S, P, V, A, T$ indicate scalar, pseudo-scalar, vector, axial-vector, and tensor, respectively. The number of parameters is larger than that of $\mathcal{L}_{\mathrm{contact}}$, Eq. (2.11), because there is no symmetry which reduces the degree of freedom as $\mathcal{L}_{\mathrm{contact}}$ where operators contain three electron fields. The model-independent and quantitative analysis for μ^--e^- was performed in Ref. [29]. They showed that the Z-dependence of decay rate depends on CLFV mechanism.

Figure 2.1: The diagrams representing μ^--e^- conversion: the one-photon-exchange photonic interaction (a) and the four Fermi contact interaction (b). The black closed circle shows the CLFV interaction. The gray shaded circle includes the complicated effects of the quantum chromodynamics.

The signal of coherent conversion process $\mu^- N \to e^- N$ is a monochromatic electron with energy of

$$E_e = m_\mu - B_\mu^{1S}, \tag{2.16}$$

where the nuclear recoil energy is ignored here. Here B_μ^{1s} is the binding energy of $1S$ muon. The binding energy depends on a kind of the nucleus, so the signal energy changes. For example, $E_e = 104.3$MeV for titanium and $E_e = 94.9$MeV for lead. Since the energy of the signal electron is much higher than typical

energy range of electrons from muon decay in orbit, the search can be performed in small physics backgrounds. It is also a great advantage that we require no coincidence measurement because the signal is only one electron.

Although the upper end point of the electron energy from free muon decay is about 52.8MeV, the tail of electron spectrum from muon decay in orbit (DIO) is extended to the same energy as the μ^--e^- conversion signal because of the nuclear recoil. The DIO electron with an energy near the end point is one of the main backgrounds. The spectra for various muonic atoms have been calculated theoretically in Ref. [28]. More careful calculation which include the nuclear recoil effect is given in Ref. [59]. According to the recent improvement [60], DIO electron spectrum for aluminum near the end-point is

$$\frac{m_\mu}{\Gamma}\frac{d\Gamma}{dE_e} \approx 1.24(3) \times 10^{-4} \times \left(\frac{E_{\max} - E_e}{m_\mu}\right)^{5.023}, \tag{2.17}$$

including radiative corrections. The energy resolution of electron near the end-point must be improved to reduce backgrounds for μ^--e^- conversion searches.

Previous searches for μ^--e^- conversion were performed by using heavy targets such as lead and gold. On the other hand, in μ^--e^- conversion experiments planned recently, aluminum or carbon (silicon carbide) will be used as the target material. COMET [24] and Mu2e [61] are the experiments planned at J-PARC (Japan) and Fermi Laboratory (USA), respectively. Both of them plan to use aluminum as the target, and their reaching sensitivities are the same level, $\mathcal{O}\left(10^{-17}\right)$. At J-PARC, DeeMe experiment [62] is also planned. DeeMe has an unique feature that pions, muon, and muonic atoms are produced in one carbon (or silicon carbide) target. Its reachable sensitivity is $\mathcal{O}\left(10^{-14}\right)$.

2.2 Tau Decay

CLFV searches with tau leptons have advantages because a number of channels are open thanks to its large mass ($m_\tau \simeq 1.78$GeV). Despite the expectation, there are some experimental difficulties using tau leptons. For example, since the lifetime of the tau lepton (2.9×10^{-13}s) is much shorter than that of the muon (2.2×10^{-6}s), the tau beam is not possible to produce. To create many tau leptons, we require a high energy electron or proton accelerator. Moreover, the tau decay must be measured by a detector which has good particle identification and energy-momentum resolution.

The rare decay of tau lepton has been studied in B-factories, such as Belle and Babar. Main aim of their experiments is measuring CP-violation phase of Cabbibo-Kobayashi-Maskawa matrix by creating a number of B-$\overline{B}$ pairs. To achieve the purpose, the center of mass energy of e^--e^+ beam is adjusted to mass of $\Upsilon(4S)$ (10.58GeV), whose branching ratio to B-$\overline{B}$ pair is almost 100% [63]. In those experiments, many tau leptons are also produced because the cross section of $\tau^+\tau^-$ pair creation is 90% of the cross section of $b\bar{b}$ pair creation. Thus the B-factory can be also called as the τ-factory, which is the best place to research detailed natures of the tau lepton. The current bounds for CLFV tau decays are shown in Table 2.2 [64].

Table 2.2: Current status of searches for tau rare decays which violate lepton flavor numbers. The second column shows current upper limit for the branching ratio.

Mode	Current upper bound	C.L.	Experiment	Year	Reference
$\tau \to e\gamma$	3.3×10^{-8}	90%	BaBar	2010	[65]
$\tau \to \mu\gamma$	4.4×10^{-8}	90%	BaBar	2010	[65]
$\tau \to eee$	2.7×10^{-8}	90%	Belle	2010	[66]
$\tau \to \mu\mu\mu$	2.1×10^{-8}	90%	Belle	2010	[66]
$\tau \to \pi^0 e$	8.0×10^{-8}	90%	Belle	2007	[67]
$\tau \to \pi^0 \mu$	1.1×10^{-7}	90%	BaBar	2007	[68]
$\tau \to \rho^0 e$	1.8×10^{-8}	90%	Belle	2011	[69]
$\tau \to \rho^0 \mu$	1.2×10^{-8}	90%	Belle	2011	[69]

The strategy for measurement of CLFV tau events in a e^+e^- collider is as follows [70]: At first, the low-multiplicity events (2 or 4 charged tracks) are selected to remove hadronic events such as $e^+e^- \to b\bar{b}$ which should have hadronic jets. The candidate events of $e^+e^- \to \tau^+\tau^-$ are divided into two hemispheres in the center of mass frame: one is a signal side, and the other is a tag side. In the tag side, we require that 1-prong tau decay ($\tau \to \ell\nu\nu$ or $\tau \to h\nu$, which are about 85% of total tau decay) is reconstructed. Of course, the standard $\tau^+\tau^-$ events can also be backgrounds. In the standard tau decays, one or more neutrinos or undetectable particles carry off energy, whereas in CLFV tau decay, all daughter particles could be detected. Therefore, it is convenient to characterize each events in two dimensions of total energy in the center-of-mass frame, E, and invariant mass, M, of all particles on the signal side. When CLFV event happens, both of $E = \sqrt{s}/2$ and $M = m_\tau$ should be satisfied.

2.3 Other CLFV search

2.3.1 Meson Decay

Not only lepton rare decays, rare decays of mesons have also been studied. The constraint on CLFV from them are summarized in Table 2.3.

Table 2.3: Current status of searches for hadron rare decays which violate lepton flavor numbers. The second column shows current upper limit for the branching ratio.

Mode	Current upper bound	C.L.	Experiment	Year	Reference
$\pi^0 \to \mu e$	3.6×10^{-10}	90%	KTeV	2008	[71]
$K_L^0 \to \mu e$	4.7×10^{-12}	90%	BNL E871	1998	[72]
$K_L^0 \to \pi^0 \mu e$	7.6×10^{-11}	90%	KTeV	2008	[71]
$K^+ \to \pi^+ \mu^+ e^-$	1.3×10^{-11}	90%	BNL E865	2005	[73]
$J/\Psi \to \mu e$	1.5×10^{-7}	90%	BESIII	2013	[74]
$J/\Psi \to \tau e$	8.3×10^{-6}	90%	BESII	2004	[75]
$J/\Psi \to \tau \mu$	2.0×10^{-6}	90%	BESII	2004	[75]
$B^0 \to \mu e$	2.8×10^{-9}	90%	LHCb	2013	[76]
$B^0 \to \tau e$	2.8×10^{-5}	90%	BaBar	2008	[77]
$B^0 \to \tau \mu$	2.2×10^{-5}	90%	BaBar	2008	[77]
$B \to K \mu e$	3.8×10^{-8}	90%	BaBar	2006	[78]
$B \to K^* \mu e$	5.1×10^{-7}	90%	BaBar	2006	[78]
$B^+ \to K^+ \tau e$	3.0×10^{-5}	90%	BaBar	2012	[79]
$B^+ \to K^+ \tau \mu$	4.8×10^{-5}	90%	BaBar	2012	[79]
$B_s^0 \to \mu e$	1.1×10^{-8}	90%	LHCb	2013	[76]
$\Upsilon(1S) \to \tau \mu$	6.0×10^{-6}	90%	CLEO	2008	[80]

The motivation of searches for the meson decays is to cover various CLFV operators. For example, $K^0 \to \mu e$ probes the CLFV operators among s, d, μ, and e, while they cannot be constrained from muon decay experiments because a muon is too light to decay into mesons with strangeness. Also, since μ^--e^- conversion has low sensitivity to operators which changes the nuclear state, the meson rare decay search is an unique method to limit such operators. Likewise, since any charmed and bottomed mesons are heavier than tau lepton, it is important to search these processes in order to limit operators including those quarks. The restrictions on four Fermi interactions including quarks are summarized in Ref. [81].

2.3.2 Z and Higgs Decay

The rare decay of Z boson and higgs particle has also been explored by using a large accelerator, such as LHC. Especially, since properties of higgs is least known in the SM, it is very important to investigate the

decay mode in detail for the verification of the SM and the search for new physics. These constraints are given in Table 2.4.

Table 2.4: Current status of searches for Z and higgs boson rare decays which violate lepton flavor numbers. The second column shows current upper limit for the branching ratio.

Mode	Current upper bound	C.L.	Experiment	Year	Reference
$Z \to \mu e$	7.5×10^{-7}	95%	LHC ATLAS	2014	[82]
$Z \to \tau e$	9.8×10^{-6}	95%	LEP OPAL	1995	[83]
$Z \to \tau \mu$	1.2×10^{-5}	95%	LEP DELPHI	1997	[84]
$h \to \mu e$	3.5×10^{-4}	95%	LHC CMS	2016	[85]
$h \to \tau e$	6.1×10^{-3}	95%	LHC CMS	2017	[86]
$h \to \tau \mu$	2.5×10^{-3}	95%	LHC CMS	2017	[86]

2.3.3 Displaced Vertex Search

Usually, rare decay processes are searched by assuming that the mediated particle X is very heavy so the CLFV interaction can be treated as contact one. However, if the X particle is lighter than the parent particle, that approach is not validated because the mediator would be created on mass shell. To search for such light new particles X, displaced vertices or invisible decays should be looked for. The current limit from past searches are shown in Table 2.5. According to Ref. [87], where X is assumed to be pseudo-scalar, most of the parameter region which can be explored by muon decay experiment has already excluded by beam-dump experiments and supernova data. On the other hand, the accessible region of tau decay remains sufficiently wide.

Table 2.5: Current status of searches for CLFV muon decays which includes invisible on-shell particle X. The second column shows order of current upper limit for the branching ratio. These results contains information on the mass, lifetime, and branching ratio of X. See reference for the details.

Mode	Current upper bound	Experiment	Year	Reference
$\mu^+ \to e^+ \gamma X$, $X \to$inv.	$\mathcal{O}\left(10^{-9}\right)$	Crystal Box	1988	[88]
$\mu^+ \to e^+ X$, $X \to$inv.	$\mathcal{O}\left(10^{-5}\right)$	TWIST	2015	[89]
$\mu^+ \to e^+ X$, $X \to e^+ e^-$	$\mathcal{O}\left(10^{-12}\right)$	SINDRUM	1986	[90]
$\mu^+ \to e^+ X$, $X \to \gamma\gamma$	$\mathcal{O}\left(10^{-10}\right)$	MEG	2012	[91]

2.3.4 Lepton Scattering

The last subject of this section is CLFV scattering processes, such as $\ell N \to \ell' X$ and $e^+ e^- \to \ell^+ \ell'^-$. In particular, the processes whose final state includes a tau lepton are very attractive. As shown in Section 2.2, searches for rare decay of tau leptons yield relatively small restriction for branching ratio, compared to muon rare decay searches, due to difficulties of tau leptons. Therefore, by a search for the scattering processes, it may be possible to explore parameter region which has not been excluded by tau rare decays.

The CLFV scattering of lepton off nucleus ($\ell N \to \ell' X$) was firstly proposed by Ref. [92]. The further discussion was given by Ref. [93, 94, 95]. Assuming the reaction of valence quark and lepton, elastic scattering at relatively low energy is favored to reduce backgrounds. On the other hand, it is effective to use scattering with a high energy lepton beam if a mediator particle with CLFV couples strongly to a heavy quark, like higgs [96]. In that case, the contribution of the DIS region is dominant, so an analysis using the parton distribution function is important. In addition, the improved calculation properly taking into account the mass of heavy quark in the final state was given in Ref. [97].

Also, discussion for $e^+e^- \to \ell^+\ell'^-$ and $e^-e^- \to \ell^-\ell'^-$, which can be searched by e^--$e^+(e^-)$ colliders, are given by Refs. [98, 99] where general four Fermi interactions are assumed. Another interesting search using electron-photon collision has been proposed [100, 101].

Chapter 3

Elementary Mechanism of $\mu^- e^- \to e^- e^-$

In this chapter, we describe an effective CLFV Lagrangian which we use for the research of the $\mu^- e^- \to e^- e^-$ process. The general effective Lagrangian on the CLFV process $\mu^- e^- \to e^- e^-$, with operators up to dimension six, is given as

$$\mathcal{L}_{CLFV} = \mathcal{L}_{\mu\to e\gamma} + \mathcal{L}_{\text{contact}}, \tag{2.10}$$

$$\mathcal{L}_{\mu\to e\gamma} = -\frac{4G_F}{\sqrt{2}} m_\mu [A_R \bar{e}\sigma^{\mu\nu} P_R \mu + A_L \bar{e}\sigma^{\mu\nu} P_L \mu] F_{\mu\nu} + [H.c.], \tag{2.1}$$

$$\begin{aligned}\mathcal{L}_{\text{contact}} = &-\frac{4G_F}{\sqrt{2}} [g_1 (\bar{e}P_R\mu)(\bar{e}P_R e) + g_2 (\bar{e}P_L\mu)(\bar{e}P_L e) \\ &+ g_3 (\bar{e}\gamma_\mu P_R\mu)(\bar{e}\gamma^\mu P_R e) + g_4 (\bar{e}\gamma_\mu P_L\mu)(\bar{e}\gamma^\mu P_L e) \\ &+ g_5 (\bar{e}\gamma_\mu P_R\mu)(\bar{e}\gamma^\mu P_L e) + g_6 (\bar{e}\gamma_\mu P_L\mu)(\bar{e}\gamma^\mu P_R e)] + [H.c.].\end{aligned} \tag{2.11}$$

This effective Lagrangian is the same one as used for the analysis for $\mu^+ \to e^+e^+e^-$ process. Here we assume the CLFV interaction that respects Lorentz and electromagnetic gauge symmetry but generally breaks parity. One can think about the extra term, $i\bar{e}\not{D}\mu + [H.c.]$, for photonic interaction. Although this term respects the symmetries assumed above, it is not physical because the kinetic-like term can be eliminated by redefining the lepton fields [102]. Therefore the operators listed in Eq. (2.1) cover all the lowest dimensional operators describing the $\mu e\gamma$ vertex. Moreover, one can show that the other possibility of four-Fermi operators, such as $(\bar{e}P_R\mu)(\bar{e}P_L e)$, are redundant by using Fierz transformation, as discussed in Appendix F. Lagrangian (2.1) and (2.11) contribute to the $\mu^- e^- \to e^- e^-$ process by the photonic process (Fig. 3.1-(a)) and the contact process (Fig. 3.1-(b)), respectively.

3.1 Photonic Interaction

The photonic interaction,

$$\mathcal{L}_{\mu\to e\gamma} = -\frac{4G_F}{\sqrt{2}} m_\mu [A_R \bar{e}\sigma^{\mu\nu} P_R \mu + A_L \bar{e}\sigma^{\mu\nu} P_L \mu] F_{\mu\nu} + [H.c.], \tag{2.1}$$

is represented by the operators with dimension five. A_R and A_L are dimensionless coupling constants, corresponding to a right-handed and left-handed muon, respectively. In the case where a muon bound to a nucleus change to an electron by this interaction, the emitted photon interacts with another bound electron by the standard electromagnetic interaction of

$$\mathcal{L}_{\text{em}} = -q_e \bar{e}\gamma^\lambda e A_\lambda, \tag{3.1}$$

Figure 3.1: The diagrams representing $\mu^- e^- \to e^- e^-$: the one-photon-exchange photonic interaction (a) and the four Fermi contact interaction (b). The black closed circle shows the CLFV interaction. Figure taken from Ref. [34]. Copyright 2018 American Physical Society.

so that the $\mu^- e^- \to e^- e^-$ process can occur (Fig. 3.1-(a)). Here $q_e = -e$ is a charge of an electron. Since the photon is a massless particle and can propagate over long distances, this process can happen even if the muon and electron are separated by a distance.

Experimental studies on the photonic interaction term are carried out mainly by measuring the CLFV decay process of anti-muon, $\mu^+ \to e^+\gamma$. The branching ratio is given as

$$Br\left(\mu^+ \to e^+\gamma\right) = 384\pi^2 \left(|A_L|^2 + |A_R|^2\right). \tag{2.3}$$

Since it is two-body decay, the experimental signal is very clear. The most accurate data were obtained from the MEG experiment at the PSI. The data-taking were completed in the summer of 2013. By this measurement, the upper limit of the branching ratio is given as 4.2×10^{-13} at confidence level of 90% [45].

3.2 Contact Interaction

We use the following form of contact interaction

$$\begin{aligned}\mathcal{L}_{\text{contact}} = -\frac{4G_F}{\sqrt{2}}[&g_1(\bar{e}P_R\mu)(\bar{e}P_Re) + g_2(\bar{e}P_L\mu)(\bar{e}P_Le) \\ &+ g_3(\bar{e}\gamma_\mu P_R\mu)(\bar{e}\gamma^\mu P_Re) + g_4(\bar{e}\gamma_\mu P_L\mu)(\bar{e}\gamma^\mu P_Le) \\ &+ g_5(\bar{e}\gamma_\mu P_R\mu)(\bar{e}\gamma^\mu P_Le) + g_6(\bar{e}\gamma_\mu P_L\mu)(\bar{e}\gamma^\mu P_Re)] + [H.c.].\end{aligned} \tag{2.11}$$

g_is $(i = 1, 2, \cdots, 6)$ represent dimensionless coupling constants. This effective Lagrangian is most general form of dimension six operators as we show in Appendix F. The first two terms are scalar-type and the next two are vector-type interactions where final electrons have the same chiralities. On the other hand, the last two terms represent interactions where the chiralities of final electrons are opposite. Unlike the photonic process, this interaction occurs at one point in space-time.

The limits on these coupling constants are mainly determined by the rare three-body decay of free muon, $\mu^+ \to e^+e^+e^-$. Assuming that photonic interaction is absent, the branching ratio for the $\mu^+ \to e^+e^+e^-$ decay of a free muon is given by

$$Br(\mu^+ \to e^+e^+e^-) = \frac{1}{8}\left(G_{12} + 16G_{34} + 8G_{56}\right), \tag{3.2}$$

where

$$G_{ij} = |g_i|^2 + |g_j|^2, \quad G'_{ij} = \text{Re}\left[g_i^* g_j\right]. \tag{2.13}$$

The recent upper limit for the branching ratio is given as 1.0×10^{-12} by the SINDRUM experiment [46].

Chapter 4

Decay Rate

In this chapter, we formulate a decay rate for the CLFV process, $\mu^- e^- \to e^- e^-$ in a muonic atom, of unpolarized muon

$$\text{Muonic Atom} \to \text{Ion}^{*2+} + e^-_{p_1} + e^-_{p_2}. \tag{4.1}$$

Here p_is $(i = 1, 2)$ are the momenta of emitted electrons. Within the independent particle model of the muonic atom and the final state, we evaluate the decay rate of two-electron emission of the muonic atom as

$$\langle \text{Ion}^{*2+}; e^-_{p_1} e^-_{p_2} | \mathcal{L} | \text{Muonic Atom} \rangle = \langle e^-_{p_1} e^-_{p_2} | \mathcal{L} | \mu^-_{\alpha_\mu} e^-_{\alpha_e} \rangle \,, \tag{4.2}$$

where $\ell^-_{\alpha_\ell}$s denote bound leptons with quantum number $\alpha_\ell = \{n_\ell, \kappa_\ell\}$ $(\ell = \mu, e)$. Since the muon trapped in a Coulomb field of a nucleus rapidly transits to a ground state (see Appendix C), we assume muon is in a $\alpha_\mu = 1S_{1/2}$ state. We take into account all electrons in the atom. Since the mass of nucleus is sufficiently larger than the muon mass, we neglect the recoil energy of nucleus and the nucleus does not play dynamical role. The transition rate is calculated from leptons bound or scattered in the nuclear Coulomb field. In our calculation, we take into account the screened potential of electron, while the correlations among electrons are not considered because it is expected to only give a small correction.

4.1 Decay rate of $\mu^- e^- \to e^- e^-$ by Koike *et al.*

We follow the method to calculate the CLFV decay rate of muonic atom by Koike *et al.* [23]. We start from the cross section σ of μ-e scattering $\mu^- e^- \to e^- e^-$ using Lagrangian (2.10). Neglecting Coulomb field of nuclei, the cross section σ is given as

$$\begin{aligned} \sigma v_{\text{rel}} =& \frac{1}{2E_\mu 2E_e} \frac{1}{2} \left(\sum_{s_1, s_2} \int \frac{d^3 p_1}{(2\pi)^3 2E_1} \frac{d^3 p_2}{(2\pi)^3 2E_2} \right) \left(\frac{1}{4} \sum_{s_\mu, s_e} \right) \\ & \times \left| \mathcal{M}\left(p_1, s_1, p_2, s_2; p_\mu, s_\mu, p_e, s_e\right) \right|^2 (2\pi)^4 \delta^{(4)}(p_1 + p_2 - p_\mu - p_e), \end{aligned} \tag{4.3}$$

where v_{rel} is the relative velocity of initial muon and electron. The transition matrix $\mathcal{M}$ is defined as

$$i\mathcal{M}(2\pi)^4 \delta^{(4)}(p_1 + p_2 - p_\mu - p_e) = \langle e^{s_1}_{p_1} e^{s_2}_{p_2} | T \left[\exp\left(i \int d^4 x \mathcal{L}_I \right) \right] | \mu^{s_\mu}_{p_\mu} e^{s_e}_{p_e} \rangle \,, \tag{4.4}$$

where $\mathcal{L}_I = \mathcal{L}_{CLFV} + \mathcal{L}_{\text{em}}$. Now, the decay rate Γ of bound muon and electron into two scattered electrons is obtained by multiplying the probability that bound electron and bound muon are at the same space point to the cross section as

$$\Gamma = \sigma v_{\text{rel}} \int d^3 r \rho_\mu(\boldsymbol{r}) \rho_e(\boldsymbol{r}). \tag{4.5}$$

Here $\rho_\mu(r)$ and $\rho_e(r)$ are density of electron and muon, which are given by the bound state wave functions as

$$\rho_\mu(\boldsymbol{r}) = \left|\psi_\mu^{1S}(\boldsymbol{r})\right|^2, \tag{4.6}$$

$$\rho_e(\boldsymbol{r}) = \left|\psi_e^{1S}(\boldsymbol{r})\right|^2. \tag{4.7}$$

Here the approximation is the factorization of CLFV mechanism and lepton wave functions. Further, we approximate the integral of muon and electron density. Since a muon is much heavier than electron, one may approximate $\left|\psi_\mu^{1S}(\boldsymbol{r})\right|^2 \simeq \delta^{(3)}(\boldsymbol{r})$.

$$\begin{aligned}\int d^3r \rho_\mu(\mathbf{r})\rho_e(\mathbf{r}) &= \int d^3r \left|\psi_\mu^{1S}(\boldsymbol{r})\right|^2 \left|\psi_e^{1S}(\boldsymbol{r})\right|^2 \\ &\simeq \left|\psi_e^{1S}(\mathbf{0})\right|^2. \end{aligned}\tag{4.8}$$

Using the solution of the Schrödinger equation with potential of a screened point charge $(Z-1)e$,

$$\psi_e^{1S}(\boldsymbol{r}) = \sqrt{\frac{\left(m_e(Z-1)\alpha_{em}\right)^3}{\pi}} \exp\left(-m_e(Z-1)\alpha_{em}\left|\boldsymbol{r}\right|\right), \tag{4.9}$$

we obtain analytic expression of the transition rate,

$$\Gamma = \frac{2\left(m_e(Z-1)\alpha_{em}\right)^3}{\pi}\sigma v_{\rm rel}. \tag{4.10}$$

For contact process, the explicit form of the transition rate is given as

$$\sigma v_{\rm rel} = \frac{1}{m_\mu^2}\frac{\left(G_F m_\mu^2\right)^2}{16\pi}G, \tag{4.11}$$

where $G = G_{12} + 16G_{34} + 4G_{56} + 8G'_{14} + 8G'_{23} - 8G'_{56}$. Therefore, using Eq. (4.10),

$$\Gamma^0_{\rm contact} = \frac{m_\mu}{8\pi^2}(Z-1)^3\alpha_{em}^3\left(G_F m_\mu^2\right)^2\left(\frac{m_e}{m_\mu}\right)^3 G. \tag{4.12}$$

Similarly, for photonic process, we obtain

$$\sigma v_{\rm rel} = \frac{4\alpha_{em}\left(G_F m_\mu^2\right)^2}{m_e^2}\left(\left|A_R\right|^2 + \left|A_L\right|^2\right), \tag{4.13}$$

and

$$\Gamma^0_{\rm photonic} = \frac{8m_e}{\pi}(Z-1)^3\alpha_{em}^4\left(G_F m_\mu^2\right)^2\left(\left|A_R\right|^2 + \left|A_L\right|^2\right). \tag{4.14}$$

The formula shows clearly dependence of cross section on CLFV interaction and atomic number Z. The decay rate is proportional to the cubic power of atomic number and increasing with Z. In our analysis in later chapters, we compare our results with respect to the above formula Γ^0.

It is noticed that $\sigma v_{\rm rel}$ is independent from the atomic system. Finite spatial size of lepton bound state and Coulomb distortion of scattering electrons are not taken into account. There is no consideration that there is a finite spread of lepton wave functions. Those approximation will be valid for $Z\alpha_{em} \ll 1$ but not for large Z. Although the obtained formula is transparent and useful, improved treatment of lepton wave function is necessary for quantitative analysis of decay rate.

4.2 Formalism

Following standard formula to obtain transition rate, the CLFV decay rate of a muonic atom with an unpolarized muon can be written as

$$\begin{aligned}\Gamma =&\frac{1}{2}\left(\sum_{s_1,s_2}\int\frac{d^3p_1d^3p_2}{(2\pi)^32E_1(2\pi)^32E_2}\right)\left(\frac{1}{2}\sum_{s_\mu}\sum_{\alpha_e,s_e}\right)\\&\times\left|\mathcal{M}\left(\boldsymbol{p}_1,s_1,\boldsymbol{p}_2,s_2;\alpha_\mu,s_\mu,\alpha_e,s_e\right)_{\alpha_\mu=1S_{1/2}}\right|^2(2\pi)\delta\left(E_1+E_2-E_{tot}^{\alpha_e}\right).\end{aligned}\tag{4.15}$$

The transition matrix of the $\mu^-e^-\to e^-e^-$ process includes information of CLFV interactions and wave functions of initial and final leptons, i.e.

$$i\mathcal{M}(2\pi)\delta\left(E_1+E_2-E_{tot}^{\alpha_e}\right)=\langle e_{\boldsymbol{p}_1}^{s_1}e_{\boldsymbol{p}_2}^{s_2}|T\left[\exp\left(i\int d^4x\mathcal{L}_I\right)\right]|\mu_{1S_{1/2}}^{s_\mu}e_{\alpha_e}^{s_e}\rangle\,,\tag{4.16}$$

where the symbol T means a time-ordered product. In calculating the transition amplitude, we take into account the overlap among lepton wave functions. Here we define $E_i=p_i^0=\sqrt{p_i^2+m_e^2}$ and $E_{tot}^{\alpha_e}=m_\mu-B_\mu^{1S_{1/2}}+m_e-B_e^{\alpha_e}$, where $B_\ell^{\alpha_\ell}$ is a binding energy of a bound lepton ℓ in a α_ℓ state. The CLFV interaction is calculated in the first order perturbation.

$$\mathcal{M}_{\rm contact}(2\pi)\delta\left(E_1+E_2-E_{tot}^{\alpha_e}\right)=\int d^4x\,\langle e_{\boldsymbol{p}_1}^{s_1}e_{\boldsymbol{p}_2}^{s_2}|\mathcal{L}_{\rm contact}(x)|\mu_{1S_{1/2}}^{s_\mu}e_{\alpha_e}^{s_e}\rangle\,,\tag{4.17}$$

for contact process. Using the explicit form of contact interaction (2.11), the transition matrix is reduced to

$$\begin{aligned}&\mathcal{M}_{\rm contact}\\&=-\frac{4G_F}{\sqrt{2}}\sum_{i=1}^{6}g_i\left[\int d^3r\overline{\psi}_e^{\boldsymbol{p}_1,s_1}(\boldsymbol{r})O_i^A\psi_\mu^{1S_{1/2},s_\mu}(\boldsymbol{r})\overline{\psi}_e^{\boldsymbol{p}_2,s_2}(\boldsymbol{r})O_i^B\psi_e^{\alpha_e,s_e}(\boldsymbol{r})-(\{\boldsymbol{p}_1,s_1\}\leftrightarrow\{\boldsymbol{p}_2,s_2\})\right],\end{aligned}\tag{4.18}$$

where Dirac matrices are defined as

$$\begin{aligned}O_1^A=O_1^B=P_R,\qquad&O_2^A=O_2^B=P_L,\\O_3^A=O_5^A=\gamma_\mu P_R,\qquad&O_3^B=O_6^B=\gamma^\mu P_R,\\O_4^A=O_6^A=\gamma_\mu P_L,\qquad&O_4^B=O_5^B=\gamma^\mu P_L.\end{aligned}\tag{4.19}$$

Similarly, the transition matrix for photonic interaction is obtained as

$$\mathcal{M}_{\rm photonic}(2\pi)\delta\left(E_1+E_2-E_{tot}^{\alpha_e}\right)=iT\int d^4x_1d^4x_2\,\langle e_{\boldsymbol{p}_1}^{s_1}e_{\boldsymbol{p}_2}^{s_2}|\mathcal{L}_{\mu\to e\gamma}(x_1)\mathcal{L}_{\rm em}(x_2)|\mu_{1S_{1/2}}^{s_\mu}e_{\alpha_e}^{s_e}\rangle\,,\tag{4.20}$$

which can be reduced to

$$\begin{aligned}\mathcal{M}_{\rm photonic}=&\left(-\frac{4G_F}{\sqrt{2}}m_\mu\right)(-q_e)\left[\int d^3r_1d^3r_2\overline{\psi}_e^{\boldsymbol{p}_1,s_1}(\boldsymbol{r}_1)\sigma^{\mu\nu}\left(A_RP_R+A_LP_L\right)\psi_\mu^{1S_{1/2},s_\mu}(\boldsymbol{r}_1)\right.\\&\left.\times2G_\nu\left(\boldsymbol{r}_1,\boldsymbol{r}_2;m_\mu-B_\mu-E_1\right)\overline{\psi}_e^{\boldsymbol{p}_2,s_2}(\boldsymbol{r}_2)\gamma_\mu\psi_e^{\alpha_e,s_e}(\boldsymbol{r}_2)-(\{\boldsymbol{p}_1,s_1\}\leftrightarrow\{\boldsymbol{p}_2,s_2\})\right].\end{aligned}\tag{4.21}$$

Here $G_\nu\left(\boldsymbol{r}_1,\boldsymbol{r}_2;q_0\right)$ is defined as

$$G_\nu\left(\boldsymbol{r}_1,\boldsymbol{r}_2;q_0\right)=i\int\frac{d^3q}{(2\pi)^3}\frac{q_\nu\exp\left\{-i\boldsymbol{q}\cdot\left(\boldsymbol{r}_1-\boldsymbol{r}_2\right)\right\}}{|\boldsymbol{q}|^2-q_0^2-i\epsilon}.\tag{4.22}$$

It should be noted that there is no delta function of three-momentum conservation, while exists that of energy conservation. Neglecting the recoil kinetic energy of nuclei, the three-body (muon-electron-nucleus) problem reduces into independent particle model of muon and electron in the Coulomb potential of nuclei, which violates translational invariance. The first factor of 1/2 due to the two identical particle, electrons, in the final state. The second factor of 1/2 is to average muon spins. Our notations for normalizations are summarized in Appendix A.

We estimate a differential decay rate with respect to the energy of an emitted electron, E_1, and the angle between two emitted electrons, θ_{12}, as well as the total decay rate. The phase space integral and delta function in Eq. (4.15) are reduced to

$$\begin{aligned}\int \frac{d^3p_1 d^3p_2}{(2\pi)^3 2E_1 (2\pi)^3 2E_2}(2\pi)\delta\left(E_1+E_2-E_{tot}^{\alpha_e}\right) =& \frac{1}{128\pi^5}\int_{m_e}^{E_{tot}^{\alpha_e}-m_e} dE_1 \int d\Omega_1 d\Omega_2 \left|\boldsymbol{p}_1\right|\left|\boldsymbol{p}_2\right| \\ =& \frac{1}{16\pi^3}\int_{m_e}^{E_{tot}^{\alpha_e}-m_e} dE_1 \int_{-1}^{1} d\cos\theta_{12} \left|\boldsymbol{p}_1\right|\left|\boldsymbol{p}_2\right|, \end{aligned} \tag{4.23}$$

where the second line is valid because the transition probability depends only relative angle between two electrons after summing over all spin of leptons. We have removed the delta function which represents energy conservation by integral on E_2, and hereafter $E_2 = E_{tot}^{\alpha_e} - E_1$ holds implicitly. Therefore that differential decay rate can be calculated by

$$\frac{d\Gamma}{dE_1 d\cos\theta_{12}} = \sum_{\alpha_e} \frac{1}{32\pi^3}\left|\boldsymbol{p}_1\right|\left|\boldsymbol{p}_2\right| \sum_{s_1,s_2}\sum_{s_\mu}\sum_{s_e} \left|\mathcal{M}\right|^2. \tag{4.24}$$

The total decay rate is obtained by integrating the partial decay rate as

$$\Gamma = \frac{1}{2}\int_{m_e}^{E_{tot}^{\alpha_e}-m_e} dE_1 \int_{-1}^{1} d\cos\theta_{12} \frac{d\Gamma}{dE_1 d\cos\theta_{12}}. \tag{4.25}$$

4.3 Plane Wave Approximation

It is useful to derive the transition rate ignoring the Coulomb potential for emitted electrons. The obtained formula can be used to test our complicated multipole expansion formula and also to understand the mechanism of the $\mu^- e^- \to e^- e^-$. Under the plane wave approximation, we can proceed with the calculation of the transition matrix element in momentum space. We use the relativistic plane wave,

$$\psi_e^{\boldsymbol{p}_i, s_i}(\boldsymbol{r}) = u_e^{s_i}(\boldsymbol{p}_i)\exp(i\boldsymbol{p}_i\cdot\boldsymbol{r}), \tag{4.26}$$

as scattering electrons in the final state. The normalization of $u_e^{s_i}(\boldsymbol{p}_i)$ is given in Appendix A. To simplify the formula further, the bound leptons are treated as nonrelativistic and we consider only bound electrons in $1S_{1/2}$ state. As wave functions of initial bound leptons, we use the solution of the Schrödinger equation with Coulomb potential of a point charge Z,

$$\psi_\mu^{1S,s_\mu}(\boldsymbol{r}) = \sqrt{\frac{\left(m_\mu Z\alpha_{em}\right)^3}{\pi}}\exp\left(-m_\mu Z\alpha_{em}\left|\boldsymbol{r}\right|\right)\begin{pmatrix}\chi_{1/2}^{s_\mu}\\ 0\end{pmatrix}, \tag{4.27}$$

$$\psi_e^{1S,s_e}(\boldsymbol{r}) = \sqrt{\frac{\left(m_e (Z-1)\alpha_{em}\right)^3}{\pi}}\exp\left(-m_e (Z-1)\alpha_{em}\left|\boldsymbol{r}\right|\right)\begin{pmatrix}\chi_{1/2}^{s_e}\\ 0\end{pmatrix}, \tag{4.28}$$

where $\chi_{1/2}^s$ is a 2-component spinor and normalized as

$$\sum_s \chi_{1/2}^s \chi_{1/2}^{s\dagger} = \mathbf{1}_2. \tag{4.29}$$

The corresponding binding energies are given as

$$B_\mu = \frac{1}{2} m_\mu (Z\alpha_{em})^2, \tag{4.30}$$

$$B_e = \frac{1}{2} m_e \left\{(Z-1)\alpha_{em}\right\}^2, \tag{4.31}$$

respectively.

4.3.1 Contact Process

Under the plane wave approximation of scattering electrons and nonrelativistic approximation of bound muon and electron,the transition matrix element of contact interaction $\mathcal{M}_{\text{contact}}$ is given as

$$\mathcal{M}_{\text{contact}} = \frac{-4G_F}{\sqrt{2}} \mathcal{F}_{\mu e}\left(\boldsymbol{p}_1 + \boldsymbol{p}_2\right) \sum_{i=1}^{6} g_i \left[C_i\left(\boldsymbol{p}_1, s_1; \boldsymbol{p}_2, s_2\right) - C_i\left(\boldsymbol{p}_2, s_2; \boldsymbol{p}_1, s_1\right)\right]. \tag{4.32}$$

The second term is the exchange of final electrons. $\mathcal{F}_{\mu e}\left(\boldsymbol{p}\right)$ is the Fourier transformation of the products of initial wave functions in coordinate space,

$$\begin{aligned}
\mathcal{F}_{\mu e}\left(\boldsymbol{p}\right) =& \int d^3 r \exp(-i\boldsymbol{p}\cdot\boldsymbol{r}) \\
& \times \sqrt{\frac{\left(m_\mu Z\alpha_{em}\right)^3}{\pi}} \exp\left(-m_\mu Z\alpha_{em}\left|\boldsymbol{r}\right|\right) \sqrt{\frac{\left(m_e(Z-1)\alpha_{em}\right)^3}{\pi}} \exp\left(-m_e(Z-1)\alpha_{em}\left|\boldsymbol{r}\right|\right) \\
=& \frac{8(m_\mu Z\alpha_{em} + m_e(Z-1)\alpha_{em})\sqrt{(m_\mu Z\alpha_{em})^3 (m_e(Z-1)\alpha_{em})^3}}{\left\{|\boldsymbol{p}|^2 + (m_\mu Z\alpha_{em} + m_e(Z-1)\alpha_{em})^2\right\}^2},
\end{aligned} \tag{4.33}$$

and C_is $(i = 1, 2, \cdots, 6)$ are defined as

$$\begin{aligned}
C_1\left(\boldsymbol{p}_1, s_1; \boldsymbol{p}_2, s_2\right) =& \overline{u}_e^{s_1}(\mathbf{p}_1) P_R \begin{pmatrix} \chi_{1/2}^{s_\mu} \\ 0 \end{pmatrix} \overline{u}_e^{s_2}(\mathbf{p}_2) P_R \begin{pmatrix} \chi_{1/2}^{s_e} \\ 0 \end{pmatrix}, \\
C_2\left(\boldsymbol{p}_1, s_1; \boldsymbol{p}_2, s_2\right) =& \overline{u}_e^{s_1}(\mathbf{p}_1) P_L \begin{pmatrix} \chi_{1/2}^{s_\mu} \\ 0 \end{pmatrix} \overline{u}_e^{s_2}(\mathbf{p}_2) P_L \begin{pmatrix} \chi_{1/2}^{s_e} \\ 0 \end{pmatrix}, \\
C_3\left(\boldsymbol{p}_1, s_1; \boldsymbol{p}_2, s_2\right) =& \overline{u}_e^{s_1}(\mathbf{p}_1) \gamma^\mu P_R \begin{pmatrix} \chi_{1/2}^{s_\mu} \\ 0 \end{pmatrix} \overline{u}_e^{s_2}(\mathbf{p}_2) \gamma_\mu P_R \begin{pmatrix} \chi_{1/2}^{s_e} \\ 0 \end{pmatrix}, \\
C_4\left(\boldsymbol{p}_1, s_1; \boldsymbol{p}_2, s_2\right) =& \overline{u}_e^{s_1}(\mathbf{p}_1) \gamma^\mu P_L \begin{pmatrix} \chi_{1/2}^{s_\mu} \\ 0 \end{pmatrix} \overline{u}_e^{s_2}(\mathbf{p}_2) \gamma_\mu P_L \begin{pmatrix} \chi_{1/2}^{s_e} \\ 0 \end{pmatrix}, \\
C_5\left(\boldsymbol{p}_1, s_1; \boldsymbol{p}_2, s_2\right) =& \overline{u}_e^{s_1}(\mathbf{p}_1) \gamma^\mu P_R \begin{pmatrix} \chi_{1/2}^{s_\mu} \\ 0 \end{pmatrix} \overline{u}_e^{s_2}(\mathbf{p}_2) \gamma_\mu P_L \begin{pmatrix} \chi_{1/2}^{s_e} \\ 0 \end{pmatrix}, \\
C_6\left(\boldsymbol{p}_1, s_1; \boldsymbol{p}_2, s_2\right) =& \overline{u}_e^{s_1}(\mathbf{p}_1) \gamma^\mu P_L \begin{pmatrix} \chi_{1/2}^{s_\mu} \\ 0 \end{pmatrix} \overline{u}_e^{s_2}(\mathbf{p}_2) \gamma_\mu P_R \begin{pmatrix} \chi_{1/2}^{s_e} \\ 0 \end{pmatrix}.
\end{aligned} \tag{4.34}$$

Since there are two identical fermions in the final state, Eq. (4.32) is antisymmetric under the exchange of their momenta and spins.

Now let $\mathcal{M}_{\text{contact}}$, Eq. (4.32), be squared and summed over the spin. It can be written as

$$\sum_{s_1, s_2} \sum_{s_\mu, s_e} \left|\mathcal{M}_{\text{contact}}\right|^2 = 8G_F^2 \left|\mathcal{F}_{\mu e}\left(\boldsymbol{p}_1 + \boldsymbol{p}_2\right)\right|^2 \sum_{i,j=1}^{6} g_i^* g_j \left[D_{ij} - E_{ij}\right], \tag{4.35}$$

where

$$D_{ij} = \sum_{s_1,s_2} \sum_{s_\mu,s_e} \left[C_i^*(\boldsymbol{p}_1, s_1; \boldsymbol{p}_2, s_2) C_j(\boldsymbol{p}_1, s_1; \boldsymbol{p}_2, s_2) + (\{\boldsymbol{p}_1, s_1\} \leftrightarrow \{\boldsymbol{p}_2, s_2\}) \right], \tag{4.36}$$

$$E_{ij} = \sum_{s_1,s_2} \sum_{s_\mu,s_e} \left[C_i^*(\boldsymbol{p}_2, s_2; \boldsymbol{p}_1, s_1) C_j(\boldsymbol{p}_1, s_1; \boldsymbol{p}_2, s_2) + (\{\boldsymbol{p}_1, s_1\} \leftrightarrow \{\boldsymbol{p}_2, s_2\}) \right]. \tag{4.37}$$

After the simple calculation for D_{ij}s and E_{ij}s, the results shown in Table 4.1 and 4.2 are obtained, respectively. Summarizing these results, we obtain

$$\sum_{s_1,s_2} \sum_{s_\mu,s_e} \left| \mathcal{M}_{\text{contact}} \right|^2 = 8G_F^2 \left| \mathcal{F}_{\mu e} \left(\boldsymbol{p}_1 + \boldsymbol{p}_2 \right) \right|^2 \left(p_1 \cdot p_2 f_1 + 8 p_1^0 p_2^0 f_2 - 2 m_e E_{tot} f_3 + 2 m_e^2 f_4 \right), \tag{4.38}$$

where the coefficients, f_is $(i = 1, 2, 3, 4)$, are defined as

$$f_1 = G_{12} + 16 G_{34} + 8 G'_{14} + 8 G'_{23} - 8 G'_{56}, \tag{4.39}$$

$$f_2 = G_{56}, \tag{4.40}$$

$$f_3 = G'_{15} + G'_{16} + G'_{25} + G'_{26} + 4 G'_{35} + 4 G'_{36} + 4 G'_{45} + 4 G'_{46}, \tag{4.41}$$

$$f_4 = G'_{12} + 4 G'_{13} + 4 G'_{24} + 16 G'_{34} + 8 G'_{56} - 2 G_{56}, \tag{4.42}$$

with $G_{ij} = \left| g_i \right|^2 + \left| g_j \right|^2$ and $G'_{ij} = \mathrm{Re}\left[g_i^* g_j \right]$.

Table 4.1: D_{ij}. Here $E_{tot} = p_1^0 + p_2^0$ does not depend on $|\boldsymbol{p}_1|$ due to the energy conservation.

$i \backslash j$	1	2	3	4	5	6
1	$2p_1^0 p_2^0$	$2m_e^2$	$2m_e^2$	$2p_1 \cdot p_2$	$m_e E_{tot}$	$m_e E_{tot}$
2	$2m_e^2$	$2p_1^0 p_2^0$	$2p_1 \cdot p_2$	$2m_e^2$	$m_e E_{tot}$	$m_e E_{tot}$
3	$2m_e^2$	$2p_1 \cdot p_2$	$8p_1 \cdot p_2$	$8m_e^2$	$-2m_e E_{tot}$	$-2m_e E_{tot}$
4	$2p_1 \cdot p_2$	$2m_e^2$	$8m_e^2$	$8p_1 \cdot p_2$	$-2m_e E_{tot}$	$-2m_e E_{tot}$
5	$m_e E_{tot}$	$m_e E_{tot}$	$-2m_e E_{tot}$	$-2m_e E_{tot}$	$8p_1^0 p_2^0$	$8m_e^2$
6	$m_e E_{tot}$	$m_e E_{tot}$	$-2m_e E_{tot}$	$-2m_e E_{tot}$	$8m_e^2$	$8p_1^0 p_2^0$

Table 4.2: E_{ij}.

$i \backslash j$	1	2	3	4	5	6
1	$2p_1^0 p_2^0 - p_1 \cdot p_2$	m_e^2	$-2m_e^2$	$-2p_1 \cdot p_2$	$2m_e E_{tot}$	$2m_e E_{tot}$
2	m_e^2	$2p_1^0 p_2^0 - p_1 \cdot p_2$	$-2p_1 \cdot p_2$	$-2m_e^2$	$2m_e E_{tot}$	$2m_e E_{tot}$
3	$-2m_e^2$	$-2p_1 \cdot p_2$	$-8p_1 \cdot p_2$	$-8m_e^2$	$2m_e E_{tot}$	$2m_e E_{tot}$
4	$-2p_1 \cdot p_2$	$-2m_e^2$	$-8m_e^2$	$-8p_1 \cdot p_2$	$2m_e E_{tot}$	$2m_e E_{tot}$
5	$2m_e E_{tot}$	$2m_e E_{tot}$	$2m_e E_{tot}$	$2m_e E_{tot}$	$4m_e^2$	$4p_1 \cdot p_2$
6	$2m_e E_{tot}$	$2m_e E_{tot}$	$2m_e E_{tot}$	$2m_e E_{tot}$	$4p_1 \cdot p_2$	$4m_e^2$

Thus, the differential decay rate Eq. (4.24) is

$$\frac{d\Gamma}{dE_1 d\cos\theta_{12}} = \frac{G_F^2}{4\pi^3} \left| \boldsymbol{p}_1 \right| \left| \boldsymbol{p}_2 \right| \left| \mathcal{F}_{\mu e} \left(\boldsymbol{p}_1 + \boldsymbol{p}_2 \right) \right|^2 \left(p_1 \cdot p_2 f_1 + 8 p_1^0 p_2^0 f_2 - 2 m_e E_{tot} f_3 + 2 m_e^2 f_4 \right). \tag{4.43}$$

By factoring out $\Gamma^0_{\text{contact}}$, which was the result by Koike *et al.*, Eq. (4.12), we get

$$\begin{aligned} &\frac{1}{\Gamma^0_{\text{contact}}} \frac{d\Gamma}{dE_1 d\cos\theta_{12}} \\ =&\frac{1}{G} \frac{128 \left(m_\mu Z \alpha_{em} \right)^3 \left(m_\mu Z \alpha_{em} + m_e (Z-1) \alpha_{em} \right)^2 \left| \boldsymbol{p}_1 \right| \left| \boldsymbol{p}_2 \right|}{\pi m_\mu^2 \left\{ |\boldsymbol{p}_1 + \boldsymbol{p}_2|^2 + (m_\mu Z \alpha_{em} + m_e (Z-1) \alpha_{em})^2 \right\}^4} \left(p_1 \cdot p_2 f_1 + 8 p_1^0 p_2^0 f_2 - 2 m_e E_{tot} f_3 + 2 m_e^2 f_4 \right). \end{aligned} \tag{4.44}$$

Now let us study the difference between this calculation and the calculation by Koike *et al.* The ratio $\Gamma/\Gamma^0_{\rm contact}$ is given as

$$\frac{\Gamma}{\Gamma^0_{\rm contact}} = \frac{1}{2}\int_{m_e}^{E_{tot}^{\alpha_e}-m_e} dE_1 \int_{-1}^{1} d\cos\theta_{12} \frac{1}{\Gamma^0_{\rm contact}} \frac{d\Gamma}{dE_1 d\cos\theta_{12}}. \tag{4.45}$$

In the previous calculation, overlap integral of final electrons and bound leptons are not taken into account assuming the typical wave length of emitted electrons is short enough compared with the size of bound state. The factor (4.45) indicates the effect of finite size of lepton wave functions for the total decay rate. We expect that Eq. (4.45) tends to be unity in limit of $Z\alpha_{em} \to 0$. When we ignore the electron mass m_e, the integral of Eq. (4.45) can be performed analytically. After the integration, the result expanded of $Z\alpha_{em}$ is given as

$$\frac{\Gamma}{\Gamma^0_{\rm contact}} \simeq 1 - \frac{2}{3}\left(3f_1 + 8f_2\right)\left(Z\alpha_{em}\right)^2 + \mathcal{O}\left(\left(Z\alpha_{em}\right)^4\right). \tag{4.46}$$

This expression of $Z\alpha_{em}$ shows clearly that $\Gamma/\Gamma^0_{\rm contact} \to 1$ as $Z\alpha_{em} \to 0$.

4.3.2 Photonic Process

The transition matrix element for the photonic interaction $\mathcal{L}_{\rm photonic}$ is given as

$$\begin{aligned}\mathcal{M}_{\rm photonic} =& 2i\frac{4G_F}{\sqrt{2}} m_\mu q_e \int \frac{d^3q}{(2\pi)^3} \frac{q_\nu}{|\boldsymbol{q}|^2 - q_0^2 - i\epsilon} \mathcal{F}_\mu\left(\boldsymbol{p}_1 + \boldsymbol{q}\right) \mathcal{F}_e\left(\boldsymbol{p}_2 - \boldsymbol{q}\right) \\ & \times \overline{u}_e^{s_1}\left(\boldsymbol{p}_1\right) \sigma^{\mu\nu} \left(A_R P_R + A_L P_L\right) \begin{pmatrix} \chi_{1/2}^{s_\mu} \\ 0 \end{pmatrix} \overline{u}_e^{s_2}\left(\boldsymbol{p}_2\right) \gamma_\mu \begin{pmatrix} \chi_{1/2}^{s_e} \\ 0 \end{pmatrix} \\ & - \left(\{\boldsymbol{p}_1, s_1\} \leftrightarrow \{\boldsymbol{p}_2, s_2\}\right), \end{aligned} \tag{4.47}$$

where the Fourier components of bound waves are also given as

$$\begin{aligned}\mathcal{F}_\mu\left(\boldsymbol{p}\right) =& \int d^3r \exp(-i\boldsymbol{p}\cdot\boldsymbol{r}) \sqrt{\frac{\left(m_\mu Z\alpha_{em}\right)^3}{\pi}} \exp\left(-m_\mu Z\alpha_{em}\left|\boldsymbol{r}\right|\right) \\ =& \frac{8\sqrt{\pi} m_\mu Z\alpha_{em} \sqrt{(m_\mu Z\alpha_{em})^3 \pi}}{\left\{|\boldsymbol{p}|^2 + (m_\mu Z\alpha_{em})^2\right\}^2}, \end{aligned} \tag{4.48}$$

and

$$\begin{aligned}\mathcal{F}_e\left(\boldsymbol{p}\right) =& \int d^3r \exp(-i\boldsymbol{p}\cdot\boldsymbol{r}) \sqrt{\frac{\left(m_e(Z-1)\alpha_{em}\right)^3}{\pi}} \exp\left(-m_e(Z-1)\alpha_{em}\left|\boldsymbol{r}\right|\right) \\ =& \frac{8\sqrt{\pi} m_e(Z-1)\alpha_{em} \sqrt{(m_e(Z-1)\alpha_{em})^3 \pi}}{\left\{|\boldsymbol{p}|^2 + (m_e(Z-1)\alpha_{em})^2\right\}^2}. \end{aligned} \tag{4.49}$$

In the first part of Eq. (4.47), q_0 means $q_0 = m_\mu - B_\mu - E_1$, while in the second part, where $\boldsymbol{p}_1$ and $\boldsymbol{p}_2$ are exchanged, $q_0 = m_\mu - B_\mu - E_2$. For the formula of photonic process, one needs convolution of form factors of two photonic vertices and virtual photon propagator.

Summing over the spins of leptons, we obtain

$$\sum_{s_1,s_2}\sum_{s_\mu,s_e} \left|\mathcal{M}_{\rm photonic}\right|^2 = 128\pi^3 G_F^2 m_\mu^2 \alpha_{em} \left(m_\mu Z\alpha_{em}\right)^5 \left(m_e(Z-1)\alpha_{em}\right)^5 \mathcal{T}\left(E_1, \cos\theta\right), \tag{4.50}$$

where we defined

$$
\begin{aligned}
&\mathcal{T}\left(E_1,\cos\theta\right)\\
=&\sum_{s_1,s_2}\sum_{s_\mu,s_e}\left|I_\nu\left(\boldsymbol{p}_1,\boldsymbol{p}_2\right)\overline{u}_e^{s_1}\left(\boldsymbol{p}_1\right)\sigma^{\mu\nu}\left(A_RP_R+A_LP_L\right)\begin{pmatrix}\chi_{1/2}^{s_\mu}\\0\end{pmatrix}\overline{u}_e^{s_2}\left(\boldsymbol{p}_2\right)\gamma_\mu\begin{pmatrix}\chi_{1/2}^{s_e}\\0\end{pmatrix}-\left(\{\boldsymbol{p}_1,s_1\}\leftrightarrow\{\boldsymbol{p}_2,s_2\}\right)\right|^2\\
=&I_\nu\left(\boldsymbol{p}_1,\boldsymbol{p}_2\right)I_{\nu'}^*\left(\boldsymbol{p}_1,\boldsymbol{p}_2\right)\\
&\times\mathrm{Tr}\left[\left(\not{p}_1+m_e\right)\sigma^{\mu\nu}\left(A_RP_R+A_LP_L\right)\frac{1+\gamma_0}{2}\left(A_R^*P_L+A_L^*P_R\right)\sigma^{\mu'\nu'}\right]\mathrm{Tr}\left[\left(\not{p}_2+m_e\right)\gamma_\mu\frac{1+\gamma_0}{2}\gamma_{\mu'}\right]\\
&-I_\nu\left(\boldsymbol{p}_1,\boldsymbol{p}_2\right)I_{\nu'}^*\left(\boldsymbol{p}_2,\boldsymbol{p}_1\right)\\
&\times\mathrm{Tr}\left[\left(\not{p}_1+m_e\right)\sigma^{\mu\nu}\left(A_RP_R+A_LP_L\right)\frac{1+\gamma_0}{2}\left(A_R^*P_L+A_L^*P_R\right)\sigma^{\mu'\nu'}\left(\not{p}_2+m_e\right)\gamma_\mu\frac{1+\gamma_0}{2}\gamma_{\mu'}\right]+\left(\boldsymbol{p}_1\leftrightarrow\boldsymbol{p}_2\right),
\end{aligned}
\tag{4.51}
$$

by using

$$
I_\nu\left(\boldsymbol{p}_1,\boldsymbol{p}_2\right)=64\pi\int\frac{d^3q}{(2\pi)^3}\frac{q_\nu}{|\boldsymbol{q}|^2-q_0^2-i\epsilon}\frac{1}{\left\{|\boldsymbol{p}_1+\boldsymbol{q}|^2+(m_\mu Z\alpha_{em})^2\right\}^2}\frac{1}{\left\{|\boldsymbol{p}_2-\boldsymbol{q}|^2+(m_e(Z-1)\alpha_{em})^2\right\}^2}.
\tag{4.52}
$$

Now $\mathcal{T}\left(E_1,\cos\theta\right)$ can be calculated straightforwardly. However the analytic result is so complicated, so it is omitted in this thesis.

By using Eq. (4.24) as in contact case, we can write down

$$
\frac{d\Gamma}{dE_1d\cos\theta_{12}}=4G_F^2m_\mu^2\alpha_{em}\left(m_\mu Z\alpha_{em}\right)^5\left(m_e(Z-1)\alpha_{em}\right)^5\left|\boldsymbol{p}_1\right|\left|\boldsymbol{p}_2\right|\mathcal{T}\left(E_1,\cos\theta\right),
\tag{4.53}
$$

and

$$
\frac{1}{\Gamma^0_{\text{photonic}}}\frac{d\Gamma}{dE_1d\cos\theta_{12}}=\frac{1}{|A_L|^2+|A_L|^2}\frac{\pi m_e^2\left(m_e(Z-1)\alpha_{em}\right)^2\left(m_\mu Z\alpha_{em}\right)^5\left|\boldsymbol{p}_1\right|\left|\boldsymbol{p}_2\right|}{2m_\mu^2}\mathcal{T}\left(E_1,\cos\theta\right).
\tag{4.54}
$$

We can confirm numerically $\Gamma/\Gamma^0_{\text{photonic}}\to1$ in $Z\alpha_{em}\to0$ limit, as the contact interaction.

4.4 Partial Wave Expansion

To take into account the distortion of Coulomb interaction for the final electrons, the first step is the partial wave expansion of the scattering wave function. In order to take into account the nuclear Coulomb potential, the momentum is no longer a good quantum number. However assuming the nuclear potential is spherical and the system has rotational symmetry, it is convenient to use the partial wave expansion.

The electron scattering state with the incoming boundary condition is expressed as

$$
\psi_e^{\boldsymbol{p},s(-)}\left(\boldsymbol{r}\right)=\sum_{\kappa,\nu,m}4\pi i^{l_\kappa}(l_\kappa,m,1/2,s|j_\kappa,\nu)Y_{l_\kappa}^{m*}(\hat{p})e^{-i\delta_\kappa}\psi_p^{\kappa,\nu}(\boldsymbol{r}),
\tag{4.55}
$$

where δ_κ is a phase shift for partial wave κ. Here the orbital angular momentum l_κ and the total angular momentum j_κ are related to κ by

$$
l_\kappa=\begin{cases}-\kappa-1 & (\kappa<0)\\ \kappa & (\kappa>0)\end{cases},
\tag{4.56}
$$

$$
j_\kappa=|\kappa|-\frac{1}{2},
\tag{4.57}
$$

which is derived from the definition of κ, Eq. (E.17). For example, $\kappa = -1$ means that $l_\kappa = 0$ and $j_\kappa = 1/2$. The wave function $\psi_p^{\kappa,\nu}(\boldsymbol{r})$, where the subscripts p and ν mean magnitude of a momentum and a spin of the partial wave, respectively, is represented with the radial part $g_p^\kappa(r)$, $f_p^\kappa(r)$ and angular-spin part χ_κ,

$$\psi_p^{\kappa,\nu}(\boldsymbol{r}) = \begin{pmatrix} g_p^\kappa(r)\chi_\kappa^\nu(\hat{r}) \\ if_p^\kappa(r)\chi_{-\kappa}^\nu(\hat{r}) \end{pmatrix}. \tag{4.58}$$

Similarly, the bound state of the lepton ℓ is also represented as

$$\psi_\ell^{\alpha_\ell,s_\ell}(\boldsymbol{r}) = \begin{pmatrix} g_{\ell,n_\ell}^{\kappa_\ell}(r)\chi_{\kappa_\ell}^{s_\ell}(\hat{r}) \\ if_{\ell,n_\ell}^{\kappa_\ell}(r)\chi_{-\kappa_\ell}^{s_\ell}(\hat{r}) \end{pmatrix}. \tag{4.59}$$

In order to clarify the structure of a result, in this analysis, the quantum number of the initial bound muon is kept as α_μ (n_μ and κ_μ), which should be $1S_{1/2}$ ($n_\mu = 1$ and $\kappa_\mu = -1$).

Inserting Eq. (4.55) into Eq. (4.18) or (4.21), we obtain

$$\begin{aligned}\mathcal{M} = &\sum_{\kappa_1,\nu_1,m_1} \sum_{\kappa_2,\nu_2,m_2} (4\pi)^2(-i)^{l_{\kappa_1}+l_{\kappa_2}} e^{i\left(\delta_{\kappa_1}+\delta_{\kappa_2}\right)} Y_{l_{\kappa_1}}^{m_1}(\hat{p}_1) Y_{l_{\kappa_2}}^{m_2}(\hat{p}_2) \\ &\times (l_{\kappa_1}, m_1, 1/2, s_1 | j_{\kappa_1}, \nu_1)(l_{\kappa_2}, m_2, 1/2, s_2 | j_{\kappa_2}, \nu_2)\tilde{\mathcal{M}}.\end{aligned} \tag{4.60}$$

Here $\tilde{\mathcal{M}}$ is an expression obtained by replacing $\psi_e^{\boldsymbol{p}_i,s_i}$ with $\psi_p^{\kappa,\nu}$ in the expression of $\mathcal{M}$, i.e.

$$\begin{aligned}\tilde{\mathcal{M}}_{\text{contact}} = &-\frac{4G_F}{\sqrt{2}} \sum_{i=1}^{6} g_i \left[\int d^3r \overline{\psi}_{p_1}^{\kappa_1,\nu_1}(\boldsymbol{r}) O_i^A \psi_\mu^{1S_{1/2},s_\mu}(\boldsymbol{r}) \right. \\ &\left. \times \overline{\psi}_{p_2}^{\kappa_2,\nu_2}(\boldsymbol{r}) O_i^B \psi_e^{\alpha_e,s_e}(\boldsymbol{r}) - (\{\beta_1,\nu_1\} \leftrightarrow \{\beta_2,\nu_2\}) \right],\end{aligned} \tag{4.61}$$

and

$$\begin{aligned}\tilde{\mathcal{M}}_{\text{photonic}} = &\left(-\frac{4G_F}{\sqrt{2}} m_\mu\right)(-q_e) \left[\int d^3r_1 d^3r_2 \overline{\psi}_{p_1}^{\kappa_1,\nu_1}(\boldsymbol{r}_1) \sigma^{\mu\nu} \left(A_R P_R + A_L P_L\right) \psi_\mu^{1S_{1/2},s_\mu}(\boldsymbol{r}_1) \right. \\ &\left. \times 2G_\nu\left(\boldsymbol{r}_1, \boldsymbol{r}_2; m_\mu - B_\mu - E_1\right) \overline{\psi}_{p_2}^{\kappa_2,\nu_2}(\boldsymbol{r}_2) \gamma_\mu \psi_e^{\alpha_e,s_e}(\boldsymbol{r}_2) - (\{\beta_1,\nu_1\} \leftrightarrow \{\beta_2,\nu_2\}) \right].\end{aligned} \tag{4.62}$$

Here p_i and κ_i are collectively written as β_i.

As shown in later derivation, $\tilde{\mathcal{M}}$s have the form of

$$\begin{aligned}\tilde{\mathcal{M}}_{\text{contact/photonic}} = &-\frac{4G_F}{\sqrt{2}} \frac{1}{4\pi} \sum_{J,M} (j_{\kappa_1}, \nu_1, j_{\kappa_2}, \nu_2 | J, M)(j_{\kappa_\mu}, s_\mu, j_{\kappa_e}, s_e | J, M) \\ &\times \sqrt{\left[j_{\kappa_1} \cdot j_{\kappa_\mu} \cdot j_{\kappa_2} \cdot j_{\kappa_e}\right]} \mathcal{N}_{\text{contact/photonic}}^{\beta_1,\beta_2}(J).\end{aligned} \tag{4.63}$$

Then the transition matrix (4.60) can be written as

$$\begin{aligned}\mathcal{M} = &\sum_{\kappa_1,\nu_1,m_1} \sum_{\kappa_2,\nu_2,m_2} (4\pi)^2 Y_{l_{\kappa_1}}^{m_1}(\hat{p}_1) Y_{l_{\kappa_2}}^{m_2}(\hat{p}_2) \\ &\times (l_{\kappa_1}, m_1, 1/2, s_1 | j_{\kappa_1}, \nu_1)(l_{\kappa_2}, m_2, 1/2, s_2 | j_{\kappa_2}, \nu_2) \sqrt{\left[j_{\kappa_1} \cdot j_{\kappa_\mu} \cdot j_{\kappa_2} \cdot j_{\kappa_e}\right]} \\ &\times \left(-\frac{4G_F}{\sqrt{2}}\right) \frac{1}{4\pi} \sum_{J,M} (j_{\kappa_1}, \nu_1, j_{\kappa_2}, \nu_2 | J, M)(j_{\kappa_\mu}, s_\mu, j_{\kappa_e}, s_e | J, M) N^{\beta_1,\beta_2}(J),\end{aligned} \tag{4.64}$$

where we define

$$N^{\beta_1,\beta_2}(J) = (-i)^{l_{\kappa_1}+l_{\kappa_2}} e^{i\left(\delta_{\kappa_1}+\delta_{\kappa_2}\right)} \left[\mathcal{N}_{\text{contact}}^{\beta_1,\beta_2}(J) + \mathcal{N}_{\text{photonic}}^{\beta_1,\beta_2}(J)\right]. \tag{4.65}$$

By Eq. (4.24), we can calculate the differential decay rate

$$\begin{aligned}\frac{d\Gamma}{dE_1 d\cos\theta_{12}} =& \sum_{\alpha_e} \frac{G_F^2}{4\pi^3} |\boldsymbol{p}_1| |\boldsymbol{p}_2| \sum_{\kappa_1,\kappa_2} \sum_{\kappa_1',\kappa_2'} \sum_{J,l} \left[J \cdot j_{\kappa_1} \cdot j_{\kappa_2} \cdot j_{\kappa_1'} \cdot j_{\kappa_2'} \cdot j_{\kappa_\mu} \cdot j_{\kappa_e}\right] \\ & \times N^{\beta_1',\beta_2'*}(J) N^{\beta_1,\beta_2}(J) P_l(\cos\theta_{12}) \\ & \times (-1)^{J-j_{\kappa_2}-j_{\kappa_2'}} \frac{1+(-1)^{l_{\kappa_1}+l_{\kappa_1'}+l}}{2} \frac{1+(-1)^{l_{\kappa_2}+l_{\kappa_2'}+l}}{2} \\ & \times (j_{\kappa_1}, 1/2, j_{\kappa_1'}, -1/2|l,0)(j_{\kappa_2}, 1/2, j_{\kappa_2'}, -1/2|l,0) W(j_{\kappa_1}, j_{\kappa_2}, j_{\kappa_1'}, j_{\kappa_2'}; J, l). \end{aligned} \tag{4.66}$$

The derivation of this formula is given by Appendix I.1. Furthermore the θ_{12} integral can be performed analytically to get

$$\frac{d\Gamma}{dE_1} = \sum_{\alpha_e} \frac{G_F^2}{2\pi^3} \left[j_{\kappa_\mu} \cdot j_{\kappa_e}\right] |\boldsymbol{p}_1| |\boldsymbol{p}_2| \sum_{\kappa_1,\kappa_2,J} \left[J \cdot j_{\kappa_1} \cdot j_{\kappa_2}\right] \left|N^{\beta_1,\beta_2}(J)\right|^2. \tag{4.67}$$

4.4.1 Contact Process

$\mathcal{N}_{\text{contact}}$ is given as

$$\mathcal{N}_{\text{contact}}^{\beta_1,\beta_2}(J) = \sum_{i=1}^{6} g_i M_i^{\beta_1,\beta_2}(J). \tag{4.68}$$

Here M_is are amplitude corresponding to g_i-type interaction, and given as

$$M_1^{\beta_1,\beta_2}(J) = \frac{1}{2}\left[X_0^-(J,0,J) - X_1^+(J,0,J) + i\left\{Y_1^+(J,0,J) + Y_0^+(J,0,J)\right\}\right], \tag{4.69}$$

$$M_2^{\beta_1,\beta_2}(J) = \frac{1}{2}\left[X_0^-(J,0,J) - X_1^+(J,0,J) - i\left\{Y_1^+(J,0,J) + Y_0^+(J,0,J)\right\}\right], \tag{4.70}$$

$$M_3^{\beta_1,\beta_2}(J) = 2\left[X_0^-(J,0,J) + X_1^+(J,0,J) + i\left\{Y_1^+(J,0,J) - Y_0^+(J,0,J)\right\}\right], \tag{4.71}$$

$$M_4^{\beta_1,\beta_2}(J) = 2\left[X_0^-(J,0,J) + X_1^+(J,0,J) - i\left\{Y_1^+(J,0,J) - Y_0^+(J,0,J)\right\}\right], \tag{4.72}$$

$$M_5^{\beta_1,\beta_2}(J) = \left[3\sum_{L=|J-1|}^{J+1} X_1^-(L,1,J) - X_0^+(J,0,J) + i\left\{3\sum_{L=|J-1|}^{J+1} Y_0^-(L,1,J) + Y_1^-(J,0,J)\right\}\right], \tag{4.73}$$

$$M_6^{\beta_1,\beta_2}(J) = \left[3\sum_{L=|J-1|}^{J+1} X_1^-(L,1,J) - X_0^+(J,0,J) - i\left\{3\sum_{L=|J-1|}^{J+1} Y_0^-(L,1,J) + Y_1^-(J,0,J)\right\}\right], \tag{4.74}$$

where

$$X_0^\pm(L,S,J) = \mathcal{X}_{L,S,J}^{\beta_1,\beta_2}(g,g,g,g) + \mathcal{X}_{L,S,J}^{\beta_1,\beta_2}(f,f,f,f) \pm \left[\mathcal{X}_{L,S,J}^{\beta_1,\beta_2}(g,f,g,f) + \mathcal{X}_{L,S,J}^{\beta_1,\beta_2}(f,g,f,g)\right], \tag{4.75}$$

$$X_1^\pm(L,S,J) = \mathcal{X}_{L,S,J}^{\beta_1,\beta_2}(g,g,f,f) + \mathcal{X}_{L,S,J}^{\beta_1,\beta_2}(f,f,g,g) \pm \left[\mathcal{X}_{L,S,J}^{\beta_1,\beta_2}(g,f,f,g) + \mathcal{X}_{L,S,J}^{\beta_1,\beta_2}(f,g,g,f)\right], \tag{4.76}$$

$$Y_1^\pm(L,S,J) = \mathcal{X}_{L,S,J}^{\beta_1,\beta_2}(g,g,g,f) - \mathcal{X}_{L,S,J}^{\beta_1,\beta_2}(f,f,f,g) \pm \left[\mathcal{X}_{L,S,J}^{\beta_1,\beta_2}(g,f,g,g) - \mathcal{X}_{L,S,J}^{\beta_1,\beta_2}(f,g,f,f)\right], \tag{4.77}$$

$$Y_0^\pm(L,S,J) = \mathcal{X}_{L,S,J}^{\beta_1,\beta_2}(g,g,f,g) - \mathcal{X}_{L,S,J}^{\beta_1,\beta_2}(f,f,g,f) \pm \left[\mathcal{X}_{L,S,J}^{\beta_1,\beta_2}(f,g,g,g) - \mathcal{X}_{L,S,J}^{\beta_1,\beta_2}(g,f,f,f)\right]. \tag{4.78}$$

Here $\mathcal{X}$ contains the radial integral of overlap among lepton wave functions and some geometric factors:

$$\begin{aligned}\mathcal{X}^{\beta_1,\beta_2}_{L,S,J}(a,b,c,d) =& \int_0^\infty dr r^2 a^{\kappa_1}_{p_1}(r) b^{\kappa_\mu}_{\mu,n_\mu}(r) c^{\kappa_2}_{p_2}(r) d^{\kappa_e}_{e,n_e}(r) \\ & \times \sqrt{[l^a_{\kappa_1}\cdot l^b_{\kappa_\mu}\cdot l^c_{\kappa_2}\cdot l^d_{\kappa_e}]}(l^a_{\kappa_1},0,l^c_{\kappa_2},0|L,0)(l^b_{\kappa_\mu},0,l^d_{\kappa_e},0|L,0) \\ & \times \begin{Bmatrix} l^a_{\kappa_1} & 1/2 & j_{\kappa_1} \\ l^c_{\kappa_2} & 1/2 & j_{\kappa_2} \\ L & S & J \end{Bmatrix} \begin{Bmatrix} l^b_{\kappa_\mu} & 1/2 & j_{\kappa_\mu} \\ l^d_{\kappa_e} & 1/2 & j_{\kappa_e} \\ L & S & J \end{Bmatrix}. \end{aligned} \tag{4.79}$$

The derivation is given by Appendix I.2.

4.4.2 Photonic Process

For photonic process, the effective CLFV interaction is finite range, it is convenient to use the multipole expansion for not only scattering electrons but also a virtual photon. At first, let us expand Eq. (4.22) with partial waves. Using a derivative operator defined as

$$\partial_\nu = \left(iq_0, \frac{\partial}{\partial r^1_1}, \frac{\partial}{\partial r^2_1}, \frac{\partial}{\partial r^3_1} \right), \tag{4.80}$$

the photon propagator (4.22) can be written as

$$G_\nu(\boldsymbol{r}_1,\boldsymbol{r}_2;q_0) = \partial_\nu \int \frac{d^3q}{(2\pi)^3} \frac{\exp\{-i\boldsymbol{q}\cdot(\boldsymbol{r}_1-\boldsymbol{r}_2)\}}{|\boldsymbol{q}|^2 - q_0^2 - i\epsilon}. \tag{4.81}$$

Using the multipole expansion of a plane wave,

$$\exp(i\boldsymbol{q}\cdot\boldsymbol{r}) = 4\pi \sum_{l,m} i^l j_l(qr) Y^{m*}_l(\hat{q}) Y^m_l(\hat{r}), \tag{4.82}$$

it is found that

$$\begin{aligned} G_\nu(\boldsymbol{r}_1,\boldsymbol{r}_2;q_0) =& \partial_\nu \frac{(4\pi)^2}{(2\pi)^3} \sum_{l,m}\sum_{l',m'} i^{l'-l} Y^{m*}_l(\hat{r}_1) Y^{m'}_{l'}(\hat{r}_2) \\ & \times \int_0^\infty dq q^2 \frac{j_l(qr_1) j_{l'}(qr_2)}{q^2-q_0^2-i\epsilon} \int d\Omega_q Y^m_l(\hat{q}) Y^{m'*}_{l'}(\hat{q}) \\ =& \partial_\nu \frac{2}{\pi} \sum_{l,m} Y^{m*}_l(\hat{r}_1) Y^m_l(\hat{r}_2) \int_0^\infty dq \frac{q^2 j_l(qr_1) j_l(qr_2)}{q^2-q_0^2-i\epsilon}. \end{aligned} \tag{4.83}$$

Now noting Eqs. (B.2)-(B.8), when $r_1 > r_2$,

$$\begin{aligned} \int_0^\infty dq \frac{q^2 j_l(qr_1) j_l(qr_2)}{q^2-q_0^2-i\epsilon} =& \frac{1}{4}\int_{-\infty}^\infty dq \left\{ \frac{q^2 h^{(1)}_l(qr_1) j_l(qr_2)}{q^2-q_0^2-i\epsilon} + \frac{q^2 h^{(2)}_l(qr_1) j_l(qr_2)}{q^2-q_0^2-i\epsilon} \right\} \\ =& \frac{i\pi|q_0|}{4} \left\{ h^{(1)}_l(|q_0|r_1) j_l(|q_0|r_2) + h^{(2)}_l(-|q_0|r_1) j_l(-|q_0|r_2) \right\} \\ =& \frac{i\pi|q_0|}{2} h^{(1)}_l(|q_0|r_1) j_l(|q_0|r_2), \end{aligned} \tag{4.84}$$

where, in the last line, we use the formulae for the spherical Bessel and Hankel function, Eqs. (B.9) and (B.10). On the other hand, when $r_1 < r_2$,

$$\int_0^\infty dq \frac{q^2 j_l(qr_1) j_l(qr_2)}{q^2-q_0^2-i\epsilon} = \frac{i\pi|q_0|}{2} h^{(1)}_l(|q_0|r_2) j_l(|q_0|r_1), \tag{4.85}$$

where r_1 and r_2 are exchanged compared to Eq. (4.84). Thus you can see that $G_\nu(\boldsymbol{r}_1, \boldsymbol{r}_2; q_0)$ can be expanded as

$$G_\nu(\boldsymbol{r}_1, \boldsymbol{r}_2; q_0) = iq_0\partial_\nu \sum_{l,m} Y_l^{m*}(\hat{r}_1) Y_l^m(\hat{r}_2) F_{l,l}^{q_0}(r_1, r_2), \tag{4.86}$$

where we have defined

$$F_{l_1,l_2}^{q_0}(r_1, r_2) = h_{l_1}^{(1)}(q_0 r_1) j_{l_2}(q_0 r_2)\theta(r_1 - r_2) + h_{l_2}^{(1)}(q_0 r_2) j_{l_1}(q_0 r_1)\theta(r_2 - r_1), \tag{4.87}$$

unifying Eqs. (4.84) and (4.85).

The calculation given in Appendix I.3 yields an explicit expression of $\mathcal{N}_{\text{photonic}}$,

$$\mathcal{N}_{\text{photonic}}^{\beta_1,\beta_2}(J) = -2im_\mu q_e \sum_{c=\pm} A_c \sum_{l=0}^{\infty} \sum_{j=|l-1|}^{l+1} \sum_{n=1}^{3} X_n^c, \tag{4.88}$$

where

$$X_1^+(l, j, \kappa_1, \kappa_2, J) = (-1)^{l+j} \left\{ Z_{gfgf}^{l,l,1,j}(J) + Z_{fggf}^{l,l,1,j}(J) - Z_{gfff}^{l,l,1,j}(J) - Z_{fgfg}^{l,l,1,j}(J) \right\}, \tag{4.89}$$

$$X_2^+(l, j, \kappa_1, \kappa_2, J) = f_j^{(2)}(l - j) \left\{ Z_{gfgg}^{l,j,0,j}(J) + Z_{fggg}^{l,j,0,j}(J) + Z_{gfff}^{l,j,0,j}(J) + Z_{fgff}^{l,j,0,j}(J) \right\}, \tag{4.90}$$

$$\begin{aligned} X_3^+(l, j, \kappa_1, \kappa_2, J) = & f_j^{(3)}(l - j) \sum_{\{l_x,l_y\}=\{l,j\},\{j,l\}} \\ & \times \left\{ Z_{gggf}^{l_x,l_y,1,j}(J) - Z_{ffgf}^{l_x,l_y,1,j}(J) - Z_{ggfg}^{l_x,l_y,1,j}(J) + Z_{fffg}^{l_x,l_y,1,j}(J) \right\}, \end{aligned} \tag{4.91}$$

$$X_1^-(l, j, \kappa_1, \kappa_2, J) = -i(-1)^{l+j} \left\{ Z_{gggf}^{l,l,1,j}(J) - Z_{ffgf}^{l,l,1,j}(J) - Z_{ggfg}^{l,l,1,j}(J) + Z_{fffg}^{l,l,1,j}(J) \right\}, \tag{4.92}$$

$$X_2^-(l, j, \kappa_1, \kappa_2, J) = -if_j^{(2)}(l - j) \left\{ Z_{gggg}^{l,j,0,j}(J) - Z_{ffgg}^{l,j,0,j}(J) + Z_{ggff}^{l,j,0,j}(J) - Z_{ffff}^{l,j,0,j}(J) \right\}, \tag{4.93}$$

$$\begin{aligned} X_3^-(l, j, \kappa_1, \kappa_2, J) = & if_j^{(3)}(l - j) \sum_{\{l_x,l_y\}=\{l,j\},\{j,l\}} \\ & \times \left\{ Z_{gfgf}^{l_x,l_y,1,j}(J) + Z_{fggf}^{l_x,l_y,1,j}(J) - Z_{gfff}^{l_x,l_y,1,j}(J) - Z_{fgfg}^{l_x,l_y,1,j}(J) \right\}. \end{aligned} \tag{4.94}$$

Here Z is defined as

$$\begin{aligned} Z_{abcd}^{l_x,l_y,s,j}(J) = & q_0^2 \int_0^\infty dr_1 r_1^2 a_{p_1}^{\kappa_1}(r_1) b_\mu^{\kappa_\mu}(r_1) \int_0^\infty dr_2 r_2^2 F_{l_x,l_y}^{q_0}(r_1, r_2) c_{p_2}^{\kappa_2}(r_2) d_e^{\kappa_e}(r_2) \\ & \times (-1)^{\kappa_1+\kappa_\mu+J+l_x+l_y} \begin{Bmatrix} j_{\kappa_1} & j_{\kappa_2} & J \\ j_{\kappa_e} & j_{\kappa_\mu} & j \end{Bmatrix} \\ & \times \left(j_{\kappa_1}, 1/2, j_{\kappa_\mu}, -1/2|j, 0\right) \left(j_{\kappa_2}, 1/2, j_{\kappa_e}, -1/2|j, 0\right) V_{l_x,1,j}^{s_a\kappa_1,s_b\kappa_\mu} V_{l_y,s,j}^{s_c\kappa_2,s_d\kappa_e} \\ & \times \frac{1 + (-1)^{l_{\kappa_1}^a + l_{\kappa_\mu}^b + l_x}}{2} \frac{1 + (-1)^{l_{\kappa_2}^c + l_{\kappa_e}^d + l_y}}{2} - (-1)^{j_{\kappa_1}+j_{\kappa_2}-J} \left(\beta_1 \leftrightarrow \beta_2\right), \end{aligned} \tag{4.95}$$

which contains two-dimensional radial integral. Here

$$s_h = \begin{cases} +1 & (h = g) \\ -1 & (h = f) \end{cases}. \tag{4.96}$$

The integral must be carefully performed because the radial wave functions of emitted electrons and the spherical Bessel function oscillate quickly compared to Bohr radius of a bound electron.

Using the explicit form of $F^{q_0}_{l_x,l_y}(r_1,r_2)$, the radial integrals are written as

$$
\begin{aligned}
I^{l_x,l_y}_r(a,b,c,d) &= \int_0^\infty dr_1 r_1^2 a^{\kappa_1}_{p_1}(r_1) b^{\kappa_\mu}_{\mu}(r_1) \int_0^\infty dr_2 r_2^2 F^{q_0}_{l_x,l_y}(r_1,r_2) c^{\kappa_2}_{p_2}(r_2) d^{\kappa_e}_{e}(r_2) \\
&= \int_0^\infty dr_1 r_1^2 a^{\kappa_1}_{p_1}(r_1) b^{\kappa_\mu}_{\mu}(r_1) \Big\{ j_{l_x}(|m_\mu - B_\mu - p_1^0|r_1) \mathcal{J}^{l_y,p_1^0}_{c,\kappa_2,d,\kappa_e}(\infty) \\
&\quad + i \left[n_{l_x}(|m_\mu - B_\mu - p_1^0|r_1) \mathcal{J}^{l_y,p_1^0}_{C,\kappa_2,D,\kappa_e}(r_1) + j_{l_x}(|m_\mu - B_\mu - p_1^0|r_1) \mathcal{N}^{l_y,p_1^0}_{C,\kappa_2,D,\kappa_e}(r_1) \right] \Big\}, \quad (4.97)
\end{aligned}
$$

where

$$
\mathcal{J}^{l_y,p_1^0}_{c,\kappa_2,d,\kappa_e}(r_1) = \int_0^{r_1} dr_2 r_2^2 j_{l_y}(|m_\mu - B_\mu - p_1^0|r_2) c^{\kappa_2}_{p_2}(r_2) d^{\kappa_e}_{e}(r_2), \quad (4.98)
$$

$$
\mathcal{N}^{l_y,p_1^0}_{c,\kappa_2,d,\kappa_e}(r_1) = \int_{r_1}^\infty dr_2 r_2^2 n_{l_y}(|m_\mu - B_\mu - p_1^0|r_2) c^{\kappa_2}_{p_2}(r_2) d^{\kappa_e}_{e}(r_2). \quad (4.99)
$$

Here it can be interpreted that the first and second line of Eq. (4.97) correspond to contributions of on-shell and off-shell photon, respectively.

Chapter 5

Asymmetry of Electron Emission by Polarized Muon

In CLFV searches such as $\mu \to e\gamma$ and $\mu \to eee$, the muon polarization have been discussed in order to distinguish CLFV mechanisms [53, 50]. For μ^--e^- conversion, muon polarization has also been discussed to reduce DIO background [35]. The numerical data of DIO spectrum in case of muon polarization was given for some muonic atoms in Ref. [103]. In this chapter, we derive formula for the parity violating asymmetry of emitted electron from polarized muon. With this observable, one might further distinguish mechanisms of CLFV interactions.

5.1 Formalism

An expression of a differential decay rate in case that the initial muon is polarized can be written as

$$\begin{aligned}\frac{d\Gamma}{dE_1 d\Omega_1 d\Omega_2} =& \frac{1}{8\pi^2}\frac{d\Gamma_{unpol.}}{dE_1 d\cos\theta_{12}}\left[1 + F\left(E_1, \cos\theta_{12}\right)\boldsymbol{P}\cdot\hat{p}_1 + F\left(E_2, \cos\theta_{12}\right)\boldsymbol{P}\cdot\hat{p}_2\right. \\ &\left. + \tilde{F}\left(E_1, \cos\theta_{12}\right)\boldsymbol{P}\cdot\left(\hat{p}_1 \times \hat{p}_2\right)\right], \end{aligned} \tag{5.1}$$

where $\Gamma_{unpol.}$ is the result for using an unpolarized muon, which is gotten by the previous analysis. Since there are two identical particles in the final state, the differential decay rate is symmetric under the exchange of p_1 and p_2. Therefore, $\tilde{F}$ must satisfy

$$\tilde{F}\left(E_2, \cos\theta_{12}\right) = -\tilde{F}\left(E_1, \cos\theta_{12}\right). \tag{5.2}$$

After integrating out the angles of the second electron and the angle around the polarization vector, we get

$$\begin{aligned}\frac{d\Gamma}{dE_1 d\cos\theta_1} =& 2\pi\int d\Omega_2 \frac{d\Gamma}{dE_1 d\Omega_1 d\Omega_2} \\ =& \frac{1}{2}\int_{-1}^{1} d\cos\theta_{12}\frac{d\Gamma_{unpol.}}{dE_1 d\cos\theta_{12}} \\ & \times\left[1 + \left\{F\left(E_1, \cos\theta_{12}\right) + F\left(E_2, \cos\theta_{12}\right)\cos\theta_{12}\right\}P\cos\theta_1\right] \\ =& \frac{1}{2}\frac{d\Gamma_{unpol.}}{dE_1}\left[1 + \alpha\left(E_1\right)P\cos\theta_1\right], \end{aligned} \tag{5.3}$$

where θ_1 is an angle between $\boldsymbol{P}$ and $\boldsymbol{p}_1$, and we defined asymmetric factor, $\alpha\left(E_1\right)$, which can be related with

$F(E_1, \cos\theta_{12})$ as

$$\alpha(E_1) = \left(\frac{d\Gamma_{unpol.}}{dE_1}\right)^{-1} \int_{-1}^{1} d\cos\theta_{12} \frac{d\Gamma_{unpol.}}{dE_1 d\cos\theta_{12}} \left\{F(E_1, \cos\theta_{12}) + F(E_2, \cos\theta_{12})\cos\theta_{12}\right\}. \tag{5.4}$$

If the asymmetry factor $\alpha(E_1)$ is positive for certain E_1, this equation means that an emitted electron with E_1 tends to go in the same direction of the polarization vector $\boldsymbol{P}$, and vice versa. Therefore we can exploit the factor as an indicator of the angular distribution of an emitted electron in the case of using polarized muons.

When $\boldsymbol{P}$ denote the muon polarization vector, the initial muon spin density ρ_μ is given by

$$\rho_\mu = \frac{\mathbf{1}_2 + \boldsymbol{\sigma}\cdot\boldsymbol{P}}{2}. \tag{5.5}$$

We already have the expressions for the transition matrices in the previous section. To utilize them in a numerical calculation, it is economical to make the expression of $\alpha(E_1)$ by N in Eq. (4.65). To generalize Eq. (4.24) for the case with polarized muon, we can write down the differential decay rate as

$$\begin{aligned}\frac{d\Gamma}{dE_1 d\Omega_1 d\Omega_2} =& \sum_{\alpha_e} \frac{1}{128\pi^5} |\boldsymbol{p}_1| |\boldsymbol{p}_2| \sum_{s_1,s_2} \sum_{s_\mu, s'_\mu} \sum_{s_e} \mathcal{M}\left(\boldsymbol{p}_1, s_1, \boldsymbol{p}_2, s_2; 1S_{1/2}, s_\mu, \alpha_e, s_e\right) \\ & \times \langle s_\mu|\rho_\mu|s'_\mu\rangle \mathcal{M}^*\left(\boldsymbol{p}_1, s_1, \boldsymbol{p}_2, s_2; 1S_{1/2}, s'_\mu, \alpha_e, s_e\right),\end{aligned} \tag{5.6}$$

which satisfies the relation to the total decay rate,

$$\Gamma = \frac{1}{2}\int_{m_e}^{E_{tot}^{\alpha_e} - m_e} dE_1 \int d\Omega_1 d\Omega_2 \frac{d\Gamma}{dE_1 d\Omega_1 d\Omega_2}. \tag{5.7}$$

Here the extra factor $\langle s_\mu|\rho_\mu|s'_\mu\rangle = \langle s_\mu|\left(\mathbf{1} + \boldsymbol{\sigma}\cdot\boldsymbol{P}\right)|s'_\mu\rangle/2$ represents the polarization of the initial muon. The term of $\mathbf{1}$ just yields the same result as the previous unpolarized one, which does not depend on the any other angles but θ_{12}. The other term $\boldsymbol{\sigma}\cdot\boldsymbol{P}$ is the additional one by polarizing muon, which should be calculated here.

By inserting Eq. (4.64) into Eq. (5.6), deforming the equation, and comparing the result to Eq. (5.1), it is found that the factor of $F(E_1, \cos\theta_{12})$ and $\tilde{F}(E_1, \cos\theta_{12})$ defined in Eq. (5.1) are given as

$$F(E_1, \cos\theta_{12}) = \frac{G_F^2}{2\pi^3}\left(\frac{d\Gamma_{unpol.}}{dE_1 d\cos\theta_{12}}\right)^{-1} \sum_{\alpha_e} |\boldsymbol{p}_1| |\boldsymbol{p}_2| \left(2j_{\kappa_e} + 1\right) f(E_1, E_2, \cos\theta_{12}), \tag{5.8}$$

$$\tilde{F}(E_1, \cos\theta_{12}) = \frac{G_F^2}{2\pi^3}\left(\frac{d\Gamma_{unpol.}}{dE_1 d\cos\theta_{12}}\right)^{-1} \sum_{\alpha_e} |\boldsymbol{p}_1| |\boldsymbol{p}_2| \left(2j_{\kappa_e} + 1\right) \tilde{f}(E_1, E_2, \cos\theta_{12}). \tag{5.9}$$

Here $f\left(E_1, E_2, \cos\theta_{12}\right)$ and $\tilde{f}\left(E_1, E_2, \cos\theta_{12}\right)$ are represented by using $N^{\beta_1,\beta_2}(J)$, Eq. (4.65), as

$$
\begin{aligned}
f\left(E_1, E_2, \cos\theta_{12}\right) =& \sqrt{6} \sum_{\kappa_1,\kappa_2} \sum_{\kappa_1',\kappa_2'} \sum_{J,J'} \sum_{l} (-1)^{J'+j_{\kappa_1'}-j_{\kappa_2'}-j_{\kappa_e}+l+1/2} N^{\beta_1',\beta_2'*}(J') N^{\beta_1,\beta_2}(J) \\
& \times \left[J \cdot J' \cdot j_{\kappa_1} \cdot j_{\kappa_2} \cdot j_{\kappa_1'} \cdot j_{\kappa_2'}\right] \sqrt{\left[l_{\kappa_1} \cdot l_{\kappa_2} \cdot l_{\kappa_1'} \cdot l_{\kappa_2'}\right]} \\
& \times \sqrt{\frac{(2l+1)(2l+3)}{l+1}} \begin{Bmatrix} J & J' & 1 \\ 1/2 & 1/2 & j_{\kappa_e} \end{Bmatrix} \\
& \times \left[P_l'\left(\cos\theta_{12}\right) \begin{pmatrix} l_{\kappa_1} & l_{\kappa_1'} & l \\ 0 & 0 & 0 \end{pmatrix} \begin{pmatrix} l_{\kappa_2} & l_{\kappa_2'} & l+1 \\ 0 & 0 & 0 \end{pmatrix} \right. \\
& \times \begin{Bmatrix} j_{\kappa_1} & j_{\kappa_1'} & l \\ l_{\kappa_1'} & l_{\kappa_1} & 1/2 \end{Bmatrix} \begin{Bmatrix} j_{\kappa_2} & j_{\kappa_2'} & l+1 \\ l_{\kappa_2'} & l_{\kappa_2} & 1/2 \end{Bmatrix} \begin{Bmatrix} j_{\kappa_1} & j_{\kappa_2} & J \\ j_{\kappa_1'} & j_{\kappa_2'} & J' \\ l & l+1 & 1 \end{Bmatrix} \\
& - P_{l+1}'\left(\cos\theta_{12}\right) \begin{pmatrix} l_{\kappa_1} & l_{\kappa_1'} & l+1 \\ 0 & 0 & 0 \end{pmatrix} \begin{pmatrix} l_{\kappa_2} & l_{\kappa_2'} & l \\ 0 & 0 & 0 \end{pmatrix} \\
& \left. \times \begin{Bmatrix} j_{\kappa_1} & j_{\kappa_1'} & l+1 \\ l_{\kappa_1'} & l_{\kappa_1} & 1/2 \end{Bmatrix} \begin{Bmatrix} j_{\kappa_2} & j_{\kappa_2'} & l \\ l_{\kappa_2'} & l_{\kappa_2} & 1/2 \end{Bmatrix} \begin{Bmatrix} j_{\kappa_1} & j_{\kappa_2} & J \\ j_{\kappa_1'} & j_{\kappa_2'} & J' \\ l+1 & l & 1 \end{Bmatrix} \right],
\end{aligned} \tag{5.10}
$$

and

$$
\begin{aligned}
\tilde{f}\left(E_1, E_2, \cos\theta_{12}\right) =& \sqrt{6} \sum_{\kappa_1,\kappa_2} \sum_{\kappa_1',\kappa_2'} \sum_{J,J'} \sum_{l} (-1)^{J'+j_{\kappa_1'}-j_{\kappa_2'}-j_{\kappa_e}+l+1/2} N^{\beta_1',\beta_2'*}(J') N^{\beta_1,\beta_2}(J) \\
& \times \left[J \cdot J' \cdot j_{\kappa_1} \cdot j_{\kappa_2} \cdot j_{\kappa_1'} \cdot j_{\kappa_2'}\right] \sqrt{\left[l_{\kappa_1} \cdot l_{\kappa_2} \cdot l_{\kappa_1'} \cdot l_{\kappa_2'}\right]} \\
& \times \frac{(2l+3)^{3/2}}{\sqrt{(l+1)(l+2)}} \begin{Bmatrix} J & J' & 1 \\ 1/2 & 1/2 & j_{\kappa_e} \end{Bmatrix} \\
& \times i P_{l+1}'\left(\cos\theta_{12}\right) \begin{pmatrix} l_{\kappa_1} & l_{\kappa_1'} & l+1 \\ 0 & 0 & 0 \end{pmatrix} \begin{pmatrix} l_{\kappa_2} & l_{\kappa_2'} & l+1 \\ 0 & 0 & 0 \end{pmatrix} \\
& \times \begin{Bmatrix} j_{\kappa_1} & j_{\kappa_1'} & l+1 \\ l_{\kappa_1'} & l_{\kappa_1} & 1/2 \end{Bmatrix} \begin{Bmatrix} j_{\kappa_2} & j_{\kappa_2'} & l+1 \\ l_{\kappa_2'} & l_{\kappa_2} & 1/2 \end{Bmatrix} \begin{Bmatrix} j_{\kappa_1} & j_{\kappa_2} & J \\ j_{\kappa_1'} & j_{\kappa_2'} & J' \\ l+1 & l+1 & 1 \end{Bmatrix}.
\end{aligned} \tag{5.11}
$$

The derivation for these formulae is given in Appendix I.4.

Thus the function defined by Eq. (5.4) is represented as

$$
\alpha(E_1) = \frac{\sum_{\alpha_e} \left(2j_{\kappa_e}+1\right) I_f^{\alpha_e}(E_1)}{2\sum_{\alpha_e}\left(2j_{\kappa_e}+1\right) \sum_{\kappa_1,\kappa_2,J} \left[J \cdot j_{\kappa_1} \cdot j_{\kappa_2}\right] \left|N^{\beta_1,\beta_2}(J)\right|^2}, \tag{5.12}
$$

where I_f in the numerator is defined as

$$
I_f^{\alpha_e}(E_1) = \int_{-1}^{1} d\cos\theta_{12} \left\{ f\left(E_1, E_2, \cos\theta_{12}\right) + f\left(E_2, E_1, \cos\theta_{12}\right) \cos\theta_{12} \right\}. \tag{5.13}
$$

By using integral relations for the Legendre function,

$$\int_{-1}^{1} dx P_l'(x) = [P_l(x)]_{-1}^{1} = P_l(1) - P_l(-1)$$
$$= \begin{cases} 2 & (l = \text{odd}) \\ 0 & (l = \text{even}) \end{cases}, \tag{5.14}$$

$$\int_{-1}^{1} dx x P_l'(x) = \begin{cases} \left[x P_l(x) - \dfrac{P_{l+1}(x) - P_{l-1}(x)}{2l+1} \right]_{-1}^{1} = P_l(1) + P_l(-1) & (l \neq 0) \\ 0 & (l = 0) \end{cases}$$
$$= \begin{cases} 2 & (l = \text{even and } l \geq 2) \\ 0 & (l = \text{odd or } l = 0) \end{cases}, \tag{5.15}$$

it is found that most terms are canceled, and we obtain

$$I_f^{\alpha_e}(E_1) = 2\sqrt{6} \sum_{\kappa_1, \kappa_2} \sum_{\kappa_1'} \sum_{J, J'} (-1)^{j_{\kappa_1} + j_{\kappa_1'} - j_{\kappa_2} - j_{\kappa_e}} \left[J \cdot J' \cdot j_{\kappa_1} \cdot j_{\kappa_1'} \cdot j_{\kappa_2} \right] \sqrt{\left[l_{\kappa_1} \cdot l_{\kappa_1'} \right]} N^{\beta_1', \beta_2 *}(J') N^{\beta_1, \beta_2}(J)$$
$$\times \begin{pmatrix} l_{\kappa_1} & l_{\kappa_1'} & 1 \\ 0 & 0 & 0 \end{pmatrix} \begin{Bmatrix} l_{\kappa_1} & l_{\kappa_1'} & 1 \\ j_{\kappa_1'} & j_{\kappa_1} & 1/2 \end{Bmatrix} \begin{Bmatrix} J & J' & 1 \\ 1/2 & 1/2 & j_{\kappa_e} \end{Bmatrix} \begin{Bmatrix} J & J' & 1 \\ j_{\kappa_1'} & j_{\kappa_1} & j_{\kappa_2} \end{Bmatrix}, \tag{5.16}$$

where Eqs. (G.19), (G.45), and (G.56) have been also used.

Chapter 6

Results and Discussions

According to the formulation in the previous chapters, observables of CLFV decay $\mu^- e^- \to e^- e^-$ of a polarized and unpolarized muon in a atom are obtained by studying the reduced matrix elements $\mathcal{N}_{\rm contact}$ and $\mathcal{N}_{\rm photonic}$ of each partial waves. Key questions are how the improved lepton wave functions affects the transition rate and how the nature of CLFV interactions shows up in the observable. At first, we examine the lepton wave functions in various approximations. Then we present our numerical results on total decay rate, angular and energy distribution of final electrons and parity violating asymmetry coefficient of electron angular distribution for polarized muon.

6.1 Lepton Wave Functions

In order to obtain the matrix elements $\mathcal{N}_{\rm contact}$ and $\mathcal{N}_{\rm photonic}$, we need the bound state wave function of muon and electron and the scattering state wave function of final electrons. The radial wave functions $g_\kappa(r)$, $f_\kappa(r)$

$$\psi^\nu_\kappa = \begin{pmatrix} g_\kappa(r)\chi^\nu_\kappa(\hat{r}) \\ i f_\kappa(r)\chi^\nu_{-\kappa}(\hat{r}) \end{pmatrix}, \tag{6.1}$$

are obtained by solving coupled equation with appropriate boundary condition

$$\frac{dg_\kappa(r)}{dr} + \frac{1+\kappa}{r} g_\kappa(r) - (E + m + e\phi(r)) f_\kappa(r) = 0, \tag{6.2}$$

$$\frac{df_\kappa(r)}{dr} + \frac{1-\kappa}{r} f_\kappa(r) + (E - m + e\phi(r)) g_\kappa(r) = 0. \tag{6.3}$$

The derivation of the equation is given in Appendix E. The Coulomb potential $\phi(r)$ is obtained from the charge distribution of nucleus $\rho(r)$ as

$$\phi(r) = \int_0^\infty \rho(r') \left[\theta(r - r') \frac{1}{r} + \theta(r' - r) \frac{1}{r'} \right] r'^2 dr'. \tag{6.4}$$

We have studied the point charge $\rho(r) = Ze\delta(r)/r^2$, uniform, and Woods-Saxon charge distributions. The uniform charge distribution is taken as

$$\rho_C(r) = \frac{3Ze}{4\pi R^3} \theta(R - r), \tag{6.5}$$

where we use $R = 1.2A^{1/3}$fm for mass number A. For each Z, we take the mass number A of the most abundant isotope [104], e.g., $A = 208$ for $Z = 82$. We have also examined the realistic form of the distribution

of nuclear charge using the Woods-Saxon form,

$$\rho_C(r) = \rho_0 \left[1 + \exp\left(\frac{r-c}{z}\right)\right]^{-1}. \tag{6.6}$$

The parameters, c and z, for ^{40}Ca, ^{120}Sn, and ^{208}Pb are listed in Table 6.1. The Woods-Saxon potential should describe the nuclear shape more accurately than the other descriptions. However the difference of wave functions between uniform and Woods-Saxon charge distributions is tiny and negligible. Actually, we found that the modification of the decay rate using Woods-Saxon charge distribution in place of uniform distribution is less than 1%. Therefore, we will not present results using Woods-Saxon charge distribution.

Table 6.1: The parameters of the charge distribution of the Woods-Saxon form for ^{40}Ca, ^{120}Sn and ^{208}Pb [105].

nuclei	c [fm]	z [fm]
^{40}Ca	3.51(7)	0.563
^{120}Sn	5.315(25)	0.576(11)
^{208}Pb	6.624(35)	0.549(8)

For bound state wave functions, we consider three cases, Nr-P, Rel-P, and Rel-U, as shown in Table 6.2, while, for wave functions of scattering state, we consider three cases, PLW, DW-P, and DW-U, as shown in Table 6.3. Our final results are obtained by using Rel-U and DW-WS, while results close to the previous works should be obtained by Nr-P and PLW.

Table 6.2: Abbreviation for bound wave functions.

Abbreviation	Equation of motion	Nuclear charge distribution
Nr-P	Schrödinger	Point
Rel-P	Dirac	Point
Rel-U	Dirac	Uniform

Table 6.3: Abbreviation for scattering wave functions. PLW denotes the Dirac plane wave, where the distortion by nuclear Coulomb potential is ignored.

Abbreviation	Equation of motion	Nuclear charge distribution
PLW	Dirac	-
DW-P	Dirac	Point
DW-U	Dirac	Uniform

6.1.1 Bound State Wave Function of Muon and Electron

The radial wave function of a muon in $1S$ bound state is shown in Fig. 6.1 and their corresponding binding energies are given in Table 6.4. The blue, green and red curves are obtained by using Nr-P, Rel-P, and Rel-U, respectively. The solid and dashed curves show $rg_{-1}(r)$ and $rf_{-1}(r)$.

Compared with point nuclear charge of non-relativistic wave function (Nr-P), $rg_{-1}(r)$ of relativistic wave function (Rel-P) shrinks a little bit towards the nucleus in the relativistic wave function and a small component $rf_{-1}(r)$, which is not negligible magnitude, appears in Rel-P. The uniform distribution of nuclear charge makes the Coulomb potential weaker around the nucleus. Since muon mass is large, the effect of finite size nucleus is larger than that for electron. The muon binding energy becomes about a half of point charge and the wave function spreads more.

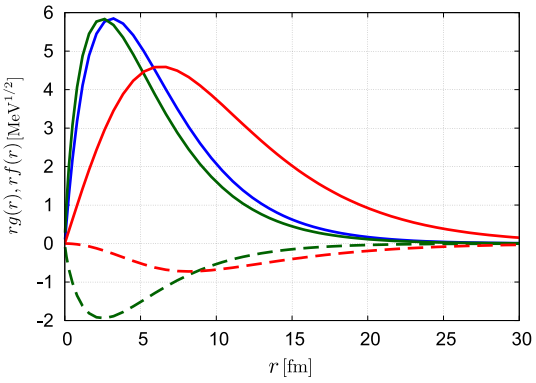

Figure 6.1: Wave functions of a $1S$ bound muon. The blue, green, and red curves are Nr-P, Rel-P, and Rel-U, respectively. For each, a solid (dashed) curve indicates $rg_{-1}(r)$ ($rf_{-1}(r)$). For Nr-P, since $f_{-1}(r) \equiv 0$, the small component is not shown.

Table 6.4: Binding energies of a $1S$ bound muon, B_μ.

	B_μ [MeV]
Nr-P	18.9
Rel-P	21.0
Rel-U	10.5

We take into account the screening effect of muon by using $(Z-1)e$ for the Coulomb potential of electron. The $1S$ bound state wave functions of electron $rg_{-1}(r)$ and $rf_{-1}(r)$ and the binding energies are shown in Fig. 6.2-(a) and in Table 6.5. The binding energy of $1S$ state essentially the same for Rel-P and Rel-U. The blue, green, and red curves are obtained by using Nr-P, Rel-P, and Rel-U, respectively. Here results of point charge (Rel-P) and uniform charge distribution (Rel-U) are almost the same. Since electron mass is about $1/200$ of muon mass, radius of electron orbit is 200 times larger than that of muon and therefore the bound state wave function is less sensitive to the finite charge distribution of nucleus. As in the muon case, the relativistic wave function around small radius is enhanced compared with the non-relativistic one. To see this more clearly, the electron wave function for $r < 30fm$ is shown in Fig. 6.2-(b). Since the contribution of the overlap integral with muon wave function is dominated in this region, large enhancement would be obtained by using the relativistic wave function of electron.

Table 6.5: Binding energies of a $1S$ electron, B_e.

	B_e [MeV]
Nr-P	8.93×10^{-2}
Rel-P	9.88×10^{-2}
Rel-U	9.88×10^{-2}

The exited states can also be calculated by the same method. We can recognize the principle quantum number n of an obtained solution by checking the number of nodes. In Fig. 6.3, we have shown wave function of $2S$, $3S$ and $4S$ states of the Rel-U model. The binding energies of those states are given in Table 6.6. The binding energies are approximately proportional to $1/n^2$, which is consistent with the property of analytic solutions for point-charge potential.

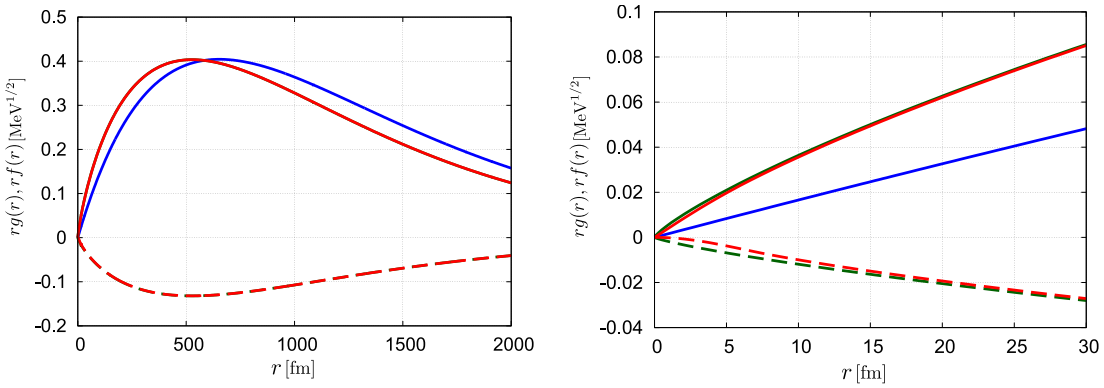

Figure 6.2: Radial wave function of $1S$ bound electrons. The meanings of curves are similar to that of Fig. 6.1. The difference between Rel-P and Rel-U is tiny so cannot be recognized in this figure. (b) is an enlarged view of (a) near the origin.

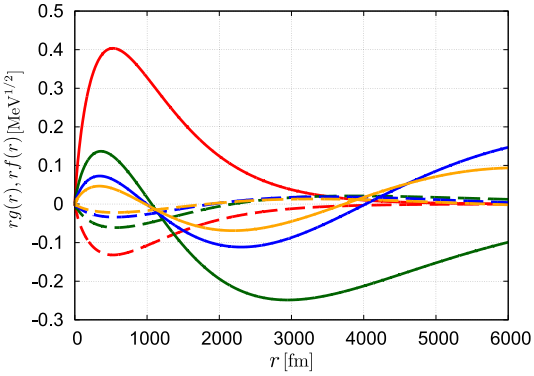

Figure 6.3: Wave functions of a bound electron in S states. The red, green, blue, and yellow curves are for $1S$, $2S$, $3S$, and $4S$, respectively. For each, a solid (dashed) curve indicates $rg_{-1}(r)$ ($rf_{-1}(r)$).

6.1.2 Electron Scattering Wave

Lastly the radial wave functions of a scattering electron for PLW, Rel-P, and Rel-U. are shown in Fig. 6.4. Here we show the results for the partial wave with $\kappa = -1$ at $p = 47.7$MeV, which has the largest contribution to the decay rate among the components of the scattering waves. The comparison between PLW and Rel-P shows that the wave function is attracted inward by the Coulomb potential, which reflects that attractive force works between an electron and a nucleus. By considering the finite size charge distribution of the nucleus, the attraction is weakened compared to the case with a point charge.

6.2 Decay Rate

By using the lepton wave functions, we have studied the decay rate Γ of $\mu^- e^- \to e^- e^-$. To examine the dependence of CLFV interaction on decay rate, we studied the following three cases assuming that only one of CLFV interaction is non-vanishing.

1. contact interaction, where the electrons are emitted with the same chirality

$$g_1 \neq 0,\ A_{L/R} = 0,\ \text{and}\ g_{j\neq 1} = 0. \tag{6.7}$$

Table 6.6: Binding energies of a bound electrons in S states.

	B_e [MeV]
$1S$	9.88×10^{-2}
$2S$	2.53×10^{-2}
$3S$	1.10×10^{-2}
$4S$	6.05×10^{-3}

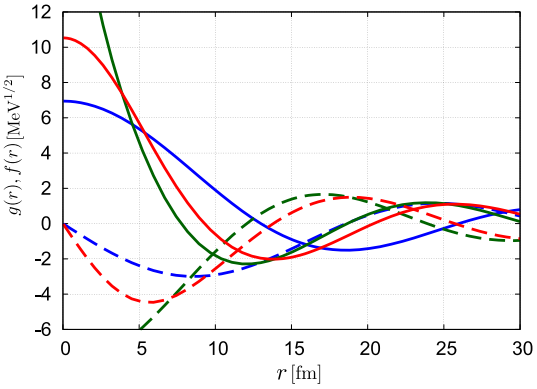

Figure 6.4: Radial wave functions of a scattering electron with $p = 47.7$MeV and $\kappa = -1$. The blue, green, and red curves are PLW, DW-P, and DW-U, respectively. For each, a solid (dashed) curve indicates $g_{-1}(r)$ ($f_{-1}(r)$).

2. contact interaction, where the electrons are emitted with the opposite chirality

$$g_5 \neq 0,\ A_{L/R} = 0,\ \text{and}\ g_{j\neq5} = 0. \tag{6.8}$$

3. photonic interaction

$$A_L \neq 0,\ A_R = 0,\ \text{and}\ g_i = 0. \tag{6.9}$$

When we average and sum all the spin states of leptons, decay rate of case 1 is the same as that for one of the coupling constant g_2, g_3 and g_4 is non-vanishing. Similarly, for case 2 (case 3), the same decay rate is obtained when only g_6 (A_R) are kept non-zero. Of course, the magnitude of a remaining coupling determines the absolute value of the transition rate. Here, we show results independent of the magnitude of the coupling, unless otherwise noted.

6.2.1 Comparison with the previous work

The formula of decay rate Γ^0 (Eqs. (4.12) and (4.14)) of the previous work is obtained in plane wave scattering state and non-relativistic bound state wave functions. Within our formalism, Γ obtained in Section 4.3 or equivalently PLW and Nr-P calculation is expected to be almost the same as Γ^0. Difference between two approach is that we have taken into account the finite spatial spread of bound state wave functions. In Fig. 6.5, The Z-dependence of ratio Γ/Γ^0 for case 1-3 is shown by solid, dashed, and dash-dotted curves, respectively. The ratio deviates from unity for large Z depending on case 1, 2, and 3 because of using the finite size bound muon wave function instead of using the plane wave in the previous estimation. It is important to take into account the finite range of bound state wave functions for large Z.

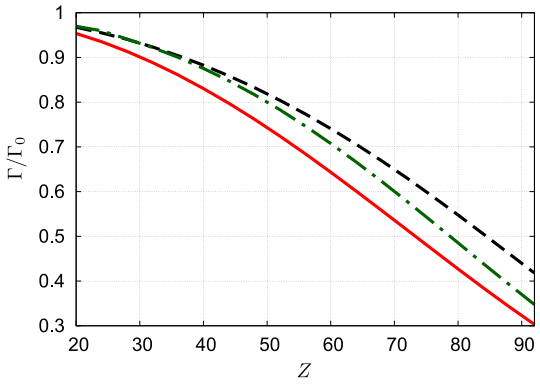

Figure 6.5: Z-dependence of the ratio Γ/Γ^0. Here Γ is calculated on the plane wave approximation introduced in Section 4.3. The solid (red), dashed (black), and dash-dotted (green) curves show Γ/Γ^0 in case 1-3, respectively.

6.2.2 Effects of Coulomb Interaction on Decay Rate

Now, let us replace used lepton wave functions with more realistic ones. In order to clarify influences of each improvement for wave functions, we examine four models for the lepton wave functions shown in Table 6.7. In model I, the bound state wave functions of the muon and electron are calculated in the nonrelativistic approximation (Non. Rel.) with Coulomb interaction of point nuclear charge (Point Coul.) and the electron scattering states are in the plane wave approximation (PLW). The model I is actually the same setting as the plane wave approximation in Section 4.3. Then the wave function of the scattering state is replaced by the solution of the Dirac equation (Rel.) in model II. In model III, both the bound state and the scattering state lepton wave functions are calculated from the Dirac equation with point nuclear charge. Finally, we used the uniform nuclear charge distribution (Uniform Coul.) in model IV.

Table 6.7: Models for the lepton wave functions.

Model	Bound state	Scattering state
I	NR-P	PLW
II	NR-P	DW-P
III	Rel-P	DW-P
IV	Rel-U	DW-U

First, contact process is considered here. We start to study the typical transition density $\rho_{\rm tr}(r)$ given by the product of lepton wave functions as

$$\rho_{\rm tr}(r) = r^2 g_{p_1}^{-1}(r) g_{\mu}^{-1}(r) g_{p_2}^{-1}(r) g_{e}^{-1}(r) \tag{6.10}$$

to find the role of the Coulomb interaction on the lepton wave function for contact process. Here we take the most important transition matrix element of the $1S$ electron and muon to the $\kappa = -1$ electrons ($\mu^-(1S) + e^-(1S) \to e^-(\kappa = -1) + e^-(\kappa = -1)$), where the two electrons are equally sharing the energy $E_1 = E_2 = E_{tot}^{1S}/2$.

The transition densities of the four models for the $\mu^- e^- \to e^- e^-$ decay of the ^{208}Pb muonic atom are shown in Fig. 6.6. The dashed curve shows transition density in model I that simulates the previous analysis. By including the Coulomb attraction for scattering electrons in model II, the transition density is enhanced around the muon Bohr radius as shown by the dash-dotted curve. Further we use the consistent lepton wave functions of the Dirac equation with point nuclear charge in model III. The transition density becomes very

large as shown by the dash-two-dotted curve, which is 1/3 of the actual transition density. However, the use of point nuclear charge would not be appropriate for an atom of large Z, where the Bohr radius of the muon can be comparable to the nuclear radius. The solid curve shows our final result by using a finite charge distribution of nucleus in model IV. The peak position of the transition density is shifted toward larger r compared with that of point nuclear charge.

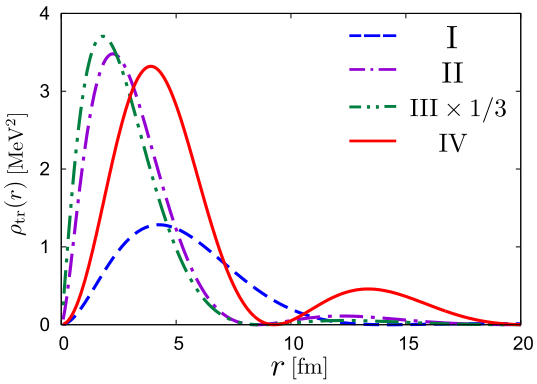

Figure 6.6: The transition density $\rho_{\rm tr}(r)$ for the $\mu^-(1S)+e^-(1S)\to e^-(\kappa=-1)+e^-(\kappa=-1)$. The dashed, dash-dotted, dash-two-dotted, and solid curves show the transition density in models I-IV, respectively. Figure taken from Ref. [33]. Copyright 2016 American Physical Society.

The decay rate Γ obtained in our calculation is shown in Fig. 6.7. Here the ratios Γ/Γ^0 are plotted, where $\Gamma^0=\Gamma^0_{\rm contact}$ is defined in Eq. (4.12). We retain only the term of g_1 and set the other gs to zero (case 1). The contribution of the dominant $1S$ bound electron is included. The dashed curve in Fig. 6.7 shows

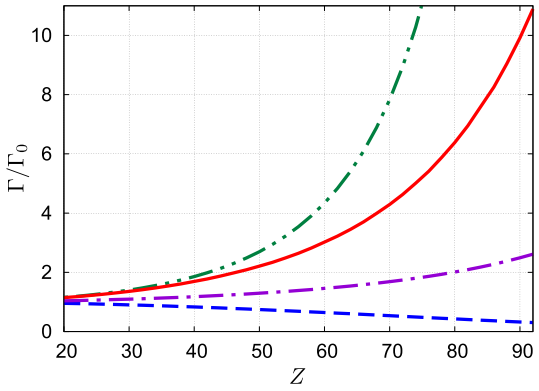

Figure 6.7: The atomic number (Z) dependence of the ratio of the decay rate Γ/Γ^0. See caption of Fig. 6.6, except dash-two-dotted curve, where we have not multiplied 1/3 for the ratio of decay rate. Figure taken from Ref. [33]. Copyright 2016 American Physical Society.

the decay rate evaluated with model I, which is the same as the solid one in Fig. 6.5. When we replace the plane wave electrons with the Dirac wave function for point nuclear charge (II), the decay rate increases as shown in the dash-dotted curve. When both bound and scattering states are described by the Dirac equation that includes the Coulomb interaction of point nuclear charge (III), the decay rate is even more enhanced as shown in the dash-two-dotted curve. A realistic description of Γ/Γ^0 is obtained by using the uniform nuclear charge distribution in model IV as shown in the solid curve in Fig. 6.7.

The results show that, while Γ^0 gives reasonable estimation for smaller $Z\sim 20$, the Z-dependence of the Γ is stronger than $(Z-1)^3$. The ratio Γ/Γ^0 is about 7.0 for the ^{208}Pb. We found slightly different

Z-dependence of Γ for two types of the effective CLFV contact interaction. The interaction of the g_i term with $i = 1, 2, 3, 4$, which leads to the same helicity states of two electrons (case 1), gives $\Gamma/\Gamma^0 \sim 7.0(1.1)$ for ^{208}Pb (^{40}Ca). For the g_i term with $i = 5, 6$, where the opposite helicity states of electrons are emitted (case 2), the decay rate is $\Gamma/\Gamma^0 \sim 6.3(1.1)$ for ^{208}Pb (^{40}Ca). Therefore, Z-dependence of the decay rate for $g_1 \sim g_4$ is slightly stronger than that of g_5 and g_6.

All the results of the decay rate were obtained by including a sufficiently large number of partial waves of final electrons. The convergence properties of the decay rate against the number of partial waves included are shown in Table 6.8. The number of partial waves needed to obtain convergent results was $|\kappa| \sim 6$ for Pb and Sn and $|\kappa| \sim 13$ for Ca. This happens because the muon Bohr radius is increasing for decreasing Z.

Table 6.8: The convergence property of the partial wave expansion of Γ/Γ^0.

Nuclei	$\lvert\kappa\rvert \leq 1$	$\lvert\kappa\rvert \leq 5$	$\lvert\kappa\rvert \leq 10$	$\lvert\kappa\rvert \leq 20$
^{40}Ca	0.141	0.847	1.11	1.15
^{120}Sn	0.731	2.17	2.21	2.21
^{208}Pb	2.89	6.94	6.96	6.96

The results shown so far were obtained including only the main transitions where the initial electrons are bound in the $1S$ state. The contributions of the electrons from the higher shell $2S, 3S, \cdots$ are estimated within the independent particle model for the atomic electrons. Contributions of higher shell electrons increase the transition rate by $\sim 20\%$ as shown in Table 6.9, which is consistent with the statement of the previous work [23].

Table 6.9: The ratio of the decay rates Γ/Γ^0 for ^{40}Ca, ^{120}Sn and ^{208}Pb. In the second (third) column, the Γ/Γ^0 including the contribution of the $1S$ ($1S$ and higher shells) is shown.

nuclei	Γ/Γ^0 (only $1S$)	$1S + 2S + \cdots$
^{40}Ca	1.15	1.35
^{120}Sn	2.21	2.67
^{208}Pb	6.96	8.78

Second, we move on to the analysis for photonic process. The ratio of decay rate Γ/Γ^0, where $\Gamma^0 = \Gamma^0_{\rm photonic}$ is defined in Eq. (4.14), is studied to examine the role of Coulomb interaction of scattering state and relativistic wave function of the bound states. For simplicity, we set $A_R = 0$ (case 3) and start discussion including only the contribution of $1S$ electron bound state again. We also consider four models summarized in Table 6.7. The ratio of decay rate in model I is shown in dashed curve of Fig. 6.8. Due to the finite size of muon wave function, the ratio is decreasing function of Z, as already discussed, which is also observed for the contact interaction. The results in model II-IV are shown in dash-dotted, dash-two-dotted, and solid curve, respectively. We use DW for the electron scattering state in these models. By taking into account the Coulomb distortion and the relativistic bound state wave function, the decay rate is strongly suppressed compared with Γ^0, which is quite different from large enhancement obtained for the contact interaction. The ratio in model IV is 0.27 (0.66) for ^{208}Pb (^{40}Ca).

To understand the mechanism of the suppression of the decay rate, we study a typical transition density,

$$\rho_{{\rm tr};\mu}(r) = r^2 j_0\left(q_0 r\right) g_{p_1}^{-1}(r) g_{1,\mu}^{-1}(r), \tag{6.11}$$

which indicates the partial transition density of a bound muon ($1S$) to a scattering electron ($\kappa = -1$) and a photon ($l = 0$). Here we choose the most important kinematical region $p_1 = (m_\mu - B_\mu)/2 = q_0$ ignoring the electron mass. The transition densities calculated by using PLW and DW electron wave functions are shown in Fig. 6.9. In the PLW case, $\rho_{{\rm tr};\mu}$ is positive definite, since the wave length of scattering electron is the

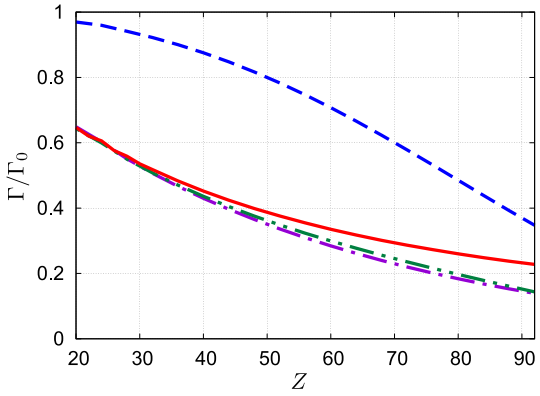

Figure 6.8: The Z-dependence of Γ/Γ^0. The ratios Γ/Γ^0 of model I-IV are shown in dashed, dash-dotted, dash-two-dotted, and solid curves, respectively, as Fig. 6.7.

same as that of virtual photon. On the other hand, $\rho_{\mathrm{tr};\mu}$ changes sign and oscillates because of the Coulomb attraction for the electron. The same mechanism also applies to the vertex of bound electron transition. Therefore the distortion of final electrons suppress the transition rate.

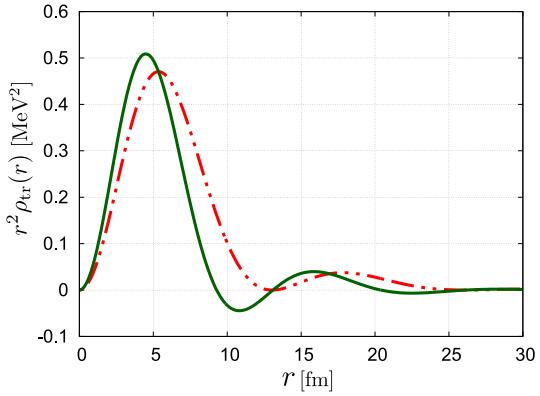

Figure 6.9: The transition density $\rho_{\mathrm{tr};\mu}(r)$ for ^{208}Pb. The dash-two-dotted and solid curves show the transition density using PLW and DW scattering electron, respectively. Here, the bound muon is treated relativistically in both curves. Figure taken from Ref. [34]. Copyright 2018 American Physical Society.

In terms of momentum space, the suppression of the decay rate for the photonic interaction can be understood as follows. The momenta of electron and virtual photon are transferred to bound muon or electron at each vertex for photonic interaction. Main contribution to the decay rate is when both electron and virtual photon carry about a half of muon mass, so that the momentum transfer to the bound states is almost zero. While this is true for the asymptotic momentum of electron, Coulomb attraction increases the local momentum of electrons close to the nucleus. This brings mismatch of the virtual photon and electron momentum and increase momentum transfer to the bound leptons and hence reduce the transition probability. Similar suppression mechanism of the transition rate was pointed out in Ref. [30] for μ^--e^- conversion process.

A sufficiently large number of partial waves of scattering electron state has to be included. Convergence property of the decay rate against partial waves is shown in Table 6.10. The convergence property is almost the same as the contact interaction. For larger Z nuclei, the decay rate converges faster due to smaller radius of the bound muon.

For photonic interaction, the effective interaction is non-local due to the propagation of virtual photon.

Table 6.10: The convergence property of Γ/Γ^0. The maximum values of $|\kappa|$ included for the decay rates in each column are given in the first row.

Nuclei	$\lvert\kappa\rvert \leq 1$	$\lvert\kappa\rvert \leq 5$	$\lvert\kappa\rvert \leq 10$	$\lvert\kappa\rvert \leq 20$
^{40}Ca	0.0762	0.482	0.641	0.663
^{120}Sn	0.125	0.396	0.406	0.406
^{208}Pb	0.109	0.270	0.271	0.271

In principle, bound electrons other than $1S$ state contribute to the decay rate. The decay rate of each atomic orbits normalized to those of $1S$ state are shown in Table 6.11. It is found the contribution of non-S wave bound electrons is larger than that of contact interaction. However it is very small compared with those of $1S$ electron. The total decay rate for ^{208}Pb is enhanced by 20% by including electrons other than $1S$ state.

Table 6.11: The CLFV decay rate coming from initial electrons in each atomic orbit under M shell and $4S$ orbit. This result is for ^{208}Pb. These are summed over spins, and normalized by $1S$ contribution.

$1S$	$2S$	$2P$	$3S$	$3P$	$3D$	$4S$	Total
1	0.15	7.3×10^{-3}	4.3×10^{-2}	2.6×10^{-3}	2.5×10^{-5}	1.8×10^{-2}	1.21

6.2.3 Branching Ratio

It is more useful to see the branching ratio $Br(\mu^-e^- \to e^-e^-)$ rather than the decay rate $\Gamma(\mu^-e^- \to e^-e^-)$ itself to discuss the relation of high energy theory with experimental observation of $\mu^-e^- \to e^-e^-$ searches. Here, by using the restriction from other CLFV experiments such as $\mu^+ \to e^+\gamma$ and $\mu^+ \to e^+e^+e^-$, let us evaluate current upper limits for $Br(\mu^-e^- \to e^-e^-)$. The branching ratio is defined by using the $\mu^-e^- \to e^-e^-$ decay rate of muonic atom $\Gamma(\mu^-e^- \to e^-e^-)$ and the total decay rate of muonic atom $1/\tilde{\tau}_\mu$,

$$Br(\mu^-e^- \to e^-e^-) = \tilde{\tau}_\mu \Gamma(\mu^-e^- \to e^-e^-). \tag{6.12}$$

First, we think about contact interactions. The CLFV branching ratio of a muonic atom is given as

$$\begin{aligned} Br\left(\mu^-e^- \to e^-e^-\right) =& \tilde{\tau}_\mu \Gamma \\ =& 24\pi(Z-1)^3\alpha_{em}^3 \left(\frac{m_e}{m_\mu}\right)^3 \frac{\tilde{\tau}_\mu}{\tau_\mu} \frac{\Gamma}{\Gamma^0_{\text{contact}}} G, \end{aligned} \tag{6.13}$$

where $\tau_\mu = 192\pi^3/(G_F^2 m_\mu^5)$ is a mean lifetime of a free muon, as shown in Eq. (C.7). The strongest limits for couplings g_1-g_6 is determined by a search for $\mu^+ \to e^+e^+e^-$ process. As denoted in Section 3.2, the branching ratio of $\mu^+ \to e^+e^+e^-$ is calculated by

$$Br\left(\mu^+ \to e^+e^+e^-\right) = \frac{1}{8}\left(G_{12} + 16G_{34} + 8G_{56}\right), \tag{3.2}$$

according to Ref. [50]. Keeping only g_1 term of CLFV interaction, we can express the branching ratio of $\mu^-e^- \to e^-e^-$ as

$$Br\left(\mu^-e^- \to e^-e^-\right) = 192\pi(Z-1)^3\alpha_{em}^3 \left(\frac{m_e}{m_\mu}\right)^3 \frac{\tilde{\tau}_\mu}{\tau_\mu} \frac{\Gamma}{\Gamma^0_{\text{contact}}} Br\left(\mu^+ \to e^+e^+e^-\right). \tag{6.14}$$

The upper limits of the branching ratio of the previous work (dashed curve) and our results with $1S$ (solid curve) and all nS electrons (dotted curve) are shown in Fig. 6.10-(a). Here we used the result of the

SINDRUM experiment $Br(\mu^+ \to e^+e^+e^-) < 1.0 \times 10^{-12}$ [46] and the data of the lifetime of muonic atoms $\tilde{\tau}_\mu$ given in [115]. For ^{208}Pb (^{238}U), the branching ratios $Br(\mu^- e^- \to e^- e^-)$ considering only $1S$ electrons and all electrons are 3.3×10^{-18} (6.9×10^{-18}) and 4.2×10^{-18} (9.8×10^{-18}), respectively. $Br(\mu^- e^- \to e^- e^-)$ reaches about 10^{-17} for ^{238}U.

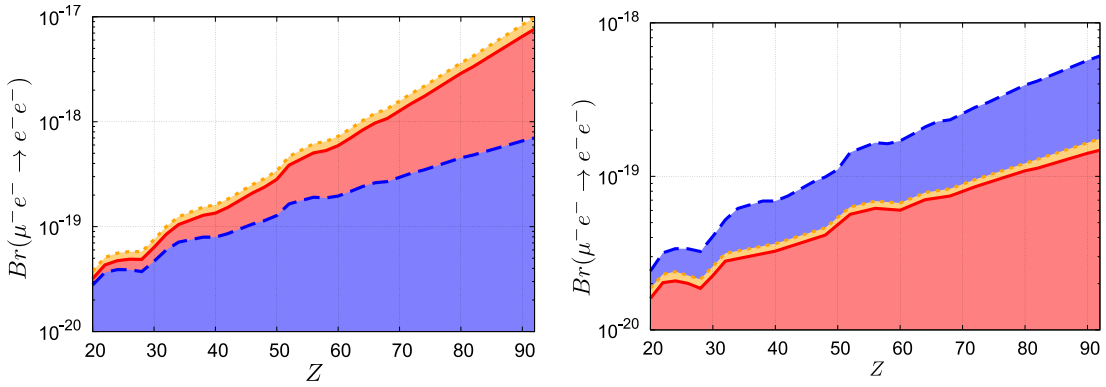

Figure 6.10: Upper limits of $Br(\mu^- e^- \to e^- e^-)$ for g_1-type interaction (a) and A_L-type interaction (b). The dashed (blue) curve shows the result of previous work [23]. Our results including only $1S$ electrons and all $1S$ electrons are shown by the solid (red) curve and the dotted (orange) curve, respectively. Figure (a) taken from Ref. [33]. Copyright 2016 American Physical Society. Figure (b) taken from Ref. [34]. Copyright 2018 American Physical Society.

Second, let us consider photonic interactions. The CLFV branching ratio is

$$Br\left(\mu^- e^- \to e^- e^-\right) = 1536\pi^2 (Z-1)^3 \alpha_{em}^4 \frac{m_e}{m_\mu} \frac{\tilde{\tau}_\mu}{\tau_\mu} \frac{\Gamma}{\Gamma^0_{\text{photonic}}} \left(|A_L|^2 + |A_R|^2\right). \tag{6.15}$$

Their coupling constants $A_{L/R}$ are restricted by searches from $\mu^+ \to e^+\gamma$ process, whose branching ratio is given as Eq. (2.3). Assuming the dominance of photonic interaction, the upper limit on $Br(\mu^- e^- \to e^- e^-)$ can be expressed by using B_{max}, which is current upper limit of $Br(\mu^+ \to e^+\gamma)$ as,

$$\begin{aligned} Br(\mu^- e^- \to e^- e^-) <& \frac{Br(\mu^- e^- \to e^- e^-)}{Br(\mu^+ \to e^+\gamma)} B_{\text{max}} \\ =& 4(Z-1)^3 \alpha_{em}^4 \frac{m_e}{m_\mu} \frac{\tilde{\tau}_\mu}{\tau_\mu} \frac{\Gamma}{\Gamma^0_{\text{photonic}}} B_{\text{max}}. \end{aligned} \tag{6.16}$$

The Z-dependence of upper limit of the branching ratio, Eq.(6.16), is calculated using $B_{\text{max}} = 4.2 \times 10^{-13}$ by MEG experiment [45]. Now, for simplicity, we take into account only A_L term of CLFV interaction. The dashed (blue) curve in Fig. 6.10-(b) shows the result of previous work [23]. Results of this work is shown in solid (red) curve and dotted (orange) curve taking into account $1S$ electrons and all bound electrons, respectively. From the improved estimation using relativistic Coulomb lepton wave function, the branching ratio $Br(\mu^- e^- \to e^- e^-)$ is about 10^{-19} for ^{208}Pb. The non-$1S$ bound electrons increase the branching ratio about 20%.

6.3 Distribution of Emitted Electrons

Next we estimate the energy and angular distribution of the electron calculated from the double differential decay rate in Eq. (4.24). This would be an important guide for search experiments to reduce backgrounds

by some kinematical cutoff. Here, we use a new dimensionless energy ϵ_1, instead of E_1, defined as

$$\epsilon_1 = \frac{E_1 - m_e}{E_{tot}^{\alpha_e} - 2m_e}, \tag{6.17}$$

which can be a value from 0 to 1 corresponding to $m_e < E_1 < E_{tot}^{\alpha_e} - m_e$.

Figs. 6.11-(a) and 6.11-(b) show $d\Gamma/d\epsilon_1/d\cos\theta_{12}$ for contact case (case 1) and photonic case (case 3), respectively. They contain contribution from only $1S$ electrons for the ^{208}Pb. The two final electrons are mainly emitted with the same energy in an opposite direction, since the momentum carried by the bound two leptons is minimized in this configuration.

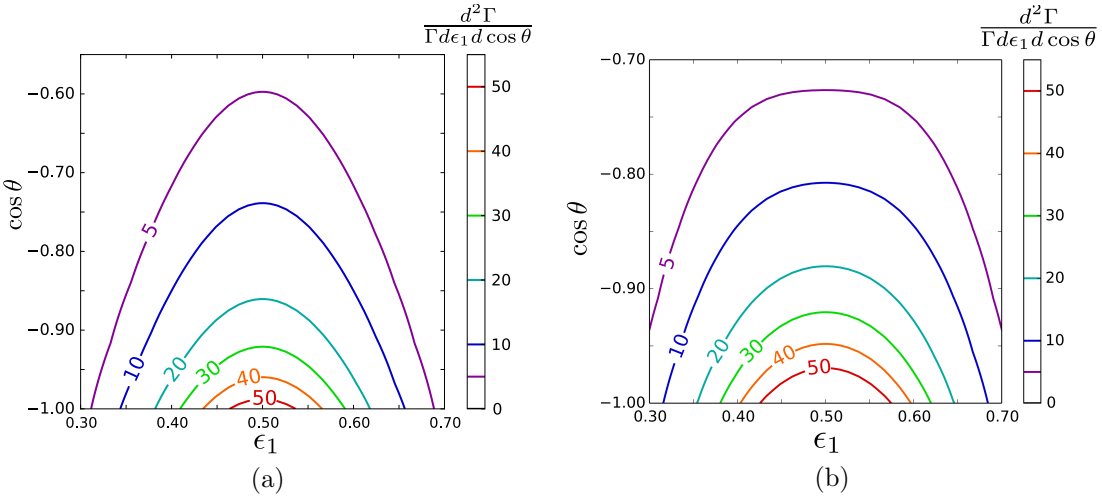

Figure 6.11: The energy and angular distribution of emitted electrons for ^{208}Pb by using g_1-type interaction (a) and A_L-type interaction (b). Figures taken from Ref. [34]. Copyright 2018 American Physical Society.

As seen in Fig. 6.11, the distribution of photonic case widens to the energy direction but shrinks in the angular direction, compared to that of contact case. That can be understood by checking carefully the difference of the distortion effect to different kinematics. As mentioned above, the most favored allotment of electron energy is the case of $\epsilon_1 = 0.5$, but the transition matrix is the most suppressed by final state distortion because the effective enhancement of local momentum of emitted electron makes a mismatch with photon momentum. On the other hand, let us consider a case where ϵ_1 is smaller or larger than 0.5. Although the suppression also occurs on the QED vertex with a bound electron, it is soften on the CLFV vertex with a bound muon where the momentum mismatch originally happens between an emitted electron and a photon. This is because the momentum mismatch is rather reduced by enhancement of the local electron momentum on the CLFV vertex. Moreover the shrink in the angular direction can be explained by each distortion effect to the transition matrix element with a partial wave of emitted electron. Generally, a distortion changes a wave function with a lower angular momentum more drastically. As Eq. (4.66), the θ_{12} distribution is described by the Legendre polynomials P_l, whose the subscript l typically indicates the angular momentum transfer between the different elements of the transition matrix. By the above discussion, it can be said that the coefficient of P_l with lower l is more suppressed than that with the higher l by final state distortion, which leads to the shrink of the distribution in the angular direction.

The electron energy spectrum normalized by decay rate $d\Gamma/d\epsilon_1/\Gamma$ and the angular distribution between the two electrons $d\Gamma/d\cos\theta_{12}/\Gamma$ are shown in Fig. 6.12 for cases 1-3. In both of these figures, the solid (red), dashed (black), and dash-dotted (green) curves indicate differential decay rates for case 1-3, respectively. The distributions for contact case 1 and 2 are almost the same, so we cannot read the discrepancy from the figures. However we can recognize that the distributions for photonic case 3 have different shapes from that for contact cases.

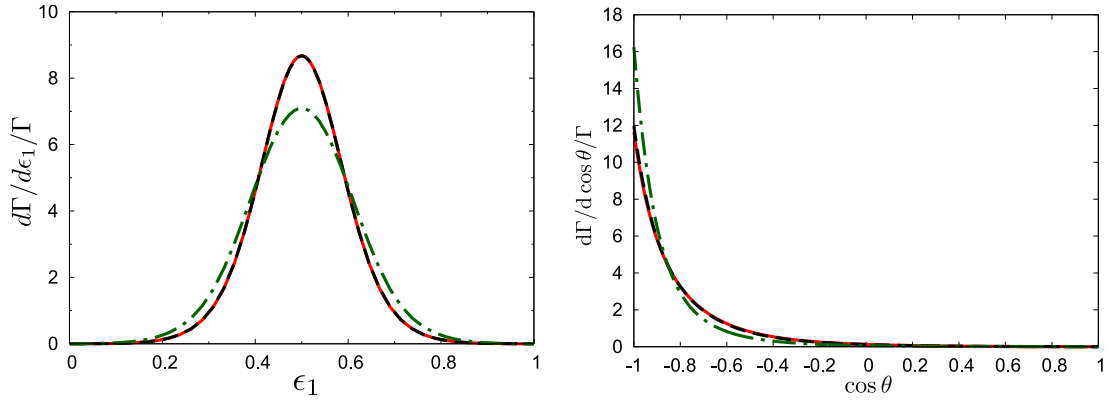

(a) (b)

Figure 6.12: The energy distribution (a) and angular distribution (b) for ^{208}Pb. The solid (red), dashed (black), and dash-dotted (green) curves correspond to model 1-3, respectively.

For the contact interaction that leads to the same chirality of final electrons, i.e., $g_1 \sim g_4$ terms of CLFV interaction (2.11), the Pauli principle prevents the final electron from having the same momentum. On the other hand, in g_5 and g_6 terms that lead to electrons with opposite chiralities, this does not apply. A difference between two interaction terms appears near $\cos\theta = 1$ as seen in Fig. 6.13. As shown so far, the detailed structure of the electron distribution depends on a kind of CLFV interaction. This result gives the possibility to identify the CLFV interaction by observing the energy-angular distribution of emitted electrons.

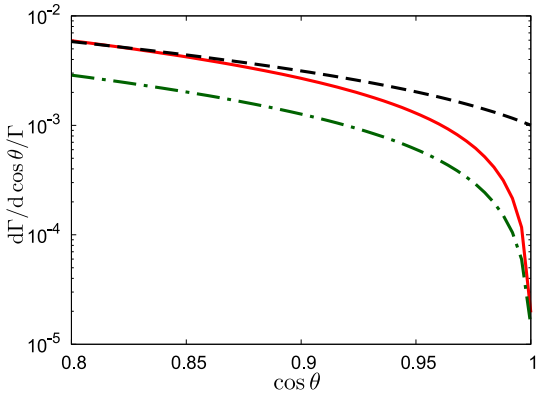

Figure 6.13: The angular distribution of emitted electrons for ^{208}Pb.

Even before the first CLFV signal is found, the information of the distribution is useful to discuss the reduction of experimental backgrounds. In a search for $\mu^- e^- \to e^- e^-$, the main background is expected to be accidental recombination of unrelated two electrons, such as electrons coming from DIO. Since the distribution of the signal electron pair is localized at $\epsilon_1 = 0.5$ and $\cos\theta_{12} = -1$, the restriction of the kinematical window in the search may be useful to reduce the accidental backgrounds. To present a material for discussing availability of the kinematical cut, we check how the efficiency of $\mu^- e^- \to e^- e^-$signal decreases by the prescription. Let us suppose to restrict the signal window to

$$\frac{1}{2} - \frac{\Delta\epsilon}{2} < \epsilon_1 < \frac{1}{2} + \frac{\Delta\epsilon}{2}, \tag{6.18}$$

and

$$-1 < \cos\theta_{12} < -1 + \Delta c. \tag{6.19}$$

When choosing these cut parameters as ($\Delta\epsilon$, Δc), how much ratio of total signal events can be detected is summarized in Table 6.12. For example, if the efficiency of 50% is needed, $(\Delta\epsilon, \Delta c) = (0.2, 0.5)$ is reasonable. So far we have assumed the rectangular signal window in ϵ_1-$\cos\theta_{12}$ plane. However it is necessary to discuss what the best shape is: e.g. the circular window could be better than the rectangular one.

Table 6.12: The ratio of detectable signals to the total $\mu^- e^- \to e^- e^-$events by using the cut parameters ($\Delta\epsilon$, Δc). The nucleus is supposed to be ^{208}Pb, and its charge distribution is taken as uniform. The second line corresponds to the case where electron pairs in the entire region are used to recombine $\mu^- e^- \to e^- e^-$events, and it should be unity.

$\Delta\epsilon$	1	0.3	0.3	0.3	0.2	0.2	0.2	0.1	0.1	0.1
Δc	2	0.5	0.25	0.1	0.5	0.25	0.1	0.5	0.25	0.1
Case 1 (g_1-type)	1.00	0.81	0.64	0.38	0.67	0.53	0.32	0.39	0.32	0.19
Case 2 (g_5-type)	1.00	0.81	0.65	0.39	0.67	0.54	0.33	0.39	0.32	0.19
Case 3 (A_L-type)	1.00	0.80	0.70	0.47	0.63	0.56	0.37	0.35	0.31	0.22

6.4 Asymmetry of Electron Angular Distribution from Polarized Muon

We study the asymmetry of electron angular distribution from polarized muon formulated in Chapter 5. The asymmetric distribution of electron is parity violating observable and the observable might be useful to further identify the nature of CLFV mechanism. We focus on the asymmetry coefficient α defined in Eq. (5.4). Here we take into account only the contribution of $1S$ bound electrons.

Since the mechanism of the asymmetry is not understood in a straight forward way, we examine the three models for bound state and scattering state wave functions as tabulated in Table 6.13.

Table 6.13: Models for the lepton wave functions.

Model	Bound state	Scattering state
I	NR-P	PLW
II	Rel-U	PLW
III	Rel-U	DW-U

At first, let us focus asymmetry obtained by using the g_1-type Lagrangian. Feature of this interaction is that two electrons in the finite state has the same chirality. The asymmetry α in model I (Non-relativistic bound state and plane wave scattering state) vanishes as shown by the dotted line in Fig. 6.14. Using the fact that g_1 term is contact interaction and emits electrons with the same chirality, the Pauli principle for the final electron pair requires that the transition amplitude is also anti-symmetric under the exchange of spins of bound muon and electron. Therefore the transition probability does not depend on spin direction of muon. This argument also applies the other contact interactions where the final electrons have the same chiralities. Explanation of this feature using explicit analytic formulae is given in Appendix H.1. Using Dirac equation with the finite size of the nucleus (Model II), α becomes actually non-zero values, shown by the dashed curve. Here the small components of bound leptons and the finite size of the nucleus play an important role. If we use point charge solution for both muon and electron bound state, α vanishes. This reason of vanishing is discussed in Appendix H.1 by using simple expressions. Finally, taking into account the distortion of final electrons (Model III), α is shown by the solid curve. The distortion of emitted electrons by the nuclear Coulomb potential gives just a small correction in this case.

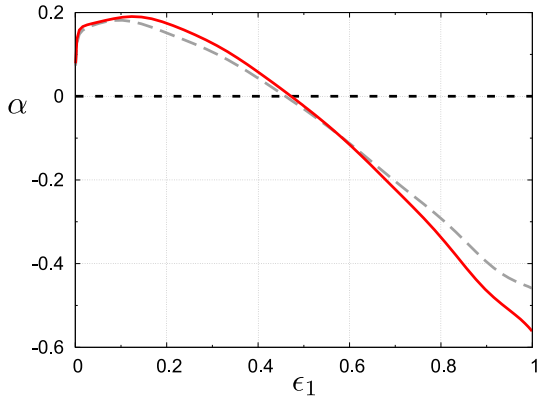

Figure 6.14: Energy dependence of the asymmetry factor α for g_1-type case. The nucleus is ^{208}Pb. The abscissa indicates the dimensionless energy ϵ_1. The dotted (black), dashed (gray), and solid (red) curves show α of model I-III, respectively.

Next, we focus on the g_5-type operator, where the emitted electrons have opposite chirality with each other. In contrast to g_1-type interaction, the asymmetry α is negative values even in model I, shown by the dotted curve in Fig. 6.15. Here due to orthogonal chirality of final electrons, the exchange term in Eq. (4.18) vanishes in the massless electron limit. For simplicity, g_5-type operator $\overline{e}_R\gamma_\mu\mu_R\overline{e}_L\gamma^\mu e_L$ can be converted into scalar-type operator $\overline{e}_L\mu_R\overline{e}_R e_L$ by the Fierz transformation. As seen in the form of this scalar-type operator, an electron coupled with muon should inherit information of the spin direction from muon. Since the electron is left-handed in g_5-type operator, the final electron has tendency to be emitted in the direction opposite to the muon polarization vector $\boldsymbol{P}$. The asymmetry factor in model II is described by the dashed curve. We can also see a drastic change of the energy dependence of α by including relativity of bound states. Since the small component of a fermion can be a spin component with the opposite direction to a spin of the large component, the relativistic effect changes the energy dependence of the asymmetry factor. The model III is shown by the solid curve, which including the distortion of emitted electrons. As in the g_1-type interaction, the effect of distortion affects α a little.

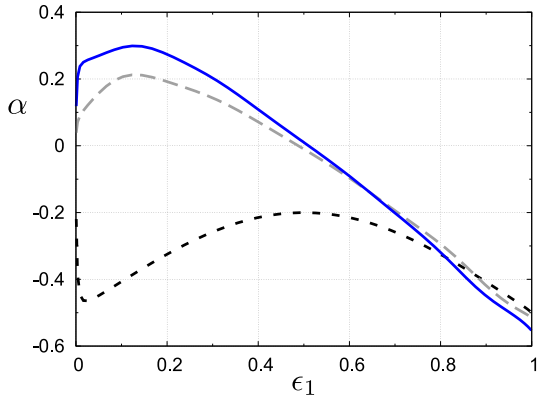

Figure 6.15: Energy dependence of the asymmetry factor α for g_5-type case. The nucleus is ^{208}Pb. The abscissa indicates the dimensionless energy ϵ_1. The dotted (black), dashed (gray), and solid (blue) curves show α of model I-III, respectively.

Fig. 6.16 shows the asymmetry factor on the A_R-type operator. The asymmetry factors in model I-III are plotted by the dotted, dashed, and solid curves, respectively. In the photonic interaction case, the distortion of emitted electrons plays a significant role.

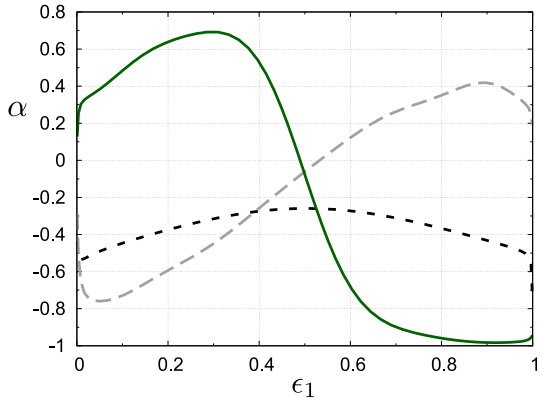

Figure 6.16: Energy dependence of the asymmetry factor α for A_R-type case. The nucleus is ^{208}Pb. The abscissa indicates the dimensionless energy ϵ_1. The dotted (black), dashed (gray), and solid (green) curves show α of model I-III, respectively.

The asymmetry coefficients for eight operators are summarized in Fig. 6.17. Eventually, we get finite values of α for all operators, which suggests that it is possible in principle to distinguish the chirality structure of CLFV interactions with parity violation by observing angular distribution of one emitted electron. According to the result, the sign of α corresponds to the chirality of muon: If the CLFV operator includes a right(left)-handed muon field, the sign of α for low and high E_1 is positive(negative) and negative(positive), respectively.

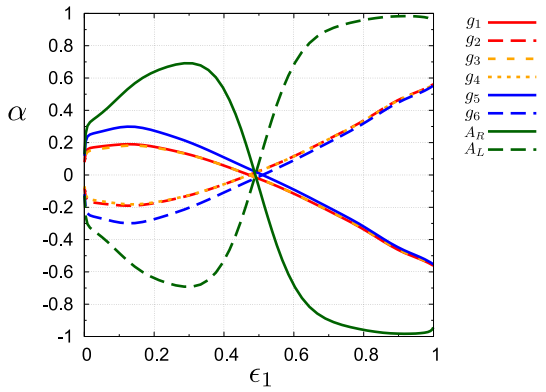

Figure 6.17: Energy dependence of the asymmetry factor α. The nucleus is ^{208}Pb. The abscissa indicates the dimensionless energy ϵ_1. Each of curves corresponds to case of single operator dominance hypothesis. Refer to the legend for what operator is supposed to be dominant.

Let us add discussion on the $\boldsymbol{P} \cdot (\hat{p}_1 \times \hat{p}_2)$ in Eq. (5.1). This observable is parity-even but CP-odd, so $\tilde{F}$ is non-zero when CP violates. $\tilde{F}$ vanishes if the emitted electrons are taken as plane wave, as long as we have assumed no CP violation of CLFV interaction. However, it is known that this type of CP violating observable is non-zero due to the final state interaction [106]. In our case the distortion of emitted electrons makes $\tilde{F}$ non-zero. Fig. 6.18 show the function $\tilde{F}$ when $\cos\theta_{12} = -1$. Since the $\boldsymbol{P} \cdot (\hat{p}_1 \times \hat{p}_2)$ is parity-even, $\tilde{F}$ of g_1 is the same as that of g_2. As shown in Fig. 6.18, $\tilde{F}$ is largest value in photonic case. The amplitude of $\tilde{F}$ is of order $\mathcal{O}\left(10^{-1}\right)$. It will be important in the future search for CP violation of CLFV interaction to notice that final state interaction should be properly included to avoid the spurious CP violating effect.

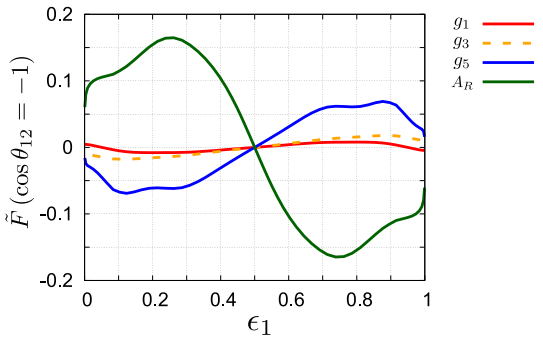

Figure 6.18: CP violating factor $\tilde{F}$ on $\cos\theta_{12} = -1$. The nucleus is ^{208}Pb. The abscissa indicates the dimensionless energy ϵ_1. Each of curves corresponds to case of single operator dominance hypothesis. Refer to the legend for what operator is supposed to be dominant.

6.5 Model Distinguishment

Once the CLFV processes is found in future, apparent question is what is the mechanism of lepton flavor violation. It is an interesting question whether we can/cannot find experimental observables to distinguish types of interactions. We discuss distinguishment of CLFV operators based on the analysis on $\mu^- e^- \to e^- e^-$ presented in the previous sections.

The first useful observable is the atomic number dependence of the decay rate, which shown in Fig. 6.19. Here, in addition to the cases defined in Eqs. (6.7)-(6.9), we have introduced the extra case

4. both of contact and photonic interactions

$$g_1 = 100 A_L \neq 0, \quad A_R = 0, \text{ and } g_{j\neq 1} = 0. \tag{6.20}$$

We have chosen $g_1/A_L = 100$ in the case 4, while $g_1/A_L \sim 270$ using the current upper limits of A_L and g_1. The ratios of the cases 1 (in a solid line) and 2 (in a dashed line) strongly increase as Z. One would need precise measurements to discriminate the case 1 from 2. On the other hand, the case 3 exhibits a moderately increase as Z. We may expect the contribution from both the photonic and the contact interactions in the case 4 and the Z-dependence is drawn as a dotted line in Fig. 6.19. Thus one of possibilities to distinguish the CLFV interactions is the Z-dependence of $\mu^- e^- \to e^- e^-$decay rate.

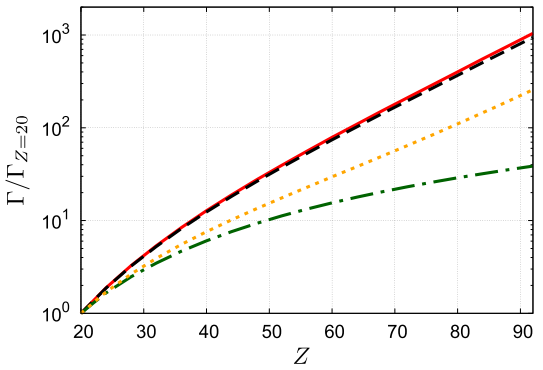

Figure 6.19: Z-dependence of $\mu^- e^- \to e^- e^-$generated by four different models. They are normalized by the rate for $Z = 20$. A solid red line shows the case 1, a dashed black line shows the case 2, a dash-dotted green one shows the case 3, and a dotted orange one shows the case 4. Figure taken from Ref. [34]. Copyright 2018 American Physical Society.

The second possibility is the energy and angular distribution of emitted electrons. As mentioned in Section 6.3, the energy-angular distribution is different between contact and photonic cases. The g_1- and g_5-type operator gives different distribution in principle, but the difference is little and it requires a very careful measurement.

By using the first and second methods, the Z-dependence of CLFV decay rate and the energy and angular distribution of emitted electrons, we could identify the contact and photonic operators clearly. Moreover, the g_1- and g_5-type operators exhibit a small difference in Z-dependence and angular distribution and precise measurement of these observables one may able to distinguish two types of interactions. So far, one cannot distinguish the g_1 term from the g_2 term by using these observables. In summary, we can identify three types of interaction, $g_1 - g_4$ type, $g_5 - g_6$ type and photonic interactions but it is difficult to identify the chiral structure of the CLFV interaction.

Finally, the third method is to observe the angular asymmetry of electron emission with polarized muon. Observation of non-zero asymmetry coefficient provides us clear evidence of parity violation of the CLFV operator. Our analysis have shown that all parity-violating operator has a finite asymmetry for an emitted electron. The asymmetry reflects the chiral structure of the CLFV interaction. Therefore, for example, g_1- and g_2-type operators could be identified by observing the sign of the asymmetry. Since the asymmetry factors for g_1-, g_3-, g_5-, and A_R-type interactions have the similar energy dependence, the careful investigation is needed to distinguish them by the asymmetry difference. The interpretation of the asymmetry is not straightforward but it depends on relativistic treatment and final state interaction. Therefore careful analysis such as done in this work is important. It is noticed further that the asymmetry is zero around the two-electrons have the same energy, where the rate is maximum. Therefore to measure asymmetry one has to observe events slightly away from the most favorable kinematics.

Chapter 7

Conclusions

We have analyzed the $\mu^- e^- \to e^- e^-$ CLFV process in muonic atoms. Coulomb interaction of leptons with finite nuclear charge distributions is taken into account by using the standard multipole expansion formalism and the numerical solutions of Dirac equations for both the electron and muon wave functions. The effects of Coulomb distortion of the emitted electron and relativistic treatments of the bound leptons are very important for quantitative estimations of the decay rate. The effects of improvement is significant for heavier atoms. When contact interaction is dominant, enhancements of the decay rates of about nine(14) times for ^{208}Pb(^{238}U), respectively, compared with the previous analysis are obtained due to the enhanced overlap integrals of the lepton wave functions. While, when photonic interaction is dominant, the decay rate is suppressed about a quarter for ^{208}Pb.

We also found that different operators of the CLFV interaction generate sizable difference in the Z-dependence of the decay rate and also the angular distribution of the emitted electrons. This is because the distortion of final electrons plays different roles between contact and photonic processes. The asymmetric angular distribution of electron form the polarized muon shows strong dependence on the chiral structure of the CLFV interaction. These results provide us a possibility to investigate a detailed nature of CLFV interaction by observation for the $\mu^- e^- \to e^- e^-$process.

In this thesis, we have not studied the possibility of several kind of CLFV interactions, which involves interference among the amplitudes. It would be so interesting to research the property of interference. For some model, contact and photonic processes are predicted to have similar strength. In that case, for example, Z-dependence of the transition probability could exhibit characteristic behavior.

Our detailed analysis of angular and energy distribution of electrons in addition to the total decay rate will be useful for simulation to search for the best configuration to catch the signal events.

Appendix A

Notations

In this appendix, the notations used throughout this thesis are summarized.

A.1 Unit

We use the natural unit, so that

$$c = \hbar = \epsilon_0 = 1, \tag{A.1}$$

where c, $\hbar$, and ϵ_0 indicate the speed of light, the Dirac constant (reduced Planck constant), and the dielectric constant of vacuum, respectively. The Heaviside-Lorentz convention is used so that the fine structure constant is given as

$$\alpha_{em} = \frac{e^2}{4\pi} \simeq \frac{1}{137}, \tag{A.2}$$

where e is the elementary charge.

A.2 Metric

The Minkovski metric used in relativity is set as

$$g_{\mu\nu} = g^{\mu\nu} = \begin{pmatrix} 1 & 0 & 0 & 0 \\ 0 & -1 & 0 & 0 \\ 0 & 0 & -1 & 0 \\ 0 & 0 & 0 & -1 \end{pmatrix}. \tag{A.3}$$

A.3 Dirac Matrix

When writing down the Dirac matrices or four-component spinors in this thesis, we use the Dirac representation:

$$\gamma^0 = \begin{pmatrix} \mathbf{1}_2 & 0 \\ 0 & -\mathbf{1}_2 \end{pmatrix}, \quad \gamma^i = \begin{pmatrix} 0 & \sigma_i \\ -\sigma_i & 0 \end{pmatrix} \quad (i = 1, 2, 3), \tag{A.4}$$

where $\mathbf{1}_2$ is the 2×2 identity matrix and σ_is are the Pauli matrices,

$$\sigma_1 = \begin{pmatrix} 0 & 1 \\ 1 & 0 \end{pmatrix}, \quad \sigma_2 = \begin{pmatrix} 0 & -i \\ i & 0 \end{pmatrix}, \quad \sigma_3 = \begin{pmatrix} 1 & 0 \\ 0 & -1 \end{pmatrix}. \tag{A.5}$$

Also, we use $\alpha_i = \gamma^0\gamma^i$ and $\beta = \gamma^0$, which can be written as

$$\alpha_i = \begin{pmatrix} 0 & \sigma_i \\ \sigma_i & 0 \end{pmatrix}, \quad \beta = \begin{pmatrix} \mathbf{1}_2 & 0 \\ 0 & -\mathbf{1}_2 \end{pmatrix}. \tag{A.6}$$

The chirality operator γ_5 is represented as

$$\gamma_5 = i\gamma_0\gamma_1\gamma_2\gamma_3 \tag{A.7}$$

$$= \begin{pmatrix} 0 & \mathbf{1}_2 \\ \mathbf{1}_2 & 0 \end{pmatrix}. \tag{A.8}$$

The projections for left-handed and right-handed component are defined as

$$P_L = \frac{1-\gamma_5}{2}$$

$$= \frac{1}{2}\begin{pmatrix} \mathbf{1}_2 & -\mathbf{1}_2 \\ -\mathbf{1}_2 & \mathbf{1}_2 \end{pmatrix}, \tag{A.9}$$

$$P_R = \frac{1+\gamma_5}{2}$$

$$= \frac{1}{2}\begin{pmatrix} \mathbf{1}_2 & \mathbf{1}_2 \\ \mathbf{1}_2 & \mathbf{1}_2 \end{pmatrix}, \tag{A.10}$$

respectively.

A.4 Field Theory

Generally, a Dirac field operator ℓ in a time-independent potential is expanded as

$$\ell(x) = \sum_{s=\uparrow,\downarrow}\left[\int \frac{d^3p}{(2\pi)^3}\frac{1}{\sqrt{2p^0}}\left\{a_\ell^{\boldsymbol{p},s}\psi_\ell^{\boldsymbol{p},s}(\boldsymbol{r}) + b_\ell^{\boldsymbol{p},s\dagger}\phi_\ell^{\boldsymbol{p},s}(\boldsymbol{r})\right\}\right.$$

$$\left. + \sum_\alpha a_\ell^{\alpha,s}\psi_\ell^{\alpha,s}(\boldsymbol{r}) + \sum_{\alpha'} b_\ell^{\alpha',s\dagger}\phi_\ell^{\alpha',s}(\boldsymbol{r})\right]\exp\left(-ip^0t\right). \tag{A.11}$$

Here the first and second terms correspond to continuum and discrete states, respectively, and $\boldsymbol{p}$ and α are their indices. Also, ψ_ℓs (ϕ_ℓs) and a_ℓs (b_ℓs) indicate the wave functions and annihilation operators for the positive (negative) energy solutions of the Dirac equation, respectively.

The state that one scattering particle ℓ exists, $|\ell_p\rangle$, is described as

$$|\ell_p^s\rangle = \sqrt{2p^0}a_\ell^{\boldsymbol{p},s\dagger}|0\rangle, \tag{A.12}$$

where $|0\rangle$ indicates the vacuum. For a bound particle, we also set

$$|\ell_\alpha^s\rangle = a_\ell^{\alpha,s\dagger}|0\rangle. \tag{A.13}$$

Corresponding to the above definition, the normalizations of ψ_ℓs are determined as

$$\int d^3r\psi_\ell^{\boldsymbol{p},s\dagger}(\boldsymbol{r})\psi_\ell^{\boldsymbol{p}',s'}(\boldsymbol{r}) = 2p^0(2\pi)^3\delta^{(3)}(\boldsymbol{p}-\boldsymbol{p}')\delta_{s,s'}, \tag{A.14}$$

$$\int d^3x\psi_\ell^{\alpha,s\dagger}(\boldsymbol{r})\psi_\ell^{\alpha',s'}(\boldsymbol{r}) = \delta_{\alpha,\alpha'}\delta_{s,s'}, \tag{A.15}$$

and a_ℓ satisfy the following anti-commutation relation:

$$\left\{a_\ell^{\boldsymbol{p},s}, a_\ell^{\boldsymbol{p}',s'\dagger}\right\} = (2\pi)^3\delta^{(3)}(\boldsymbol{p}-\boldsymbol{p}')\delta_{s,s'}, \tag{A.16}$$

$$\left\{a_\ell^{\alpha,s}, a_\ell^{\alpha',s'\dagger}\right\} = \delta_{\alpha,\alpha'}\delta_{s,s'}. \tag{A.17}$$

A.5 Other Abbreviations

For simplicity, we sometimes use the square brackets as

$$[j_1 \cdot j_2 \cdot \cdots \cdot j_n] = (2j_1 + 1)\,(2j_2 + 1) \cdots (2j_n + 1)\,. \tag{A.18}$$

Appendix B

Useful Special Functions

B.1 Spherical Bessel Function

The spherical Bessel function is a solution of the differential equation

$$\frac{d^2f}{dr^2} + \frac{2}{r}\frac{df}{dr} + \left\{1 - \frac{l(l+1)}{r^2}\right\} f = 0. \tag{B.1}$$

Of two kinds of linearly independent solutions, the regular solution $j_l(r)$ is called as the spherical Bessel function, while the solution irregular at the origin $n_l(r)$ is called as the spherical Neumann function. The linear combination $h_l^{(1)}(r) = j_l(r) + in_l(r)$ is called as the spherical Hankel function of the first kind, and $h_l^{(2)}(r) = j_l(r) - in_l(r)$ is called as the spherical Hankel function of the second kind. Therefore the $j_l(z)$ is represented by $h_l^{(1)}(r)$ and $h_l^{(2)}(r)$ as

$$j_l(z) = \frac{h_l^{(1)}(z) + h_l^{(2)}(z)}{2}. \tag{B.2}$$

Their asymptotic forms near the origin are given as

$$j_l(z) \overset{z\to 0}{\to} \frac{1}{(2l+1)!!} z^l, \tag{B.3}$$

$$n_l(z) \overset{z\to 0}{\to} (2l+1)!! \frac{-1}{z^{l+1}}, \tag{B.4}$$

where $(2l+1)!! = (2l+1)(2l-1)\cdots 5\cdot 3\cdot 1$. On the other hand, their asymptotic behaviors at $|z| \to \infty$ are represented as

$$j_l(z) \overset{z\to\infty}{\to} \frac{1}{z}\cos\left(z - \frac{l+1}{2}\pi\right), \tag{B.5}$$

$$n_l(z) \overset{z\to\infty}{\to} \frac{1}{z}\sin\left(z - \frac{l+1}{2}\pi\right), \tag{B.6}$$

$$h_l^{(1)}(z) \overset{z\to\infty}{\to} (-i)^{n+1}\frac{e^{iz}}{z}, \tag{B.7}$$

$$h_l^{(2)}(z) \overset{z\to\infty}{\to} i^{n+1}\frac{e^{-iz}}{z}. \tag{B.8}$$

The spherical Bessel functions have the following symmetry under flipping the sign of its argument, $z = -z$:

$$j_n(-z) = (-1)^n j_n(z), \tag{B.9}$$

$$h_n^{(2)}(-z) = (-1)^n h_n^{(1)}(z). \tag{B.10}$$

Derivative of the spherical Bessel functions can be represented as

$$\frac{d}{dr}\mathfrak{j}_n(r) = \frac{n}{r}\mathfrak{j}_n(r) - \mathfrak{j}_{n+1}(r) \tag{B.11}$$

$$= \mathfrak{j}_{n-1}(r) - \frac{n+1}{r}\mathfrak{j}_n(r), \tag{B.12}$$

where $\mathfrak{j}_l(r)$ indicates all of the spherical Bessel, Neumann, and Hankel functions.

B.2 Confluent Hypergeometric Function

The confluent hypergeometric function ${}_1F_1(a,b;z)$ satisfies the Kummer's differential equation,

$$z\frac{d^2f}{dz^2} + (b-z)\frac{df}{dz} - af = 0. \tag{B.13}$$

At $z \sim 0$, this equation (B.13) reduces to

$$z\frac{d^2f}{dz^2} + b\frac{df}{dz} = 0. \tag{B.14}$$

Therefore there are two independent solutions, which behaves as z^0 and z^{1-b} near the origin. The solution of z^0 is the confluent hypergeometric function ${}_1F_1(a,b;z)$, normalized to be ${}_1F_1(a,b;0) = 1$.

${}_1F_1(a,b;z)$ has the power series near the origin,

$${}_1F_1(a,b;z) = 1 + \frac{a}{b}z + \frac{a(a+1)}{b(b+1)}\frac{z^2}{2!} + \mathcal{O}\left(z^3\right). \tag{B.15}$$

Moreover the confluent hypergeometric function satisfies the following relations:

$$\frac{d}{dz}{}_1F_1(a,b;z) = \frac{a}{b}{}_1F_1(a,b;z) \tag{B.16}$$

$$= \frac{a-b}{b}{}_1F_1(a,b+1;z) + {}_1F_1(a,b;z), \tag{B.17}$$

$$e^{-z/2}{}_1F_1(a,b;z) = e^{z/2}{}_1F_1(-a+b,b;-z), \tag{B.18}$$

$$z{}_1F_1(a+1,b+1;z) = b\left[{}_1F_1(a+1,b;z) - {}_1F_1(a,b;z)\right]. \tag{B.19}$$

Appendix C

Muonic Atom

In this appendix, we outline phenomenology of muons and muonic atoms.

C.1 Muon

Here, let us describe the nature of muon. Except for its mass, a muon has nearly the same properties as an electron, so that it is a fermion with the same electric charge as an electron. The mass of a muon and of an electron are

$$m_\mu = 105.6583715(35)\ [\mathrm{MeV}], \tag{C.1}$$
$$m_e = 0.510998928(11)\ [\mathrm{MeV}], \tag{C.2}$$

and its mass ratio m_μ/m_e is about 207 [63].

C.1.1 Decays

The most important property of muons different from electrons is that muons are unstable and decay into lighter particles. A negative and positive muon decays into an electron and two neutrinos as

$$\mu^- \to e^- \nu_\mu \overline{\nu}_e, \tag{C.3}$$
$$\mu^+ \to e^+ \overline{\nu}_\mu \nu_e, \tag{C.4}$$

respectively. The decay is called as the Michel decay [107].

The muon decay is described by four-Fermi interaction,

$$\mathcal{L}_{\mathrm{Fermi}} = -\frac{4G_F}{\sqrt{2}} \left(\overline{\nu}_\mu \gamma^\mu P_L \mu\right) \left(\overline{e} \gamma_\mu P_L \nu_e\right) + [H.c.], \tag{C.5}$$

where G_F is the Fermi constant. In the SM, it is represented as

$$G_F = \frac{g^2}{4\sqrt{2} m_W^2}, \tag{C.6}$$

at tree level. Here g is the $SU(2)_L$ gauge coupling constant and m_W is the mass of W boson. The value of the Fermi constant is $G_F = 1.166 \times 10^{-5} \mathrm{GeV}^{-2}$. In terms of those parameters, the lifetime of free muon is written as

$$\tau_\mu = 192\pi^3/(G_F^2 m_\mu^5). \tag{C.7}$$

The experimental value is $2.1969811(22) \times 10^{-6}$s [63].

C.2 Muonic Atom

When a negative muon stops in a material, it is trapped by a nucleus and forms an "atom" while some electrons are knocked out. This is called a muonic atom. Just after the muon being captured by the nuclear Coulomb field, it is in a high excited state, $n \approx 14$. However, since the Pauli exclusion rule is not applied between a muon and any electrons, the muon cascades down to $1S$ state rapidly while photons and Auger electrons are emitted [108].

Since a muon has 207 times heavier than an electron, the Bohr radius of a muon is 1/207 of that of an electron. In other words, the muon is localized very close to the nucleus, its wave function is greatly affected by the charge distribution of the nucleus which could not be a problem in the case of the electron.

C.2.1 Decays

As mentioned above, the lifetime of free muons is about 2.2 ms. However, in the case of muonic atoms, in addition to the Michel decay of the muon on orbit (Decay In Orbit, DIO), the process that a proton in the nucleus captures the muon,

$$\mu^- p \to \nu_\mu n, \tag{C.8}$$

also occurs. Using the decay rate Γ_c due to the muonic capture of a proton and the decay rate Γ_d due to the Michel decay, the total decay rate of muonic atoms Γ_t is expressed as

$$\Gamma_t = \Gamma_c + Q\Gamma_d. \tag{C.9}$$

Here Q is called as Huff factor, which describes the effect of decreasing the Michel decay rate of bound muons as compared to free muons. Now, there are three conceivable effects as the cause that the decay rate of bound muons changes from that of free muons. First effect is due to the phase space of the final state suppressed by the bound energy of the muon, which make the decay rate smaller. Secondly, it should be also considered that the wave function of the final state electron is attracted by the nuclear Coulomb potential, and the overlap with the muon wave function becomes large. This effect leads to an increase in decay rate. As the third effect, there is also a relativistic time lag due to bound muons moving at the average velocity $Z\alpha_{em}$, which also has the effect of lowering the decay rate. When considering the energy spectrum of emitted electrons, this effect of relativistic time delay is much smaller than those of the previous two. However, when calculating the total decay rate, unless electrons can not escape the Coulomb potential, the first and second of these three effects are almost canceled because of the electromagnetic gauge symmetry [26, 109]. Therefore, the Michel decay of a muon bound to nuclei whose atomic number is not so large is mainly suppressed by relativistic time lag. The energy distribution of DIO electron for a various muonic atom is given in Ref. [28]. After Ref. [28], there have been some improvement to include the nuclear recoil effect and the QED radiative correction [59, 110, 111, 60].

Next let us consider the reaction in which muons are absorbed in nuclei. If the atomic nucleus is taken as a point charge, the radius of the wave function of the bound muon decreases as Z^{-1}. As a result, the value at the origin of the muon wave function increases in proportion to Z^3. Also, since the number of proton, which can capture muon, also increases in proportion to Z, of course, the decay rate of the muon capture process is roughly expected to be proportional to Z^4. However, taking into account the finite volume of the nucleus, the most part of the bound muon wave function could overlap the nucleus. For this reason, it is convenient to use the effective proton number Z_{eff} to consider the nuclear finite volume. Z_{eff} is defined as [112, 113]

$$Z_{eff} = Z \left[\int d^3r \left|\psi_\mu(\boldsymbol{r})\right|^2 \mathcal{D}(\boldsymbol{r}) \right]^{1/4}. \tag{C.10}$$

Moreover, since general nuclei have more neutrons than protons, the Pauli exclusion principle restricts transitions from protons to neutrons. Taking into account that the reaction rate is reduced by this effect, the

muon capture rate of a proton is rewritten as [114]

$$\Gamma_c = Z_{eff}^4 X_1 \left[1 - X_2 \left(\frac{A-Z}{2A}\right)\right]. \tag{C.11}$$

Here, the first parameter X_1 denotes the muon capture rate for muonic hydrogens, and the second one X_2 is the effect of decreasing the rate by the exclusion principle. These values are determined as

$$X_1 = 170 \left[\mathrm{s}^{-1}\right], \quad X_2 = 3.125, \tag{C.12}$$

by experiments.

For the total decay rate of muonic atoms, Γ_t, the contribution of the muon decay in orbit, $Q\Gamma_d$, is major when the atomic number is small, but as the atomic number increases, the contribution of the capture process by the nucleus, Γ_c, becomes dominant. The Z-dependence of the measured lifetime is as shown in Fig. C.1. The lifetime of muonic hydrogens is almost the same as that of free muon, which is about 2.2 ms, but in the case of muonic leads where the capture process dominates, it is about 82 ns [115].

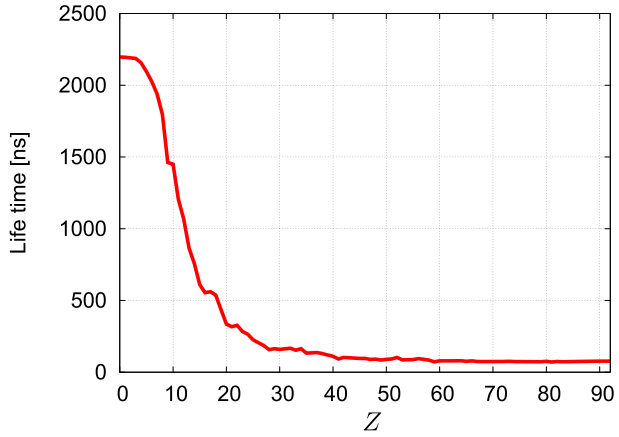

Figure C.1: Mean lifetimes of a muonic atom with atomic number Z [115]

.

Appendix D

Solution for Dirac Equation with Point-Charge Coulomb Potential

This appendix describes the way to obtain the analytic solution of the Dirac equation with point-charge Coulomb potential $\psi(r) = (Ze)/(4\pi r)$ [108, 116].

The coupled equation to solve here is

$$\frac{dg_\kappa(r)}{dr} + \frac{1+\kappa}{r} g_\kappa(r) - (E + m + \frac{Z\alpha_{em}}{r}) f_\kappa(r) = 0, \tag{D.1}$$

$$\frac{df_\kappa(r)}{dr} + \frac{1-\kappa}{r} f_\kappa(r) + (E - m + \frac{Z\alpha_{em}}{r}) g_\kappa(r) = 0, \tag{D.2}$$

which is derived from Eqs. (E.23)-(E.24) in Appendix E, by choosing $\psi(r) = (Ze)/(4\pi r)$. For convenience, let us define new functions G and F as

$$G = r g_\kappa(r), \tag{D.3}$$

$$F = r f_\kappa(r), \tag{D.4}$$

respectively, and the coupled equation is rewritten as

$$\frac{dG}{dr} + \frac{\kappa}{r} G - \left(E + m + \frac{Z\alpha_{em}}{r} \right) F = 0, \tag{D.5}$$

$$\frac{dF}{dr} - \frac{\kappa}{r} F + \left(E - m + \frac{Z\alpha_{em}}{r} \right) G = 0. \tag{D.6}$$

This equation has both of solutions with discrete and continuum spectrum, and they are called as bound solutions and scattering solutions, respectively. We show those derivations in order below.

D.1 Bound State

In this section, we describe the method for finding the bound solutions and its energies of Eq (D.5)-(D.6).

First, let us consider a behavior of Eqs. (D.5)-(D.6) in the region where r is small. Assuming that $(E \pm m)$ is negligible compared to $Z\alpha_{em}/r$, Eqs. (D.5)-(D.6) become

$$\frac{dG}{dr} + \frac{\kappa}{r} G - \frac{Z\alpha_{em}}{r} F = 0, \tag{D.7}$$

$$\frac{dF}{dr} - \frac{\kappa}{r} F + \frac{Z\alpha_{em}}{r} G = 0, \tag{D.8}$$

respectively. Suppose that both of $G_\kappa(r)$ and $F_\kappa(r)$ are analytic near the origin, the lowest order of its Taylor expansion is a leading term. Let γ be the lowest order, and represent $G \sim ar^\gamma$, $F \sim br^\gamma$ where a and b are constants. Inserting them into Eq. (D.7)-(D.8), we can get

$$a\gamma r^{\gamma-1} + \kappa a r^{\gamma-1} - Z\alpha_{em} b r^{\gamma-1} = 0, \tag{D.9}$$

$$b\gamma r^{\gamma-1} - \kappa b r^{\gamma-1} + Z\alpha_{em} a r^{\gamma-1} = 0, \tag{D.10}$$

which lead to the relation of γ, a, and b,

$$\begin{pmatrix} \gamma+\kappa & -Z\alpha_{em} \\ Z\alpha_{em} & \gamma-\kappa \end{pmatrix} \begin{pmatrix} a \\ b \end{pmatrix} = 0. \tag{D.11}$$

The condition that both a and b can have finite values is

$$\begin{vmatrix} \gamma+\kappa & -Z\alpha_{em} \\ Z\alpha_{em} & \gamma-\kappa \end{vmatrix} = \gamma^2 - \kappa^2 + (Z\alpha_{em})^2 = 0, \tag{D.12}$$

or,

$$\gamma = \pm\sqrt{\kappa^2 - (Z\alpha_{em})^2}. \tag{D.13}$$

Now, assuming $Z\alpha_{em} \approx Z/137 < 1$, it is guaranteed that γ is a real number. Moreover, according to the definition of γ, γ should be positive to obtain a regular solution. Here, we choose positive one,

$$\gamma = \sqrt{\kappa^2 - (Z\alpha_{em})^2}, \tag{D.14}$$

and let us consider the regular solution of the coupled equation (D.5)-(D.6).

Before beginning to solve Eqs. (D.5)-(D.6), let us define

$$\rho = 2\lambda r, \tag{D.15}$$

$$\lambda = \sqrt{m^2 - E^2}. \tag{D.16}$$

Since $d/dr = 2\lambda d/d\rho$, Eqs. (D.5)-(D.6) become

$$\frac{dG(\rho)}{d\rho} = -\frac{\kappa G(\rho)}{\rho} + \left[\frac{m+E}{2\lambda} + \frac{Z\alpha_{em}}{\rho}\right] F(\rho), \tag{D.17}$$

$$\frac{dF(\rho)}{d\rho} = \left[\frac{m-E}{2\lambda} - \frac{Z\alpha_{em}}{\rho}\right] G(\rho) + \frac{\kappa F(\rho)}{\rho}. \tag{D.18}$$

Now, research the behavior of $G(\rho)$ and $F(\rho)$ at $\rho \to \infty$. If ρ is sufficiently large, $1/\rho$ terms can be neglected, it reduces to

$$\frac{dG(\rho)}{d\rho} = \frac{E+m}{2\lambda} F(\rho), \tag{D.19}$$

$$\frac{dF(\rho)}{d\rho} = -\frac{E-m}{2\lambda} G(\rho). \tag{D.20}$$

Connecting them, it is found that

$$\begin{aligned} \frac{d^2G(\rho)}{d\rho^2} &= \frac{m^2-E^2}{4\lambda^2} G(\rho) \\ &= \frac{1}{4} G(\rho). \end{aligned} \tag{D.21}$$

Therefore it can be expected that $G(\rho) \sim e^{\pm\rho/2}$ at sufficiently large ρ. Here we exclude the solution of $e^{\rho/2}$, which diverges at infinity. We can also obtain the similar result for $F(\rho)$. Now assuming that G and F can be represented by linear combination of certain functions $\phi_1(\rho)$ and $\phi_2(\rho)$:

$$G(\rho) = \sqrt{m+E}e^{-\rho/2}\left(\phi_1(\rho) + \phi_2(\rho)\right), \tag{D.22}$$

$$F(\rho) = \sqrt{m-E}e^{-\rho/2}\left(\phi_1(\rho) - \phi_2(\rho)\right). \tag{D.23}$$

After substituting them into (D.17)-(D.18), we have

$$\frac{d}{d\rho}(\phi_1+\phi_2) = \left(\frac{1}{2} - \frac{\kappa}{\rho}\right)(\phi_1+\phi_2) + \left[\frac{m+E}{2\lambda} + \frac{Z\alpha_{em}}{\rho}\right]\frac{m-E}{\lambda}(\phi_1-\phi_2), \tag{D.24}$$

$$\frac{d}{d\rho}(\phi_1-\phi_2) = \left[\frac{m-E}{2\lambda} - \frac{Z\alpha_{em}}{\rho}\right]\frac{m+E}{\lambda}(\phi_1+\phi_2) + \left(\frac{1}{2} + \frac{\kappa}{\rho}\right)(\phi_1-\phi_2), \tag{D.25}$$

or

$$\frac{d\phi_1}{d\rho} = \left(1 - \frac{Z\alpha_{em}E}{\lambda\rho}\right)\phi_1 - \left(\frac{\kappa}{\rho} + \frac{Z\alpha_{em}m}{\lambda\rho}\right)\phi_2, \tag{D.26}$$

$$\frac{d\phi_2}{d\rho} = \left(-\frac{\kappa}{\rho} + \frac{Z\alpha_{em}m}{\lambda\rho}\right)\phi_1 + \frac{Z\alpha_{em}E}{\lambda\rho}\phi_2. \tag{D.27}$$

Here, suppose that ϕ_1 and ϕ_2 can be expanded in power series. As shown above, the lowest order of power expansion of G and F are λ. Let us factor it out to write

$$\phi_1 = \rho^\lambda \sum_{i=0}^{\infty} \alpha_i \rho^i, \tag{D.28}$$

$$\phi_2 = \rho^\lambda \sum_{i=0}^{\infty} \beta_i \rho^i. \tag{D.29}$$

Substituting them into Eqs. (D.26)-(D.27), we obtain

$$\sum_i \alpha_i(i+\gamma)\rho^{i+\gamma-1} = \sum_i \alpha_i \rho^{i+\gamma} - \frac{Z\alpha_{em}E}{\lambda}\sum_i \alpha_i\rho^{i+\gamma-1} - \left(\kappa + \frac{Z\alpha_{em}m}{\lambda}\right)\sum_i \beta_i\rho^{i+\gamma-1}, \tag{D.30}$$

$$\sum_i \beta_i(i+\gamma)\rho^{i+\gamma-1} = \left(-\kappa + \frac{Z\alpha_{em}m}{\lambda}\right)\sum_i \alpha_i\rho^{i+\gamma-1} + \frac{Z\alpha_{em}E}{\lambda}\sum_i \beta_i\rho^{i+\gamma-1}. \tag{D.31}$$

Therefore the following relation is given by comparing coefficients of the left and right hand side:

$$(i+\gamma)\alpha_i = \alpha_{i-1} - \frac{Z\alpha_{em}E}{\lambda}\alpha_i - \left(\kappa + \frac{Z\alpha_{em}m}{\lambda}\right)\beta_n, \tag{D.32}$$

$$(i+\gamma)\beta_i = \left(-\kappa + \frac{Z\alpha_{em}m}{\lambda}\right)\alpha_i + \frac{Z\alpha_{em}E}{\lambda}\beta_i. \tag{D.33}$$

Eq. (D.33) leads to

$$\frac{\beta_i}{\alpha_i} = \frac{\kappa - Z\alpha_{em}m/\lambda}{n' - i}, \tag{D.34}$$

where we have defined

$$n' = \frac{Z\alpha_{em}E}{\lambda} - \gamma. \tag{D.35}$$

Then, we can get the recursion formula for α_i from Eq. (D.32):

$$\alpha_i = -\frac{n' - i}{i(2\gamma + i)}\alpha_{i-1}. \tag{D.36}$$

Solving this, we know the general formula of α_i to be

$$\alpha_i = \frac{(1 - n')(2 - n')\cdots(i - n')}{i!(2\gamma + 1)\cdots(2\gamma + i)}\alpha_0. \tag{D.37}$$

Also, Eq. (D.34) yields a formula of β_i including α_0,

$$\beta_i = \frac{\kappa - Z\alpha_{em}m/\lambda}{n' - i}\frac{(1 - n')(2 - n')\cdots(i - n')}{i!(2\gamma + 1)\cdots(2\gamma + i)}\alpha_0. \tag{D.38}$$

Using Eq. (D.34) for $i = 0$,

$$\alpha_0 = \frac{n'}{\kappa - Z\alpha_{em}m/\lambda}\beta_0, \tag{D.39}$$

β_i is given as

$$\beta_i = (-1)^i\frac{n'(n' - 1)\cdots(n' - i)}{i!(2\gamma + 1)\cdots(2\gamma + i)}\beta_0. \tag{D.40}$$

We have the definite forms of α_i and β_i. Then, let us return to Eqs. (D.28)-(D.29) and determine ϕ_1, ϕ_2. Using the power series of confluent hypergeometric function, Eq. (B.15), ϕ_1 and ϕ_2 are represented as

$$\phi_1 = \alpha_0\rho^\gamma {}_1F_1(1 - n', 2\gamma + 1; \rho), \tag{D.41}$$

$$\begin{aligned}\phi_2 =& \beta_0\rho^\gamma {}_1F_1(-n', 2\gamma + 1; \rho)\\ =& \left(\frac{\kappa - Z\alpha_{em}m/\lambda}{n'}\right)\alpha_0\rho^\gamma {}_1F_1(-n', 2\gamma + 1; \rho).\end{aligned} \tag{D.42}$$

However, in order to normalize the wave function, ϕ_1 and ϕ_2 must be polynomials of finite order at most. This requirement is equivalent to that n' is non-zero integer:

$$n' = 0, 1, 2, \cdots. \tag{D.43}$$

Now we define the principle quantum number n:

$$n = n' + |\kappa|, \qquad n = 1, 2, 3, \cdots. \tag{D.44}$$

According to Eqs. (D.14), (D.16), and (D.35), the eigen-energy E is represented as

$$E = m\left[1 + \left(\frac{Z\alpha_{em}}{n - |\kappa| + \sqrt{\kappa^2 - (Z\alpha_{em})^2}}\right)^2\right]^{-1/2}. \tag{D.45}$$

Although energies with the same principle number n are degenerate in nonrelativistic theory, it is found that the energies split by the relativistic effect and they are in order of the magnitude of angular momentum $j = |\kappa| - 1/2$.

Finally, the formula of radial wave function is written down. By normalizing by the condition

$$\int_0^\infty \left(g^2 + f^2\right) r^2 dr = 1, \tag{D.46}$$

the radial functions are represented as

$$\begin{aligned}\begin{pmatrix} g_\kappa(r) \\ f_\kappa(r) \end{pmatrix} =& \frac{\pm 1}{\Gamma(2\gamma+1)} \sqrt{\frac{2\lambda^5 (m \pm E)\Gamma(2\gamma + n' + 1)}{m^2 Z\alpha_{em}(mZ\alpha_{em} - \lambda\kappa) n'!}} (2\lambda r)^{\gamma-1} e^{-\lambda r} \\ & \times \left\{ \left(\frac{mZ\alpha_{em}}{\lambda} - \kappa \right) {}_1F_1(-n', 2\gamma+1; 2\lambda r) \mp n' {}_1F_1(1-n', 2\gamma+1; 2\lambda r) \right\}. \end{aligned} \tag{D.47}$$

Especially, the wave function for $1S_{1/2}$ state is obtained by choosing $n = 1$, $\kappa = -1$:

$$g_{-1}(r) = \sqrt{\frac{mZ\alpha_{em}(1+\gamma)}{\Gamma(2\gamma+1)}} \frac{(2mZ\alpha_{em}r)^\gamma}{r} \exp(-mZ\alpha_{em}r), \tag{D.48}$$

$$f_{-1}(r) = -\sqrt{\frac{mZ\alpha_{em}(1-\gamma)}{\Gamma(2\gamma+1)}} \frac{(2mZ\alpha_{em}r)^\gamma}{r} \exp(-mZ\alpha_{em}r). \tag{D.49}$$

The binding energy B for the $1S_{1/2}$ state is

$$\begin{aligned} B =& -(E-m) \\ =& m\left(1 - \sqrt{1 - (Z\alpha_{em})^2}\right). \end{aligned} \tag{D.50}$$

D.2 Scattering State

Next the solution in continuous spectrum is considered.

Let us the general solution of the coupled equation (D.5)-(D.6) for $E > m$. Now introduce a new variable $x = 2ipr$ where p is defined as

$$p = \sqrt{E^2 - m^2}. \tag{D.51}$$

After variable transformation, since $d/dr = 2ipd/dx$, Eqs. (D.5)-(D.6) become

$$\frac{dG}{dx} = -\frac{\kappa}{x}G + \left(\frac{E+m}{2ip} + \frac{Z\alpha_{em}}{x}\right)F, \tag{D.52}$$

$$\frac{dF}{dx} = \frac{\kappa}{x}F - \left(\frac{E-m}{2ip} + \frac{Z\alpha_{em}}{x}\right)G. \tag{D.53}$$

Here we write the solution G and F of the Dirac equation as

$$G = \sqrt{E+m}(\phi_1 + \phi_2), \tag{D.54}$$

$$F = i\sqrt{E-m}(\phi_1 - \phi_2). \tag{D.55}$$

According to Eqs. (D.52)-(D.53), it yields

$$\frac{d}{dx}(\phi_1 + \phi_2) = -\frac{\kappa}{x}(\phi_1 + \phi_2) + \left[\frac{1}{2} + \frac{iZ\alpha_{em}}{px}(E-m)\right](\phi_1 - \phi_2), \tag{D.56}$$

$$\frac{d}{dx}(\phi_1 - \phi_2) = \frac{\kappa}{x}(\phi_1 - \phi_2) + \left[\frac{1}{2} + \frac{iZ\alpha_{em}}{px}(E+m)\right](\phi_1 + \phi_2), \tag{D.57}$$

or

$$\frac{d\phi_1}{dx} = \left(\frac{1}{2} + \frac{iZ\alpha_{em}E}{px}\right)\phi_1 - \left(\frac{\kappa}{x} - \frac{iZ\alpha_{em}m}{px}\right)\phi_2, \tag{D.58}$$

$$\frac{d\phi_2}{dx} = -\left(\frac{\kappa}{x} + \frac{iZ\alpha_{em}m}{px}\right)\phi_1 - \left(\frac{1}{2} + \frac{iZ\alpha_{em}E}{px}\right)\phi_2. \tag{D.59}$$

Now let us consider the complex conjugate of Eqs. (D.58)-(D.59). Since x is pure imaginary, we get

$$\frac{d\phi_1^*}{dx} = -\left(\frac{1}{2} + \frac{iZ\alpha_{em}E}{px}\right)\phi_1^* - \left(\frac{\kappa}{x} + \frac{iZ\alpha_{em}m}{px}\right)\phi_2^*, \tag{D.60}$$

$$\frac{d\phi_2^*}{dx} = -\left(\frac{\kappa}{x} - \frac{iZ\alpha_{em}m}{px}\right)\phi_1^* + \left(\frac{1}{2} + \frac{iZ\alpha_{em}E}{px}\right)\phi_2^*. \tag{D.61}$$

Comparing Eqs. (D.58)-(D.59) and Eqs. (D.60)-(D.61), it is found that these are equivalent if it is satisfied that

$$\phi_1 = \phi_2^*, \qquad \phi_2 = \phi_1^*. \tag{D.62}$$

This is requirement for G and F to be real functions.

Now, according to Eq. (D.58), ϕ_2 can be represented by ϕ_1 and $d\phi_1/dx$ as

$$\phi_2 = \frac{px}{iZ\alpha_{em}m - \kappa p}\frac{d\phi_1}{dx} - \left(\frac{px}{2} + iZ\alpha_{em}E\right)\frac{1}{iZ\alpha_{em}m - \kappa p}\phi_1. \tag{D.63}$$

By combining Eqs. (D.59) and (D.63), we can write $d\phi_2/dx$ as

$$\begin{aligned}\frac{d\phi_2}{dx} =& -\left(\frac{\kappa}{x} + \frac{iZ\alpha_{em}m}{px}\right)\phi_1 \\ & - \left(\frac{1}{2} + \frac{iZ\alpha_{em}E}{px}\right)\frac{1}{iZ\alpha_{em}m - \kappa p}\left(px\left(\frac{d\phi_1}{dx} - \frac{1}{2}\phi_1\right) - iZ\alpha_{em}E\phi_1\right).\end{aligned} \tag{D.64}$$

Differentiating both sides of Eq. (D.58) with respect to x, and eliminating ψ_2 by using Eqs. (D.63)-(D.64), the second order differential equation for ϕ_1 with respect to x is given as

$$\frac{d^2\phi_1}{dx^2} + \frac{1}{x}\frac{d\phi_1}{dx} - \left[\frac{1}{4} + \left(\frac{1}{2} + \frac{iZ\alpha_{em}E}{p}\right)\frac{1}{x} + \frac{\gamma^2}{x^2}\right]\phi_1 = 0, \tag{D.65}$$

where $\gamma^2 = \kappa^2 - (Z\alpha_{em})^2$. Setting $W = x^{1/2}\phi_1$, this equation reduces to

$$\frac{d^2W}{dx^2} - \left[\frac{1}{4} + \left(\frac{1}{2} + \frac{iZ\alpha_{em}E}{p}\right)\frac{1}{x} + \frac{\gamma^2 - 1/4}{x^2}\right]W = 0. \tag{D.66}$$

This is known as the Whittaker differential equation, which has two independent solutions: a regular solution,

$$W = x^{\gamma+1/2}e^{-x/2}{}_1F_1(\gamma + 1 + iy, 2\gamma + 1; x), \tag{D.67}$$

and a solution irregular at the origin,

$$W = x^{-\gamma+1/2}e^{-x/2}{}_1F_1(-\gamma + 1 + iy, -2\gamma + 1; x), \tag{D.68}$$

where ${}_1F_1(a, b; x)$ is the confluent hypergeometiric function and y is

$$y = \frac{Z\alpha_{em}E}{p}. \tag{D.69}$$

In case of a pure point charge, the irregular solution is rejected, so we do not have to consider it for a while. On the other hand, in case of a charge with a finite size, the irregular solution is also necessary. We will discuss it later.

As result, ϕ_1 is represented as

$$\phi_1 = N(\gamma + iy)e^{i\eta}(2p)^\gamma\phi(r), \tag{D.70}$$

where

$$\phi(r) = r^{\gamma} e^{-ipr}{}_1F_1(\gamma + 1 + iy, 2\gamma + 1; 2ipr). \tag{D.71}$$

N is a real normalized factor. Here η is introduced as a phase adjusted to satisfy Eq. (D.62). Rewriting Eq. (D.58) as a function of r and setting $\phi_2 = \phi_1^*$, it yields

$$\frac{d\phi_1}{dr} = \left(ip + \frac{iZ\alpha_{em}E}{pr}\right)\phi_1 + \left(-\frac{\kappa}{r} + \frac{iZ\alpha_{em}m}{pr}\right)\phi_1^*. \tag{D.72}$$

Inserting Eq. (D.70) into this equation, we have

$$\begin{aligned} N(\gamma + iy)e^{i\eta}(2p)^{\gamma}\frac{d\phi(r)}{dr} =& \left(ip + \frac{iZ\alpha_{em}E}{pr}\right)N(\gamma + iy)e^{i\eta}(2p)^{\gamma}\phi(r) \\ &+ \left(-\frac{\kappa}{r} + \frac{iZ\alpha_{em}m}{pr}\right)N(\gamma - iy)e^{-i\eta}(2p)^{\gamma}\phi^*(r). \end{aligned} \tag{D.73}$$

Simplify it and obtain the expression for η:

$$e^{-2i\eta} = -\frac{\gamma + iy}{\gamma - iy}\frac{r}{\kappa - iym/E}\left[\frac{d\phi}{dr} - ip\left(1 + \frac{y}{pr}\right)\phi\right]\frac{1}{\phi^*}. \tag{D.74}$$

According to the relation for the confluent hypergeometric function, Eqs. (B.16)-(B.19), it is straightforwardly found that

$$\left[\frac{d\phi}{dr} - ip\left(1 + \frac{y}{pr}\right)\phi\right] = \frac{\phi^*(\gamma - iy)}{r}. \tag{D.75}$$

Thus the phase η should be chosen to satisfy

$$e^{2i\eta} = -\frac{\kappa - iym/E}{\gamma + iy}. \tag{D.76}$$

Now, returning to Eqs. (D.54)-(D.55), we know that G and F can be represented as

$$\begin{aligned} G =& 2N\sqrt{E + m}(2pr)^{\gamma}\mathrm{Re}\Phi(r), \\ F =& -2N\sqrt{E - m}(2pr)^{\gamma}\mathrm{Im}\Phi(r), \end{aligned} \tag{D.77}$$

where

$$\Phi(r) = (\gamma + iy)e^{-ipr + i\eta}{}_1F_1(\gamma + 1 + iy, 2\gamma + 1; 2ipr). \tag{D.78}$$

Moreover, by Eqs. (D.3)-(D.4), $g_\kappa(r)$ and $f_\kappa(r)$ are written as

$$g_\kappa(r) = 2N\sqrt{E + m}\frac{(2pr)^{\gamma}}{r}\mathrm{Re}\Phi(r), \tag{D.79}$$

$$f_\kappa(r) = -2N\sqrt{E - m}\frac{(2pr)^{\gamma}}{r}\mathrm{Im}\Phi(r), \tag{D.80}$$

respectively.

Here let us consider the asymptotic form of $g_\kappa(r)$ at $r \to \infty$. Since confluent hypergeometric function tend to

$${}_1F_1(a, b; z) \to \frac{\Gamma(b)}{\Gamma(a)}z^{a-b}e^z, \tag{D.81}$$

at $r \to \infty$, the asymptotic form of $g_\kappa(r)$ is given as

$$\begin{aligned} g_\kappa(r) \to & 2N\sqrt{E+m}\mathrm{Re}\left[(\gamma+iy)\frac{\Gamma(2\gamma+1)}{\Gamma(\gamma+1+iy)}\frac{(2ipr)^{iy}}{r}i^{-\gamma}e^{i(pr+\eta)}\right] \\ = & \frac{2N\sqrt{E+m}e^{-\pi y/2}\Gamma(2\gamma+1)}{|\Gamma(\gamma+iy)|}\mathrm{Re}\left[\frac{1}{r}e^{i(pr+y\ln(2pr)-\arg\Gamma(\gamma+iy)-\pi\gamma/2+\eta)}\right] \\ = & \frac{2N\sqrt{E+m}e^{-\pi y/2}\Gamma(2\gamma+1)}{|\Gamma(\gamma+iy)|}\frac{\cos(pr-\frac{l_\kappa+1}{2}\pi+\delta_C)}{r}. \end{aligned} \tag{D.82}$$

As $g_\kappa(r)$, it is found that $f_\kappa(r)$ should satisfy

$$f_\kappa(r) \to -\frac{2N\sqrt{E-m}e^{-\pi y/2}\Gamma(2\gamma+1)}{|\Gamma(\gamma+iy)|}\frac{\sin(pr-\frac{l_\kappa+1}{2}\pi+\delta_C)}{r}, \tag{D.83}$$

where δ_C represents the phase shift by Coulomb potential compared to a free particle and is given as

$$\delta_C = y\ln(2pr) - \arg\Gamma(\gamma+iy) + \frac{\pi}{2}(l_\kappa+1-\gamma) + \eta. \tag{D.84}$$

Here let the normalized factor N be

$$N = \frac{|\Gamma(\gamma+iy)|e^{\pi y/2}}{2p\Gamma(2\gamma+1)}, \tag{D.85}$$

and determine $g_\kappa(r), f_\kappa(r)$:

$$g_\kappa(r) = 2\sqrt{E+m}(2pr)^{\gamma-1}\frac{|\Gamma(\gamma+iy)|e^{\pi y/2}}{\Gamma(2\gamma+1)}\mathrm{Re}\Phi(r), \tag{D.86}$$

$$f_\kappa(r) = -2\sqrt{E-m}(2pr)^{\gamma-1}\frac{|\Gamma(\gamma+iy)|e^{\pi y/2}}{\Gamma(2\gamma+1)}\mathrm{Im}\Phi(r). \tag{D.87}$$

These $g_\kappa(r)$ and $f_\kappa(r)$ are the (regular) solution for the Dirac equation with point-charge Coulomb potential. The asymptotic forms of $g_\kappa(r)$ and $f_\kappa(r)$ determined above can be written as

$$g_\kappa(r) \to \frac{\sqrt{E+m}}{pr}\cos(pr-\frac{l_\kappa+1}{2}\pi+\delta_C), \tag{D.88}$$

$$f_\kappa(r) \to -\frac{\sqrt{E-m}}{pr}\sin(pr-\frac{l_\kappa+1}{2}\pi+\delta_C), \tag{D.89}$$

which are similar to that of plane wave, Eqs. (E.63)-(E.64).

When we consult the analysis using Coulomb potential by a charge with a finite size, we need not only the regular solution, but also an irregular solution singular at the origin. Let us construct the other solution using the irregular solution (D.68), which was rejected above. As in the previous analysis, even if we choose the irregular solution (D.68) as the solution for Eq. (D.66), instead of the regular solution (D.67), we can proceed the same discussion. By replacement of $\gamma \to -\gamma$, the solution $\tilde{g}_\kappa(r)$ and $\tilde{f}_\kappa(r)$ in this case is as follows:

$$\tilde{g}_\kappa(r) = 2\sqrt{E+m}(2pr)^{-\gamma-1}\frac{|\Gamma(-\gamma+iy)|e^{\pi y/2}}{\Gamma(-2\gamma+1)}\mathrm{Re}\tilde{\Phi}(r), \tag{D.90}$$

$$\tilde{f}_\kappa(r) = -2\sqrt{E-m}(2pr)^{-\gamma-1}\frac{|\Gamma(-\gamma+iy)|e^{\pi y/2}}{\Gamma(-2\gamma+1)}\mathrm{Im}\tilde{\Phi}(r), \tag{D.91}$$

where

$$\tilde{\Phi}(r) = (-\gamma+iy)e^{-ipr+i\tilde{\eta}}{}_1F_1(-\gamma+1+iy, -2\gamma+1; 2ipr), \tag{D.92}$$

and $\tilde{\eta}$ satisfies

$$e^{2i\tilde{\eta}} = -\frac{\kappa - iym/E}{-\gamma + iy}. \tag{D.93}$$

Also, the asymptotic forms at $r \to \infty$ are given as

$$\tilde{g}_\kappa(r) \to \frac{\sqrt{E+m}}{pr} \cos(pr - \frac{l_\kappa + 1}{2}\pi + \tilde{\delta}_C), \tag{D.94}$$

$$\tilde{f}_\kappa(r) \to -\frac{\sqrt{E-m}}{pr} \sin(pr - \frac{l_\kappa + 1}{2}\pi + \tilde{\delta}_C), \tag{D.95}$$

where

$$\tilde{\delta}_C = y \ln(2pr) - \arg\Gamma(-\gamma + iy) + \frac{\pi}{2}(l_\kappa + 1 + \gamma) + \tilde{\eta}. \tag{D.96}$$

For convenience, using

$$\begin{aligned} \Delta =& \tilde{\delta}_C - \delta_C \\ =& \arg\left(\sqrt{\frac{-\gamma - iy}{\gamma - iy}} \frac{\Gamma(\gamma + iy)}{\Gamma(-\gamma + iy)}\right) + \pi\gamma, \end{aligned} \tag{D.97}$$

we define $g^{\rm irr}(r)$ and $f^{\rm irr}(r)$ as

$$g^{\rm irr}(r) = \frac{\cos\Delta}{\sin\Delta} g(r) - \frac{1}{\sin\Delta}\tilde{g}(r), \tag{D.98}$$

$$f^{\rm irr}(r) = \frac{\cos\Delta}{\sin\Delta} f(r) - \frac{1}{\sin\Delta}\tilde{f}(r). \tag{D.99}$$

The asymptotic forms at $r \to \infty$ of them are

$$g^{\rm irr}(r) \to \frac{\sqrt{E+m}}{pr} \sin(pr - \frac{l_\kappa + 1}{2}\pi + \delta_C), \tag{D.100}$$

$$f^{\rm irr}(r) \to \frac{\sqrt{E-m}}{pr} \cos(pr - \frac{l_\kappa + 1}{2}\pi + \delta_C). \tag{D.101}$$

Appendix E

Lepton Wave Functions

In this appendix, we discuss the way to describe a wave function of muon and electron in the presence of Coulomb potential $\phi(\boldsymbol{r})$. When the source of Coulomb potential is not point charge, the Dirac equation cannot be analytically solved, so the numerical calculation would be needed. Here we assume that the charge distribution of the nucleus is spherically symmetric and $\phi(\boldsymbol{r}) = \phi(r)$ is spherically symmetric.

E.1 Dirac Equation with Coulomb Potential

The relativistic wave function of a free fermion obeys the Dirac equation,

$$[\partial\!\!\!/ + m]\,\psi = 0, \tag{E.1}$$

where m is a mass of the fermion. It is known that the motion of particles with electric charge $(-e)$ in the electromagnetic potential A_μ is described by the equation with replacement

$$\partial_\mu \to \partial_\mu + i(-e)A_\mu, \tag{E.2}$$

in the equation without electromagnetic field. According to this procedure, Eq. (E.1) is modified as

$$[\partial\!\!\!/ - ieA\!\!\!/ + m]\,\psi = 0. \tag{E.3}$$

Now, let the electromagnetic field be a static potential which is spherically symmetric:

$$A_0 = \phi(r), \qquad A_i = 0 \quad (i = 1, 2, 3). \tag{E.4}$$

In addition, assuming the wave function as $e^{-Et}\psi(\boldsymbol{r})$ to separate a time component, $\psi(\boldsymbol{r})$ obeys

$$E\psi(\boldsymbol{r}) = [-i\alpha \cdot \nabla + m\beta - e\phi(r)]\,\psi(\boldsymbol{r}). \tag{E.5}$$

Corresponding to the Schrödinger equation,

$$H = -i\alpha \cdot \nabla + m\beta - e\phi(r), \tag{E.6}$$

is called Hamiltonian.

E.1.1 Angular Momentum and Spherical Wave Solution

Now let us consider angular momentum in the Dirac equation. A orbital angular momentum operator L_i is defined by

$$\begin{aligned} L_i &= -\,i\,(\boldsymbol{r} \times \nabla)_i \\ &= -\,i\epsilon_{ijk} r_j \partial_k, \end{aligned} \tag{E.7}$$

as in case of nonrelativistic theory. The commutation relation between L_i and the Dirac Hamiltonian Eq. (E.6), if the potential is spherically symmetric, is

$$[H, L_i] = -\epsilon_{ijk}\alpha_j\partial_k. \tag{E.8}$$

Unlike the case of nonrelativity, the orbital momentum does not commutate with the Hamiltonian. In other words, the orbital angular momentum is not conserved alone in the Dirac equation.

Next, a spin angular momentum operator S_i is defined as

$$S_i = \frac{1}{2}\begin{pmatrix}\sigma_i & 0\\ 0 & \sigma_i\end{pmatrix}, \tag{E.9}$$

which is extended from $\sigma_i/2$ used in nonrelativity. As in the orbital angular momentum, since the commutation relation with the Hamiltonian is

$$[H, S_i] = \epsilon_{ijk}\alpha_j\partial_k. \tag{E.10}$$

Therefore S_i is not a conserved quantity.

However, as you can be readily seen in comparing Eq. (E.8) and (E.10), the total angular momentum

$$\boldsymbol{J} = \boldsymbol{L} + \boldsymbol{S}, \tag{E.11}$$

is commutative to the Hamiltonian. That is, the sum of orbital and spin angular momentum is conserved in the Dirac equation with a spherical potential. Therefore, it is convenient to use eigenstates of the total angular momentum $\boldsymbol{J}$.

Now let us solve the Dirac equation (E.5) to obtain an eigenstate with the total angular momentum $\boldsymbol{J}$. Let $j(j+1)$ and ν be the eigenvalues of $\boldsymbol{J}^2$ and J_z, respectively, and write its eigenfunction as

$$\psi_j^\nu = \begin{pmatrix}\xi_j^\nu\\ \eta_j^\nu\end{pmatrix}, \tag{E.12}$$

where ξ_j^ν and η_j^ν represent two-component wave functions. Here, the total angular momentum operator $\boldsymbol{J}$ is represented by

$$\boldsymbol{J} = \begin{pmatrix}\boldsymbol{j} & 0\\ 0 & \boldsymbol{j}\end{pmatrix}, \qquad \boldsymbol{j} = \boldsymbol{l} + \frac{\boldsymbol{\sigma}}{2}, \tag{E.13}$$

as the sum of the orbital angular momentum operator $\boldsymbol{l}$ and the spin angular momentum operator $\boldsymbol{\sigma}/2$ for the two components, and both ξ_j^ν and η_j^ν satisfy

$$\boldsymbol{j}^2\chi_j^\nu = j(j+1)\chi_j^\nu, \qquad j_z\chi_j^\nu = \nu\chi_j^\nu, \tag{E.14}$$

where χ_j^ν represents ξ_j^ν or η_j^ν.

There are two independent solutions of Eq. (E.14) as follows:

$$\begin{aligned}\chi_j^{\nu(+)} =& \sqrt{\frac{l+1/2+\nu}{2l+1}}Y_l^{\nu-1/2}(\hat{r})\begin{pmatrix}1\\0\end{pmatrix} + \sqrt{\frac{l+1/2-\nu}{2l+1}}Y_l^{\nu+1/2}(\hat{r})\begin{pmatrix}0\\1\end{pmatrix}\\ =& \sum_{m,s}(l,m,1/2,s|l+1/2,\nu)Y_l^m(\hat{r})\chi_{1/2}^s,\end{aligned} \tag{E.15}$$

$$\begin{aligned}\chi_j^{\nu(-)} =& -\sqrt{\frac{l+1/2-\nu}{2l+1}}Y_l^{\nu-1/2}(\hat{r})\begin{pmatrix}1\\0\end{pmatrix} + \sqrt{\frac{l+1/2+\nu}{2l+1}}Y_l^{\nu+1/2}(\hat{r})\begin{pmatrix}0\\1\end{pmatrix}\\ =& \sum_{m,s}(l,m,1/2,s|l-1/2,\nu)Y_l^m(\hat{r})\chi_{1/2}^s.\end{aligned} \tag{E.16}$$

where l means magnitude of the orbital angular momentum. The former and the latter of these correspond to $j = l + 1/2$ and $j = l - 1/2$, respectively.

It is convenient to introduce a quantum number κ:

$$\kappa = \begin{cases} -(l+1) = -(j+1/2) & (j = l + 1/2) \\ l = j + 1/2 & (j = l - 1/2) \end{cases}. \tag{E.17}$$

By using this, $\chi_j^{\nu(\pm)}$ can be collectively rewritten as χ_κ^ν.

$$\chi_\kappa^\nu(\hat{r}) = \begin{cases} \chi_j^{\nu(+)} & (\kappa < 0) \\ \chi_j^{\nu(-)} & (\kappa > 0). \end{cases}. \tag{E.18}$$

Then ψ_j^ν can generally be written as

$$\psi_j^\nu = \begin{pmatrix} g_\kappa(r)\chi_\kappa^\nu(\hat{r}) + g_{-\kappa}(r)\chi_{-\kappa}^\nu(\hat{r}) \\ if_\kappa(r)\chi_{-\kappa}^\nu(\hat{r}) + if_{-\kappa}(r)\chi_\kappa^\nu(\hat{r}) \end{pmatrix}, \tag{E.19}$$

using radial functions $g_\kappa(r)$, $f_\kappa(r)$. Substituting this into equation (E.5) yields the simultaneous equation,

$$\begin{aligned} &\boldsymbol{\sigma} \cdot \nabla \left[f_\kappa(r)\chi_{-\kappa}^\nu(\hat{r}) + f_{-\kappa}(r)\chi_\kappa^\nu(\hat{r}) \right] \\ &\qquad + (m - E - e\phi(r)) \left[g_\kappa(r)\chi_\kappa^\nu(\hat{r}) + g_{-\kappa}(r)\chi_{-\kappa}^\nu(\hat{r}) \right] = 0, \end{aligned} \tag{E.20}$$

$$\begin{aligned} &\boldsymbol{\sigma} \cdot \nabla \left[g_\kappa(r)\chi_\kappa^\nu(\hat{r}) + g_{-\kappa}(r)\chi_{-\kappa}^\nu(\hat{r}) \right] \\ &\qquad + (m + E + e\phi(r)) \left[f_\kappa(r)\chi_{-\kappa}^\nu(\hat{r}) + f_{-\kappa}(r)\chi_\kappa^\nu(\hat{r}) \right] = 0. \end{aligned} \tag{E.21}$$

Furthermore, using the relation that holds for arbitrary function $G(r)$ that depends only on the distance from the origin,

$$\boldsymbol{\sigma} \cdot \nabla \left[G(r)\chi_\kappa^\nu(\hat{r}) \right] = -\left[\frac{dG(r)}{dr} + \frac{1+\kappa}{r} G(r) \right] \chi_{-\kappa}^\nu(\hat{r}), \tag{E.22}$$

it gives equations for $g_\kappa(r)$, $f_\kappa(r)$ as follows:

$$\frac{dg_\kappa(r)}{dr} + \frac{1+\kappa}{r} g_\kappa(r) - (E + m + e\phi(r)) f_\kappa(r) = 0, \tag{E.23}$$

$$\frac{df_\kappa(r)}{dr} + \frac{1-\kappa}{r} f_\kappa(r) + (E - m + e\phi(r)) g_\kappa(r) = 0. \tag{E.24}$$

The equations for $g_{-\kappa}(r)$, $f_{-\kappa}(r)$ are also obtained by replacing κ with $-\kappa$. In summary, ψ_j^ν, Eq. (E.19), is represented by superposition of two independent solutions, ψ_κ^ν and $\psi_{-\kappa}^\nu$, which is defined as

$$\psi_\kappa^\nu = \begin{pmatrix} g_\kappa(r)\chi_\kappa^\nu(\hat{r}) \\ if_\kappa(r)\chi_{-\kappa}^\nu(\hat{r}) \end{pmatrix}. \tag{E.25}$$

Even if an arbitrary spherical potential exists, since the angular component of the wave function can be obtained analytically, the equations are reduced to the radial equations (E.23) and (E.24). When $\phi(r)$ is the Coulomb potential of the point charge, its solution can be obtained analytically. The derivation is shown in Appendix D. However, for general case, an analytic solution rarely exists, and the numerical calculation is necessary to solve the equation. We assume that the potential $\phi(r)$ has a finite value at the origin and behaves as the point-charge potential at infinity.

E.2 Bound State

Here we describe the method to calculate the wave function and the energy of the bound state by numerically solving Eqs. (E.23)-(E.24). Now it is convenient to define

$$G_\kappa(r) = r g_\kappa(r), \tag{E.26}$$
$$F_\kappa(r) = r f_\kappa(r), \tag{E.27}$$

and rewrite Eqs. (E.23)-(E.24) as

$$\frac{dG_\kappa(r)}{dr} + \frac{\kappa}{r} G_\kappa(r) - (E + m + e\phi(r))\, F_\kappa(r) = 0, \tag{E.28}$$
$$\frac{dF_\kappa(r)}{dr} - \frac{\kappa}{r} F_\kappa(r) + (E - m + e\phi(r))\, G_\kappa(r) = 0. \tag{E.29}$$

The definition of the bound state is a solution that can satisfy the normalization condition

$$\int_0^\infty dr \left[G_\kappa(r)^2 + F_\kappa(r)^2 \right] = 1, \tag{E.30}$$

by multiplying by a constant.

At first, let us discuss the behavior of Eqs. (E.28)-(E.29) near the origin. Since wave functions must be square-integrable, we require the boundary condition at the origin,

$$G_\kappa(0) = F_\kappa(0) = 0. \tag{E.31}$$

In order to obtain more detailed information, let the solution be analytic near the origin:

$$G_\kappa(r) \sim A r^\alpha, \tag{E.32}$$
$$F_\kappa(r) \sim B r^\beta, \tag{E.33}$$

where α and β are defined as the lowest order of $G_\kappa(r)$ and $F_\kappa(r)$, respectively, so A and B are a non-zero constant. To satisfy the boundary condition (E.31), α and β must be a positive value. Substituting those expressions into Dirac equation (E.28)-(E.29) near the origin, we get

$$A(\alpha + \kappa) r^{\alpha - 1} - B(E + m + e\phi_0) r^\beta \sim 0, \tag{E.34}$$
$$B(\beta - \kappa) r^{\beta - 1} + A(E - m + e\phi_0) r^\alpha \sim 0, \tag{E.35}$$

where $\phi_0 = \phi(0)$.

Let us consider the case of $\kappa < 0$. If $\alpha > \beta - 1$, the first term dominates in Eq. (E.35) when $r \sim 0$. Therefore it is required that

$$B(\beta - \kappa) r^{\beta - 1} \sim 0, \tag{E.36}$$

up to $\mathcal{O}\left(r^{\beta-1}\right)$. Since B is non-zero by definition, $\beta = \kappa < 0$ must be satisfied but β is defined as a positive number. Moreover, if $\alpha < \beta - 1$, Eqs. (E.34)-(E.35) yield

$$\alpha = -\kappa, \tag{E.37}$$
$$E = m - e\phi_0. \tag{E.38}$$

However, since the energy condition is obviously unphysical, we do not have to consider this case. Thus we conclude $\alpha = \beta - 1$ if $\kappa < 0$. Using the relation and Eq. (E.34), we get

$$\alpha = -\kappa, \tag{E.39}$$

so Eq. (E.35) yields

$$\frac{B}{A} = \frac{E - m + e\phi_0}{2\kappa - 1}. \tag{E.40}$$

On the other hand, for case of $\kappa > 0$, we can obtain $\alpha = \beta + 1$ and

$$\beta = \kappa, \tag{E.41}$$

$$\frac{B}{A} = \frac{2\kappa + 1}{E + m + e\phi_0}. \tag{E.42}$$

In summary, the ratio between $G_\kappa(r)$ and $F_\kappa(r)$ near the origin is

$$\frac{F_\kappa(r)}{G_\kappa(r)} \overset{r\to 0}{\to} \begin{cases} \dfrac{E - m + e\phi_0}{2\kappa - 1} r & (\kappa < 0) \\ \dfrac{2\kappa + 1}{E + m + e\phi_0} \dfrac{1}{r} & (\kappa > 0) \end{cases}. \tag{E.43}$$

Next we move on to discuss discussion about the behavior of Eqs. (E.28)-(E.29) in $r \sim \infty$. Then we can neglect the terms proportional to $1/r$, Eqs. (E.23)-(E.24) tend to be

$$\frac{dG_\kappa(r)}{dr} - (E + m)F_\kappa(r) \sim 0, \tag{E.44}$$

$$\frac{dF_\kappa(r)}{dr} + (E - m)G_\kappa(r) \sim 0. \tag{E.45}$$

By eliminating $F_\kappa(r)$ from the coupled equations, we can obtain the closed equation for $G_\kappa(r)$,

$$\frac{d^2G_\kappa(r)}{dr^2} \sim \left(m^2 - E^2\right) G_\kappa(r). \tag{E.46}$$

This differential equation can be solved, and we obtain the form of $G_\kappa(r)$ in $r \sim \infty$,

$$G_\kappa(r) \sim \tilde{A} \exp\left(-\sqrt{m^2 - E^2} r\right), \tag{E.47}$$

where $\tilde{A}$ is a constant depending on the normalization condition. Therefore, the form of $F_\kappa(r)$ is also determined as

$$F_\kappa(r) \sim -\sqrt{\frac{m - E}{m + E}} G_\kappa(r). \tag{E.48}$$

Thus, we obtain

$$\frac{F_\kappa(r)}{G_\kappa(r)} \overset{r\to\infty}{\to} -\sqrt{\frac{m - E}{m + E}}. \tag{E.49}$$

Now we discuss the numerical method to get the energy and wave functions of a bound state. The way to calculate the bound state is basically as follows: Choose an arbitrary energy, start solving the differential equation from the asymptotic behavior of either the origin or far, and adopt the energy if the obtained wave function satisfies the boundary condition on the other side as solution. Various methods may be conceivable, but the two simplest methods are introduced here:

- To solve from outside to inside.
- To solve from inside to outside.

The initial condition used when starting to solve the differential equation from one end are obtained above. In case to solve it from outside, you would proceed for the origin from initial condition of

$$G_\kappa(r_\infty) = C, \tag{E.50}$$

$$F_\kappa(r_\infty) = -\sqrt{\frac{m-E}{m+E}}C. \tag{E.51}$$

Since the wave function will be normalized finally, C can be an arbitrary value. Even if you solve it from inside, the procedure is the same except for the used initial condition.

In order to search an energy of a bound state, we should use a numerical techniques, such as the secant method. Then we should discuss which test function is effective, by comparing some different methods. $G^E_\kappa(r)$ and $F^E_\kappa(r)$ are functions obtained as a result of solving the Dirac equation using Energy E, regardless of whether they are a bound state or not.

Practically, it is difficult to actually evaluate differential equations at the origin or at infinity. Therefore, when solving the differential equation from outside and evaluating the boundary condition of the origin, extrapolation is performed using the value near the origin. The point at infinity is considered as a finite value r_∞ in numerical calculation.

1. Method 1. We decide the value of the function to protect the behavior at infinity and solve the Dirac equation for the origin. The test function is

$$H^1_\kappa(E) = G^E_\kappa(0). \tag{E.52}$$

   The energy of bound states gives the zero point of this function.

2. Method 2. As method 1, we solve the Dirac equation from the infinity point to the origin. The test function is

$$H^2_\kappa(E) = G^E_\kappa(0)^2 + F^E_\kappa(0)^2. \tag{E.53}$$

   The energy of bound states gives the zero point or local minimum of this function.

3. Method 3. We solve the Dirac equation from the origin to the infinity. The test function is

$$H^3_\kappa(E) = G^E_\kappa(r_\infty). \tag{E.54}$$

   The energy of bound states gives the zero point of this function.

4. Method 4. As method 3, we solve the Dirac equation from the origin to the infinity. The test function is

$$H^4_\kappa(E) = G^E_\kappa(r_\infty)^2 + F^E_\kappa(r_\infty)^2. \tag{E.55}$$

   The energy of bound states gives the zero point or local minimum of this function.

Fig. E.1 shows test functions, $H^i_\kappa(E)$ $(i = 1, 2, 3, 4)$, for $\kappa = -1$ (a) and $\kappa = +1$ (b). The point which changes the sign of $H^1_\kappa(E)$ and $H^3_\kappa(E)$ yields the energy of the solution, while the minimum of $H^2_\kappa(E)$ and $H^4_\kappa(E)$ does. Comparing them, all methods seem to give consistent results. Although it seems that there is a difference in each method for shallow binding energy, this is because we did not take r_∞ sufficiently large when drawing the figure.

The results of calculating bound states are shown below. Whichever method are used, we set

$$r_\infty = 20 r^n_B, \tag{E.56}$$

where $r^n_B = n/(m_e(Z-1)\alpha_{em})$ and n indicates the principle quantum number of the state we want. This means that about 20 times the Bohr radius obtained in the case of the point charge potential is regarded

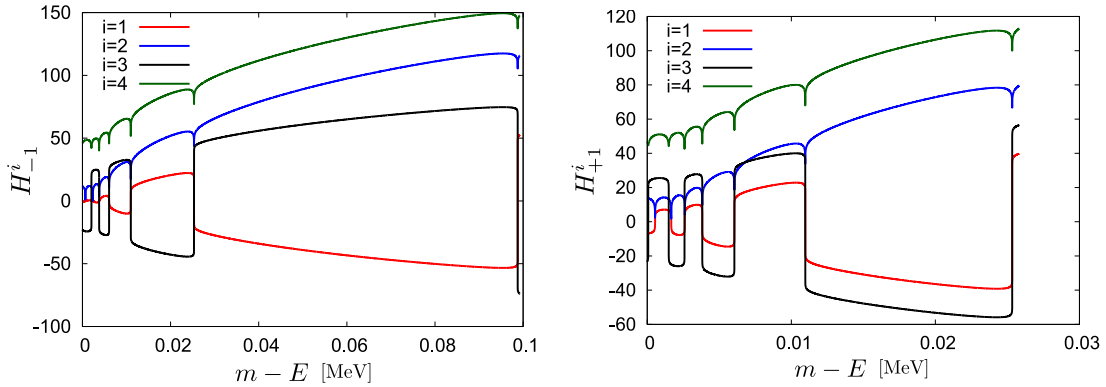

(a) (b)

Figure E.1: $H^i_{-1}(E)$ (a) and $H^i_{+1}(E)$ (b). E which gives $H_\kappa(E)=0$ is important, while the magnitude of H_κ has no meaning. Since H_κs used here have large values for large range of E, we plot $(\ln H_\kappa + 1)$ if $H^i_\kappa(E) > 1$, and $(-\ln|H_\kappa| - 1)$ if $H^i_\kappa(E) < -1$, instead of H_κ.

as infinity. In the methods 1 and 2 (3 and 4), we solved the differential equations to $r_0 = r_\infty/200000$ (from $r_0 = 197.3 \times 10^{-10}$fm) with 200000 steps. Here we assume that the nucleus is ^{208}Pb and its charge distribution is uniform. However, since we use the code for electron bound states in a muon atom, considering the screening effect of the muon, the proton number of the Coulomb potential in this calculation is taken as $Z - 1 = 81$.

The found binding energies $m - E$ are shown in Table E.1-E.2. Even using different methods, it is found

Table E.1: Comparison among four numerical methods for $\kappa = -1$. The second, third, and fourth columns show the binding energies (keV) corresponding to each quantum states. The fifth column shows the time (seconds) to calculate the ground state.

Method	$1s$	$2s$	$3s$	time($1s$)
1	98.7615338034228407	25.3231186851013979	10.9657992683473982	3.2224121
2	98.7615343958235803	25.3231187872899333	10.9657992872963517	3.6384277
3	98.7615343962585657	25.3231187874320973	10.9657992974631080	3.3044434
4	98.7615343958241354	25.3231187870084362	10.9657992868976706	3.6933594

Table E.2: Comparison among four numerical methods for $\kappa = +1$. See the caption of Table E.1 for the meaning of each column.

Method	$2p$	$3p$	$4p$	time($2p$)
1	25.3327712221007584	10.9686504182404665	6.05112807567942390	10.302246
2	25.3327711874804518	10.9686503735209051	6.05112806559748861	11.138184
3	25.3327712191353527	10.9686504148879260	6.05112805511720531	10.525391
4	25.3327711875487860	10.9686503742800756	6.05112804622587319	10.914307

that consistent results are obtained with about 8 significant digits.

The obtained wave functions are shown in Figs. E.2-E.3.

As results, all methods yield sufficiently consistent bound states. In order to get the more accurate results or the higher excited state, for all methods, it is basically necessary to make (1) r_∞ larger and (2) spacial

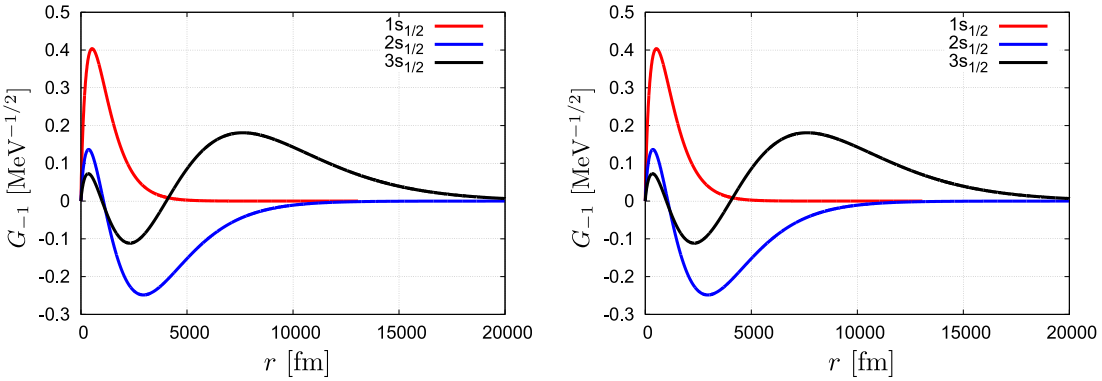

Figure E.2: Obtained $G_{-1}(r)$ (a) and $F_{-1}(r)$ (b).

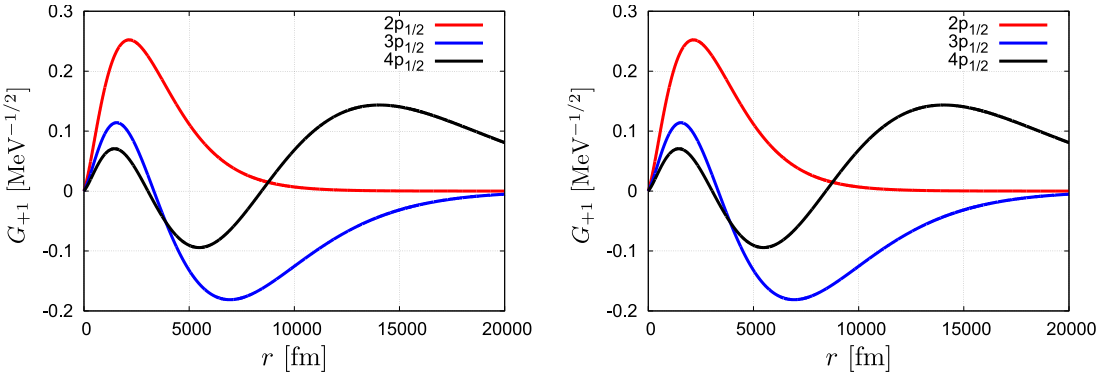

Figure E.3: Obtained $G_{+1}(r)$ (a) and $F_{+1}(r)$ (b).

mesh finer. In addition, by tightening a termination condition of the secant method, we have to improve the resolution of energy search.

However, unnecessarily setting r_∞ too large or r_0 too small would make the calculation not work. When using the obtained wave function, it is essential to output the wave function once.

E.3 Scattering State

Next, the wave function of the final state scattered electrons is calculated. Before describing the calculation method, we show how the wave function of the scattering state should be represented by superposing the eigenfunctions of the angular momentum, which can be calculated by Eqs. (E.23)-(E.24).

E.3.1 Partial Wave Expansion

The wave function distorted by the nuclear Coulomb potential can be expressed by superposition of the eigenstates of the angular momentum, that is, partial waves. This expansion is called partial wave expansion. Here we briefly derive the expression.

First of all, for preparation, let us derive the expansion of a plane wave,

$$\psi_{\rm pl}^{p,s}(\boldsymbol{r}) = \sqrt{E+m}\begin{pmatrix} \mathbf{1}_2 \\ \dfrac{1}{i}\dfrac{\boldsymbol{\sigma}\cdot\nabla}{E+m} \end{pmatrix} e^{i\boldsymbol{p}\cdot\boldsymbol{r}}\chi^s, \tag{E.57}$$

with spherical waves of the free Dirac equation. By using the formula

$$\exp\left(i\boldsymbol{q}\cdot\boldsymbol{r}\right) = 4\pi\sum_{l,m} i^l j_l(qr) Y_l^{m*}\left(\hat{q}\right) Y_l^m\left(\hat{r}\right), \tag{4.82}$$

we can rewrite Eq. (E.57) as

$$\begin{aligned}
\psi_{\rm pl}^{p,s}(\boldsymbol{r}) =& \sqrt{E+m}\sum_{L,M} 4\pi i^L Y_L^{M*}(\hat{p})\begin{pmatrix} \mathbf{1}_2 \\ \dfrac{1}{i}\dfrac{\boldsymbol{\sigma}\cdot\nabla}{E+m} \end{pmatrix} j_L(pr) Y_L^M(\hat{r})\chi^s \\
=& \sqrt{E+m}\sum_{L,M} 4\pi i^L Y_L^{M*}(\hat{p})\begin{pmatrix} \mathbf{1}_2 \\ \dfrac{1}{i}\dfrac{\boldsymbol{\sigma}\cdot\nabla}{E+m} \end{pmatrix} j_L(pr)\sum_{J,m}(L,M,1/2,s|J,m)\chi_J^m \\
=& \sqrt{E+m}\sum_{\kappa,m} 4\pi i^{l_\kappa}(l_\kappa,m-s,1/2,s|j_\kappa,m) Y_{l_\kappa}^{m-s*}(\hat{p})\begin{pmatrix} \mathbf{1}_2 \\ \dfrac{1}{i}\dfrac{\boldsymbol{\sigma}\cdot\nabla}{E+m} \end{pmatrix} j_{l_\kappa}(pr)\chi_\kappa^m.
\end{aligned} \tag{E.58}$$

In addition, by using Eq. (E.22), we obtain

$$\psi_{\rm pl}^{p,s}(\boldsymbol{r}) = \sum_{\kappa,m} 4\pi i^{l_\kappa} Y_{l_\kappa}^{m-s*}(\hat{p})(l_\kappa,m-s,1/2,s|j_\kappa,m)\begin{pmatrix} g_\kappa^{\rm pl}(r)\chi_\kappa^m \\ i f_\kappa^{\rm pl}(r)\chi_{-\kappa}^m \end{pmatrix}. \tag{E.59}$$

Here

$$g_\kappa^{\rm pl}(r) = \sqrt{E+m} j_{l_\kappa}(pr), \tag{E.60}$$

$$f_\kappa^{\rm pl}(r) = \sqrt{E-m} S_\kappa j_{l_{-\kappa}}(pr), \tag{E.61}$$

where S_κ is the sign of κ. Since the Bessel function $j_{l_\kappa}(pr)$ behaves at $r\to\infty$ as

$$j_{l_\kappa}(pr) \to \frac{1}{pr}\cos\left(pr - \frac{l_\kappa+1}{2}\pi\right), \tag{E.62}$$

$g_\kappa^{\rm pl}(r)$ and $f_\kappa^{\rm pl}(r)$ tend to be

$$g_\kappa^{\rm pl}(r) \to \frac{\sqrt{E+m}}{pr}\cos\left(pr - \frac{l_\kappa+1}{2}\pi\right), \tag{E.63}$$

$$\begin{aligned}
f_\kappa^{\rm pl}(r) \to& \frac{\sqrt{E-m}S_\kappa}{pr}\cos\left(pr - \frac{l_{-\kappa}+1}{2}\pi\right) \\
=& -\frac{\sqrt{E-m}}{pr}\sin\left(pr - \frac{l_\kappa+1}{2}\pi\right),
\end{aligned} \tag{E.64}$$

at $r\to\infty$.

Next let us consider a wave distorted by the Coulomb potential. If the potential is spherical, only the radial part is changed but the angular part is not. Therefore the expansion of plane wave (E.59) should be modified for distorted wave as

$$\psi^{p,s}(\boldsymbol{r}) = \sum_{\kappa,m} 4\pi i^{l_\kappa} Y_{l_\kappa}^{m-s*}(\hat{p})(l_\kappa,m-s,1/2,s|j_\kappa,m) c_\kappa \begin{pmatrix} g_\kappa(r)\chi_\kappa^m \\ i f_\kappa(r)\chi_{-\kappa}^m \end{pmatrix}. \tag{E.65}$$

Here $g_\kappa(r)$ and $f_\kappa(r)$ are a solution of the Dirac equation (E.23)-(E.24) and the coefficients c_κ indicate weights of each partial wave.

In order to determine c_κ, let us consider the behavior of $\psi^{p,s}(\boldsymbol{x})$ at $r \to \infty$. Since the nuclear Coulomb potential is asymptotically close to the point-charge potential at $r \to \infty$, the shape of the wave function at $r \to \infty$ can be represented by superposition of the solutions of the Dirac equation with the point-charge potential. The set of these solutions is given in Appendix D. Suppose that, at $r \to \infty$, $g_\kappa(r)$ and $f_\kappa(r)$ are written by linear combination of a regular solution and an irregular solution as follows:

$$\begin{pmatrix} g_\kappa(r) \\ f_\kappa(r) \end{pmatrix} \to \cos\delta_\kappa \begin{pmatrix} g_\kappa^{\rm reg}(r) \\ f_\kappa^{\rm reg}(r) \end{pmatrix} - \sin\delta_\kappa \begin{pmatrix} g_\kappa^{\rm irr}(r) \\ f_\kappa^{\rm irr}(r) \end{pmatrix}. \tag{E.66}$$

By using the asymptotic form of point-charge solution, we obtain

$$\begin{aligned} g_\kappa(r) \to & \frac{\sqrt{E+m}}{pr}\left(\cos\delta_\kappa \cos\left(pr - \frac{l_\kappa+1}{2}\pi + \delta_C\right) - \sin\delta_\kappa \sin\left(pr - \frac{l_\kappa+1}{2}\pi + \delta_C\right)\right) \\ = & \frac{\sqrt{E+m}}{pr}\cos\left(pr - \frac{l_\kappa+1}{2}\pi + \delta_C + \delta_\kappa\right), \end{aligned} \tag{E.67}$$

$$\begin{aligned} f_\kappa(r) \to & \frac{\sqrt{E-m}}{pr}\left(-\cos\delta_\kappa \sin\left(pr - \frac{l_\kappa+1}{2}\pi + \delta_C\right) - \sin\delta_\kappa \cos\left(pr - \frac{l_\kappa+1}{2}\pi + \delta_C\right)\right) \\ = & -\frac{\sqrt{E-m}}{pr}\sin\left(pr - \frac{l_\kappa+1}{2}\pi + \delta_C + \delta_\kappa\right). \end{aligned} \tag{E.68}$$

The expression shows that δ_κ indicates the phase shift from the solution in a point-charge Coulomb potential. Now defining

$$z = pr - \frac{l_\kappa+1}{2}\pi + \delta_C, \tag{E.69}$$

we can write

$$\begin{aligned} \cos(z+\delta_\kappa) = & \frac{e^{i(z+\delta_\kappa)} + e^{-i(z+\delta_\kappa)}}{2} \\ = & e^{\mp i\delta_\kappa}\left[\frac{e^{iz} + e^{-iz} - e^{\pm iz} + e^{\pm iz \pm 2i\delta_\kappa}}{2}\right] \\ = & e^{\mp i\delta_\kappa}\cos z + \frac{e^{\mp i\delta_\kappa}}{2}(e^{\pm 2i\delta_\kappa} - 1)e^{\pm iz}, \end{aligned} \tag{E.70}$$

$$\begin{aligned} \sin(z+\delta_\kappa) = & \frac{e^{i(z+\delta_\kappa)} - e^{-i(z+\delta_\kappa)}}{2i} \\ = & e^{\mp i\delta_\kappa}\left[\frac{e^{iz} - e^{-iz} \mp e^{\pm iz} \pm e^{\pm iz \pm 2i\delta_\kappa}}{2i}\right] \\ = & e^{\mp i\delta_\kappa}\sin z \pm \frac{e^{\mp i\delta_\kappa}}{2i}(e^{\pm 2i\delta_\kappa} - 1)e^{\pm iz}. \end{aligned} \tag{E.71}$$

By this formula, we rewrite

$$\begin{pmatrix} g_\kappa(r) \\ f_\kappa(r) \end{pmatrix} \to e^{\mp i\delta_\kappa}\left[\frac{1}{pr}\begin{pmatrix} \sqrt{E+m}\cos z \\ -\sqrt{E-m}\sin z \end{pmatrix} + \frac{(e^{\pm 2i\delta_\kappa} - 1)e^{\pm iz}}{2pr}\begin{pmatrix} E+m \\ \mp i(E-m) \end{pmatrix}\right]. \tag{E.72}$$

Compared to Eq. (E.63)-(E.64), it is found that the first and second terms should correspond to the plane-wave part and the additional part by δ_κ, respectively. In order to interpret the first term as plane wave, c_κ must be

$$c_\kappa = e^{\pm i\delta_\kappa}. \tag{E.73}$$

We note that, since the Coulomb interaction is long-range, δ_C contains r and the first term is not perfectly equal to that of the plane wave. Thus, the partial wave expansion for distorted Dirac wave is written as

$$\psi^{p,s}(\boldsymbol{r}) = \sum_{\kappa,m} 4\pi i^{l_\kappa} Y_{l_\kappa}^{m-s*}(\hat{p})(l_\kappa, m-s, 1/2, s|j_\kappa, m) e^{\pm i\delta_\kappa} \begin{pmatrix} g_\kappa(r)\chi_{\kappa,m} \\ i f_\kappa(r)\chi_{-\kappa,m} \end{pmatrix}. \tag{E.74}$$

Here $g_\kappa(r)$ and $f_\kappa(r)$ are represented by using the regular solution $(g_\kappa^{\rm reg}(r), f_\kappa^{\rm reg})$ and the irregular solution $\left(g_\kappa^{\rm irr}(r), f_\kappa^{\rm irr}\right)$, which are given in Appendix D:

$$\begin{pmatrix} g_\kappa(r) \\ f_\kappa(r) \end{pmatrix} \to \cos\delta_\kappa \begin{pmatrix} g_\kappa^{\rm reg}(r) \\ f_\kappa^{\rm reg}(r) \end{pmatrix} - \sin\delta_\kappa \begin{pmatrix} g_\kappa^{\rm irr}(r) \\ f_\kappa^{\rm irr}(r) \end{pmatrix}. \tag{E.66}$$

The value of δ_κ have to be calculated by numerical calculation for each κ.

The sign $+/-$ of the second term corresponds to the outgoing/incoming boundary condition. For our purpose to obtain the wave function of the final scattering state, we have to choose the incoming boundary condition [117].

E.3.2 Numerical Calculation

We have discussed how to superpose partial waves in the previous subsection. Next we describe how to obtain each partial waves numerically. As bound states, the equation to solve is the coupled equation (E.23)-(E.24). In calculation for bound states, the energy was to be found, while, for scattering states, the energy is given before calculation.

Let us suppose that $\phi(r)$ has finite value ϕ_0 at the origin and $\phi(r)$ is sufficiently smooth near the origin. Then Eqs. (E.23)-(E.24) can be written near the origin as

$$\frac{dg_\kappa(r)}{dr} + \frac{1+\kappa}{r} g_\kappa(r) - (E + m + e\phi_0) f_\kappa(r) \sim 0, \tag{E.75}$$

$$\frac{df_\kappa(r)}{dr} + \frac{1-\kappa}{r} f_\kappa(r) + (E - m + e\phi_0) g_\kappa(r) \sim 0. \tag{E.76}$$

Define $\tilde{E} = E + e\phi_0$ and $\tilde{p} = \sqrt{\tilde{E}^2 - m^2}$, and the solution of the Dirac equation near the origin should behave as

$$g_\kappa(r) = N\sqrt{\tilde{E} + m} j_{l_\kappa}(\tilde{p}r), \tag{E.77}$$

$$f_\kappa(r) = N\sqrt{\tilde{E} - m} S_\kappa j_{l_{-\kappa}}(\tilde{p}r), \tag{E.78}$$

where N is a common constant. Therefore, the following equations hold for sufficiently small $r_{\rm ini}$:

$$g_\kappa(r_{\rm ini}) = N\sqrt{\tilde{E} + m} j_{l_\kappa}(\tilde{p}r_{\rm ini}), \tag{E.79}$$

$$f_\kappa(r_{\rm ini}) = N\sqrt{\tilde{E} - m} S_\kappa j_{l_{-\kappa}}(\tilde{p}r_{\rm ini}). \tag{E.80}$$

Using this as an initial value, we numerically solve the differential equation (E.23)-(E.24) from inside to outside by the fourth-order Runge-Kutta method.

Next the phase shift δ_κ have to be found. Let us remember that the solution satisfy the boundary condition (E.66). We have to determine δ_κ to connect smoothly the function solved from inside and the asymptotic form (E.66) at a "sufficiently" infinity point $r_{\rm con}$. $r_{\rm con}$ should be chosen to be a point where the form of the potential can be taken as that of point-charge potential. Especially, if the nuclear charge distribution is assumed to be the finite distribution with a radius R, it is good to choose $r_{\rm con} = R$. The word "connected smoothly" means matching of their logarithmic derivatives. Define a function of δ,

$$W_g(\delta) = \frac{(g_\kappa(r_{\rm con}))'}{g_\kappa(r_{\rm con})} - \frac{\left(\cos\delta g_\kappa^{\rm reg}(r_{\rm con}) - \sin\delta g_\kappa^{\rm irr}(r_{\rm con})\right)'}{\cos\delta g_\kappa^{\rm reg}(r_{\rm con}) - \sin\delta g_\kappa^{\rm irr}(r_{\rm con})}, \tag{E.81}$$

which is called as Wronskian. Search δ to satisfy $W_g(\delta) = 0$ numerically, and the found δ can be recognized as δ_κ. When δ_κ can be determined by the above way, the asymptotic form of $g_\kappa(r)$ is also given. Finally, normalize $g_\kappa(r)$ to connect its asymptotic form at $r = r_{\rm con}$, and the partial wave is obtained.

Appendix F

Fierz Transformation

Here, we derive Fierz transformation in order to prove the generality of contact Lagrangian, Eq. (2.11).

F.1 Products of Dirac Matrices

As a notation in this appendix, let Dirac matrices and their products be represented by subscripting Γ as shown in Table F.1.

Table F.1: Products of Dirac matrices. Here, $\sigma^{\mu\nu} = i\gamma^\mu\gamma^\nu$.

Γ^1	Γ^2	Γ^3	Γ^4	Γ^5	Γ^6	Γ^7	Γ^8	Γ^9	Γ^{10}	Γ^{11}	Γ^{12}	Γ^{13}	Γ^{14}	Γ^{15}	Γ^{16}
$\mathbf{1}$	γ^0	γ^1	γ^2	γ^3	σ^{01}	σ^{02}	σ^{03}	σ^{12}	σ^{23}	σ^{31}	$\gamma^0\gamma^5$	$\gamma^1\gamma^5$	$\gamma^2\gamma^5$	$\gamma^3\gamma^5$	γ^5

Here we note some properties of Γs.
A trace of two Γ^a satisfies

$$\mathrm{Tr}\left[\Gamma^a\Gamma^b\right] = \mathrm{Tr}\left[\left(\Gamma^a\right)^2\right]\delta_{a,b}. \tag{F.1}$$

Also, the set of Γ^a forms an orthogonal basis for 4×4 matrices, so that an arbitrary 4×4 matrix, X, can be represented by their linear combination,

$$X = \frac{1}{4}\sum_a s_a \mathrm{Tr}\left[X\Gamma^a\right]\Gamma^a, \qquad s_a = \frac{1}{4}\mathrm{Tr}\left[(\Gamma^a)^2\right]. \tag{F.2}$$

Since the square of any Γ^a equals to identity matrix, it is clear that $s_a = \pm 1$.

F.2 Derivation of Fierz Transformation

Let us derive the formula,

$$\left(\overline{\psi}_1\Gamma^a\psi_2\right)\left(\overline{\psi}_3\Gamma^a\psi_4\right) = -\frac{1}{16}\sum_b \mathrm{Tr}\left[\left(\Gamma^a\Gamma^b\right)^2\right]\left(\overline{\psi}_1\Gamma^a\psi_4\right)\left(\overline{\psi}_3\Gamma^a\psi_2\right), \tag{F.3}$$

which is called as the Fierz transformation. This transformation shows that four-Fermi contact operators can rewritten by operators where fermion pairs are exchanged.

Now Lorentz invariant interactions that can be constructed by four Dirac fields (ψ_1, ψ_2, ψ_3, ψ_4) are the following five:

$$\mathcal{L}^S(\psi_1,\psi_2,\psi_3,\psi_4) = \left(\overline{\psi}_1\psi_2\right)\left(\overline{\psi}_3\psi_4\right), \tag{F.4}$$
$$\mathcal{L}^V(\psi_1,\psi_2,\psi_3,\psi_4) = \left(\overline{\psi}_1\gamma^\mu\psi_2\right)\left(\overline{\psi}_3\gamma_\mu\psi_4\right), \tag{F.5}$$
$$\mathcal{L}^T(\psi_1,\psi_2,\psi_3,\psi_4) = \left(\overline{\psi}_1\sigma^{\mu\nu}\psi_2\right)\left(\overline{\psi}_3\sigma_{\mu\nu}\psi_4\right), \tag{F.6}$$
$$\mathcal{L}^A(\psi_1,\psi_2,\psi_3,\psi_4) = \left(\overline{\psi}_1\gamma^\mu\gamma^5\psi_2\right)\left(\overline{\psi}_3\gamma_\mu\gamma^5\psi_4\right), \tag{F.7}$$
$$\mathcal{L}^P(\psi_1,\psi_2,\psi_3,\psi_4) = \left(\overline{\psi}_1\gamma^5\psi_2\right)\left(\overline{\psi}_3\gamma^5\psi_4\right). \tag{F.8}$$

These can be written by $\Gamma^a_{\alpha\beta}\Gamma^a_{\rho\eta}$ shown in Table F.1. For example, $\mathcal{L}^V$ is rewritten as

$$\begin{aligned}\mathcal{L}^V(\psi_1,\psi_2,\psi_3,\psi_4) &= \left(\overline{\psi}_1\gamma^0\psi_2\right)\left(\overline{\psi}_3\gamma^0\psi_4\right) - \left(\overline{\psi}_1\gamma^k\psi_2\right)\left(\overline{\psi}_3\gamma^k\psi_4\right) \\ &= \left(\overline{\psi}_1\right)_\alpha\left(\psi_2\right)_\beta\left(\overline{\psi}_3\right)_\rho\left(\psi_4\right)_\eta\left(\Gamma^2_{\alpha\beta}\Gamma^2_{\rho\eta} - \Gamma^3_{\alpha\beta}\Gamma^3_{\rho\eta} - \Gamma^4_{\alpha\beta}\Gamma^4_{\rho\eta} - \Gamma^5_{\alpha\beta}\Gamma^5_{\rho\eta}\right).\end{aligned} \tag{F.9}$$

Here, β and ρ are fixed and a 4×4 matrix $M^{\alpha\beta\rho}$ is defined as

$$M^{a\beta\rho}_{\alpha\eta} = \Gamma^a_{\alpha\beta}\Gamma^a_{\rho\eta}, \tag{F.10}$$

where α and η mean indices of the matrix. This matrix can be expressed using the completeness of the Γ^a matrices, Eq. (F.2), as

$$M^{a\beta\rho} = \frac{1}{4}\sum_b s_b \mathrm{Tr}\left[M^{a\beta\rho}\Gamma^b\right]\Gamma^b. \tag{F.11}$$

The trace part is calculated by the definition of $M^{a\beta\rho}$, Eq. (F.10), and the completeness relation, Eq. (F.2), again, as

$$\begin{aligned}\mathrm{Tr}\left[M^{a\beta\rho}\Gamma^b\right] &= \sum_{\alpha,\eta}\Gamma^a_{\alpha\beta}\Gamma^a_{\rho\eta}\Gamma^b_{\eta\alpha} \\ &= \left(\Gamma^a\Gamma^b\Gamma^a\right)_{\rho\beta} \\ &= \left(\frac{1}{4}\sum_c s_c \mathrm{Tr}\left[\Gamma^a\Gamma^b\Gamma^a\Gamma^c\right]\Gamma^c\right)_{\rho\beta}.\end{aligned} \tag{F.12}$$

Since it is known that the product of Γ matrices is proportional to another Γ matrices, let us replace $\Gamma^a\Gamma^b$ and $\Gamma^a\Gamma^c$ with Γ^d and Γ^e, respectively. Therefore, it is found that

$$\mathrm{Tr}\left[\Gamma^a\Gamma^b\Gamma^a\Gamma^c\right] \propto \mathrm{Tr}\left[\Gamma^d\Gamma^e\right] \propto \delta_{d,e}. \tag{F.13}$$

Since $d=e$ implies $b=c$, we also get

$$\mathrm{Tr}\left[\Gamma^a\Gamma^b\Gamma^a\Gamma^c\right] = \mathrm{Tr}\left[\left(\Gamma^a\Gamma^b\right)^2\right]\delta_{b,c}. \tag{F.14}$$

In addition to the above discussion, by using $s_b^2 = 1$, we obtain

$$\Gamma^a_{\alpha\beta}\Gamma^a_{\rho\eta} = \frac{1}{16}\sum_b \mathrm{Tr}\left[\left(\Gamma^a\Gamma^b\right)^2\right]\Gamma^b_{\alpha\eta}\Gamma^b_{\rho\beta}. \tag{F.15}$$

This formula leads to the Fierz transformation,

$$\left(\overline{\psi}_1\Gamma^a\psi_2\right)\left(\overline{\psi}_3\Gamma^a\psi_4\right) = -\frac{1}{16}\sum_b \mathrm{Tr}\left[\left(\Gamma^a\Gamma^b\right)^2\right]\left(\overline{\psi}_1\Gamma^a\psi_4\right)\left(\overline{\psi}_3\Gamma^a\psi_2\right). \tag{F.3}$$

The negative sign that appears here comes from the exchange of the fermion fields.

Using this result, it becomes possible to express the operators (F.4)-(F.8) by superposition of operators in which ψ_2 and ψ_4 are replaced:

$$\mathcal{L}^X(\psi_1,\psi_2,\psi_3,\psi_4) = \sum_{Y=S,V,T,A,P} C_{XY}\mathcal{L}^Y(\psi_1,\psi_4,\psi_3,\psi_2), \tag{F.16}$$

where the coefficients are given as shown in Table F.2.

Table F.2: The value of the coefficients C_{XY}.

X\Y	S	V	T	A	P
S	-1/4	-1/4	-1/8	1/4	-1/4
V	-1	1/2	0	1/2	1
T	-3	0	1/2	0	-3
A	1	1/2	0	1/2	-1
P	-1/4	1/4	-1/8	-1/4	-1/4

The Lagrangians considered in Eqs. (F.4)-(F.8) look invariant to the parity conversion. However, in order to consider Lagrangian which breaks the parity, it is possible to set $\psi_1 \to P_L\psi_1$, etc., and Table F.2 can be applied similarly.

F.3 Generality of Contact Lagrangian

Here we discuss that the contact Lagrangian (2.11) given in the chapter 3 holds generality.

Not distinguishing between terms related by replacement of $L \leftrightarrow R$ or by Hermite transformation, there are three types of interaction term present in Eq. (2.11),

$$(\bar{e}P_R\mu)(\bar{e}P_Re);\ (\bar{e}\gamma_\mu P_R\mu)(\bar{e}\gamma^\mu P_Re);\ (\bar{e}\gamma_\mu P_R\mu)(\bar{e}\gamma^\mu P_Le). \tag{F.17}$$

One may come up with other three terms which respect the Lorentz symmetry but are absent in Eq. (2.11),

$$(\bar{e}P_R\mu)(\bar{e}P_Le);\ (\bar{e}\sigma_{\mu\nu}P_R\mu)(\bar{e}\sigma^{\mu\nu}P_Re);\ (\bar{e}\sigma_{\mu\nu}P_R\mu)(\bar{e}\sigma^{\mu\nu}P_Le). \tag{F.18}$$

Now, we show that the members of Eq. (F.18) can be rewritten to those of Eq. (F.17) by using the Fierz transformation.

First of all, let us consider scalar-type interaction $(\bar{e}P_R\mu)(\bar{e}P_Le)$. Setting $\psi_1 = P_Le$, $\psi_2 = P_R\mu$, $\psi_3 = P_Re$, $\psi_4 = P_Le$, $X = S$ in Eq. F.16, it is found that

$$\begin{aligned}(\bar{e}P_R\mu)(\bar{e}P_Le) =& (\overline{P_Le}P_R\mu)(\overline{P_Re}P_Le)\\ =& -\frac{1}{4}(\overline{P_Le}\gamma_\mu P_Le)(\overline{P_Re}\gamma^\mu P_R\mu) + \frac{1}{4}(\overline{P_Le}\gamma_\mu\gamma_5 P_Le)(\overline{P_Re}\gamma^\mu\gamma_5 P_R\mu)\\ =& -\frac{1}{2}(\bar{e}\gamma^\mu P_R\mu)(\bar{e}\gamma_\mu P_Le),\end{aligned} \tag{F.19}$$

where we used some relations for projection operators such as $P_LP_R = P_RP_L = 0$ and $\gamma_5P_R = P_R$, $\gamma_5P_L = -P_L$. Thus, $(\bar{e}P_R\mu)(\bar{e}P_Le)$ is equivalent to $(\bar{e}\gamma^\mu P_R\mu)(\bar{e}\gamma_\mu P_Le)$ except for the overall constant factor.

Next we discuss $(\bar{e}\sigma_{\mu\nu}P_R\mu)(\bar{e}\sigma^{\mu\nu}P_Re)$. A similar calculation gives

$$\begin{aligned}(\bar{e}\sigma_{\mu\nu}P_R\mu)(\bar{e}\sigma^{\mu\nu}P_Re) =& (\overline{P_Le}\sigma_{\mu\nu}P_R\mu)(\overline{P_Le}\sigma^{\mu\nu}P_Re)\\ =& -3(\overline{P_Le}P_Re)(\overline{P_Le}P_R\mu) + \frac{1}{2}(\overline{P_Le}\sigma_{\mu\nu}P_Re)(\overline{P_Le}\sigma^{\mu\nu}P_R\mu)\\ & -3(\overline{P_Le}\gamma_5P_R\mu)(\overline{P_Le}\gamma_5P_Re)\\ =& -6(\bar{e}P_R\mu)(\bar{e}P_Re) + \frac{1}{2}(\bar{e}\sigma_{\mu\nu}P_R\mu)(\bar{e}\sigma^{\mu\nu}P_Re).\end{aligned} \tag{F.20}$$

Therefore we get

$$(\overline{e}\sigma_{\mu\nu}P_R\mu)(\overline{e}\sigma^{\mu\nu}P_Re) = -12(\overline{e}P_R\mu)(\overline{e}P_Re). \tag{F.21}$$

It is proved that the tensor-type interaction $(\overline{e}\sigma_{\mu\nu}P_R\mu)(\overline{e}\sigma^{\mu\nu}P_Re)$ has exactly the same property as the scalar-type one $(\overline{e}P_R\mu)(\overline{e}P_Re)$.

Finally, the remaining one, $(\overline{e}\sigma_{\mu\nu}P_R\mu)(\overline{e}\sigma^{\mu\nu}P_Le)$, is considered. However, the same operation gives zero to this operator:

$$(\overline{e}\sigma_{\mu\nu}P_R\mu)(\overline{e}\sigma^{\mu\nu}P_Le) = 0. \tag{F.22}$$

Therefore, this interaction is not worth considering.

As the result, it is shown that all of the interaction terms absent in Eq. (2.11) are certainly redundant.

Appendix G

Angular Momentum Coupling

Here, we summarize the angular momentum algebra, such as the Clebsch-Gordan coefficient [118]. They are necessary for analyzing the angular component of the wave function.

G.1 Clebsch-Gordan Coefficient

Let $\psi_{j_i}^{m_i}$ $(i = 1, 2)$ be an eigenfunction for an angular momentum operator $\boldsymbol{J}_i$, which holds

$$\boldsymbol{J}_i^2 \psi_{j_i}^{m_i} = j_i(j_i+1)\psi_{j_i}^{m_i}, \tag{G.1}$$

$$J_{iz} \psi_{j_i}^{m_i} = m_i \psi_{j_i}^{m_i}, \tag{G.2}$$

where $-j_i \leq m_i \leq j_i$. Now the direct product of two eigenfunctions, $\psi_{j_1}^{m_1}\psi_{j_2}^{m_2}$, is also an eigenfunction of four operators, such as $\boldsymbol{J}_1^2$, J_{1z}, $\boldsymbol{J}_2^2$, J_{2z}. In other words, the above four operators are diagonal on the $\left\{\psi_{j_1}^{m_1}\psi_{j_2}^{m_2}\right\}$ basis. In practice, however, this basis is not useful because each of angular momenta is not conserved in usual cases. On the other hand, the total momentum,

$$\boldsymbol{J} = \boldsymbol{J}_1 + \boldsymbol{J}_2, \tag{G.3}$$

should be a good conserved quantity as long as the system has the spherical symmetry. Therefore, it is more useful to properly rebuild the basis of eigenfunctions.

Now let us look for the basis where $\boldsymbol{J}^2$ and J_z are diagonal as well as $\boldsymbol{J}_1^2$ and $\boldsymbol{J}_2^2$. A new representation, ψ_j^m, should be related to the old one by some unitary transformation as follows:

$$\psi_j^m = \sum_{m_1,m_2} (j_1, m_1, j_2, m_2|j, m)\, \psi_{j_1}^{m_1}\psi_{j_2}^{m_2}. \tag{G.4}$$

The expansion coefficients, $(j_1, m_1, j_2, m_2|j, m)$, are called as the Clebsch-Gordan coefficient.

Some formulea for Clebsch-Gordan coefficient are shown here. First, the unitarity of this transformation requires

$$\sum_{m_1,m_2} (j_1, m_1, j_2, m_2|j, m)(j_1, m_1, j_2, m_2|j', m') = \delta_{j,j'}\delta_{m,m'}, \tag{G.5}$$

$$\sum_{j,m} (j_1, m_1, j_2, m_2|j, m)(j_1, m_1', j_2, m_2'|j, m) = \delta_{m_1,m_1'}\delta_{m_2,m_2'}. \tag{G.6}$$

Next, if $m \neq m_1 + m_2$, Clebsch-Gordan coefficients are zero because you can prove

$$(m - m_1 - m_2)\,(j_1, m_1, j_2, m_2|j, m) = 0. \tag{G.7}$$

It is easy to confirm this relation by operating J_z to ψ_j^m. Also, the allowed ranges of the quantum numbers of coupled representation are given as

$$-j \leq m \leq j, \tag{G.8}$$
$$|j_1 - j_2| \leq j \leq j_1 + j_2. \tag{G.9}$$

The explicit form of the Clebsch-Gordan coefficient is given as

$$\begin{aligned}(j_1, m_1, j_2, m_2|j, m) &= \delta_{m_1+m_2,m} \\ &\times \left[(2j+1)\frac{(j+j_1-j_2)!(j-j_1+j_2)!(j_1+j_2-j_3)!(j+m)!(j-m)!}{(j_1+j_2+j+1)!(j_1-m_1)!(j_1+m_1)!(j_2-m_2)!(j_2+m_2)!}\right]^{1/2} \\ &\times \sum_\nu \frac{(-1)^{\nu+j_2+m_2}}{\nu!}\frac{(j_2+j+m_1-\nu)!(j_1-m_1+\nu)!}{(j-j_1+j_2-\nu)!(j+m-\nu)!(\nu+j_1-j_2-m)!}.\end{aligned} \tag{G.10}$$

Here the sum on ν is over all integers, but it is sufficient in practice to consider only the integers which make arguments of any factorials non-negative. Especially, in the case of $j = 0$ and $m = 0$, its formula becomes

$$(j_1, m_1, j_2, m_2|0, 0) = \frac{(-1)^{j_1-m_1}}{\sqrt{2j_1+1}}\delta_{j_1,j_2}\delta_{m_1,-m_2}. \tag{G.11}$$

By the formula (G.10), we can prove the following symmetry for exchange of pair of indices and parity inversion:

$$(j_1, m_1, j_2, m_2|j, m) = (-1)^{j_1+j_2-j}(j_1, -m_1, j_2, -m_2|j, -m) \tag{G.12}$$
$$= (-1)^{j_1+j_2-j}(j_2, m_2, j_1, m_1|j, m) \tag{G.13}$$
$$= (-1)^{j_1-m_1}\sqrt{\frac{2j+1}{2j_2+1}}(j_1, m_1, j, -m|j_2, -m_2). \tag{G.14}$$

Now it is convenient to introduce the Wigner's $3j$ symbol. The symbol is defined as

$$\begin{pmatrix} j_1 & j_2 & j \\ m_1 & m_2 & -m \end{pmatrix} = \frac{(-1)^{j_1-j_2+m}}{\sqrt{2j+1}}(j_1, m_1, j_2, m_2|j, m). \tag{G.15}$$

The advantage of notation is that the appearance of factors by replacing indices is simplified, as noted below. Suppose three indices $\{a, b, c\}$ are replaced into $\{p, q, r\}$ and some extra factor C is multiplied:

$$\begin{pmatrix} j_a & j_b & j_c \\ m_a & m_b & m_c \end{pmatrix} = C\begin{pmatrix} j_p & j_q & j_r \\ m_p & m_q & m_r \end{pmatrix}. \tag{G.16}$$

The value of C is summarized as follows:

1. $C = 1$ if $\{p, q, r\}$ is even permutation of $\{a, b, c\}$.
2. $C = (-1)^{j_a+j_b+j_c}$ if $\{p, q, r\}$ is odd permutation of $\{a, b, c\}$.
3. $C = (-1)^{j_a+j_b+j_c}$ if $\{m_p, m_q, m_r\} = \{-m_a, -m_b, -m_c\}$.

Moreover, the orthogonal relation for the $3j$ symbol is represented as

$$\sum_{j,m}(2j+1)\begin{pmatrix} j_a & j_b & j \\ m_a & m_b & m \end{pmatrix}\begin{pmatrix} j_a & j_b & j \\ m'_a & m'_b & m \end{pmatrix} = \delta_{m_a,m'_a}\delta_{m_b,m'_b}, \tag{G.17}$$

$$\sum_{m_a,m_b}\begin{pmatrix} j_a & j_b & j \\ m_a & m_b & m \end{pmatrix}\begin{pmatrix} j_a & j_b & j' \\ m_a & m_b & m' \end{pmatrix} = \frac{\delta_{j,j'}\delta_{m,m'}}{2j+1}. \tag{G.18}$$

In terms of $3j$ symbol, Eq. (G.11) can be rewritten as

$$\begin{pmatrix} j_1 & j_2 & 0 \\ m_1 & m_2 & 0 \end{pmatrix} = \frac{(-1)^{j_1-m_1}}{\sqrt{2j_1+1}} \delta_{j_1,j_2} \delta_{m_1,-m_2}. \tag{G.19}$$

In this thesis, the following notation is used:

$$\begin{aligned} [A_{L_a} \otimes B_{L_b}]^M_J &= \sum_{M_a,M_b} (L_a, M_a, L_b, M_b | J, M)\, A^{M_a}_{L_a} \otimes B^{M_b}_{L_b} \\ &= \sum_{M_a,M_b} (-1)^{L_a - L_b + M} \sqrt{2J+1} \begin{pmatrix} L_a & L_b & J \\ M_a & M_b & -M \end{pmatrix} A^{M_a}_{L_a} \otimes B^{M_b}_{L_b}, \end{aligned} \tag{G.20}$$

where A and B are spherical tensor operators. The definition of the spherical tensor operator is given in the next section.

G.2 Spherical Tensor Operator

The function $R\psi^m_j$ obtained by rotating the eigenfunction of the angular momentum ψ^m_l in the three-dimensional space is expressed by using the angular momentum operator $\boldsymbol{J}$ and the rotation parameter $\boldsymbol{\theta}$ as

$$R(\boldsymbol{\theta})\psi^m_j = \exp(-i\boldsymbol{\theta}\cdot\boldsymbol{J})\psi^m_j. \tag{G.21}$$

Since the operator $\boldsymbol{J}^2$ commutes with any components of operator $\boldsymbol{J}$, it is also commutative for the rotation operator $R(\boldsymbol{\theta})$. This fact means that the magnitude of the angular momentum does not depend on the direction of the coordinates. On the other hand, however, $R(\boldsymbol{\theta})\psi^m_j$ is no longer the eigenstate of the operator J_z. Generally, it can be represented by a superposition of angular momentum eigenstates with the same quantum number j as follows:

$$R(\boldsymbol{\theta})\psi^m_j = \sum_{m'} \langle jm' | e^{-i\boldsymbol{\theta}\cdot\boldsymbol{J}} | jm \rangle\, \psi^{m'}_j. \tag{G.22}$$

Three degrees of freedom are required for the parameter to represent the rotation of the three-dimension space. These can be taken as three components of $\boldsymbol{\theta}$ as above, but the description using Euler angles is useful. Let the original coordinate be (x, y, z), and consider the coordinate rotation by the following procedure.

1. Rotate the angle α around the z axis. Call the new coordinates (x', y', z').
2. Rotate the angle β around the y' axis. Call the new coordinates (x'', y'', z'').
3. Rotate the angle γ around the z'' axis.

α, β, γ defined here are called Euler angles. By them, the rotation operator can be written as

$$R(\alpha, \beta, \gamma) = e^{-i\gamma J_{z''}} e^{-i\beta J_{y'}} e^{-i\alpha J_z}. \tag{G.23}$$

Here, since the y' axis is obtained by rotating the original y axis by the angle α, it can be expressed as

$$e^{-i\beta J_{y'}} = e^{-i\alpha J_z} e^{-i\beta J_y} e^{i\alpha J_z}. \tag{G.24}$$

Similarly,

$$\begin{aligned} e^{-i\gamma J_{z''}} =& e^{-i\beta J_{y'}} e^{-i\gamma J_{z'}} e^{i\beta_{y'}} \\ =& e^{-i\alpha J_z} e^{-i\beta J_y} e^{-i\gamma J_z} e^{i\beta J_y} e^{i\alpha J_z}. \end{aligned} \tag{G.25}$$

Using these expressions, the rotation operator is denoted in terms of the original axes as

$$R(\alpha,\beta,\gamma) = e^{-i\alpha J_z} e^{-i\beta J_y} e^{-i\gamma J_z}. \tag{G.26}$$

Hereafter, let us denote the rotation using the Euler angle and let $D_j^{m'm}(\alpha,\beta,\gamma)$ be the matrix element written in Eq. (G.22):

$$R(\alpha,\beta,\gamma)\psi_j^m = \sum_{m'} D_j^{m'm}(\alpha,\beta,\gamma)\psi_j^{m'}. \tag{G.27}$$

The matrix element $D_j^{m'm}(\alpha,\beta,\gamma)$ of the rotation operator is given by

$$\begin{aligned} D_j^{m'm}(\alpha,\beta,\gamma) =& \langle jm'|e^{-i\alpha J_z} e^{-i\beta J_y} e^{-i\gamma J_z}|jm\rangle \\ =& e^{-im'\alpha} \langle jm'|e^{-i\beta J_y}|jm\rangle e^{-im\gamma}. \end{aligned} \tag{G.28}$$

It is known that the matrix element $\langle jm'|e^{-i\beta J_y}|jm\rangle$ is given by

$$\begin{aligned} \langle jm'|e^{-i\beta J_y}|jm\rangle =& \sqrt{(j+m)!(j-m)!(j+m')!(j-m')!} \\ & \times \sum_\kappa \frac{(-1)^\kappa}{(j-m'-\kappa)!(j+m-\kappa)!(\kappa+m'-m)!\kappa!} \\ & \times \left(\cos\frac{\beta}{2}\right)^{2j+m-m'-2\kappa} \left(-\sin\frac{\beta}{2}\right)^{m'-m+2\kappa}. \end{aligned} \tag{G.29}$$

Here, the sum on κ runs over only integers where all factorial arguments are non-negative.

When a set of $(2k+1)$ operators is transformed under a rotation R as

$$R(\alpha,\beta,\gamma)T_k^q R^{-1}(\alpha\beta\gamma) = \sum_{q'} D_k^{q'q}(\alpha\beta\gamma)T_k^{q'}, \tag{G.30}$$

we call T_k^q as an irreducible tensor operator of rank k.

The projected quantum number dependence of $\langle j'm'|T_k^q|jm\rangle$ can be factored out in the form of a Clebsch-Gordan coefficient as

$$\langle j'm'|T_k^q|jm\rangle = \frac{(j,m,k,q|j',m')}{\sqrt{2j'+1}} \langle j'||T_k||j\rangle. \tag{G.31}$$

This is called the Wigner-Eckart theorem. Here, $\langle j'||T_k||j\rangle$ is independent of any projection quantum numbers and is called a reduced matrix element, which can be calculated by the equation

$$\langle j'||T_k||j\rangle = \sum_{m',q,m} \frac{(j,m,k,q|j',m')}{\sqrt{2j'+1}} \langle j'm'|T_k^q|jm\rangle, \tag{G.32}$$

which is obtained from Eq. (G.31). Especially, for the identity, the reduced matrix element is given by

$$\langle j'||1||j\rangle = \sqrt{2j+1}\delta_{j,j'}. \tag{G.33}$$

G.2.1 Spherical Basis

For calculation using the partial wave expansion, it is convenient to use the spherical basis. Let $\boldsymbol{A}$ be a three-component vector: $\boldsymbol{A} = (A_x, A_y, A_z)$. Then $\boldsymbol{A}$ can also be called as a tensor operator of rank 1. The representation of $\boldsymbol{A}$ in the spherical basis, $\left(A^{+1}, A^0, A^{-1}\right)$, is defined as

$$A^{\pm 1} = \frac{-1}{\sqrt{2}}\left(\pm A_x + iA_y\right), \quad A^0 = A_z. \tag{G.34}$$

In terms of the spherical basis, the inner product and outer product are written as

$$\begin{aligned}\boldsymbol{A}\cdot\boldsymbol{B} &= \sum_{s=\pm1,0}(-1)^s A^s B^{-s} \\ &= -\sqrt{3}\,[A\otimes B]^0_0\,,\end{aligned} \tag{G.35}$$

and

$$(\boldsymbol{A}\times\boldsymbol{B})^m = -i\sqrt{2}\,[A\otimes B]^m_1\,, \tag{G.36}$$

respectively. Eq. (G.35) can be generalized to the tensor operator of rank l as follows:

$$\begin{aligned}\boldsymbol{A}_L\cdot\boldsymbol{B}_L &= \sum_{M=-L}^{L}(-1)^M A^M_L B^{-M}_L \\ &=(-1)^L\sqrt{2L+1}\,[A_L\otimes B_L]^0_0\,.\end{aligned} \tag{G.37}$$

G.3 $3nj$ Symbols

Generally, we can discuss more complicated cases with more than two angular momenta. In the cases, we would like to need the unitary transformation between basis where different angular momenta are coupled. Here $6j$ and $9j$ symbols are introduced.

G.3.1 $6j$ Symbol

In the above discussion, we have just considered a sum of two angular momenta, $\boldsymbol{J}=\boldsymbol{J}_1+\boldsymbol{J}_2$, and a unitary transformation from the base diagonal for J_{1z} and J_{2z} to the base diagonal for J_z and $\boldsymbol{J}^2$. Next let us think about a case of three angular momenta and research a unitary transformation between different basis again.

Suppose that there are three angular momenta, $\boldsymbol{J}_1$, $\boldsymbol{J}_2$, and $\boldsymbol{J}_3$. Then it is easily found that we can simultaneously diagonalize six operaters in the simple direct product: $\boldsymbol{J}_1^2$, J_{1z}, $\boldsymbol{J}_2^2$, J_{2z}, $\boldsymbol{J}_3^2$, and J_{3z}. Let us think about another base where $\boldsymbol{J}^2$ and J_z are diagonal. In such a base, the diagonal six operators are $\boldsymbol{J}_1^2$, $\boldsymbol{J}_2^2$, $\boldsymbol{J}_3^2$, $\boldsymbol{J}_{ij}^2$, $\boldsymbol{J}^2$, and J_z. Here, for example, $\boldsymbol{J}_{ij}=\boldsymbol{J}_{12}=\boldsymbol{J}_1+\boldsymbol{J}_2$. There are three choices for ij: The other choices are $\boldsymbol{J}_{23}=\boldsymbol{J}_2+\boldsymbol{J}_3$ and $\boldsymbol{J}_{31}=\boldsymbol{J}_3+\boldsymbol{J}_1$. Now let us study the relation between two of these basis.

Let $\psi(j_{12})$ and $\psi(j_{23})$ be an eigenfunction of $\boldsymbol{J}_{12}^2$ and $\boldsymbol{J}_{23}^2$, respectively, and their indices j_{12} and j_{23} indicate the eigenvalues of $\boldsymbol{J}_{12}^2$ and $\boldsymbol{J}_{23}^2$, respectively. Moreover, suppose that both of them are also an eigenfunction of $\boldsymbol{J}_1^2$, $\boldsymbol{J}_2^2$, $\boldsymbol{J}_3^2$, $\boldsymbol{J}^2$, and J_z. These eigenfunctions can be constructed by coupling the direct product representation of four eigenfunctions, $\psi_{j_1}^{m_1}\psi_{j_2}^{m_2}\psi_{j_3}^{m_3}\psi_{j_4}^{m_4}$, in terms of Clebsch-Gordan coefficients. Then $\psi(j_{12})$ and $\psi(j_{23})$ should be related by some unitary transformation as follows:

$$\psi(j_{12}) = \sum_{j_{23}}\sqrt{[j_{12}\cdot j_{23}]}W\left(j_1,j_2,j,j_3;j_{12},j_{23}\right)\psi(j_{23}). \tag{G.38}$$

The W is called as the Racah coefficient.

The Racah coefficient W can be represented by the more symmetric $6j$ symbols as

$$W\left(j_1,j_2,j,j_3;j_{12},j_{23}\right) = (-1)^{j_1+j_2+j_3+j}\begin{Bmatrix} j_1 & j_2 & j_{12} \\ j_3 & j & j_{23}\end{Bmatrix}. \tag{G.39}$$

The orthogonality of the $6j$ symbol is given as

$$\sum_{j_3}[j_3\cdot j_6]\begin{Bmatrix} j_1 & j_2 & j_3 \\ j_4 & j_5 & j_6\end{Bmatrix}\begin{Bmatrix} j_1 & j_2 & j_3 \\ j_4 & j_5 & j_6'\end{Bmatrix} = \delta_{j_6,j_6'}. \tag{G.40}$$

We can write down the following relation by using the $6j$ symbol:

$$\left[\left[A_{L_a}\otimes B_{L_b}\right]_{L_{ab}}\otimes C_{L_c}\right]_J^M = (-1)^{L_a+L_b+L_c+J} \times \sum_{L_{bc}} \sqrt{[L_{ab}\cdot L_{bc}]} \begin{Bmatrix} L_a & L_b & L_{ab} \\ L_c & J & L_{bc} \end{Bmatrix} \left[A_{L_a}\otimes\left[B_{L_b}\otimes C_{L_c}\right]_{L_{bc}}\right]_J^M . \tag{G.41}$$

The $6j$ symbols have the following symmetry for the replacement of its indices:

1. invariant under any replacement of columns:

$$\begin{Bmatrix} j_1 & j_2 & j_3 \\ j_4 & j_5 & j_6 \end{Bmatrix} = \begin{Bmatrix} j_2 & j_1 & j_3 \\ j_5 & j_4 & j_6 \end{Bmatrix} = \begin{Bmatrix} j_3 & j_2 & j_1 \\ j_6 & j_5 & j_4 \end{Bmatrix} = \begin{Bmatrix} j_1 & j_3 & j_2 \\ j_4 & j_6 & j_5 \end{Bmatrix} = \begin{Bmatrix} j_2 & j_3 & j_1 \\ j_5 & j_6 & j_4 \end{Bmatrix} = \begin{Bmatrix} j_3 & j_1 & j_2 \\ j_6 & j_4 & j_5 \end{Bmatrix}. \tag{G.42}$$

2. invariant under interchange of lower and upper arguments in any two columns:

$$\begin{Bmatrix} j_1 & j_2 & j_3 \\ j_4 & j_5 & j_6 \end{Bmatrix} = \begin{Bmatrix} j_4 & j_5 & j_3 \\ j_1 & j_2 & j_6 \end{Bmatrix} = \begin{Bmatrix} j_4 & j_2 & j_6 \\ j_1 & j_5 & j_3 \end{Bmatrix} = \begin{Bmatrix} j_1 & j_5 & j_6 \\ j_4 & j_2 & j_3 \end{Bmatrix}. \tag{G.43}$$

In special case, we have a simple form of $6j$ symbol:

$$\begin{Bmatrix} j_1 & j_1 & 1 \\ j_2 & j_2 & j \end{Bmatrix} = (-1)^{j_1+j_2+j} \frac{j(j+1)-j_1(j_1+1)-j_2(j_2+1)}{2\sqrt{j_1(j_1+1)(2j_1+1)j_2(j_2+1)(2j_2+1)}}, \tag{G.44}$$

$$\begin{Bmatrix} j & j' & 0 \\ l' & l & J \end{Bmatrix} = \frac{(-1)^{j+l+J}}{\sqrt{[j\cdot l]}} \delta_{j,j'}\delta_{l,l'}, \tag{G.45}$$

and

$$\begin{pmatrix} l_a & l_b & L \\ 0 & 0 & 0 \end{pmatrix} \begin{Bmatrix} j_a & j_b & L \\ l_a & l_b & 1/2 \end{Bmatrix} = \frac{-1}{\sqrt{[l_a\cdot l_b]}} \begin{pmatrix} j_a & j_b & L \\ 1/2 & -1/2 & 0 \end{pmatrix} \frac{1+(-1)^{l_a+l_b+L}}{2}. \tag{G.46}$$

The relation with $3j$ symbol is given as

$$\sum_{\text{all } m} (-1)^{j_4-m_4+j_5-m_5+j_6-m_6} \begin{pmatrix} j_1 & j_2 & j_3 \\ m_1 & m_2 & m_3 \end{pmatrix} \begin{pmatrix} j_1 & j_5 & j_6 \\ m_1 & -m_5 & m_6 \end{pmatrix} \times \begin{pmatrix} j_4 & j_2 & j_6 \\ m_4 & m_2 & -m_6 \end{pmatrix} \begin{pmatrix} j_4 & j_5 & j_3 \\ -m_4 & m_5 & m_3 \end{pmatrix} = \begin{Bmatrix} j_1 & j_2 & j_3 \\ j_4 & j_5 & j_6 \end{Bmatrix}, \tag{G.47}$$

or

$$\sum_{m_1,m_2,m_4,m_5,m_6} (-1)^{j_4-m_4+j_5-m_5+j_6-m_6} \begin{pmatrix} j_1 & j_2 & j_3 \\ m_1 & m_2 & m_3 \end{pmatrix} \begin{pmatrix} j_1 & j_5 & j_6 \\ m_1 & -m_5 & m_6 \end{pmatrix} \times \begin{pmatrix} j_4 & j_2 & j_6 \\ m_4 & m_2 & -m_6 \end{pmatrix} \begin{pmatrix} j_4 & j_5 & j_3 \\ -m_4 & m_5 & m_3 \end{pmatrix} = \frac{1}{[j_3]} \begin{Bmatrix} j_1 & j_2 & j_3 \\ j_4 & j_5 & j_6 \end{Bmatrix}. \tag{G.48}$$

Another relation between $6j$ and $3j$ symbols can be derived:

$$\begin{pmatrix} l_1 & l_2 & l_3 \\ n_1 & n_2 & n_3 \end{pmatrix} \begin{Bmatrix} l_1 & l_2 & l_3 \\ j_1 & j_2 & j_3 \end{Bmatrix} = \sum_{m_1,m_2,m_3} (-1)^{j_1+j_2+j_3+m_1+m_2+m_3} \begin{pmatrix} j_1 & j_2 & l_3 \\ m_1 & -m_2 & n_3 \end{pmatrix} \begin{pmatrix} j_2 & j_3 & l_1 \\ m_2 & -m_3 & n_1 \end{pmatrix} \begin{pmatrix} j_3 & j_1 & l_2 \\ m_3 & -m_1 & n_2 \end{pmatrix}. \tag{G.49}$$

G.3.2 $9j$ Symbol

Next consider the coupling of four angular momenta, $\boldsymbol{J}_1$, $\boldsymbol{J}_2$, $\boldsymbol{J}_3$, and $\boldsymbol{J}_4$. In the case, by dividing the four angular momenta into two sets, combining with each other, and combining the two combined angular momentums again, a diagonal expression can be generated for $\boldsymbol{J}^2$ and J_z, where $\boldsymbol{J}$ is the total angular momentum. Then the number of operators which can be diagonal simultaneously are eight: $\boldsymbol{J}_1^2$, $\boldsymbol{J}_2^2$, $\boldsymbol{J}_3^2$, $\boldsymbol{J}_4^2$, $\boldsymbol{J}_a^2$, $\boldsymbol{J}_b^2$, $\boldsymbol{J}^2$, and J_z. Here $\boldsymbol{J}_a^2$ and $\boldsymbol{J}_b^2$ are the two angular momenta obtained by initial couplings. We get different representations, depending on choice of initial angular-momentum sets. Now let $\psi(j_{12}, j_{34})$ be an eigenfunction in case with $\boldsymbol{J}_a = \mathbf{J}_{12} = \boldsymbol{J}_1 + \boldsymbol{J}_2$ and $\boldsymbol{J}_b = \boldsymbol{J}_{34} = \boldsymbol{J}_3 + \boldsymbol{J}_4$, and let $\psi(j_{13}, j_{24})$ be an eigenfunction in case with $\boldsymbol{J}_a = \boldsymbol{J}_{13} = \boldsymbol{J}_1 + \boldsymbol{J}_3$, $\boldsymbol{J}_b = \boldsymbol{J}_{24} = \boldsymbol{J}_2 + \boldsymbol{J}_4$. These eigenfunctions should be related by some unitary transformation again as

$$\psi(j_{12}, j_{34}) = \sum_{j_{13}, j_{24}} \sqrt{[j_{12} \cdot j_{34} \cdot j_{13} \cdot j_{24}]} \begin{Bmatrix} j_1 & j_2 & j_{12} \\ j_3 & j_4 & j_{34} \\ j_{13} & j_{24} & j \end{Bmatrix} \psi(j_{13}, j_{24}). \tag{G.50}$$

This is the definition of the $9j$ symbol.

The $9j$ symbol can be represented by $6j$ symbols or $3j$ symbols as follows:

$$\begin{Bmatrix} J_1 & J_2 & J_{12} \\ J_3 & J_4 & J_{34} \\ J_{13} & J_{24} & J \end{Bmatrix} = \sum_{J'} (-1)^{2J'} [J'] \begin{Bmatrix} J_1 & J_3 & J_{13} \\ J_{24} & J & J' \end{Bmatrix} \begin{Bmatrix} J_2 & J_4 & J_{24} \\ J_3 & J' & J_{34} \end{Bmatrix} \begin{Bmatrix} J_{12} & J_{34} & J \\ J' & J_1 & J_2 \end{Bmatrix} \tag{G.51}$$

$$= \sum_{\text{all } M} \begin{pmatrix} J_1 & J_2 & J_{12} \\ M_1 & M_2 & M_{12} \end{pmatrix} \begin{pmatrix} J_3 & J_4 & J_{34} \\ M_3 & M_4 & M_{34} \end{pmatrix} \begin{pmatrix} J_{13} & J_{24} & J \\ M_{13} & M_{24} & M \end{pmatrix}$$
$$\times \begin{pmatrix} J_1 & J_3 & J_{13} \\ M_1 & M_3 & M_{13} \end{pmatrix} \begin{pmatrix} J_2 & J_4 & J_{24} \\ M_2 & M_4 & M_{24} \end{pmatrix} \begin{pmatrix} J_{12} & J_{34} & J \\ M_{12} & M_{34} & M \end{pmatrix}. \tag{G.52}$$

The symmetry of $9j$ symbol is as follows:

1. invariant under even permutation of any rows or columns: e.g.

$$\begin{Bmatrix} J_1 & J_2 & J_{12} \\ J_3 & J_4 & J_{34} \\ J_{13} & J_{24} & J \end{Bmatrix} = \begin{Bmatrix} J_3 & J_4 & J_{34} \\ J_{13} & J_{24} & J \\ J_1 & J_2 & J_{12} \end{Bmatrix}. \tag{G.53}$$

2. invariant under transposition:

$$\begin{Bmatrix} J_1 & J_2 & J_{12} \\ J_3 & J_4 & J_{34} \\ J_{13} & J_{24} & J \end{Bmatrix} = \begin{Bmatrix} J_1 & J_3 & J_{13} \\ J_2 & J_4 & J_{24} \\ J_{12} & J_{34} & J \end{Bmatrix}. \tag{G.54}$$

3. multiplying phase factor $(-1)^P$ under odd permutation of any rows or columns, where P is the sum of all arguments of the $9j$ symbol: e.g.

$$\begin{Bmatrix} J_1 & J_2 & J_{12} \\ J_3 & J_4 & J_{34} \\ J_{13} & J_{24} & J \end{Bmatrix} = (-1)^{J_1+J_2+J_{12}+J_3+J_4+J_{34}+J_{13}+J_{24}+J} \begin{Bmatrix} J_3 & J_4 & J_{34} \\ J_1 & J_2 & J_{12} \\ J_{13} & J_{24} & J \end{Bmatrix}. \tag{G.55}$$

For specific cases, $9j$ symbols can be reduced to $6j$ symbols as follows:

$$\begin{Bmatrix} J & j_1 & j_2 \\ J' & j_1' & j_2' \\ L & L' & 0 \end{Bmatrix} = \frac{(-1)^{j_1+j_2+J'+L}}{\sqrt{[j_2 \cdot L]}} \begin{Bmatrix} J & j_1 & j_2 \\ j_1' & J' & L \end{Bmatrix} \delta_{j_2, j_2'} \delta_{L, L'}. \tag{G.56}$$

G.4 Spherical Harmonics

In quantum mechanics, the orbital angular momentum operator $\boldsymbol{L}$ is defined by an outer product of the position operator $\boldsymbol{r}$ and the momentum operator $-i\boldsymbol{\nabla}$ as

$$\boldsymbol{L} = \boldsymbol{r} \times (-i\boldsymbol{\nabla}) . \tag{G.57}$$

This operator contains three components, but it is not possible to diagonalize the angular momenta in more than one direction simultaneously because each of them does not commute with the other ones. However, since $\boldsymbol{L}^2 = L_x^2 + L_y^2 + L_z^2$ is commutable with each of L_x, L_y, and L_z, we can define an eigenfunction of $\boldsymbol{L}^2$ and one of three operators.

The spherical harmonics $Y_l^m(\hat{r})$ is defined as the simultaneous eigenfunction of $\boldsymbol{L}^2$ and L_z, which satisfies

$$\boldsymbol{L}^2 Y_l^m(\hat{r}) = l(l+1) Y_l^m(\hat{r}), \tag{G.58}$$
$$L_z Y_l^m(\hat{r}) = m Y_l^m(\hat{r}). \tag{G.59}$$

Usually, it is normalized as

$$\int d\Omega_r Y_{l'}^{m'*}(\hat{r}) Y_l^m(\hat{r}) = \delta_{l,l'}\delta_{m,m'}. \tag{G.60}$$

The explicit form is given as

$$Y_l^m(\hat{r}) = \sqrt{\frac{2l+1}{4\pi}\frac{(l-m)!}{(l+m)!}} \frac{1}{2^l l!} e^{im\phi} (-\sin\theta)^m \left[\frac{d}{d(\cos\theta)}\right]^{l+m} \left(\cos^2\theta - 1\right)^l . \tag{G.61}$$

Especially, for $m = 0$, it is represented as

$$Y_l^0(\hat{r}) = \sqrt{\frac{2l+1}{4\pi}} P_l(\cos\theta) , \tag{G.62}$$

where $P_l(\cos\theta)$ is the Legendre function. Also, from the explicit form of spherical harmonics, we can prove directly

$$Y_l^{m*}(\hat{r}) = (-1)^m Y_l^{-m}(\hat{r}). \tag{G.63}$$

In addition, the formula of combining two spherical harmonics,

$$\begin{aligned}[Y_{l_1}(\hat{r}) \otimes Y_{l_2}(\hat{r})]_l^m &= \sum_{m_1,m_2} (l_1, m_1, l_2, m_2 | l, m) Y_{l_1}^{m_1}(\hat{r}) Y_{l_2}^{m_2}(\hat{r}) \\ &= \left[\frac{(2l_1+1)(2l_2+1)}{4\pi(2l+1)}\right]^{1/2} (l_1, 0, l_2, 0 | l, 0) Y_l^m(\hat{r}),\end{aligned} \tag{G.64}$$

is also useful. This is also written as

$$\begin{aligned}Y_{l_1}^{m_1}(\hat{p}) Y_{l_2}^{m_2 *}(\hat{p}) &= (-1)^{m_2} Y_{l_1}^{m_1}(\hat{p}) Y_{l_2}^{-m_2}(\hat{p}) \\ &= \sum_{l,m} (-1)^{m_1} \sqrt{\frac{[l_1 \cdot l_2 \cdot l]}{4\pi}} \begin{pmatrix} l_1 & l_2 & l \\ 0 & 0 & 0 \end{pmatrix} \begin{pmatrix} l_1 & l_2 & l \\ m_1 & -m_2 & -m \end{pmatrix} Y_l^m(\hat{p}).\end{aligned} \tag{G.65}$$

Let $f(r)$ be a function which is independent of direction $\hat{r}$. Then the following formula is satisfied:

$$\begin{aligned}\nabla^s Y_l^m(\hat{r}) f(r) =& \sqrt{\frac{l+1}{2l+3}}(l,m,1,s|l+1,m+s) Y_{l+1}^{m+s}(\hat{r}) \left(\frac{d}{dr} - \frac{l}{r}\right) f(r) \\ & - \sqrt{\frac{l}{2l-1}}(l,m,1,s|l-1,m+s) Y_{l-1}^{m+s}(\hat{r}) \left(\frac{d}{dr} + \frac{l+1}{r}\right) f(r) \qquad \text{(G.66)} \\ =& (-1)^s \sqrt{\frac{l+1}{2l+1}}(l+1,m+s,1,-s|l,m) Y_{l+1}^{m+s}(\hat{r}) \left(\frac{l}{r} - \frac{d}{dr}\right) f(r) \\ & + (-1)^s \sqrt{\frac{l}{2l+1}}(l-1,m+s,1,-s|l,m) Y_{l-1}^{m+s}(\hat{r}) \left(\frac{d}{dr} + \frac{l+1}{r}\right) f(r). \qquad \text{(G.67)}\end{aligned}$$

This is called the gradient formula.

Let $\cos\theta_{12} = \hat{p}_1 \cdot \hat{p}_2$, we can relate spherical harmonics with Legendre polynomial P_l:

$$\sum_n (-1)^n Y_l^n(\hat{p}_1) Y_l^{-n}(\hat{p}_2) = \frac{[l]}{4\pi} P_l(\cos\theta_{12}). \qquad \text{(G.68)}$$

Moreover, the following formulae are also satisfied:

$$[Y_l(\hat{p}_1) \otimes Y_{l+1}(\hat{p}_2)]_1^n = \frac{(-1)^{l-1}}{4\pi} \sqrt{\frac{3}{l+1}} \left\{\hat{p}_1^n P_l'(\cos\theta_{12}) - \hat{p}_2^n P_{l+1}'(\cos\theta_{12})\right\}, \qquad \text{(G.69)}$$

$$[Y_l(\hat{p}_1) \otimes Y_l(\hat{p}_2)]_1^n = \frac{(-1)^{l-1}}{4\pi} \sqrt{\frac{3(2l+1)}{l(l+1)}} i (\hat{p}_1 \times \hat{p}_2)^n P_l'(\cos\theta_{12}), \qquad \text{(G.70)}$$

$$[Y_l(\hat{p}_1) \otimes Y_{l-1}(\hat{p}_2)]_1^n = \frac{(-1)^{l-1}}{4\pi} \sqrt{\frac{3}{l}} \left\{\hat{p}_1^n P_l'(\cos\theta_{12}) - \hat{p}_2^n P_{l-1}'(\cos\theta_{12})\right\}. \qquad \text{(G.71)}$$

Appendix H

Plane Wave Approximation for Asymmetry Factor

The asymmetry factor $\alpha(E_1)$ of emitted electron is described by Eq. (5.12) in Chapter 5. This appendix gives the explicit formula of $\alpha(E_1)$ by using the plane wave approximation in order to understand the difference between the chiral structures of contact interactions.

Here we define simple two scalar-type interaction:

$$\begin{aligned}\mathcal{L}_{RR} =& g_{RR}\left(\overline{e}P_R\mu\right)\left(\overline{e}P_R e\right) + [H.c.],\\ \mathcal{L}_{RL} =& g_{RL}\left(\overline{e}P_R\mu\right)\left(\overline{e}P_L e\right) + [H.c.].\end{aligned} \tag{H.1}$$

Now let us discuss whether the observable can or cannot have the information of chirality. $\mathcal{L}_{RR}$ and $\mathcal{L}_{RL}$ correspond to g_1- and g_5-type interaction, respectively. The discussion here do not include photonic interactions.

In this appendix, we treat the final electrons as plane waves and the initial leptons as nonrelativistic waves. The transition amplitudes of $\mu^- e^- \to e^- e^-$ for each of g_{RR}- and g_{RL}-type interaction are, respectively,

$$iM_{RR} = ig_{RR}\int d^3r \exp\left(-i\boldsymbol{p}\cdot\boldsymbol{r}\right)\overline{u}^{s_1}_{e,p_1}P_R u^{s_\mu}_{\mu,b}\overline{u}^{s_2}_{e,p_2}P_R u^{s_e}_{e,b} - \left(\{p_1,s_1\}\leftrightarrow\{p_2,s_2\}\right), \tag{H.2}$$

$$iM_{RL} = ig_{RL}\int d^3r \exp\left(-i\boldsymbol{p}\cdot\boldsymbol{r}\right)\overline{u}^{s_1}_{e,p_1}P_R u^{s_\mu}_{\mu,b}\overline{u}^{s_2}_{e,p_2}P_L u^{s_e}_{e,b} - \left(\{p_1,s_1\}\leftrightarrow\{p_2,s_2\}\right), \tag{H.3}$$

where $\boldsymbol{p} = \boldsymbol{p}_1 + \boldsymbol{p}_2$ is a sum of momenta of final electrons.

Using the Dirac representation, the Dirac structure of scattering and bound states can be written down as

$$u^s_{e,p} = \sqrt{E+m}\begin{pmatrix}1\\ \dfrac{\sigma\cdot\boldsymbol{p}}{E+m}\end{pmatrix}\chi^s, \tag{H.4}$$

and

$$u^s_{\ell,b} = \begin{pmatrix}g_\ell(r)\\ -if_\ell(r)\sigma\cdot\hat{r}\end{pmatrix}\chi^s, \tag{H.5}$$

respectively. Hereafter, neglecting electron mass for simplicity, we use

$$u^s_{e,p} = \sqrt{E}\begin{pmatrix}1\\ \sigma\cdot\hat{p}\end{pmatrix}\chi^s. \tag{H.6}$$

Then, we can write

$$P_L u^s_{e,p} = \frac{\sqrt{E}}{2}\begin{pmatrix} 1-\sigma\cdot\hat{p} \\ -1+\sigma\cdot\hat{p}\end{pmatrix}\chi^s, \tag{H.7}$$

$$P_R u^s_{e,p} = \frac{\sqrt{E}}{2}\begin{pmatrix} 1+\sigma\cdot\hat{p} \\ 1+\sigma\cdot\hat{p}\end{pmatrix}\chi^s. \tag{H.8}$$

H.1 Interaction with the Same Chirality of Final Electrons

First, we explore $\mathcal{L}_{RR}$. At the beginning, let us treat the bound waves nonrelativistically: i.e. let $f_\ell(r)$ be zero. Ignoring the irrelevant factor for discussion of polarization, we consider

$$\begin{aligned} N_{RR} =& \int d^3r \exp\left(-i\boldsymbol{p}\cdot\boldsymbol{r}\right) \overline{u}^{s_1}_{e,p_1} P_R u^{s_\mu}_{\mu,1s} \overline{u}^{s_2}_{e,p_2} P_R u^{s_e}_{e,\alpha} - (\{p_1,s_1\}\leftrightarrow\{p_2,s_2\}) \\ =& \pi I_{gg}(p)\sqrt{E_1E_2}\chi^{s_1\dagger}\left(1-\sigma\cdot\hat{p}_1\right)\chi^{s_\mu}\chi^{s_2\dagger}\left(1-\sigma\cdot\hat{p}_2\right)\chi^{s_e} - (\{p_1,s_1\}\leftrightarrow\{p_2,s_2\}), \end{aligned} \tag{H.9}$$

where I_{gg} is the Fourier component of an overlap between bound radial wave functions,

$$I_{gg}\left(p\right) = \int dr r^2 g_\mu(r) g_e(r) j_0\left(pr\right). \tag{H.10}$$

Here p indicates the magnitude of momentum $\boldsymbol{p} = \boldsymbol{p}_1 + \boldsymbol{p}_2$, which can be written as

$$p = \sqrt{E_1^2 + E_2^2 + 2E_1E_2\cos\theta_{12}}. \tag{H.11}$$

Squaring N_{RR} and summing over spins of all electrons, we can write

$$\begin{aligned} \frac{1}{\pi^2 I_{gg}^2\left(p\right)E_1E_2}\sum_{s_1,s_2,s_e}\left|N_{RR}\right|^2 =& \sum_{s_1,s_2,s_e}\left|\chi^{s_1\dagger}\left(1-\sigma\cdot\hat{p}_1\right)\chi^{s_\mu}\chi^{s_2\dagger}\left(1-\sigma\cdot\hat{p}_2\right)\chi^{s_e} - (\{p_1,s_1\}\leftrightarrow\{p_2,s_2\})\right|^2 \\ =& D_{RR} - E_{RR}, \end{aligned} \tag{H.12}$$

where

$$\begin{aligned} D_{RR} =& \sum_{s_1,s_2,s_e}\chi^{s_\mu\dagger}\left(1-\sigma\cdot\hat{p}_1\right)\chi^{s_1}\chi^{s_e\dagger}\left(1-\sigma\cdot\hat{p}_2\right)\chi^{s_2} \\ & \times\chi^{s_1\dagger}\left(1-\sigma\cdot\hat{p}_1\right)\chi^{s_\mu}\chi^{s_2\dagger}\left(1-\sigma\cdot\hat{p}_2\right)\chi^{s_e} + (p_1\leftrightarrow p_2), \end{aligned} \tag{H.13}$$

and

$$\begin{aligned} E_{RR} =& \sum_{s_1,s_2,s_e}\chi^{s_\mu\dagger}\left(1-\sigma\cdot\hat{p}_2\right)\chi^{s_2}\chi^{s_e\dagger}\left(1-\sigma\cdot\hat{p}_1\right)\chi^{s_1} \\ & \times\chi^{s_1\dagger}\left(1-\sigma\cdot\hat{p}_1\right)\chi^{s_\mu}\chi^{s_2\dagger}\left(1-\sigma\cdot\hat{p}_2\right)\chi^{s_e} + (p_1\leftrightarrow p_2). \end{aligned} \tag{H.14}$$

Now it does not lose generality to put the spin of initial muon so that

$$\chi^{s_\mu} = \begin{pmatrix}1\\0\end{pmatrix}. \tag{H.15}$$

Then using the relation

$$\sum_s \chi^s\chi^{s\dagger} = 1, \tag{H.16}$$

we can rewrite D_{RR} as

$$\begin{aligned}
D_{RR} =& \sum_{s_1,s_2,s_e} \chi^{s_\mu\dagger}\left(1-\sigma\cdot\hat{p}_1\right)\chi^{s_1}\chi^{s_e\dagger}\left(1-\sigma\cdot\hat{p}_2\right)\chi^{s_2} \\
& \times \chi^{s_1\dagger}\left(1-\sigma\cdot\hat{p}_1\right)\chi^{s_\mu}\chi^{s_2\dagger}\left(1-\sigma\cdot\hat{p}_2\right)\chi^{s_e} + (p_1 \leftrightarrow p_2) \\
=& \mathrm{Tr}\left[\begin{pmatrix}1 & 0\\ 0 & 0\end{pmatrix}\left(1-\sigma\cdot\hat{p}_1\right)^2\right]\mathrm{Tr}\left[\left(1-\sigma\cdot\hat{p}_2\right)^2\right] + (p_1 \leftrightarrow p_2) \\
=& 4\mathrm{Tr}\left[\begin{pmatrix}1 & 0\\ 0 & 0\end{pmatrix}\left(1-\sigma\cdot\hat{p}_1\right)\right]\mathrm{Tr}\left[\left(1-\sigma\cdot\hat{p}_2\right)\right] + (p_1 \leftrightarrow p_2) \\
=& 8\left(1-\cos\theta_1\right) + (p_1 \leftrightarrow p_2) \\
=& 8\left(2-\cos\theta_1-\cos\theta_2\right),
\end{aligned} \tag{H.17}$$

where θ_i indicates the angle between the direction of the polarization vector and the momentum of the emitted electron i. Similarly, E_{RR} is also rewritten as

$$\begin{aligned}
E_{RR} =& \sum_{s_1,s_2,s_e} \chi^{s_\mu\dagger}\left(1-\sigma\cdot\hat{p}_2\right)\chi^{s_2}\chi^{s_e\dagger}\left(1-\sigma\cdot\hat{p}_1\right)\chi^{s_1} \\
& \times \chi^{s_1\dagger}\left(1-\sigma\cdot\hat{p}_1\right)\chi^{s_\mu}\chi^{s_2\dagger}\left(1-\sigma\cdot\hat{p}_2\right)\chi^{s_e} + (p_1 \leftrightarrow p_2) \\
=& \mathrm{Tr}\left[\begin{pmatrix}1 & 0\\ 0 & 0\end{pmatrix}\left(1-\sigma\cdot\hat{p}_2\right)^2\left(1-\sigma\cdot\hat{p}_1\right)^2\right] + (p_1 \leftrightarrow p_2) \\
=& 4\mathrm{Tr}\left[\begin{pmatrix}1 & 0\\ 0 & 0\end{pmatrix}\left(1-\sigma\cdot\hat{p}_1\right)\left(1-\sigma\cdot\hat{p}_2\right)\right] + (p_1 \leftrightarrow p_2) \\
=& 4\mathrm{Tr}\left[\begin{pmatrix}1 & 0\\ 0 & 0\end{pmatrix}\left(1+\hat{p}_1\cdot\hat{p}_2-\sigma\cdot\hat{p}_1-\sigma\cdot\hat{p}_2\right)\right] + (p_1 \leftrightarrow p_2) \\
=& 8\left(1+\cos\theta_{12}-\cos\theta_1-\cos\theta_2\right).
\end{aligned} \tag{H.18}$$

Therefore we obtain the result:

$$D_{LL} - E_{LL} = 8\left(1-\hat{p}_1\cdot\hat{p}_2\right), \tag{H.19}$$

or

$$\frac{1}{8\pi^2 E_1 E_2}\sum_{s_1,s_2,s_e}\left|N_{RR}\right|^2 = I_{gg}^2(p)\left(1-\cos\theta_{12}\right). \tag{H.20}$$

We can see that the transition rate does not include θ_1 and θ_2. This finding means that we cannot observe the difference between $\mathcal{L}_{RR}$ and $\mathcal{L}_{LL}$ by muon polarization. However this unexciting conclusion is drastically changed by the relativistic effect for initial leptons, where the small component of Dirac solution has an important role.

More general formula which includes relativity can be represented as

$$\begin{aligned}
\frac{1}{8\pi^2 E_1 E_2}\sum_{s_1,s_2,s_e}\left|N_{RR}\right|^2 =& \left\{I_{gg}^2(p) + 2I_{gf}^2(p) + I_{fg}^2(p) - 2I_{gf}^2(p)I_{fg}^2(p)\right\}\left(1-\cos\theta_{12}\right) \\
& + 2I_{gg}(p)\left\{I_{gf}^2(p) - I_{fg}^2(p)\right\}\left(1-\cos\theta_{12}\right)\frac{E_1\cos\theta_1 + E_2\cos\theta_2}{p},
\end{aligned} \tag{H.21}$$

where I_{gf} and I_{fg} are defined as

$$I_{gf}(p) = \int dr r^2 g_\mu(r) f_e(r) j_1(pr), \tag{H.22}$$

$$I_{fg}(p) = \int dr r^2 f_\mu(r) g_e(r) j_1(pr). \tag{H.23}$$

Note that in this formula we have ignored the term including an overlap of small components of the bound muon and electron because the term is more suppressed by a factor of $Z\alpha_{em}$ than other terms. As seen in the second line of Eq. (H.21), it is found that the seed of asymmetry factor comes from small components of bound lepton wave functions. However we notice that the term proportional to $(I_{gf} - I_{fg})$ vanishes if $g_\mu(r)/f_\mu(r) = g_e(r)/f_e(r)$ holds. If we assume that the nucleus is a point-charge, the condition is approximately satisfied and the asymmetry factor is suppressed. When the nuclear finite size is taken into account, large asymmetry of electron emission is obtained.

H.2 Interaction with the Opposite Chirality of Final Electrons

Next we think about $\mathcal{L}_{RL}$. As $\mathcal{L}_{RR}$, we define

$$\begin{aligned} N_{RL} =& \int d^3r \exp\left(-i\boldsymbol{p}\cdot\boldsymbol{r}\right) \overline{u}^{s_1}_{e,p_1} P_R u^{s_\mu}_{\mu,1s} \overline{u}^{s_2}_{e,p_2} P_L u^{s_e}_{e,\alpha} - (\{p_1,s_1\} \leftrightarrow \{p_2,s_2\}) \\ =& \pi I_{gg}(p) \sqrt{E_1 E_2} \chi^{s_1\dagger} (1-\sigma\cdot\hat{p}_1) \chi^{s_\mu} \chi^{s_2\dagger} (1+\sigma\cdot\hat{p}_2) \chi^{s_e} - (\{p_1,s_1\} \leftrightarrow \{p_2,s_2\}) . \end{aligned} \tag{H.24}$$

Squaring it and summing over electron spins, it is found that

$$\begin{aligned} \frac{1}{\pi^2 I_{gg}^2(p) E_1 E_2} \sum_{s_1,s_2,s_e} |N_{RL}|^2 =& \sum_{s_1,s_2,s_e} \left| \chi^{s_1\dagger} (1-\sigma\cdot\hat{p}_1) \chi^{s_\mu} \chi^{s_2\dagger} (1+\sigma\cdot\hat{p}_2) \chi^{s_e} - (\{p_1,s_1\} \leftrightarrow \{p_2,s_2\}) \right|^2 \\ =& D_{RL} - E_{RL}, \end{aligned} \tag{H.25}$$

where

$$\begin{aligned} D_{RL} =& \sum_{s_1,s_2,s_e} \chi^{s_\mu\dagger} (1-\sigma\cdot\hat{p}_1) \chi^{s_1} \chi^{s_e\dagger} (1+\sigma\cdot\hat{p}_2) \chi^{s_2} \\ & \times \chi^{s_1\dagger} (1-\sigma\cdot\hat{p}_1) \chi^{s_\mu} \chi^{s_2\dagger} (1+\sigma\cdot\hat{p}_2) \chi^{s_e} + (p_1 \leftrightarrow p_2) , \end{aligned} \tag{H.26}$$

and

$$\begin{aligned} E_{RL} =& \sum_{s_1,s_2,s_e} \chi^{s_\mu\dagger} (1-\sigma\cdot\hat{p}_2) \chi^{s_2} \chi^{s_e\dagger} (1+\sigma\cdot\hat{p}_1) \chi^{s_1} \\ & \times \chi^{s_1\dagger} (1-\sigma\cdot\hat{p}_1) \chi^{s_\mu} \chi^{s_2\dagger} (1+\sigma\cdot\hat{p}_2) \chi^{s_e} + (p_1 \leftrightarrow p_2) . \end{aligned} \tag{H.27}$$

We can write down

$$\begin{aligned} D_{RL} =& \sum_{s_1,s_2,s_e} \chi^{s_\mu\dagger} (1-\sigma\cdot\hat{p}_1) \chi^{s_1} \chi^{s_e\dagger} (1+\sigma\cdot\hat{p}_2) \chi^{s_2} \\ & \times \chi^{s_1\dagger} (1-\sigma\cdot\hat{p}_1) \chi^{s_\mu} \chi^{s_2\dagger} (1+\sigma\cdot\hat{p}_2) \chi^{s_e} + (p_1 \leftrightarrow p_2) \\ =& \mathrm{Tr}\left[\begin{pmatrix} 1 & 0 \\ 0 & 0 \end{pmatrix} (1-\sigma\cdot\hat{p}_1)^2 \right] \mathrm{Tr}\left[(1+\sigma\cdot\hat{p}_2)^2 \right] + (p_1 \leftrightarrow p_2) \\ =& 4\mathrm{Tr}\left[\begin{pmatrix} 1 & 0 \\ 0 & 0 \end{pmatrix} (1-\sigma\cdot\hat{p}_1) \right] \mathrm{Tr}\left[(1+\sigma\cdot\hat{p}_2) \right] + (p_1 \leftrightarrow p_2) \\ =& 8(1-\cos\theta_1) + (p_1 \leftrightarrow p_2) \\ =& 8(2-\cos\theta_1-\cos\theta_2) , \end{aligned} \tag{H.28}$$

and

$$\begin{aligned} E_{RL} =& \sum_{s_1,s_2,s_e} \chi^{s_\mu\dagger} (1-\sigma\cdot\hat{p}_2) \chi^{s_2} \chi^{s_e\dagger} (1+\sigma\cdot\hat{p}_1) \chi^{s_1} \\ & \times \chi^{s_1\dagger} (1-\sigma\cdot\hat{p}_1) \chi^{s_\mu} \chi^{s_2\dagger} (1+\sigma\cdot\hat{p}_2) \chi^{s_e} + (p_1 \leftrightarrow p_2) \\ =& 0. \end{aligned} \tag{H.29}$$

Thus we have

$$D_{RL} - E_{RL} = 8\left(2 - \cos\theta_1 - \cos\theta_2\right), \tag{H.30}$$

or

$$\frac{1}{8\pi^2 E_1 E_2} \sum_{s_1,s_2,s_e} |N_{RL}|^2 = I_{gg}^2(p)\left(2 - \cos\theta_1 - \cos\theta_2\right). \tag{H.31}$$

This equation shows that final electrons tend to emit in the opposite direction as the direction of muon polarization.

Within this approximation, the further calculation yields the asymmetry factor as

$$\alpha(E_1) = -\frac{1}{2} - \frac{\int d\cos\theta_{12} \cos\theta_{12} I_{gg}^2(p)}{\int d\cos\theta_{12} I_{gg}^2(p)}. \tag{H.32}$$

Using the expression of nonrelativistic wave function in point charge potential, Eq. (4.27), we can recognize the radial wave function of muon as

$$g_\mu(r) = \sqrt{\frac{\left(m_\mu Z\alpha_{em}\right)^3}{\pi}} \exp\left(-m_\mu Z\alpha_{em} r\right), \tag{H.33}$$

and we obtain an approximate representation,

$$\alpha(E_1) = -\frac{1}{2} + \frac{4E_1E_2\left(E_1^2 + E_2^2 + (m_\mu Z\alpha_{em})^2\right)}{3\left(E_1^2 + E_2^2 + (m_\mu Z\alpha_{em})^2\right)^2 + 4E_1^2E_2^2}, \tag{H.34}$$

where $g_e(r) \sim 1$ is assumed. The second term indicates a correction from the value of $-1/2$, which gives a peak at $E_1 = E_2 = E_{tot}/2$. This formula approximately gives the dotted curve in Fig. 6.15, actually.

The formula which includes relativity is given as

$$\begin{aligned}
&\frac{1}{8\pi^2 E_1 E_2} \sum_{s_1,s_2,s_e} |N_{RL}|^2 \\
=&2\left\{I_{gg}^2(p) + I_{gf}^2(p) + I_{fg}^2(p)\right\} + 2I_{gg}(p)\left\{I_{gf}(p) + I_{fg}(p)\right\}\frac{E_{tot}}{p}(1 + \cos\theta_{12}) \\
&+ 4I_{gf}(p)I_{fg}(p)\frac{E_1 + E_2\cos\theta_{12}}{p}\frac{E_2 + E_1\cos\theta_{12}}{p} \\
&- \left\{I_{gg}^2(p) + I_{gf}^2(p) - I_{fg}^2(p)\right\}(\cos\theta_1 + \cos\theta_2) - 4I_{gg}(p)I_{fg}(p)\frac{E_1\cos\theta_1 + E_2\cos\theta_2}{p} \\
&- 2I_{gg}(p)I_{gf}(p)\left\{\frac{E_2 + E_1\cos\theta_{12}}{p}\cos\theta_1 + \frac{E_1 + E_2\cos\theta_{12}}{p}\cos\theta_2\right\} \\
&- 2I_{fg}(p)\left\{I_{gf}(p) + I_{fg}(p)\right\}\frac{E_{tot}}{p}\frac{E_1\cos\theta_1 + E_2\cos\theta_2}{p}(1 + \cos\theta_{12}).
\end{aligned} \tag{H.35}$$

Appendix I

Details of Calculations

The details of some calculations in the text are given here.

I.1 Derivation for Eq. (4.66)

Inserting Eq. (4.64) into Eq. (4.24), we get

$$
\begin{aligned}
\frac{d\Gamma}{dE_1 d\cos\theta_{12}} =& \sum_{\alpha_e} \frac{1}{32\pi^3} |\boldsymbol{p}_1| \, |\boldsymbol{p}_2| \sum_{s_1,s_2} \sum_{s_\mu} \sum_{s_e} \Bigg| \sum_{\kappa_1,\nu_1,m_1} \sum_{\kappa_2,\nu_2,m_2} (4\pi)^2 Y^{m_1}_{l_{\kappa_1}}(\hat{p}_1) Y^{m_2}_{l_{\kappa_2}}(\hat{p}_2) \\
& \times (l_{\kappa_1}, m_1, 1/2, s_1 | j_{\kappa_1}, \nu_1)(l_{\kappa_2}, m_2, 1/2, s_2 | j_{\kappa_2}, \nu_2) \sqrt{\left[j_{\kappa_1} \cdot j_{\kappa_\mu} \cdot j_{\kappa_2} \cdot j_{\kappa_e} \right]} \\
& \times \left(-\frac{4G_F}{\sqrt{2}} \right) \frac{1}{4\pi} \sum_{J,M} (j_{\kappa_1}, \nu_1, j_{\kappa_2}, \nu_2 | J, M)(j_{\kappa_\mu}, s_\mu, j_{\kappa_e}, s_e | J, M) N^{\beta_1,\beta_2}(J) \Bigg|^2 \\
=& \sum_{\alpha_e} \frac{4G_F^2}{\pi} |\boldsymbol{p}_1| \, |\boldsymbol{p}_2| \sum_{s_1,s_2} \sum_{s_\mu} \sum_{s_e} \sum_{\kappa_1,\nu_1,m_1} \sum_{\kappa_2,\nu_2,m_2} \sum_{\kappa_1',\nu_1',m_1'} \sum_{\kappa_2',\nu_2',m_2'} \\
& \times Y^{m_1'*}_{l_{\kappa_1'}}(\hat{p}_1) Y^{m_2'*}_{l_{\kappa_2'}}(\hat{p}_2) Y^{m_1}_{l_{\kappa_1}}(\hat{p}_1) Y^{m_2}_{l_{\kappa_2}}(\hat{p}_2) \\
& \times (l_{\kappa_1'}, m_1', 1/2, s_1 | j_{\kappa_1'}, \nu_1')(l_{\kappa_2'}, m_2', 1/2, s_2 | j'_{\kappa_2}, \nu_2') \\
& \times (l_{\kappa_1}, m_1, 1/2, s_1 | j_{\kappa_1}, \nu_1)(l_{\kappa_2}, m_2, 1/2, s_2 | j_{\kappa_2}, \nu_2) \\
& \times \sqrt{\left[j_{\kappa_1} \cdot j_{\kappa_2} \cdot j_{\kappa_1'} \cdot j_{\kappa_2'} \right]} \left[j_{\kappa_\mu} \cdot j_{\kappa_e} \right] \\
& \times \sum_{J',M'} (j_{\kappa_1'}, \nu_1', j_{\kappa_2'}, \nu_2' | J', M')(j_{\kappa_\mu}, s_\mu, j_{\kappa_e}, s_e | J', M') N^{\beta_1',\beta_2'*}(J') \\
& \times \sum_{J,M} (j_{\kappa_1}, \nu_1, j_{\kappa_2}, \nu_2 | J, M)(j_{\kappa_\mu}, s_\mu, j_{\kappa_e}, s_e | J, M) N^{\beta_1,\beta_2}(J). \qquad \text{(I.1)}
\end{aligned}
$$

By the relation of Clebsch-Gordan coefficients, it is reduced to

$$\begin{aligned}\frac{d\Gamma}{dE_1 d\cos\theta_{12}} =& \sum_{\alpha_e} \frac{4G_F^2}{\pi} |\boldsymbol{p}_1| |\boldsymbol{p}_2| \sum_{s_1,s_2} \sum_{\kappa_1,\nu_1,m_1} \sum_{\kappa_2,\nu_2,m_2} \sum_{\kappa_1',\nu_1',m_1'} \sum_{\kappa_2',\nu_2',m_2'} \\ & \times Y_{l_{\kappa_1'}}^{m_1'*}(\hat{p}_1) Y_{l_{\kappa_2'}}^{m_2'*}(\hat{p}_2) Y_{l_{\kappa_1}}^{m_1}(\hat{p}_1) Y_{l_{\kappa_2}}^{m_2}(\hat{p}_2) \\ & \times (l_{\kappa_1'}, m_1', 1/2, s_1 | j_{\kappa_1'}, \nu_1') (l_{\kappa_2'}, m_2', 1/2, s_2 | j_{\kappa_2}', \nu_2') \\ & \times (l_{\kappa_1}, m_1, 1/2, s_1 | j_{\kappa_1}, \nu_1) (l_{\kappa_2}, m_2, 1/2, s_2 | j_{\kappa_2}, \nu_2) \\ & \times \sqrt{\left[j_{\kappa_1} \cdot j_{\kappa_2} \cdot j_{\kappa_1'} \cdot j_{\kappa_2'}\right]} \left[j_{\kappa_\mu} \cdot j_{\kappa_e}\right] \\ & \times \sum_{J,M} (j_{\kappa_1'}, \nu_1', j_{\kappa_2'}, \nu_2' | J, M) N^{\beta_1',\beta_2'*}(J) \\ & \times (j_{\kappa_1}, \nu_1, j_{\kappa_2}, \nu_2 | J, M) N^{\beta_1,\beta_2}(J). \end{aligned} \tag{I.2}$$

Now let us rewrite Clebsch-Gordon coefficients with $3j$ symbols,

$$\begin{aligned}\frac{d\Gamma}{dE_1 d\cos\theta_{12}} =& \sum_{\alpha_e} \frac{4G_F^2}{\pi} |\boldsymbol{p}_1| |\boldsymbol{p}_2| \sum_{s_1,s_2} \sum_{\kappa_1,\nu_1,m_1} \sum_{\kappa_2,\nu_2,m_2} \sum_{\kappa_1',\nu_1',m_1'} \sum_{\kappa_2',\nu_2',m_2'} \sum_{J,M} \\ & \times \left[J \cdot j_{\kappa_1} \cdot j_{\kappa_2} \cdot j_{\kappa_1'} \cdot j_{\kappa_2'} \cdot j_{\kappa_\mu} \cdot j_{\kappa_e}\right] N^{\beta_1',\beta_2'*}(J) N^{\beta_1,\beta_2}(J) \\ & \times (-1)^{l_{\kappa_1}+l_{\kappa_2}+l_{\kappa_1'}+l_{\kappa_2'}+j_{\kappa_1}+j_{\kappa_1'}-j_{\kappa_2}-j_{\kappa_2'}} Y_{l_{\kappa_1'}}^{m_1'*}(\hat{p}_1) Y_{l_{\kappa_1}}^{m_1}(\hat{p}_1) Y_{l_{\kappa_2'}}^{m_2'*}(\hat{p}_2) Y_{l_{\kappa_2}}^{m_2}(\hat{p}_2) \\ & \times \begin{pmatrix} l_{\kappa_1} & 1/2 & j_{\kappa_1} \\ m_1 & s_1 & -\nu_1 \end{pmatrix} \begin{pmatrix} l_{\kappa_2} & 1/2 & j_{\kappa_2} \\ m_2 & s_2 & -\nu_2 \end{pmatrix} \begin{pmatrix} l_{\kappa_1'} & 1/2 & j_{\kappa_1'} \\ m_1' & s_1 & -\nu_1' \end{pmatrix} \begin{pmatrix} l_{\kappa_2'} & 1/2 & j_{\kappa_2'} \\ m_2' & s_2 & -\nu_2' \end{pmatrix} \\ & \times \begin{pmatrix} j_{\kappa_1} & j_{\kappa_2} & J \\ \nu_1 & \nu_2 & -M \end{pmatrix} \begin{pmatrix} j_{\kappa_1'} & j_{\kappa_2'} & J \\ \nu_1' & \nu_2' & -M \end{pmatrix}. \end{aligned} \tag{I.3}$$

In addition, we use the formula for the spherical harmonics, Eq. (G.65), we obtain

$$\begin{aligned}\frac{d\Gamma}{dE_1 d\cos\theta_{12}} =& \sum_{\alpha_e} \frac{G_F^2}{\pi^2} |\boldsymbol{p}_1| |\boldsymbol{p}_2| \sum_{s_1,s_2} \sum_{\kappa_1,\nu_1,m_1} \sum_{\kappa_2,\nu_2,m_2} \sum_{\kappa_1',\nu_1',m_1'} \sum_{\kappa_2',\nu_2',m_2'} \sum_{J,M} \sum_{l_1,n_1} \sum_{l_2,n_2} \\ & \times \left[J \cdot j_{\kappa_1} \cdot j_{\kappa_2} \cdot j_{\kappa_1'} \cdot j_{\kappa_2'} \cdot j_{\kappa_\mu} \cdot j_{\kappa_e}\right] \\ & \times \sqrt{\left[l_{\kappa_1} \cdot l_{\kappa_2} \cdot l_{\kappa_1'} \cdot l_{\kappa_2'} \cdot l_1 \cdot l_2\right]} N^{\beta_1',\beta_2'*}(J) N^{\beta_1,\beta_2}(J) \\ & \times (-1)^{l_{\kappa_1}+l_{\kappa_2}+l_{\kappa_1'}+l_{\kappa_2'}+j_{\kappa_1}+j_{\kappa_1'}-j_{\kappa_2}-j_{\kappa_2'}+m_1+m_2} Y_{l_1}^{n_1}(\hat{p}_1) Y_{l_2}^{n_2}(\hat{p}_2) \\ & \times \begin{pmatrix} j_{\kappa_1} & j_{\kappa_2} & J \\ \nu_1 & \nu_2 & -M \end{pmatrix} \begin{pmatrix} j_{\kappa_1'} & j_{\kappa_2'} & J \\ \nu_1' & \nu_2' & -M \end{pmatrix} \begin{pmatrix} l_{\kappa_1} & l_{\kappa_1'} & l_1 \\ 0 & 0 & 0 \end{pmatrix} \begin{pmatrix} l_{\kappa_2} & l_{\kappa_2'} & l_2 \\ 0 & 0 & 0 \end{pmatrix} \\ & \times \begin{pmatrix} l_{\kappa_1} & l_{\kappa_1'} & l_1 \\ m_1 & -m_1' & -n_1 \end{pmatrix} \begin{pmatrix} l_{\kappa_1} & 1/2 & j_{\kappa_1} \\ m_1 & s_1 & -\nu_1 \end{pmatrix} \begin{pmatrix} l_{\kappa_1'} & 1/2 & j_{\kappa_1'} \\ m_1' & s_1 & -\nu_1' \end{pmatrix} \\ & \times \begin{pmatrix} l_{\kappa_2} & l_{\kappa_2'} & l_2 \\ m_2 & -m_2' & -n_2 \end{pmatrix} \begin{pmatrix} l_{\kappa_2} & 1/2 & j_{\kappa_2} \\ m_2 & s_2 & -\nu_2 \end{pmatrix} \begin{pmatrix} l_{\kappa_2'} & 1/2 & j_{\kappa_2'} \\ m_2' & s_2 & -\nu_2' \end{pmatrix}. \end{aligned} \tag{I.4}$$

In order to simplify it more, using the sum rule for $3j$ symbols, Eq. (G.49), we get a relation as

$$\begin{aligned}
&\sum_{s_1,m_1,m_1'} (-1)^{l_{\kappa_1}+l_{\kappa_1'}+m_1} \begin{pmatrix} l_{\kappa_1} & l_{\kappa_1'} & l_1 \\ m_1 & -m_1' & -n_1 \end{pmatrix} \begin{pmatrix} l_{\kappa_1} & 1/2 & j_{\kappa_1} \\ m_1 & s_1 & -\nu_1 \end{pmatrix} \begin{pmatrix} l_{\kappa_1'} & 1/2 & j_{\kappa_1'} \\ m_1' & s_1 & -\nu_1' \end{pmatrix} \\
=& \sum_{s_1,m_1,m_1'} (-1)^{\nu_1'-1/2+l_{\kappa_1}+l_{\kappa_1'}+1/2+m_1+m_1'-s_1} \\
&\times \begin{pmatrix} l_{\kappa_1} & l_{\kappa_1'} & l_1 \\ m_1 & -m_1' & -n_1 \end{pmatrix} \begin{pmatrix} l_{\kappa_1'} & 1/2 & j_{\kappa_1'} \\ m_1' & s_1 & -\nu_1' \end{pmatrix} \begin{pmatrix} 1/2 & l_{\kappa_1} & j_{\kappa_1} \\ -s_1 & -m_1 & \nu_1 \end{pmatrix} \\
=&(-1)^{\nu_1'-1/2} \begin{pmatrix} j_{\kappa_1'} & j_{\kappa_1} & l_1 \\ -\nu_1' & \nu_1 & -n_1 \end{pmatrix} \begin{Bmatrix} j_{\kappa_1'} & j_{\kappa_1} & l_1 \\ l_{\kappa_1} & l_{\kappa_1'} & 1/2 \end{Bmatrix}.
\end{aligned} \tag{I.5}$$

Therefore,

$$\begin{aligned}
\frac{d\Gamma}{dE_1 d\cos\theta_{12}} =& \sum_{\alpha_e} \frac{G_F^2}{\pi^2} |\boldsymbol{p}_1| |\boldsymbol{p}_2| \sum_{\kappa_1,\nu_1} \sum_{\kappa_2,\nu_2} \sum_{\kappa_1',\nu_1'} \sum_{\kappa_2',\nu_2'} \sum_{J,M} \sum_{l_1,n_1} \sum_{l_2,n_2} \\
&\times \left[J \cdot j_{\kappa_1} \cdot j_{\kappa_2} \cdot j_{\kappa_1'} \cdot j_{\kappa_2'} \cdot j_{\kappa_\mu} \cdot j_{\kappa_e}\right] \\
&\times \sqrt{\left[l_{\kappa_1} \cdot l_{\kappa_2} \cdot l_{\kappa_1'} \cdot l_{\kappa_2'} \cdot l_1 \cdot l_2\right]} N^{\beta_1',\beta_2'*}(J) N^{\beta_1,\beta_2}(J) \\
&\times (-1)^{j_{\kappa_1}+j_{\kappa_1'}-j_{\kappa_2}-j_{\kappa_2'}+M-1} Y_{l_1}^{n_1}(\hat{p}_1) Y_{l_2}^{n_2}(\hat{p}_2) \\
&\times \begin{pmatrix} j_{\kappa_1} & j_{\kappa_2} & J \\ \nu_1 & \nu_2 & -M \end{pmatrix} \begin{pmatrix} j_{\kappa_1'} & j_{\kappa_2'} & J \\ \nu_1' & \nu_2' & -M \end{pmatrix} \begin{pmatrix} l_{\kappa_1} & l_{\kappa_1'} & l_1 \\ 0 & 0 & 0 \end{pmatrix} \begin{pmatrix} l_{\kappa_2} & l_{\kappa_2'} & l_2 \\ 0 & 0 & 0 \end{pmatrix} \\
&\times \begin{pmatrix} j_{\kappa_1'} & j_{\kappa_1} & l_1 \\ -\nu_1' & \nu_1 & -n_1 \end{pmatrix} \begin{Bmatrix} j_{\kappa_1'} & j_{\kappa_1} & l_1 \\ l_{\kappa_1} & l_{\kappa_1'} & 1/2 \end{Bmatrix} \begin{pmatrix} j_{\kappa_2'} & j_{\kappa_2} & l_2 \\ -\nu_2' & \nu_2 & -n_2 \end{pmatrix} \begin{Bmatrix} j_{\kappa_2'} & j_{\kappa_2} & l_2 \\ l_{\kappa_2} & l_{\kappa_2'} & 1/2 \end{Bmatrix}.
\end{aligned} \tag{I.6}$$

Notice that non-zero contributions come from only the case that

$$l_2 = l_1, \qquad n_2 = -n_1, \tag{I.7}$$

because of the condition for Clebsch-Gordan coefficients. Moreover, since $\nu_1 = \nu_1' + n_1$ is a half-integer,

$$-1 = (-1)^{2\nu_1} = (-1)^{\nu_1+\nu_1'+n_1}. \tag{I.8}$$

By using them, it can be written as

$$\begin{aligned}
\frac{d\Gamma}{dE_1 d\cos\theta_{12}} =& \sum_{\alpha_e} \frac{G_F^2}{\pi^2} |\boldsymbol{p}_1| |\boldsymbol{p}_2| \sum_{\kappa_1,\nu_1} \sum_{\kappa_2,\nu_2} \sum_{\kappa_1',\nu_1'} \sum_{\kappa_2',\nu_2'} \sum_{J,M} \sum_{l,n} \\
&\times \left[J \cdot l \cdot j_{\kappa_1} \cdot j_{\kappa_2} \cdot j_{\kappa_1'} \cdot j_{\kappa_2'} \cdot j_{\kappa_\mu} \cdot j_{\kappa_e}\right] \\
&\times \sqrt{\left[l_{\kappa_1} \cdot l_{\kappa_2} \cdot l_{\kappa_1'} \cdot l_{\kappa_2'}\right]} N^{\beta_1',\beta_2'*}(J) N^{\beta_1,\beta_2}(J) \\
&\times (-1)^{j_{\kappa_1}+j_{\kappa_1'}-j_{\kappa_2}-j_{\kappa_2'}+M+\nu_1+\nu_1'+n} Y_l^n(\hat{p}_1) Y_l^{-n}(\hat{p}_2) \\
&\times \begin{pmatrix} j_{\kappa_1} & j_{\kappa_2} & J \\ \nu_1 & \nu_2 & -M \end{pmatrix} \begin{pmatrix} j_{\kappa_1'} & j_{\kappa_2'} & J \\ \nu_1' & \nu_2' & -M \end{pmatrix} \begin{pmatrix} l_{\kappa_1} & l_{\kappa_1'} & l \\ 0 & 0 & 0 \end{pmatrix} \begin{pmatrix} l_{\kappa_2} & l_{\kappa_2'} & l \\ 0 & 0 & 0 \end{pmatrix} \\
&\times \begin{pmatrix} j_{\kappa_1'} & j_{\kappa_1} & l \\ -\nu_1' & \nu_1 & -n \end{pmatrix} \begin{Bmatrix} j_{\kappa_1'} & j_{\kappa_1} & l \\ l_{\kappa_1} & l_{\kappa_1'} & 1/2 \end{Bmatrix} \begin{pmatrix} j_{\kappa_2'} & j_{\kappa_2} & l \\ -\nu_2' & \nu_2 & n \end{pmatrix} \begin{Bmatrix} j_{\kappa_2'} & j_{\kappa_2} & l \\ l_{\kappa_2} & l_{\kappa_2'} & 1/2 \end{Bmatrix}.
\end{aligned} \tag{I.9}$$

Now we use Eq. (G.48) and perform the remaining summation over projection quantum numbers but n:

$$\begin{aligned}
&\sum_{\nu_1,\nu_2,\nu_1',\nu_2',M} (-1)^{M+\nu_1+\nu_1'} \\
&\times \begin{pmatrix} j_{\kappa_1} & j_{\kappa_2} & J \\ \nu_1 & \nu_2 & -M \end{pmatrix} \begin{pmatrix} j_{\kappa_1'} & j_{\kappa_2'} & J \\ \nu_1' & \nu_2' & -M \end{pmatrix} \begin{pmatrix} j_{\kappa_1'} & j_{\kappa_1} & l \\ -\nu_1' & \nu_1 & -n \end{pmatrix} \begin{pmatrix} j_{\kappa_2'} & j_{\kappa_2} & l \\ -\nu_2' & \nu_2 & n \end{pmatrix} \\
=&\sum_{\nu_1,\nu_2,\nu_1',\nu_2',M} (-1)^{-\nu_1-\nu_1'-M} \\
&\times \begin{pmatrix} j_{\kappa_2'} & j_{\kappa_2} & l \\ -\nu_2' & \nu_2 & n \end{pmatrix} \begin{pmatrix} j_{\kappa_2'} & j_{\kappa_1'} & J \\ -\nu_2' & -\nu_1' & M \end{pmatrix} \begin{pmatrix} j_{\kappa_1} & j_{\kappa_2} & J \\ \nu_1 & \nu_2 & -M \end{pmatrix} \begin{pmatrix} j_{\kappa_1} & j_{\kappa_1'} & l \\ -\nu_1 & \nu_1' & n \end{pmatrix} \\
=&\frac{(-1)^{j_{\kappa_1}+j_{\kappa_1'}+J}}{[l]} \begin{Bmatrix} j_{\kappa_2'} & j_{\kappa_2} & l \\ j_{\kappa_1} & j_{\kappa_1'} & J \end{Bmatrix} = \frac{(-1)^{j_{\kappa_1}+j_{\kappa_1'}+J}}{[l]} \begin{Bmatrix} j_{\kappa_1} & j_{\kappa_2} & J \\ j_{\kappa_2'} & j_{\kappa_1'} & l \end{Bmatrix}.
\end{aligned} \tag{I.10}$$

In addition, we can sum over n by Eq. (G.68) and get

$$\begin{aligned}
\frac{d\Gamma}{dE_1 d\cos\theta_{12}} =& \sum_{\alpha_e} \frac{G_F^2}{4\pi^3} |\boldsymbol{p}_1| |\boldsymbol{p}_2| \sum_{\kappa_1,\kappa_2} \sum_{\kappa_1',\kappa_2'} \sum_{J,l} \\
&\times \left[J \cdot l \cdot j_{\kappa_1} \cdot j_{\kappa_2} \cdot j_{\kappa_1'} \cdot j_{\kappa_2'} \cdot j_{\kappa_\mu} \cdot j_{\kappa_e}\right] \\
&\times \sqrt{\left[l_{\kappa_1} \cdot l_{\kappa_2} \cdot l_{\kappa_1'} \cdot l_{\kappa_2'}\right]} N^{\beta_1',\beta_2'*}(J) N^{\beta_1,\beta_2}(J) P_l(\cos\theta_{12}) \\
&\times (-1)^{J-j_{\kappa_2}-j_{\kappa_2'}} \begin{pmatrix} l_{\kappa_1} & l_{\kappa_1'} & l \\ 0 & 0 & 0 \end{pmatrix} \begin{pmatrix} l_{\kappa_2} & l_{\kappa_2'} & l \\ 0 & 0 & 0 \end{pmatrix} \\
&\times \begin{Bmatrix} j_{\kappa_1'} & j_{\kappa_1} & l \\ l_{\kappa_1} & l_{\kappa_1'} & 1/2 \end{Bmatrix} \begin{Bmatrix} j_{\kappa_2'} & j_{\kappa_2} & l \\ l_{\kappa_2} & l_{\kappa_2'} & 1/2 \end{Bmatrix} \begin{Bmatrix} j_{\kappa_1} & j_{\kappa_2} & J \\ j_{\kappa_2'} & j_{\kappa_1'} & l \end{Bmatrix}.
\end{aligned} \tag{I.11}$$

Using the formula for a product of $3j$ and $6j$ symbols (G.46), we can reduce it to

$$\begin{aligned}
\frac{d\Gamma}{dE_1 d\cos\theta_{12}} =& \sum_{\alpha_e} \frac{G_F^2}{4\pi^3} |\boldsymbol{p}_1| |\boldsymbol{p}_2| \sum_{\kappa_1,\kappa_2} \sum_{\kappa_1',\kappa_2'} \sum_{J,l} \left[J \cdot l \cdot j_{\kappa_1} \cdot j_{\kappa_2} \cdot j_{\kappa_1'} \cdot j_{\kappa_2'} \cdot j_{\kappa_\mu} \cdot j_{\kappa_e}\right] \\
&\times N^{\beta_1',\beta_2'*}(J) N^{\beta_1,\beta_2}(J) P_l(\cos\theta_{12}) \\
&\times (-1)^{J-j_{\kappa_2}-j_{\kappa_2'}} \frac{1+(-1)^{l_{\kappa_1}+l_{\kappa_1'}+l}}{2} \frac{1+(-1)^{l_{\kappa_2}+l_{\kappa_2'}+l}}{2} \\
&\times \begin{pmatrix} j_{\kappa_1'} & j_{\kappa_1} & l \\ 1/2 & -1/2 & 0 \end{pmatrix} \begin{pmatrix} j_{\kappa_2'} & j_{\kappa_2} & l \\ 1/2 & -1/2 & 0 \end{pmatrix} \begin{Bmatrix} j_{\kappa_1} & j_{\kappa_2} & J \\ j_{\kappa_2'} & j_{\kappa_1'} & l \end{Bmatrix}.
\end{aligned} \tag{I.12}$$

By rewriting it by Clebsch-Gordan and Racah coefficients, we finally obtain

$$\begin{aligned}
\frac{d\Gamma}{dE_1 d\cos\theta_{12}} =& \sum_{\alpha_e} \frac{G_F^2}{4\pi^3} |\boldsymbol{p}_1| |\boldsymbol{p}_2| \sum_{\kappa_1,\kappa_2} \sum_{\kappa_1',\kappa_2'} \sum_{J,l} \left[J \cdot j_{\kappa_1} \cdot j_{\kappa_2} \cdot j_{\kappa_1'} \cdot j_{\kappa_2'} \cdot j_{\kappa_\mu} \cdot j_{\kappa_e}\right] \\
&\times N^{\beta_1',\beta_2'*}(J) N^{\beta_1,\beta_2}(J) P_l(\cos\theta_{12}) \\
&\times (-1)^{J-j_{\kappa_2}-j_{\kappa_2'}} \frac{1+(-1)^{l_{\kappa_1}+l_{\kappa_1'}+l}}{2} \frac{1+(-1)^{l_{\kappa_2}+l_{\kappa_2'}+l}}{2} \\
&\times (j_{\kappa_1}, 1/2, j_{\kappa_1'}, -1/2|l,0)(j_{\kappa_2}, 1/2, j_{\kappa_2'}, -1/2|l,0) W(j_{\kappa_1}, j_{\kappa_2}, j_{\kappa_1'}, j_{\kappa_2'}; J, l).
\end{aligned} \tag{4.66}$$

I.2 Derivation for Eq. (4.68)

For the calculation, it is convenient to use the Dirac basis rather than the chiral basis. Now we define useful values as

$$M_{ij}^{\beta_1,\nu_1;\beta_2,\nu_2} = \int d^3r \overline{\psi}_{p_1}^{\kappa_1,\mu_1}(\boldsymbol{r})\Gamma_i\psi_{\mu}^{\alpha_\mu,s_\mu}(\boldsymbol{r})\overline{\psi}_{p_2}^{\kappa_2,\mu_2}(\boldsymbol{r})\Gamma_j\psi_{e}^{\alpha_e,s_e}(\boldsymbol{r}), \tag{I.13}$$

$$\Gamma_i = \begin{cases} 1 & (i=S) \\ \gamma_5 & (i=P) \\ \gamma^\mu & (i=V) \\ \gamma^\mu\gamma_5 & (i=A) \end{cases}, \quad \Gamma_j = \begin{cases} 1 & (j=S) \\ \gamma_5 & (j=P) \\ \gamma_\mu & (j=V) \\ \gamma_\mu\gamma_5 & (j=A) \end{cases}. \tag{I.14}$$

Using this expression, Eq. (4.61) is rewritten as

$$\tilde{\mathcal{M}}_{\text{contact}} = -\frac{4G_F}{\sqrt{2}}\sum_{i,j} g_{ij}\left[M_{ij}^{\beta_1,\nu_1;\beta_2,\nu_2} - M_{ij}^{\beta_2,\nu_2;\beta_1,\nu_1}\right], \tag{I.15}$$

where i and j run over S, P, V, A, and the coupling constants g_{ij} are defined as

$$g_{SS} = g_{PP} = \frac{1}{4}(g_1+g_2), \tag{I.16}$$

$$g_{SP} = g_{PS} = \frac{1}{4}(g_1-g_2), \tag{I.17}$$

$$g_{VV} = \frac{1}{4}(g_3+g_4+g_5+g_6), \tag{I.18}$$

$$g_{AA} = \frac{1}{4}(g_3+g_4-g_5-g_6), \tag{I.19}$$

$$g_{VA} = \frac{1}{4}(g_3-g_4-g_5+g_6), \tag{I.20}$$

$$g_{AV} = \frac{1}{4}(g_3-g_4+g_5-g_6). \tag{I.21}$$

For the first example, let us pay attention to M_{SS}, which is

$$\begin{aligned} M_{SS}^{\beta_1,\nu_1;\beta_2,\nu_2} =& \int d^3r \left[g_{p_1}^{\kappa_1}(r)g_{\mu,n_\mu}^{\kappa_\mu}(r)\chi_{\kappa_1}^{\nu_1\dagger}(\hat{r})\,\chi_{\kappa_\mu}^{s_\mu}(\hat{r}) - f_{p_1}^{\kappa_1}(r)f_{\mu,n_\mu}^{\kappa_\mu}(r)\chi_{-\kappa_1}^{\nu_1\dagger}(\hat{r})\,\chi_{-\kappa_\mu}^{s_\mu}(\hat{r})\right] \\ &\times\left[g_{p_2}^{\kappa_2}(r)g_{e,n_e}^{\kappa_e}(r)\chi_{\kappa_2}^{\nu_2\dagger}(\hat{r})\,\chi_{\kappa_e}^{s_e}(\hat{r}) - f_{p_2}^{\kappa_2}(r)f_{e,n_e}^{\kappa_e}(r)\chi_{-\kappa_2}^{\nu_2\dagger}(\hat{r})\,\chi_{-\kappa_e}^{s_e}(\hat{r})\right] \\ =& \int drr^2d\Omega\left[g_{p_1}^{\kappa_1}(r)g_{\mu,n_\mu}^{\kappa_\mu}(r)g_{p_2}^{\kappa_2}(r)g_{e,n_e}^{\kappa_e}(r)\chi_{\kappa_1}^{\nu_1\dagger}(\hat{r})\,\chi_{\kappa_\mu}^{s_\mu}(\hat{r})\,\chi_{\kappa_2}^{\nu_2\dagger}(\hat{r})\,\chi_{\kappa_e}^{s_e}(\hat{r})\right. \\ &+ f_{p_1}^{\kappa_1}(r)f_{\mu,n_\mu}^{\kappa_\mu}(r)f_{p_2}^{\kappa_2}(r)f_{e,n_e}^{\kappa_e}(r)\chi_{-\kappa_1}^{\nu_1\dagger}(\hat{r})\,\chi_{-\kappa_\mu}^{s_\mu}(\hat{r})\,\chi_{-\kappa_2}^{\nu_2\dagger}(\hat{r})\,\chi_{-\kappa_e}^{s_e}(\hat{r}) \\ &- g_{p_1}^{\kappa_1}(r)g_{\mu,n_\mu}^{\kappa_\mu}(r)f_{p_2}^{\kappa_2}(r)f_{e,n_e}^{\kappa_e}(r)\chi_{\kappa_1}^{\nu_1\dagger}(\hat{r})\,\chi_{\kappa_\mu}^{s_\mu}(\hat{r})\,\chi_{-\kappa_2}^{\nu_2\dagger}(\hat{r})\,\chi_{-\kappa_e}^{s_e}(\hat{r}) \\ &\left.- f_{p_1}^{\kappa_1}(r)f_{\mu,n_\mu}^{\kappa_\mu}(r)g_{p_2}^{\kappa_2}(r)g_{e,n_e}^{\kappa_e}(r)\chi_{-\kappa_1}^{\nu_1\dagger}(\hat{r})\,\chi_{-\kappa_\mu}^{s_\mu}(\hat{r})\,\chi_{\kappa_2}^{\nu_2\dagger}(\hat{r})\,\chi_{\kappa_e}^{s_e}(\hat{r})\right]. \end{aligned} \tag{I.22}$$

Each term can be divided into radial integral part and angular integral part. Now focusing on the angular

integral of the first term I_Ω,

$$\begin{aligned}
I_\Omega &= \int d\Omega \chi_{\kappa_1}^{\nu_1\dagger}(\hat{r})\,\chi_{\kappa_\mu}^{s_\mu}(\hat{r})\,\chi_{\kappa_2}^{\nu_2\dagger}(\hat{r})\,\chi_{\kappa_e}^{s_e}(\hat{r}) \\
&= \int d\Omega [Y_{l_{\kappa_1}}(\hat{r})\otimes\chi_{1/2}(1)]_{j\kappa_1}^{\nu_1\dagger}[Y_{l_{\kappa_\mu}}(\hat{r})\otimes\chi_{1/2}(1)]_{j\kappa_\mu}^{s_\mu} \\
&\quad\times[Y_{l_{\kappa_2}}(\hat{r})\otimes\chi_{1/2}(2)]_{j\kappa_2}^{\nu_2\dagger}[Y_{l_{\kappa_e}}(\hat{r})\otimes\chi_{1/2}(2)]_{j\kappa_e}^{s_e} \\
&= \int d\Omega \left[[Y_{l_{\kappa_1}}(\hat{r})\otimes\chi_{1/2}(1)]_{j\kappa_1}^{\nu_1}\otimes[Y_{l_{\kappa_2}}(\hat{r})\otimes\chi_{1/2}(2)]_{j\kappa_2}^{\nu_2}\right]^\dagger \\
&\quad\times\left[[Y_{l_{\kappa_\mu}}(\hat{r})\otimes\chi_{1/2}(1)]_{j\kappa_\mu}^{s_\mu}\otimes[Y_{l_{\kappa_e}}(\hat{r})\otimes\chi_{1/2}(2)]_{j\kappa_e}^{s_e}\right].
\end{aligned} \tag{I.23}$$

Here the suffixes (1) and (2) attached to $\chi_{1/2}$s are for emphasizing that these spinors are in different spaces. By using the Clebsch-Gordan coefficient, it is possible to represent the direct product of angular momentum eigenstates with the sum of the irreducible representation:

$$\begin{aligned}
I_\Omega = \int d\Omega \sum_{J,M}(j_{\kappa_1},\nu_1,j_{\kappa_2},\nu_2|J,M)\left[[Y_{l_{\kappa_1}}(\hat{r})\otimes\chi_{1/2}(1)]_{j\kappa_1}\otimes[Y_{l_{\kappa_2}}(\hat{r})\otimes\chi_{1/2}(2)]_{j\kappa_2}\right]_J^{M\dagger} \\
\times\sum_{J',M'}\left(j_{\kappa_\mu},s_\mu,j_{\kappa_e},s_e|J',M'\right)\left[[Y_{l_{\kappa_\mu}}(\hat{r})\otimes\chi_{1/2}(1)]_{j\kappa_\mu}\otimes[Y_{l_{\kappa_e}}(\hat{r})\otimes\chi_{1/2}(2)]_{j\kappa_e}\right]_{J'}^{M'}.
\end{aligned} \tag{I.24}$$

Moreover, using the $9j$ symbols, we deform the equation to separate the orbital part and the spin part:

$$\begin{aligned}
I_\Omega &= \int d\Omega \sum_{J,M}\sum_{J',M'}(j_{\kappa_1},\nu_1,j_{\kappa_2},\nu_2|J,M)\left(j_{\kappa_\mu},s_\mu,j_{\kappa_e},s_e|J',M'\right) \\
&\quad\times\sum_{L,S}\sqrt{[j_{\kappa_1}\cdot j_{\kappa_2}\cdot L\cdot S]}\begin{Bmatrix} l_{\kappa_1} & 1/2 & j_{\kappa_1} \\ l_{\kappa_2} & 1/2 & j_{\kappa_2} \\ L & S & J\end{Bmatrix} \\
&\quad\times\left[[Y_{l_{\kappa_1}}(\hat{r})\otimes Y_{l_{\kappa_2}}(\hat{r})]_L\otimes[\chi_{1/2}(1)\otimes\chi_{1/2}(2)]_S\right]_J^{M\dagger} \\
&\quad\times\sum_{L',S'}\sqrt{\left[j_{\kappa_\mu}\cdot j_{\kappa_e}\cdot L'\cdot S'\right]}\begin{Bmatrix} l_{\kappa_\mu} & 1/2 & j_{\kappa_\mu} \\ l_{\kappa_e} & 1/2 & j_{\kappa_e} \\ L' & S' & J'\end{Bmatrix} \\
&\quad\times\left[[Y_{l_{\kappa_\mu}}(\hat{r})\otimes Y_{l_{\kappa_e}}(\hat{r})]_{L'}\otimes[\chi_{1/2}(1)\otimes\chi_{1/2}(2)]_{S'}\right]_{J'}^{M'}.
\end{aligned} \tag{I.25}$$

By Eq. (G.64), we can combine the spherical harmonics:

$$\begin{aligned}
I_\Omega &= \int d\Omega \sum_{J,M}\sum_{J',M'}(j_{\kappa_1},\nu_1,j_{\kappa_2},\nu_2|J,M)\left(j_{\kappa_\mu},s_\mu,j_{\kappa_e},s_e|J',M'\right) \\
&\quad\times\sum_{L,S}\sum_{L',S'}\begin{Bmatrix} l_{\kappa_1} & 1/2 & j_{\kappa_1} \\ l_{\kappa_2} & 1/2 & j_{\kappa_2} \\ L & S & J\end{Bmatrix}\begin{Bmatrix} l_{\kappa_\mu} & 1/2 & j_{\kappa_\mu} \\ l_{\kappa_e} & 1/2 & j_{\kappa_e} \\ L' & S' & J'\end{Bmatrix} \\
&\quad\times\sqrt{\left[j_{\kappa_1}\cdot j_{\kappa_2}\cdot j_{\kappa_\mu}\cdot j_{\kappa_e}\cdot j_{\kappa_e}\cdot l_{\kappa_1}\cdot l_{\kappa_2}\cdot l_{\kappa_\mu}\cdot l_{\kappa_e}\cdot S\cdot S'\right]} \\
&\quad\times\frac{1}{4\pi}(l_{\kappa_1},0,l_{\kappa_2},0|L,0)(l_{\kappa_\mu},0,l_{\kappa_e},0|L',0)\left\langle LS;JM|1|L'S';J'M'\right\rangle.
\end{aligned} \tag{I.26}$$

Here we have introduced a notation,

$$\begin{aligned}
&\left\langle LS;JM|\mathcal{O}|L'S';J'M'\right\rangle \\
&= \int d\Omega\left[Y_L(\hat{r})\otimes[\chi_{1/2}(1)\otimes\chi_{1/2}(2)]_S\right]_J^{M\dagger}\mathcal{O}\left[Y_{L'}(\hat{r})\otimes[\chi_{1/2}(1)\otimes\chi_{1/2}(2)]_{S'}\right]_{J'}^{M'},
\end{aligned} \tag{I.27}$$

where $\mathcal{O}$ indicates an arbitrary operator. In this case, $\mathcal{O}$ is an identity. According to the Wigner-Eckart theorem, we obtain

$$\begin{aligned}
\langle LS;JM|1|L'S';J'M'\rangle =&\frac{(J',M',0,0|J,M)}{\sqrt{[J]}}\langle LS;J||1||L'S';J\rangle \\
=&\frac{\delta_{JJ'}\delta_{MM'}}{\sqrt{[J]}}\langle LS;J||1||L'S';J\rangle \\
=&\frac{\delta_{JJ'}\delta_{MM'}}{\sqrt{[J]}}\sqrt{[J\cdot J]}\begin{Bmatrix} L & S & J \\ L' & S' & J \\ 0 & 0 & 0 \end{Bmatrix}\langle L||1||L'\rangle\langle S||1||S'\rangle \\
=&\delta_{JJ'}\delta_{MM'}\sqrt{[J]}\frac{\delta_{LL'}\delta_{SS'}}{\sqrt{[L\cdot S\cdot J]}}\delta_{LL'}\sqrt{[L]}\delta_{SS'}\sqrt{[S]} \\
=&\delta_{JJ'}\delta_{MM'}\delta_{LL'}\delta_{SS'}.
\end{aligned} \tag{I.28}$$

Using this reduction, the formula for I_Ω is given as

$$\begin{aligned}
I_\Omega =&\frac{1}{4\pi}\sum_{J,M}(j_{\kappa_1},\nu_1,j_{\kappa_2},\nu_2|J,M)(j_{\kappa_\mu},s_\mu,j_{\kappa_e},s_e|J,M) \\
&\sqrt{\left[j_{\kappa_1}\cdot j_{\kappa_2}\cdot j_{\kappa_\mu}\cdot j_{\kappa_e}\cdot l_{\kappa_1}\cdot l_{\kappa_2}\cdot l_{\kappa_\mu}\cdot l_{\kappa_e}\right]} \\
&\times\sum_{L,S}\times[S]\begin{Bmatrix} l_{\kappa_1} & 1/2 & j_{\kappa_1} \\ l_{\kappa_2} & 1/2 & j_{\kappa_2} \\ L & S & J \end{Bmatrix}\begin{Bmatrix} l_{\kappa_\mu} & 1/2 & j_{\kappa_\mu} \\ l_{\kappa_e} & 1/2 & j_{\kappa_e} \\ L & S & J \end{Bmatrix} \\
&\times(l_{\kappa_1},0,l_{\kappa_2},0|L,0)(l_{\kappa_\mu},0,l_{\kappa_e},0|L,0).
\end{aligned} \tag{I.29}$$

Now we define

$$\begin{aligned}
\mathcal{X}^{\beta_1,\beta_2}_{L,S,J}(a,b,c,d) =&\int_0^\infty drr^2 a^{\kappa_1}_{p_1}(r)b^{\kappa_\mu}_{\mu,n_\mu}(r)c^{\kappa_2}_{p_2}(r)d^{\kappa_e}_{e,n_e}(r) \\
&\times\sqrt{[l^a_{\kappa_1}\cdot l^b_{\kappa_\mu}\cdot l^c_{\kappa_2}\cdot l^d_{\kappa_e}]}(l^a_{\kappa_1},0,l^c_{\kappa_2},0|L,0)(l^b_{\kappa_\mu},0,l^d_{\kappa_e},0|L,0) \\
&\times\begin{Bmatrix} l^a_{\kappa_1} & 1/2 & j_{\kappa_1} \\ l^c_{\kappa_2} & 1/2 & j_{\kappa_2} \\ L & S & J \end{Bmatrix}\begin{Bmatrix} l^b_{\kappa_\mu} & 1/2 & j_{\kappa_\mu} \\ l^d_{\kappa_e} & 1/2 & j_{\kappa_e} \\ L & S & J \end{Bmatrix},
\end{aligned} \tag{4.79}$$

where a, b, c, and d are g or f. In addition, l^g_κ and l^f_κ is defined as

$$l^h_\kappa=\begin{cases} l_{+\kappa} & (h=g) \\ l_{-\kappa} & (h=f) \end{cases}. \tag{I.30}$$

By the above calculation for I_Ω, it was found that the first term of Eq. (I.22) can be rewritten as

$$\begin{aligned}
&\int drr^2 d\Omega g^{\kappa_1}_{p_1}(r)g^{\kappa_\mu}_{\mu,n_\mu}(r)g^{\kappa_2}_{p_2}(r)g^{\kappa_e}_{e,n_e}(r)\chi^{\nu_1\dagger}_{\kappa_1}(\hat{r})\,\chi^{s_\mu}_{\kappa_\mu}(\hat{r})\,\chi^{\nu_2\dagger}_{\kappa_2}(\hat{r})\,\chi^{s_e}_{\kappa_e}(\hat{r}) \\
=&\frac{1}{4\pi}\sum_{J,M}(j_{\kappa_1},\nu_1,j_{\kappa_2},\nu_2|J,M)(j_{\kappa_\mu},s_\mu,j_{\kappa_e},s_e|J,M)\sqrt{\left[j_{\kappa_1}\cdot j_{\kappa_\mu}\cdot j_{\kappa_2}\cdot j_{\kappa_e}\right]} \\
&\times\sum_{L,S}[S]\mathcal{X}^{\beta_1,\beta_2}_{L,S,J}(g,g,g,g).
\end{aligned} \tag{I.31}$$

After the same analyses for all other terms of Eq. (I.22), we obtain

$$
\begin{aligned}
&M_{SS}^{\beta_1,\nu_1;\beta_2,\nu_2} \\
=&\frac{1}{4\pi}\sum_{J,M}(j_{\kappa_1},\nu_1,j_{\kappa_2},\nu_2|J,M)(j_{\kappa_\mu},s_\mu,j_{\kappa_e},s_2|JM)\sqrt{\left[j_{\kappa_1}\cdot j_{\kappa_\mu}\cdot j_{\kappa_2}\cdot j_{\kappa_e}\right]} \\
&\times\sum_{L,S}[S]\left[\mathcal{X}_{L,S,J}^{\beta_1,\beta_2}(g,g,g,g)+\mathcal{X}_{L,S,J}^{\beta_1,\beta_2}(f,f,f,f)-\mathcal{X}_{L,S,J}^{\beta_1,\beta_2}(g,g,f,f)-\mathcal{X}_{L,S,J}^{\beta_1,\beta_2}(f,f,g,g)\right].
\end{aligned}
\tag{I.32}
$$

Similarly, the calculation can be performed for other M_{ij}. However, unlike scalar terms, more general formula is needed for calculating the vector terms because they contains the terms including the Pauli matrices. For example, let us see M_{VV},

$$
\begin{aligned}
M_{VV}^{\beta_1,\nu_1;\beta_2,\nu_2} =& \int drr^2d\Omega\left[g_{p_1}^{\kappa_1}(r)g_{\mu,n_\mu}^{\kappa_\mu}(r)g_{p_2}^{\kappa_2}(r)g_{e,n_e}^{\kappa_e}(r)\chi_{\kappa_1}^{\nu_1\dagger}(\hat{r})\,\chi_{\kappa_\mu}^{s_\mu}(\hat{r})\,\chi_{\kappa_2}^{\nu_2\dagger}(\hat{r})\,\chi_{\kappa_e}^{s_e}(\hat{r})\right. \\
&+f_{p_1}^{\kappa_1}(r)f_{\mu,n_\mu}^{\kappa_\mu}(r)f_{p_2}^{\kappa_2}(r)f_{e,n_e}^{\kappa_e}(r)\chi_{-\kappa_1}^{\nu_1\dagger}(\hat{r})\,\chi_{-\kappa_\mu}^{s_\mu}(\hat{r})\,\chi_{-\kappa_2}^{\nu_2\dagger}(\hat{r})\,\chi_{-\kappa_e}^{s_e}(\hat{r}) \\
&+g_{p_1}^{\kappa_1}(r)g_{\mu,n_\mu}^{\kappa_\mu}(r)f_{p_2}^{\kappa_2}(r)f_{e,n_e}^{\kappa_e}(r)\chi_{\kappa_1}^{\nu_1\dagger}(\hat{r})\,\chi_{\kappa_\mu}^{s_\mu}(\hat{r})\,\chi_{-\kappa_2}^{\nu_2\dagger}(\hat{r})\,\chi_{-\kappa_e}^{s_e}(\hat{r}) \\
&+f_{p_1}^{\kappa_1}(r)f_{\mu,n_\mu}^{\kappa_\mu}(r)g_{p_2}^{\kappa_2}(r)g_{e,n_e}^{\kappa_e}(r)\chi_{-\kappa_1}^{\nu_1\dagger}(\hat{r})\,\chi_{-\kappa_\mu}^{s_\mu}(\hat{r})\,\chi_{\kappa_2}^{\nu_2\dagger}(\hat{r})\,\chi_{\kappa_e}^{s_e}(\hat{r}) \\
&+g_{p_1}^{\kappa_1}(r)f_{\mu,n_\mu}^{\kappa_\mu}(r)g_{p_2}^{\kappa_2}(r)f_{e,n_e}^{\kappa_e}(r)\chi_{\kappa_1}^{\nu_1\dagger}(\hat{r})\,\sigma_i\chi_{-\kappa_\mu}^{s_\mu}(\hat{r})\,\chi_{\kappa_2}^{\nu_2\dagger}(\hat{r})\,\sigma_i\chi_{-\kappa_e}^{s_e}(\hat{r}) \\
&+f_{p_1}^{\kappa_1}(r)g_{\mu,n_\mu}^{\kappa_\mu}(r)f_{p_2}^{\kappa_2}(r)g_{e,n_e}^{\kappa_e}(r)\chi_{-\kappa_1}^{\nu_1\dagger}(\hat{r})\,\sigma_i\chi_{\kappa_\mu}^{s_\mu}(\hat{r})\,\chi_{-\kappa_2}^{\nu_2\dagger}(\hat{r})\,\sigma_i\chi_{\kappa_e}^{s_e}(\hat{r}) \\
&-g_{p_1}^{\kappa_1}(r)f_{\mu,n_\mu}^{\kappa_\mu}(r)f_{p_2}^{\kappa_2}(r)g_{e,n_e}^{\kappa_e}(r)\chi_{\kappa_1}^{\nu_1\dagger}\sigma_i\chi_{-\kappa_\mu}^{s_\mu}\chi_{-\kappa_2}^{\nu_2\dagger}\sigma_i\chi_{\kappa_e}^{s_e} \\
&\left.-f_{p_1}^{\kappa_1}(r)g_{\mu,n_\mu}^{\kappa_\mu}(r)g_{p_2}^{\kappa_2}(r)f_{e,n_e}^{\kappa_e}(r)\chi_{-\kappa_1}^{\nu_1\dagger}\sigma_i\chi_{\kappa_\mu}^{s_\mu}\chi_{\kappa_2}^{\nu_2\dagger}\sigma_i\chi_{-\kappa_e}^{s_e}(\hat{r})\right],
\end{aligned}
\tag{I.33}
$$

where the latter four terms include the Pauli matrices. Now let us calculate

$$
I'_\Omega = \int d\Omega\chi_{\kappa_1}^{\nu_1\dagger}(\hat{r})\,\sigma_i\chi_{\kappa_\mu}^{s_\mu}(\hat{r})\,\chi_{\kappa_2}^{\nu_2\dagger}(\hat{r})\,\sigma_i\chi_{\kappa_e}^{s_e}(\hat{r}).
\tag{I.34}
$$

The similar modification can be used to obtain

$$
\begin{aligned}
I'_\Omega =& \sum_{J,M}\sum_{J',M'}(j_{\kappa_1},\nu_1,j_{\kappa_2},\nu_2|J,M)(j_{\kappa_\mu},s_\mu,j_{\kappa_e},s_e|J',M') \\
&\times\sum_{L,S}\sum_{L',S'}\begin{Bmatrix} l_{\kappa_1} & 1/2 & j_{\kappa_1} \\ l_{\kappa_2} & 1/2 & j_{\kappa_2} \\ L & S & J \end{Bmatrix}\begin{Bmatrix} l_{\kappa_\mu} & 1/2 & j_{\kappa_\mu} \\ l_{\kappa_e} & 1/2 & j_{\kappa_e} \\ L' & S' & J' \end{Bmatrix} \\
&\times\sqrt{\left[j_{\kappa_1}\cdot j_{\kappa_2}\cdot j_{\kappa_\mu}\cdot j_{\kappa_e}\cdot l_{\kappa_1}\cdot l_{\kappa_2}\cdot l_{\kappa_\mu}\cdot l_{\kappa_e}\cdot S\cdot S'\right]} \\
&\times\frac{1}{4\pi}(l_{\kappa_1},0,l_{\kappa_2},0|L,0)(l_{\kappa_\mu},0,l_{\kappa_e},0|L',0) \\
&\times\delta_{JJ'}\delta_{MM'}\delta_{LL'}\frac{1}{\sqrt{[S]}}\langle S||\sigma_i(1)\otimes\sigma_i(2)||S'\rangle.
\end{aligned}
\tag{I.35}
$$

$\sigma_i(1)\otimes\sigma_i(2)$ is represented by the total spin operator

$$
S_i = \frac{\sigma_i(1)}{2}+\frac{\sigma_i(2)}{2},
\tag{I.36}
$$

as

$$
\sigma_i(1)\otimes\sigma_i(2) = 2\hat{S}^2-3,
\tag{I.37}
$$

because

$$\begin{aligned}\hat{S}^2 =& \left(\frac{\sigma_i(1)}{2}\right)^2 + \left(\frac{\sigma_i(2)}{2}\right)^2 + \frac{\sigma_i(1)\otimes\sigma_i(2)}{2} \\ =& \frac{3}{2} + \frac{\sigma_i(1)\otimes\sigma_i(2)}{2}.\end{aligned} \tag{I.38}$$

Furthermore, since $||S\rangle$ is the eigenstate of $\hat{S}$ with an eigenvalue of S, we find

$$\sigma_i(1)\otimes\sigma_i(2)\,||S\rangle = \begin{cases} -3\,||S\rangle & (S=0) \\ ||S\rangle & (S=1) \end{cases}. \tag{I.39}$$

Thus we obtain

$$\begin{aligned} I'_\Omega =& \frac{1}{4\pi}\sum_{J,M}(j_{\kappa_1},\nu_1,j_{\kappa_2},\nu_2|J,M)(j_{\kappa_\mu},s_\mu,j_{\kappa_e},s_e|J,M) \\ & \times\sqrt{\left[j_{\kappa_1}\cdot j_{\kappa_2}\cdot j_{\kappa_\mu}\cdot j_{\kappa_e}\cdot l_{\kappa_1}\cdot l_{\kappa_2}\cdot l_{\kappa_\mu}\cdot l_{\kappa_e}\right]} \\ & \times\sum_{LS}[S]\begin{Bmatrix} l_{\kappa_1} & 1/2 & j_{\kappa_1} \\ l_{\kappa_2} & 1/2 & j_{\kappa_2} \\ L & S & J \end{Bmatrix}\begin{Bmatrix} l_{\kappa_\mu} & 1/2 & j_{\kappa_e} \\ l_{\kappa_\mu} & 1/2 & j_{\kappa_e} \\ L & S & J \end{Bmatrix} \\ & \times(l_{\kappa_1},0,l_{\kappa_2},0,|L,0)(l_{\kappa_\mu},0,l_{\kappa_e},0|L,0)\Sigma(S), \end{aligned} \tag{I.40}$$

where $\Sigma(S)$ is defined as

$$\Sigma(S) = \begin{cases} -3 & (S=0) \\ 1 & (S=1) \end{cases}. \tag{I.41}$$

Thus

$$\begin{aligned} & M_{VV}^{\beta_1,\nu_1;\beta_2,\nu_2} \\ =& \frac{1}{4\pi}\sum_{J,M}(j_{\kappa_1},\nu_1,j_{\kappa_2},\nu_2|J,M)(j_{\kappa_\mu},s_\mu,j_{\kappa_e},s_e|J,M)\sqrt{\left[j_{\kappa_1}\cdot j_{\kappa_\mu}\cdot j_{\kappa_2}\cdot j_{\kappa_e}\right]} \\ & \times\sum_{L,S}[S]\left[\mathcal{X}^{\beta_1,\beta_2}_{L,S,J}(g,g,g,g)+\mathcal{X}^{\beta_1,\beta_2}_{L,S,J}(f,f,f,f)+\mathcal{X}^{\beta_1,\beta_2}_{L,S,J}(g,g,f,f)+\mathcal{X}^{\beta_1,\beta_2}_{L,S,J}(f,f,g,g)\right. \\ & \left.+\Sigma(S)\left\{\mathcal{X}^{\beta_1,\beta_2}_{L,S,J}(g,f,g,f)+\mathcal{X}^{\beta_1,\beta_2}_{L,S,J}(f,g,f,g)-\mathcal{X}^{\beta_1,\beta_2}_{L,S,J}(g,f,f,g)-\mathcal{X}^{\beta_1,\beta_2}_{L,S,J}(f,g,g,f)\right\}\right]. \end{aligned} \tag{I.42}$$

Now we can evaluate all M_{ij}s by the similar way. Combining the expressions for M_{ij}s and Eq. (I.15), $\tilde{\mathcal{M}}_{\rm contact}$ is written down as follows:

$$\begin{aligned} \tilde{\mathcal{M}}_{\rm contact} =& -\frac{4G_F}{\sqrt{2}}\frac{1}{4\pi}\sum_{J,M}(j_{\kappa_1},\nu_1,j_{\kappa_2},\nu_2|J,M)(j_{\kappa_\mu},s_\mu,j_{\kappa_e},s_e|J,M)\sqrt{\left[j_{\kappa_1}\cdot j_{\kappa_\mu}\cdot j_{\kappa_2}\cdot j_{\kappa_e}\right]} \\ & \times\sum_{i,j}g_{ij}\sum_{L,S}[S]\left[M^{\beta_1,\beta_2}_{ij;L,S,J}-(-1)^{j_{\kappa_1}+j_{\kappa_2}-J}M^{\beta_2,\beta_1}_{ij;L,S,J}\right], \end{aligned} \tag{I.43}$$

where $M^{\beta_1,\beta_2}_{ij;L,S,J}$s are defined as

$$M^{\beta_1,\beta_2}_{SS;L,S,J} = \mathcal{X}^{\beta_1,\beta_2}_{L,S,J}(g,g,g,g)+\mathcal{X}^{\beta_1,\beta_2}_{L,S,J}(f,f,f,f)-\mathcal{X}^{\beta_1,\beta_2}_{L,S,J}(g,g,f,f)-\mathcal{X}^{\beta_1,\beta_2}_{L,S,J}(f,f,g,g), \tag{I.44}$$

$$M^{\beta_1,\beta_2}_{PP;L,S,J} = -\mathcal{X}^{\beta_1,\beta_2}_{L,S,J}(g,f,g,f)-\mathcal{X}^{\beta_1,\beta_2}_{L,S,J}(f,g,f,g)-\mathcal{X}^{\beta_1,\beta_2}_{L,S,J}(g,f,f,g)-\mathcal{X}^{\beta_1,\beta_2}_{L,S,J}(f,g,g,f), \tag{I.45}$$

$$M^{\beta_1,\beta_2}_{SP;L,S,J} = i\left[\mathcal{X}^{\beta_1,\beta_2}_{L,S,J}(g,g,g,f)-\mathcal{X}^{\beta_1,\beta_2}_{L,S,J}(f,f,f,g)+\mathcal{X}^{\beta_1,\beta_2}_{L,S,J}(g,g,f,g)-\mathcal{X}^{\beta_1,\beta_2}_{L,S,J}(f,f,g,f)\right], \tag{I.46}$$

$$M^{\beta_1,\beta_2}_{PS;L,S,J} = i\left[\mathcal{X}^{\beta_1,\beta_2}_{L,S,J}(g,f,g,g)-\mathcal{X}^{\beta_1,\beta_2}_{L,S,J}(f,g,f,f)+\mathcal{X}^{\beta_1,\beta_2}_{L,S,J}(f,g,g,g)-\mathcal{X}^{\beta_1,\beta_2}_{L,S,J}(g,f,f,f)\right], \tag{I.47}$$

$$
\begin{aligned}
&M^{\beta_1,\beta_2}_{VV;L,S,J}\\
=&\mathcal{X}^{\beta_1,\beta_2}_{L,S,J}(g,g,g,g)+\mathcal{X}^{\beta_1,\beta_2}_{L,S,J}(f,f,f,f)+\mathcal{X}^{\beta_1,\beta_2}_{L,S,J}(g,g,f,f)+\mathcal{X}^{\beta_1,\beta_2}_{L,S,J}(f,f,g,g)\\
&+\Sigma(S)\left\{\mathcal{X}^{\beta_1,\beta_2}_{L,S,J}(g,f,g,f)+\mathcal{X}^{\beta_1,\beta_2}_{L,S,J}(f,g,f,g)-\mathcal{X}^{\beta_1,\beta_2}_{L,S,J}(g,f,f,g)-\mathcal{X}^{\beta_1,\beta_2}_{L,S,J}(f,g,g,f)\right\}, \qquad \text{(I.48)}\\
&M^{\beta_1,\beta_2}_{AA;L,S,J}\\
=&-\mathcal{X}^{\beta_1,\beta_2}_{L,S,J}(g,f,g,f)-\mathcal{X}^{\beta_1,\beta_2}_{L,S,J}(f,g,f,g)+\mathcal{X}^{\beta_1,\beta_2}_{L,S,J}(g,f,f,g)+\mathcal{X}^{\beta_1,\beta_2}_{L,S,J}(f,g,g,f)\\
&-\Sigma(S)\left\{\mathcal{X}^{\beta_1,\beta_2}_{L,S,J}(g,g,g,g)+\mathcal{X}^{\beta_1,\beta_2}_{L,S,J}(f,f,f,f)+\mathcal{X}^{\beta_1,\beta_2}_{L,S,J}(g,g,f,f)+\mathcal{X}^{\beta_1,\beta_2}_{L,S,J}(f,f,g,g)\right\}, \qquad \text{(I.49)}\\
&M^{\beta_1,\beta_2}_{VA;L,S,J}\\
=&i\left[\mathcal{X}^{\beta_1,\beta_2}_{L,S,J}(g,g,g,f)-\mathcal{X}^{\beta_1,\beta_2}_{L,S,J}(f,f,f,g)-\mathcal{X}^{\beta_1,\beta_2}_{L,S,J}(g,g,f,g)+\mathcal{X}^{\beta_1,\beta_2}_{L,S,J}(f,f,g,f)\right.\\
&\left.-\Sigma(S)\left\{\mathcal{X}^{\beta_1,\beta_2}_{L,S,J}(g,f,g,g)-\mathcal{X}^{\beta_1,\beta_2}_{L,S,J}(f,g,f,f)-\mathcal{X}^{\beta_1,\beta_2}_{L,S,J}(f,g,g,g)+\mathcal{X}^{\beta_1,\beta_2}_{L,S,J}(g,f,f,f)\right\}\right], \qquad \text{(I.50)}\\
&M^{\beta_1,\beta_2}_{AV;L,S,J}\\
=&i\left[\mathcal{X}^{\beta_1,\beta_2}_{L,S,J}(g,f,g,g)-\mathcal{X}^{\beta_1,\beta_2}_{L,S,J}(f,g,f,f)-\mathcal{X}^{\beta_1,\beta_2}_{L,S,J}(f,g,g,g)+\mathcal{X}^{\beta_1,\beta_2}_{L,S,J}(g,f,f,f)\right.\\
&\left.-\Sigma(S)\left\{\mathcal{X}^{\beta_1,\beta_2}_{L,S,J}(g,g,g,f)-\mathcal{X}^{\beta_1,\beta_2}_{L,S,J}(f,f,f,g)-\mathcal{X}^{\beta_1,\beta_2}_{L,S,J}(g,g,f,g)+\mathcal{X}^{\beta_1,\beta_2}_{L,S,J}(f,f,g,f)\right\}\right]. \qquad \text{(I.51)}
\end{aligned}
$$

We can simplify the formula more by unifying $M^{\beta_1,\beta_2}_{ij;L,S,J}$ and $M^{\beta_2,\beta_1}_{ij;L,S,J}$. For that purpose, let us consider the relation between $\mathcal{X}^{\beta_1,\beta_2}_{L,S,J}(a,b,c,d)$ and $\mathcal{X}^{\beta_2,\beta_1}_{L,S,J}(a,b,c,d)$, which is given by

$$
\begin{aligned}
\mathcal{X}^{\beta_2,\beta_1}_{L,S,J}(a,b,c,d)=&\int_0^\infty drr^2a^{\kappa_2}_{p_2}(r)b^{\kappa_\mu}_{\mu,n_\mu}(r)c^{\kappa_1}_{p_1}(r)d^{\kappa_e}_{e,n_e}(r)\\
&\times[S]\sqrt{\left[j_{\kappa_2}\cdot j_{\kappa_\mu}\cdot j_{\kappa_1}\cdot j_{\kappa_e}\cdot l^a_{\kappa_2}\cdot l^b_{\kappa_\mu}\cdot l^c_{\kappa_1}\cdot l^d_{\kappa_e}\right]}\\
&\times\begin{Bmatrix} l^a_{\kappa_2} & 1/2 & j_{\kappa_2}\\ l^c_{\kappa_1} & 1/2 & j_{\kappa_1}\\ L & S & J\end{Bmatrix}\begin{Bmatrix} l^b_{\kappa_\mu} & 1/2 & j_{\kappa_\mu}\\ l^d_{\kappa_e} & 1/2 & j_{\kappa_e}\\ L & S & J\end{Bmatrix}\\
&\times(l^a_{\kappa_2},0,l^c_{\kappa_1},0|L,0)(l^b_{\kappa_\mu},0,l^d_{\kappa_e},0|L,0). \qquad \text{(I.52)}
\end{aligned}
$$

Using some relations for Clebsch-Gordan coefficients, we obtain

$$
\begin{aligned}
\mathcal{X}^{\beta_2,\beta_1}_{L,S,J}(a,b,c,d)=&\int_0^\infty drr^2c^{\kappa_1}_{p_1}(r)b^{\kappa_\mu}_{\mu,n_\mu}(r)a^{\kappa_2}_{p_2}(r)d^{\kappa_e}_{e,n_e}(r)\\
&\times[S]\sqrt{\left[j_{\kappa_1}\cdot j_{\kappa_\mu}\cdot j_{\kappa_2}\cdot j_{\kappa_e}\cdot l^c_{\kappa_1}\cdot l^b_{\kappa_\mu}\cdot l^a_{\kappa_2}\cdot l^d_{\kappa_e}\right]}\\
&\times(-1)^{1+S+j_{\kappa_1}+j_{\kappa_2}+J}\begin{Bmatrix} l^c_{\kappa_1} & 1/2 & j_{\kappa_1}\\ l^a_{\kappa_2} & 1/2 & j_{\kappa_2}\\ L & S & J\end{Bmatrix}\begin{Bmatrix} l^b_{\kappa_\mu} & 1/2 & j_{\kappa_\mu}\\ l^d_{\kappa_e} & 1/2 & j_{\kappa_e}\\ L & S & J\end{Bmatrix}\\
&\times(l^c_{\kappa_1},0,l^a_{\kappa_2},0|L,0)(l^b_{\kappa_\mu},0,l^d_{\kappa_e},0|L,0)\\
=&(-1)^{1+S+j_{\kappa_1}+j_{\kappa_2}+J}\mathcal{X}^{\beta_1,\beta_2}_{L,S,J}(c,b,a,d). \qquad \text{(I.53)}
\end{aligned}
$$

Now it is useful to define

$$
\begin{aligned}
&M^{\beta_1,\beta_2}_{ij\pm i'j';L,S,J}\\
=&\left(M^{\beta_1,\beta_2}_{ij;L,S,J}-(-1)^{j_{\kappa_1}+j_{\kappa_2}-J}M^{\beta_2,\beta_1}_{ij;L,S,J}\right)\pm\left(M^{\beta_1,\beta_2}_{i'j';L,S,J}-(-1)^{j_{\kappa_1}+j_{\kappa_2}-J}M^{\beta_2,\beta_1}_{i'j';L,S,J}\right), \qquad \text{(I.54)}
\end{aligned}
$$

and represent $\tilde{\mathcal{M}}_{\rm contact}$ as

$$\begin{aligned}\tilde{\mathcal{M}}_{\rm contact} =& -\frac{4G_F}{\sqrt{2}}\frac{1}{4\pi}\sum_{J,M}(j_{\kappa_1},\nu_1,j_{\kappa_2},\nu_2|J,M)(j_{\kappa_\mu},s_\mu,j_{\kappa_e},s_e|J,M)\\ &\times\sum_{i,j,i',j'} g_{ij\pm i'j'}\sum_{L,S}[S]M^{\beta_1,\beta_2}_{ij\pm i'j';L,S,J}.\end{aligned} \tag{I.55}$$

Here new coupling constants are defined as

$$g_{SS+PP} = \frac{g_{SS}+g_{PP}}{2} = \frac{g_1+g_2}{4}, \tag{I.56}$$

$$g_{SS-PP} = \frac{g_{SS}-g_{PP}}{2} = 0, \tag{I.57}$$

$$g_{SP+PS} = \frac{g_{SP}+g_{PS}}{2} = \frac{g_1-g_2}{4}, \tag{I.58}$$

$$g_{SP-PS} = \frac{g_{SP}-g_{PS}}{2} = 0, \tag{I.59}$$

$$g_{VV+AA} = \frac{g_{VV}+g_{AA}}{2} = \frac{g_3+g_4}{4}, \tag{I.60}$$

$$g_{VV-AA} = \frac{g_{VV}-g_{AA}}{2} = \frac{g_5+g_6}{4}, \tag{I.61}$$

$$g_{VA+AV} = \frac{g_{VA}+g_{AV}}{2} = \frac{g_3-g_4}{4}, \tag{I.62}$$

$$g_{VA-AV} = \frac{g_{VA}-g_{AV}}{2} = -\frac{g_5-g_6}{4}. \tag{I.63}$$

Now a few examples of $M_{ij\pm i'j'}$ are shown. Let i, j, i', and j' be S, S, P and P, respectively.

$$\begin{aligned}&M^{\beta_1,\beta_2}_{SS\pm PP;L,S,J}\\ =&\mathcal{X}^{\beta_1,\beta_2}_{L,S,J}(g,g,g,g)+\mathcal{X}^{\beta_1,\beta_2}_{L,S,J}(f,f,f,f)-\mathcal{X}^{\beta_1,\beta_2}_{L,S,J}(g,g,f,f)-\mathcal{X}^{\beta_1,\beta_2}_{L,S,J}(f,f,g,g)\\ &\pm\left\{-\mathcal{X}^{\beta_1,\beta_2}_{L,S,J}(g,f,g,f)-\mathcal{X}^{\beta_1,\beta_2}_{L,S,J}(f,g,f,g)-\mathcal{X}^{\beta_1,\beta_2}_{L,S,J}(g,f,f,g)-\mathcal{X}^{\beta_1,\beta_2}_{L,S,J}(f,g,g,f)\right\}\\ &+(-1)^S\left[\mathcal{X}^{\beta_1,\beta_2}_{L,S,J}(g,g,g,g)+\mathcal{X}^{\beta_1,\beta_2}_{L,S,J}(f,f,f,f)-\mathcal{X}^{\beta_1,\beta_2}_{L,S,J}(f,g,g,f)-\mathcal{X}^{\beta_1,\beta_2}_{L,S,J}(g,f,f,g)\right.\\ &\left.\pm\left\{-\mathcal{X}^{\beta_1,\beta_2}_{L,S,J}(g,f,g,f)-\mathcal{X}^{\beta_1,\beta_2}_{L,S,J}(f,g,f,g)-\mathcal{X}^{\beta_1,\beta_2}_{L,S,J}(f,f,g,g)-\mathcal{X}^{\beta_1,\beta_2}_{L,S,J}(g,g,f,f)\right\}\right]\\ =&(1+(-1)^S)\left[\mathcal{X}^{\beta_1,\beta_2}_{L,S,J}(g,g,g,g)+\mathcal{X}^{\beta_1,\beta_2}_{L,S,J}(f,f,f,f)\mp\left\{\mathcal{X}^{\beta_1,\beta_2}_{L,S,J}(g,f,g,f)+\mathcal{X}^{\beta_1,\beta_2}_{L,S,J}(f,g,f,g)\right\}\right]\\ &+(1\pm(-1)^S)\left[-\mathcal{X}^{\beta_1,\beta_2}_{L,S,J}(g,g,f,f)-\mathcal{X}^{\beta_1,\beta_2}_{L,S,J}(f,f,g,g)\right.\\ &\left.\mp\left\{\mathcal{X}^{\beta_1,\beta_2}_{L,S,J}(g,f,f,g)+\mathcal{X}^{\beta_1,\beta_2}_{L,S,J}(f,g,g,f)\right\}\right].\end{aligned} \tag{I.64}$$

Similarly, for $ij \pm i'j' = VV \pm AA$,

$$
\begin{aligned}
&M^{\beta_1,\beta_2}_{VV\pm AA;L,S,J} \\
=&\mathcal{X}^{\beta_1,\beta_2}_{L,S,J}(g,g,g,g) + \mathcal{X}^{\beta_1,\beta_2}_{L,S,J}(f,f,f,f) + \mathcal{X}^{\beta_1,\beta_2}_{L,S,J}(g,g,f,f) + \mathcal{X}^{\beta_1,\beta_2}_{L,S,J}(f,f,g,g) \\
&+ \Sigma(S)\left\{\mathcal{X}^{\beta_1,\beta_2}_{L,S,J}(g,f,g,f) + \mathcal{X}^{\beta_1,\beta_2}_{L,S,J}(f,g,f,g) - \mathcal{X}^{\beta_1,\beta_2}_{L,S,J}(g,f,f,g) - \mathcal{X}^{\beta_1,\beta_2}_{L,S,J}(f,g,g,f)\right\} \\
&\pm\left\{-\mathcal{X}^{\beta_1,\beta_2}_{L,S,J}(g,f,g,f) - \mathcal{X}^{\beta_1,\beta_2}_{L,S,J}(f,g,f,g) + \mathcal{X}^{\beta_1,\beta_2}_{L,S,J}(g,f,f,g) + \mathcal{X}^{\beta_1,\beta_2}_{L,S,J}(f,g,g,f)\right. \\
&\left.+\Sigma(S)\left\{-\mathcal{X}^{\beta_1,\beta_2}_{L,S,J}(g,g,g,g) - \mathcal{X}^{\beta_1,\beta_2}_{L,S,J}(f,f,f,f) - \mathcal{X}^{\beta_1,\beta_2}_{L,S,J}(g,g,f,f) - \mathcal{X}^{\beta_1,\beta_2}_{L,S,J}(f,f,g,g)\right\}\right\} \\
&+ (-1)^S\left[\mathcal{X}^{\beta_1,\beta_2}_{L,S,J}(g,g,g,g) + \mathcal{X}^{\beta_1,\beta_2}_{L,S,J}(f,f,f,f) + \mathcal{X}^{\beta_1,\beta_2}_{L,S,J}(f,g,g,f) + \mathcal{X}^{\beta_1,\beta_2}_{L,S,J}(g,f,f,g)\right. \\
&+ \Sigma(S)\left\{\mathcal{X}^{\beta_1,\beta_2}_{L,S,J}(g,f,g,f) + \mathcal{X}^{\beta_1,\beta_2}_{L,S,J}(f,g,f,g) - \mathcal{X}^{\beta_1,\beta_2}_{L,S,J}(f,f,g,g) - \mathcal{X}^{\beta_1,\beta_2}_{L,S,J}(g,g,f,f)\right\} \\
&\pm\left\{-\mathcal{X}^{\beta_1,\beta_2}_{L,S,J}(g,f,f,g) - \mathcal{X}^{\beta_1,\beta_2}_{L,S,J}(f,g,f,g) + \mathcal{X}^{\beta_1,\beta_2}_{L,S,J}(f,f,g,g) + \mathcal{X}^{\beta_1,\beta_2}_{L,S,J}(g,g,f,f)\right. \\
&\left.\left.+\Sigma(S)\left\{-\mathcal{X}^{\beta_1,\beta_2}_{L,S,J}(g,g,g,g) - \mathcal{X}^{\beta_1,\beta_2}_{L,S,J}(f,f,f,f) - \mathcal{X}^{\beta_1,\beta_2}_{L,S,J}(f,g,g,f) - \mathcal{X}^{\beta_1,\beta_2}_{L,S,J}(g,f,f,g)\right\}\right\}\right] \\
=&(1+(-1)^S)(1\mp\Sigma(S)) \\
&\times\left[\mathcal{X}^{\beta_1,\beta_2}_{L,S,J}(g,g,g,g) + \mathcal{X}^{\beta_1,\beta_2}_{L,S,J}(f,f,f,f) \mp \left\{\mathcal{X}^{\beta_1,\beta_2}_{L,S,J}(g,f,g,f) + \mathcal{X}^{\beta_1,\beta_2}_{L,S,J}(f,g,f,g)\right\}\right] \\
&+ (1\pm(-1)^S)(1\mp\Sigma(S)) \\
&\times\left[\mathcal{X}^{\beta_1,\beta_2}_{L,S,J}(g,g,f,f) + \mathcal{X}^{\beta_1,\beta_2}_{L,S,J}(f,f,g,g) \pm \left\{\mathcal{X}^{\beta_1,\beta_2}_{L,S,J}(g,f,f,g) + \mathcal{X}^{\beta_1,\beta_2}_{L,S,J}(f,g,g,f)\right\}\right].
\end{aligned}
\tag{I.65}
$$

Since the sum of two lepton spin S is allowed to be only 0 or 1, we can use

$$1+(-1)^S = 2\delta_{S,0}, \tag{I.66}$$

$$1-(-1)^S = 2\delta_{S,1}. \tag{I.67}$$

Eventually, we get the formula for contact process,

$$
\begin{aligned}
\tilde{\mathcal{M}}_{\text{contact}} =& -\frac{4G_F}{\sqrt{2}}\frac{1}{4\pi}\sum_{J,M}(j_{\kappa_1},\nu_1,j_{\kappa_2},\nu_2|J,M)(j_{\kappa_\mu},s_\mu,j_{\kappa_e},s_e|J,M)\sqrt{[j_{\kappa_1}\cdot j_{\kappa_\mu}\cdot j_{\kappa_2}\cdot j_{\kappa_e}]} \\
&\times\sum_{i,j,i',j'} g_{ij\pm i'j'}M^{\beta_1,\beta_2}_{ij\pm i'j'}(J),
\end{aligned}
\tag{I.68}
$$

where

$$M^{\beta_1,\beta_2}_{ij\pm i'j'}(J) = \sum_{L,S}[S]M^{\beta_1,\beta_2}_{ij\pm i'j';J}. \tag{I.69}$$

Here $M^{\beta_1,\beta_2}_{ij\pm i'j'}(J)$s are given as

$$M^{\beta_1,\beta_2}_{SS+PP}(J) = 2\left[X^-_0(J,0,J) - X^+_1(J,0,J)\right], \tag{I.70}$$

$$M^{\beta_1,\beta_2}_{SS-PP}(J) = 2\left[X^+_0(J,0,J) - 3\sum_{L=|J-1|}^{J+1}X^-_1(L,1,J)\right], \tag{I.71}$$

$$M^{\beta_1,\beta_2}_{SP+PS}(J) = 2i\left[Y^+_1(J,0,J) + Y^+_0(J,0,J)\right], \tag{I.72}$$

$$M^{\beta_1,\beta_2}_{SP-PS}(J) = 2i\left[Y^-_1(J,0,J) + 3\sum_{L=|J-1|}^{J+1}Y^-_0(L,1,J)\right], \tag{I.73}$$

$$M^{\beta_1,\beta_2}_{VV+AA}(J) =8\left[X^-_0(J,0,J)+X^+_1(J,0,J)\right], \tag{I.74}$$

$$M^{\beta_1,\beta_2}_{VV-AA}(J) =-4\left[X^+_0(J,0,J)-3\sum_{L=|J-1|}^{J+1}X^-_1(L,1,J)\right], \tag{I.75}$$

$$M^{\beta_1,\beta_2}_{VA+AV}(J) =8i\left[Y^+_1(J,0,J)-Y^+_0(J,0,J)\right], \tag{I.76}$$

$$M^{\beta_1,\beta_2}_{VA-AV}(J) =-4i\left[Y^-_1(J,0,J)+3\sum_{L=|J-1|}^{J+1}Y^-_0(L,1,J)\right], \tag{I.77}$$

where

$$X^\pm_0(L,S,J) =\mathcal{X}^{\beta_1,\beta_2}_{L,S,J}(g,g,g,g)+\mathcal{X}^{\beta_1,\beta_2}_{L,S,J}(f,f,f,f)\pm\left[\mathcal{X}^{\beta_1,\beta_2}_{L,S,J}(g,f,g,f)+\mathcal{X}^{\beta_1,\beta_2}_{L,S,J}(f,g,f,g)\right], \tag{4.75}$$

$$X^\pm_1(L,S,J) =\mathcal{X}^{\beta_1,\beta_2}_{L,S,J}(g,g,f,f)+\mathcal{X}^{\beta_1,\beta_2}_{L,S,J}(f,f,g,g)\pm\left[\mathcal{X}^{\beta_1,\beta_2}_{L,S,J}(g,f,f,g)+\mathcal{X}^{\beta_1,\beta_2}_{L,S,J}(f,g,g,f)\right], \tag{4.76}$$

$$Y^\pm_1(L,S,J) =\mathcal{X}^{\beta_1,\beta_2}_{L,S,J}(g,g,g,f)-\mathcal{X}^{\beta_1,\beta_2}_{L,S,J}(f,f,f,g)\pm\left[\mathcal{X}^{\beta_1,\beta_2}_{L,S,J}(g,f,g,g)-\mathcal{X}^{\beta_1,\beta_2}_{L,S,J}(f,g,f,f)\right], \tag{4.77}$$

$$Y^\pm_0(L,S,J) =\mathcal{X}^{\beta_1,\beta_2}_{L,S,J}(g,g,f,g)-\mathcal{X}^{\beta_1,\beta_2}_{L,S,J}(f,f,g,f)\pm\left[\mathcal{X}^{\beta_1,\beta_2}_{L,S,J}(f,g,g,g)-\mathcal{X}^{\beta_1,\beta_2}_{L,S,J}(g,f,f,f)\right]. \tag{4.78}$$

We can rewrite this by g_i $(i=1,2,\cdots,6)$ as

$$\begin{aligned}\tilde{\mathcal{M}}_{\rm contact} =&-\frac{4G_F}{\sqrt{2}}\frac{1}{4\pi}\sum_{J,M}(j_{\kappa_1},\nu_1,j_{\kappa_2},\nu_2|J,M)(j_{\kappa_\mu},s_\mu,j_{\kappa_e},s_e|J,M)\sqrt{\left[j_{\kappa_1}\cdot j_{\kappa_\mu}\cdot j_{\kappa_2}\cdot j_{\kappa_e}\right]}\\ &\times\sum_{i=1}^{6}g_iM^{\beta_1,\beta_2}_i(J),\end{aligned} \tag{I.78}$$

where

$$M^{\beta_1,\beta_2}_1(J) =\frac{1}{2}\left[X^-_0(J,0,J)-X^+_1(J,0,J)+i\left\{Y^+_1(J,0,J)+Y^+_0(J,0,J)\right\}\right], \tag{4.69}$$

$$M^{\beta_1,\beta_2}_2(J) =\frac{1}{2}\left[X^-_0(J,0,J)-X^+_1(J,0,J)-i\left\{Y^+_1(J,0,J)+Y^+_0(J,0,J)\right\}\right], \tag{4.70}$$

$$M^{\beta_1,\beta_2}_3(J) =2\left[X^-_0(J,0,J)+X^+_1(J,0,J)+i\left\{Y^+_1(J,0,J)-Y^+_0(J,0,J)\right\}\right], \tag{4.71}$$

$$M^{\beta_1,\beta_2}_4(J) =2\left[X^-_0(J,0,J)+X^+_1(J,0,J)-i\left\{Y^+_1(J,0,J)-Y^+_0(J,0,J)\right\}\right], \tag{4.72}$$

$$M^{\beta_1,\beta_2}_5(J) =\left[3\sum_{L=|J-1|}^{J+1}X^-_1(L,1,J)-X^+_0(J,0,J)+i\left\{3\sum_{L=|J-1|}^{J+1}Y^-_0(L,1,J)+Y^-_1(J,0,J)\right\}\right], \tag{4.73}$$

$$M^{\beta_1,\beta_2}_6(J) =\left[3\sum_{L=|J-1|}^{J+1}X^-_1(L,1,J)-X^+_0(J,0,J)-i\left\{3\sum_{L=|J-1|}^{J+1}Y^-_0(L,1,J)+Y^-_1(J,0,J)\right\}\right]. \tag{4.74}$$

Compared to Eq. (4.63), we conclude that

$$\mathcal{N}^{\beta_1,\beta_2}_{\rm contact}(J)=\sum_{i=1}^{6}g_iM^{\beta_1,\beta_2}_i(J). \tag{4.68}$$

I.3 Derivation for Eq. (4.88)

Here let us calculate $\tilde{\mathcal{M}}_{\text{photonic}}$. As contact interaction, it is convenient to use the Dirac basis. Therefore let us rewrite Eq. (4.62) as

$$\begin{aligned}\tilde{\mathcal{M}}_{\text{photonic}} =& \left(-\frac{4G_F}{\sqrt{2}}m_\mu\right)(-q_e)\left[\int d^3r_1 d^3r_2 \overline{\psi}_{p_1}^{\kappa_1,\nu_1}(\boldsymbol{r}_1)\sigma^{\mu\nu}\left(A_+ + A_-\gamma_5\right)\psi_\mu^{1S_{1/2},s_\mu}(\boldsymbol{r}_1)\right.\\ &\left.\times 2G_\nu\left(\boldsymbol{r}_1,\boldsymbol{r}_2;m_\mu - B_\mu - E_1\right)\overline{\psi}_{p_2}^{\kappa_2,\nu_2}(\boldsymbol{r}_2)\gamma_\mu\psi_e^{\alpha_e,s_e}(\boldsymbol{r}_2) - (\{\beta_1,\nu_1\}\leftrightarrow\{\beta_2,\nu_2\})\right],\end{aligned} \tag{I.79}$$

where the couplings $A_\pm$ are related to $A_{L/R}$ as

$$A_+ = \frac{A_R + A_L}{2}, \tag{I.80}$$

$$A_- = \frac{A_R - A_L}{2}. \tag{I.81}$$

By inserting the partial wave expansion form of $G_\nu\left(\boldsymbol{r}_1,\boldsymbol{r}_2;q_0\right)$, Eq. (4.86), $\tilde{\mathcal{M}}_{\text{photonic}}$ becomes

$$\begin{aligned}\tilde{\mathcal{M}}_{\text{photonic}} =& 2i\frac{4G_F}{\sqrt{2}}m_\mu q_e\left[q_0\int d^3r_1 d^3r_2\overline{\psi}_{p_1}^{\kappa_1,\nu_1}(\boldsymbol{r}_1)\sigma^{\mu\nu}\left(A_+ + A_-\gamma_5\right)\psi_\mu^{1S_{1/2},s_\mu}(\boldsymbol{r}_1)\right.\\ &\left.\times\sum_{l,m}\partial_\nu\left\{Y_l^{m*}\left(\hat{r}_1\right)Y_l^m\left(\hat{r}_2\right)F_{l,l}^{q_0}(r_1,r_2)\right\}\overline{\psi}_{p_2}^{\kappa_2,\nu_2}(\boldsymbol{r}_2)\gamma_\mu\psi_e^{\alpha_e,s_e}(\boldsymbol{r}_2) - (\{\beta_1,\nu_1\}\leftrightarrow\{\beta_2,\nu_2\})\right],\end{aligned} \tag{I.82}$$

where $q_0 = m_\mu - B_\mu - E_1$ in the first term, while $q_0 = m_\mu - B_\mu - E_2$ in the exchange term, again. For convenience, we define a non-local operator

$$\begin{aligned}\mathcal{O}_{ph}^{q_0}\left(\boldsymbol{r}_1,\boldsymbol{r}_2\right) =& q_0\sum_{l,m}\partial_\nu\left\{Y_l^{m*}\left(\hat{r}_1\right)Y_l^m\left(\hat{r}_2\right)F_{l,l}^{q_0}(r_1,r_2)\right\}\left[\sigma^{\mu\nu}\left(A_+ + A_-\gamma_5\right)\right]\otimes\left[\gamma_\mu\right]\\ =& q_0\sum_{l,m}\partial_\nu\left\{Y_l^{m*}\left(\hat{r}_1\right)Y_l^m\left(\hat{r}_2\right)F_{l,l}^{q_0}(r_1,r_2)\right\}\left[\sigma^{\mu\nu}\begin{pmatrix}A_+ & A_-\\ A_- & A_+\end{pmatrix}\right]\otimes\left[\gamma_\mu\right],\end{aligned} \tag{I.83}$$

and write $\tilde{\mathcal{M}}_{\text{photonic}}$ as

$$\begin{aligned}\tilde{\mathcal{M}}_{\text{photonic}} =& 2i\frac{4G_F}{\sqrt{2}}m_\mu q_e\left[\int d^3r_1 d^3r_2\left\{\overline{\psi}_{p_1}^{\kappa_1,\nu_1}(\boldsymbol{r}_1)\otimes\overline{\psi}_{p_2}^{\kappa_2,\nu_2}(\boldsymbol{r}_2)\right\}\right.\\ &\left.\times\mathcal{O}_{ph}^{q_0}\left(\boldsymbol{r}_1,\boldsymbol{r}_2\right)\left\{\psi_\mu^{1S_{1/2},s_\mu}(\boldsymbol{r}_1)\otimes\psi_e^{\alpha_e,s_e}(\boldsymbol{r}_2)\right\} - (\{\beta_1,\nu_1\}\leftrightarrow\{\beta_2,\nu_2\})\right].\end{aligned} \tag{I.84}$$

In the definition of $\mathcal{O}_{ph}^{q_0}\left(\boldsymbol{r}_1,\boldsymbol{r}_2\right)$, Eq. (I.83), the brackets are written to emphasize difference of operating spaces.

Let us focus on the operator $\mathcal{O}_{ph}^{q_0}\left(\boldsymbol{r}_1,\boldsymbol{r}_2\right)$. Since σ^{i0} is

$$\sigma^{i0} = \frac{i}{2}\left[\gamma^i,\gamma^0\right] = i\begin{pmatrix}0 & \sigma^i\\ -\sigma^i & 0\end{pmatrix}\begin{pmatrix}1 & 0\\ 0 & -1\end{pmatrix} = -i\sigma^i\begin{pmatrix}0 & 1\\ 1 & 0\end{pmatrix}, \tag{I.85}$$

the part of $\nu = 0$ is

$$\begin{aligned}\left[\partial_0\sigma^{i0}\begin{pmatrix}A_+ & A_-\\ A_- & A_+\end{pmatrix}\right]\otimes\left[\gamma_i\right] =& \left[q_0\sigma^i\begin{pmatrix}A_- & A_+\\ A_+ & A_-\end{pmatrix}\right]\otimes\left[\sigma^i\begin{pmatrix}0 & -1\\ 1 & 0\end{pmatrix}\right]\\ =& q_0\boldsymbol{\sigma}(1)\cdot\boldsymbol{\sigma}(2)\left[\begin{pmatrix}A_- & A_+\\ A_+ & A_-\end{pmatrix}\right]\otimes\left[\begin{pmatrix}0 & -1\\ 1 & 0\end{pmatrix}\right].\end{aligned} \tag{I.86}$$

Similarly, the part of $\mu = 0$ is

$$\left[\partial_j \sigma^{0j} \begin{pmatrix} A_+ & A_- \\ A_- & A_+ \end{pmatrix}\right] \otimes [\gamma_0] = i\nabla \cdot \boldsymbol{\sigma}(1) \left[\begin{pmatrix} A_- & A_+ \\ A_+ & A_- \end{pmatrix}\right] \otimes \left[\begin{pmatrix} 1 & 0 \\ 0 & -1 \end{pmatrix}\right]. \tag{I.87}$$

Lastly, the remaining part for σ_{ij} is

$$\begin{aligned}\left[\partial_j \sigma^{ij} \begin{pmatrix} A_+ & A_- \\ A_- & A_+ \end{pmatrix}\right] \otimes [\gamma_i] =& \left[\partial_j \epsilon^{ijk} \sigma^k \begin{pmatrix} A_+ & A_- \\ A_- & A_+ \end{pmatrix}\right] \otimes \left[\sigma^i \begin{pmatrix} 0 & -1 \\ 1 & 0 \end{pmatrix}\right] \\ =& \nabla \cdot (\boldsymbol{\sigma}(1) \times \boldsymbol{\sigma}(2)) \left[\begin{pmatrix} A_+ & A_- \\ A_- & A_+ \end{pmatrix}\right] \otimes \left[\begin{pmatrix} 0 & -1 \\ 1 & 0 \end{pmatrix}\right],\end{aligned} \tag{I.88}$$

where we used

$$\begin{aligned}\sigma^{ij} =& \frac{i}{2} \left[\gamma^i, \gamma^j\right] \\ =& \frac{i}{2} \begin{pmatrix} -\left[\sigma^i, \sigma^j\right] & 0 \\ 0 & -\left[\sigma^i, \sigma^j\right] \end{pmatrix} \\ =& \epsilon^{ijk} \begin{pmatrix} \sigma^k & 0 \\ 0 & \sigma^k \end{pmatrix}.\end{aligned} \tag{I.89}$$

Collecting Eqs. (I.86), (I.87), and (I.88), we get

$$\begin{aligned}\left[\partial_\nu \sigma^{\mu\nu} \left(A_+ + A_- \gamma_5\right)\right] \otimes [\gamma_\mu] =& q_0 \boldsymbol{\sigma}(1) \cdot \boldsymbol{\sigma}(2) \left[\begin{pmatrix} A_- & A_+ \\ A_+ & A_- \end{pmatrix}\right] \otimes \left[\begin{pmatrix} 0 & -1 \\ 1 & 0 \end{pmatrix}\right] \\ &+ i\nabla \cdot \boldsymbol{\sigma}(1) \left[\begin{pmatrix} A_- & A_+ \\ A_+ & A_- \end{pmatrix}\right] \otimes \left[\begin{pmatrix} 1 & 0 \\ 0 & -1 \end{pmatrix}\right] \\ &+ \nabla \cdot (\boldsymbol{\sigma}(1) \times \boldsymbol{\sigma}(2)) \left[\begin{pmatrix} A_+ & A_- \\ A_- & A_+ \end{pmatrix}\right] \otimes \left[\begin{pmatrix} 0 & -1 \\ 1 & 0 \end{pmatrix}\right],\end{aligned} \tag{I.90}$$

so the operator $\mathcal{O}_{ph}^{q_0}(\boldsymbol{p}_1, \boldsymbol{p}_2)$ is divided into three parts:

$$\mathcal{O}_{ph}^{q_0}(\boldsymbol{r}_1, \boldsymbol{r}_2) = \sum_{i=1}^{3} \mathcal{O}_{ph;i}(\boldsymbol{r}_1, \boldsymbol{r}_2), \tag{I.91}$$

where

$$\mathcal{O}_{ph;1}^{q_0}(\boldsymbol{r}_1, \boldsymbol{r}_2) = q_0^2 \sum_{l,m} Y_l^m(\hat{r}_1) F_{l,l}^{q_0}(r_1, r_2) Y_l^{m*}(\hat{r}_2) \boldsymbol{\sigma}(1) \cdot \boldsymbol{\sigma}(2) \left[\begin{pmatrix} A_- & A_+ \\ A_+ & A_- \end{pmatrix}\right] \otimes \left[\begin{pmatrix} 0 & -1 \\ 1 & 0 \end{pmatrix}\right] \tag{I.92}$$

$$\mathcal{O}_{ph;2}^{q_0}(\boldsymbol{r}_1, \boldsymbol{r}_2) = iq_0 \sum_{l,m} \left(\nabla Y_l^m(\hat{r}_1) F_{l,l}^{q_0}(r_1, r_2)\right) \cdot \boldsymbol{\sigma}(1) Y_l^{m*}(\hat{r}_2) \left[\begin{pmatrix} A_- & A_+ \\ A_+ & A_- \end{pmatrix}\right] \otimes \left[\begin{pmatrix} 1 & 0 \\ 0 & -1 \end{pmatrix}\right] \tag{I.93}$$

$$\begin{aligned}\mathcal{O}_{ph;3}^{q_0}(\boldsymbol{r}_1, \boldsymbol{r}_2) =& q_0 \sum_{l,m} \left(\nabla Y_l^m(\hat{r}_1) F_{l,l}^{q_0}(r_1, r_2)\right) \cdot (\boldsymbol{\sigma}(1) \times \boldsymbol{\sigma}(2)) Y_l^{m*}(\hat{r}_2) \\ &\times \left[\begin{pmatrix} A_+ & A_- \\ A_- & A_+ \end{pmatrix}\right] \otimes \left[\begin{pmatrix} 0 & -1 \\ 1 & 0 \end{pmatrix}\right].\end{aligned} \tag{I.94}$$

First, let us focus on $\mathcal{O}_{ph;1}$. We can rewrite inner products as

$$\begin{aligned}&\sum_{l,m} Y_l^m(\hat{r}_1) F_{l,l}^{q_0}(r_1, r_2) Y_l^{m*}(\hat{r}_2) \boldsymbol{\sigma}(1) \cdot \boldsymbol{\sigma}(2) \\ =& \sum_l F_{l,l}^{q_0}(r_1, r_2) (-1)^{l+1} \sqrt{3(2l+1)} \left[\left[Y_l(\hat{r}_1) \otimes Y_l(\hat{r}_2)\right]_0 \otimes \left[\sigma(1) \otimes \sigma(2)\right]_0\right]_0^0.\end{aligned} \tag{I.95}$$

Using the $9j$ symbol to recombine angular momenta, it yields

$$\begin{aligned}
&\left[\left[Y_l(\hat{r}_1)\otimes Y_l(\hat{r}_2)\right]_0\otimes\left[\sigma(1)\otimes\sigma(2)\right]_0\right]_0^0\\
=&\sum_{j_1,j_2}\sqrt{(2j_1+1)(2j_2+1)}\begin{Bmatrix} l & l & 0\\ 1 & 1 & 0\\ j_1 & j_2 & 0\end{Bmatrix}\left[\left[Y_l(\hat{r}_1)\otimes\sigma(1)\right]_{j_1}\otimes\left[Y_l(\hat{r}_2)\otimes\sigma(2)\right]_{j_2}\right]_0^0\\
=&\sum_{j=|l-1|}^{l+1}\sqrt{\frac{2j+1}{3(2l+1)}}\left[\left[Y_l(\hat{r}_1)\otimes\sigma(1)\right]_j\otimes\left[Y_l(\hat{r}_2)\otimes\sigma(2)\right]_j\right]_0^0\\
=&\sum_{j=|l-1|}^{l+1}\frac{(-1)^j}{\sqrt{3(2l+1)}}\boldsymbol{T}_{l,1,j}(1)\cdot\boldsymbol{T}_{l,1,j}(2).
\end{aligned}\tag{I.96}$$

Here, we have defined a tensor with rank j,

$$T^m_{l,1,j}(n)=\left[Y_l(\hat{r}_n)\otimes\sigma(n)\right]^m_j,\tag{I.97}$$

where $n=1,2$. Therefore, it is given as

$$\begin{aligned}
&\sum_{l,m}Y_l^m(\hat{r}_1)F^{q_0}_{l,l}(r_1,r_2)Y_l^{m*}(\hat{r}_2)\boldsymbol{\sigma}(1)\cdot\boldsymbol{\sigma}(2)\\
=&\sum_l\sum_{j=|l-1|}^{l+1}(-1)^{l+1+j}F^{q_0}_{l,l}(r_1,r_2)\boldsymbol{T}_{l,1,j}(1)\cdot\boldsymbol{T}_{l,1,j}(2),
\end{aligned}\tag{I.98}$$

and we obtain

$$\begin{aligned}
\mathcal{O}^{q_0}_{ph;1}(\boldsymbol{r}_1,\boldsymbol{r}_2)=&q_0^2\sum_l\sum_{j=|l-1|}^{l+1}(-1)^{l+1+j}F^{q_0}_{l,l}(r_1,r_2)\boldsymbol{T}_{l,1,j}(1)\cdot\boldsymbol{T}_{l,1,j}(2)\\
&\times\left[\begin{pmatrix}A_- & A_+\\ A_+ & A_-\end{pmatrix}\right]\otimes\left[\begin{pmatrix}0 & -1\\ 1 & 0\end{pmatrix}\right].
\end{aligned}\tag{I.99}$$

Next, for $\mathcal{O}_{ph;2}$, let us concentrate on

$$\begin{aligned}
&\sum_{l,m}\left(\nabla Y_l^m(\hat{r}_1)F^{q_0}_{l,l}(r_1,r_2)\right)\cdot\boldsymbol{\sigma}(1)Y_l^{m*}(\hat{r}_2)\\
=&\sum_{l,m}\sum_{s=\pm1,0}(-1)^s\left(\nabla^s Y_l^m(\hat{r}_1)F^{q_0}_{l,l}(r_1,r_2)\right)\sigma^{-s}(1)Y_l^{m*}(\hat{r}_2).
\end{aligned}\tag{I.100}$$

According to the gradient formula (G.67), we get

$$\begin{aligned}
&\nabla^s Y_l^m(\hat{r}_1)F^{q_0}_{l,l}(r_1,r_2)\\
=&(-1)^s\sqrt{\frac{l+1}{2l+1}}(l+1,m+s,1,-s|l,m)Y_{l+1}^{m+s}(\hat{r}_1)\left(\frac{l}{r_1}-\frac{d}{dr_1}\right)F^{q_0}_{l,l}(r_1,r_2)\\
&+(-1)^s\sqrt{\frac{l}{2l+1}}(l-1,m+s,1,-s|l,m)Y_{l-1}^{m+s}(\hat{r}_1)\left(\frac{d}{dr_1}+\frac{l+1}{r_1}\right)F^{q_0}_{l,l}(r_1,r_2).
\end{aligned}\tag{I.101}$$

Here,

$$\begin{aligned}\frac{d}{dr_1}F^{q_0}_{l,l}(r_1,r_2) =&\frac{d}{dr_1}\left\{h^{(1)}_l(q_0r_1)j_l(q_0r_2)\theta(r_1-r_2)+h^{(1)}_l(q_0r_2)j_l(|q_0|r_1)\theta(r_2-r_1)\right\}\\ =&\left\{\frac{d}{dr_1}h^{(1)}_l(q_0r_1)\right\}j_l(q_0r_2)\theta(r_1-r_2)+h^{(1)}_l(q_0r_1)j_l(q_0r_2)\delta(r_1-r_2)\\ &+h^{(1)}_l(q_0r_2)\left\{\frac{d}{dr_1}j_l(q_0r_1)\right\}\theta(r_2-r_1)-h^{(1)}_l(q_0r_2)j_l(q_0r_1)\delta(r_1-r_2)\\ =&\left\{\frac{d}{dr_1}h^{(1)}_l(q_0r_1)\right\}j_l(q_0r_2)\theta(r_1-r_2)+h^{(1)}_l(q_0r_2)\left\{\frac{d}{dr_1}j_l(q_0r_1)\right\}\theta(r_2-r_1).\end{aligned}\tag{I.102}$$

Using the derivative formula of spherical Bessel or Hankel function, Eq. (B.12), it yields

$$\begin{aligned}\frac{d}{dr_1}F^{q_0}_{l,l}(r_1,r_2) =&q_0\left(\frac{l}{q_0r_1}h^{(1)}_l(q_0r_1)-h^{(1)}_{l+1}(q_0r_1)\right)j_l(q_0r_2)\theta(r_1-r_2)\\ &+q_0h^{(1)}_l(q_0r_2)\left(\frac{l}{q_0r_1}j_l(q_0r_1)-j_{l+1}(q_0r_1)\right)\theta(r_2-r_1)\\ =&\frac{l}{r_1}F^{q_0}_{l,l}(r_1,r_2)-q_0F^{q_0}_{l+1,l}(r_1,r_2),\end{aligned}\tag{I.103}$$

or

$$\begin{aligned}\frac{d}{dr_1}F^{q_0}_{l,l}(r_1,r_2) =&q_0\left(h^{(1)}_{l-1}(q_0r_1)-\frac{l+1}{q_0r_1}h^{(1)}_l(q_0r_1)\right)j_l(q_0r_2)\theta(r_1-r_2)\\ &+q_0h^{(1)}_l(q_0r_2)\left(j_{l-1}(q_0r_1)-\frac{l+1}{q_0r_1}j_l(q_0r_1)\right)\theta(r_2-r_1)\\ =&q_0F^{q_0}_{l-1,l}(r_1,r_2)-\frac{l+1}{r_1}F^{q_0}_{l,l}(r_1,r_2).\end{aligned}\tag{I.104}$$

Therefore,

$$\begin{aligned}\nabla^sY^m_l(\hat{r}_1)F^{q_0}_{l,l}(r_1,r_2) =&q_0(-1)^s\sqrt{\frac{l+1}{2l+1}}(l+1,m+s,1,-s|l,m)Y^{m+s}_{l+1}(\hat{r}_1)F^{q_0}_{l+1,l}(r_1,r_2)\\ &+q_0(-1)^s\sqrt{\frac{l}{2l+1}}(l-1,m+s,1,-s|l,m)Y^{m+s}_{l-1}(\hat{r}_1)F^{q_0}_{l-1,l}(r_1,r_2)\\ =&q_0(-1)^s\sum_{h=\pm1}f^{(2)}_l(h)(l+h,m+s,1,-s|l,m)Y^{m+s}_{l+h}(\hat{r}_1)F^{q_0}_{l+h,l}(r_1,r_2),\end{aligned}\tag{I.105}$$

where we defined

$$f^{(2)}_l(h)=\begin{cases}\sqrt{\dfrac{l+1}{2l+1}} & (h=+1)\\ \sqrt{\dfrac{l}{2l+1}} & (h=-1)\end{cases}.\tag{I.106}$$

Multiplying Eq. (I.105) by $(-1)^s\sigma^{-s}(1)$ and summing over s, we get

$$\begin{aligned}&\sum_s(-1)^s\nabla^sY^m_l(\hat{r}_1)F^{q_0}_{l,l}(r_1,r_2)\sigma^{-s}(1)\\ =&q_0\sum_{h=\pm1}f^{(2)}_l(h)\sum_s(l+h,m+s,1,-s|l,m)Y^{m+s}_{l+h}(\hat{r}_1)\sigma^{-s}(1)F^{q_0}_{l+h,l}(r_1,r_2)\\ =&q_0\sum_{h=\pm1}f^{(2)}_l(h)T^m_{l+h,1,l}(1)F^{q_0}_{l+h,l}(r_1,r_2).\end{aligned}\tag{I.107}$$

This yields

$$\begin{aligned}
&\sum_{l,m}\left(\nabla Y_l^m(\hat{r}_1)F_{l,l}^{q_0}(r_1,r_2)\right)\cdot\boldsymbol{\sigma}(1)Y_l^{m*}(\hat{r}_2)\\
=&\sum_{l,m}q_0\sum_{h=\pm1}f_l^{(2)}(h)T_{l+h,1,l}^{m}(1)F_{l+h,l}^{q_0}(r_1,r_2)(-1)^m T_{l,0,l}^{-m}(2)\\
=&q_0\sum_{l}\sum_{h=\pm1}f_l^{(2)}(h)F_{l+h,l}^{q_0}(r_1,r_2)\boldsymbol{T}_{l+h,1,l}(1)\cdot\boldsymbol{T}_{l,0,l}(2)\\
=&q_0\sum_{l}\sum_{j=l\pm1\geq0}f_l^{(2)}(j-l)F_{j,l}^{q_0}(r_1,r_2)\boldsymbol{T}_{j,1,l}(1)\cdot\boldsymbol{T}_{l,0,l}(2)\\
=&q_0\sum_{l}\sum_{j=l\pm1\geq0}f_j^{(2)}(l-j)F_{l,j}^{q_0}(r_1,r_2)\boldsymbol{T}_{l,1,j}(1)\cdot\boldsymbol{T}_{j,0,j}(2),
\end{aligned}\tag{I.108}$$

where

$$T_{l,0,l}^{m}(n)=\left[Y_l(\hat{x}_n)\otimes\hat{1}(n)\right]_l^m.\tag{I.109}$$

The last equal holds because the exchange of indices, $l\leftrightarrow j=l+h$, does not change the sum over l and j. Therefore we obtain

$$\begin{aligned}
\mathcal{O}_{ph;2}^{q_0}(\boldsymbol{r}_1,\boldsymbol{r}_2)=&iq_0^2\sum_{l}\sum_{j=l\pm1\geq0}f_j(l-j)F_{l,j}^{q_0}(r_1,r_2)\boldsymbol{T}_{l,1,j}(1)\cdot\boldsymbol{T}_{j,0,j}(2)\\
&\times\left[\begin{pmatrix}A_- & A_+\\ A_+ & A_-\end{pmatrix}\right]\otimes\left[\begin{pmatrix}1 & 0\\ 0 & -1\end{pmatrix}\right].
\end{aligned}\tag{I.110}$$

Lastly, let us consider the third one, $\mathcal{O}_{ph;3}$. Similarly as $\mathcal{O}_{ph;2}$, using the gradient formula, Eq. (G.67), we obtain

$$\begin{aligned}
&\sum_{l,m}\left(\nabla Y_l^m(\hat{r}_1)F_{l,l}^{q_0}(r_1,r_2)\right)\cdot\left(\boldsymbol{\sigma}(1)\times\boldsymbol{\sigma}(2)\right)Y_l^{m*}(\hat{r}_2)\\
=&-i\sqrt{2}\sum_{l,m}\sum_{s=\pm1,0}(-1)^s\left(\nabla^s Y_l^m(\hat{r}_1)F_{l,l}^{q_0}(r_1,r_2)\right)\left[\sigma(1)\otimes\sigma(2)\right]_1^{-s}Y_l^{m*}(\hat{r}_2)\\
=&-i\sqrt{2}q_0\sum_{l,m}\sum_{h=\pm1}f_l^{(2)}(h)\\
&\times\sum_{s=\pm1,0}(l+h,m+s,1,-s|l,m)Y_{l+h}^{m+s}(\hat{r}_1)F_{l+h,l}^{q_0}(r_1,r_2)\left[\sigma(1)\otimes\sigma(2)\right]_1^{-s}Y_l^{m*}(\hat{r}_2)\\
=&-i\sqrt{2}q_0\sum_{l,m}\sum_{h=\pm1}f_l^{(2)}(h)F_{l+h,l}^{q_0}(r_1,r_2)\\
&\times\sum_{s=\pm1,0}(-1)^{l+1+s}\sqrt{\frac{2l+1}{3}}(l+h,m+s,l,-m|1,s)Y_{l+h}^{m+s}(\hat{r}_1)\left[\sigma(1)\otimes\sigma(2)\right]_1^{-s}Y_l^{-m}(\hat{r}_2)\\
=&-i\sqrt{2}q_0\sum_{l}\sum_{h=\pm1}f_l^{(2)}(h)F_{l+h,l}^{q_0}(r_1,r_2)\\
&\times\sum_{s=\pm1,0}(-1)^{l+1+s}\sqrt{\frac{2l+1}{3}}\left[Y_{l+h}(\hat{r}_1)\otimes Y_l(\hat{r}_2)\right]_1^s\left[\sigma(1)\otimes\sigma(2)\right]_1^{-s}\\
=&i\sqrt{2}q_0\sum_{l}\sum_{h=\pm1}f_l^{(2)}(h)F_{l+h,l}^{q_0}(r_1,r_2)(-1)^{l+1}\sqrt{2l+1}\left[\left[Y_{l+h}(\hat{r}_1)\otimes Y_l(\hat{r}_2)\right]_1\otimes\left[\sigma(1)\otimes\sigma(2)\right]_1\right]_0^0.
\end{aligned}\tag{I.111}$$

Moreover recombining the angular momenta,

$$
\begin{aligned}
&[[Y_{l+h}(\hat{r}_1)\otimes Y_l(\hat{r}_2)]_1\otimes[\sigma(1)\otimes\sigma(2)]_1]_0^0\\
=&\sum_{j_1,j_2} 3\sqrt{(2j_1+1)(2j_2+1)}\begin{Bmatrix} l+h & l & 1\\ 1 & 1 & 1\\ j_1 & j_2 & 0\end{Bmatrix}[T_{l+h,1,j_1}(1)\otimes T_{l,1,j_2}(2)]_0^0\\
=&\sum_j(-1)^{j+l}\sqrt{3(2j+1)}\begin{Bmatrix} l+h & l & 1\\ 1 & 1 & j\end{Bmatrix}[T_{l+h,1,j}(1)\otimes T_{l,1,j}(2)]_0^0\\
=&(-1)^l\sqrt{3}\sum_j\begin{Bmatrix} l+h & l & 1\\ 1 & 1 & j\end{Bmatrix}\boldsymbol{T}_{l+h,1,j}(1)\cdot\boldsymbol{T}_{l,1,j}(2)\\
=&(-1)^l\sqrt{3}\left(\begin{Bmatrix} l+h & l & 1\\ 1 & 1 & l\end{Bmatrix}\boldsymbol{T}_{l+h,1,l}(1)\cdot\boldsymbol{T}_{l,1,l}(2)\right.\\
&\qquad\left.+\begin{Bmatrix} l+h & l & 1\\ 1 & 1 & l+h\end{Bmatrix}\boldsymbol{T}_{l+h,1,l+h}(1)\cdot\boldsymbol{T}_{l,1,l+h}(2)\right).
\end{aligned}
\tag{I.112}
$$

According to symmetry of the $6j$ symbol and Eq. (G.44), we can write

$$
\begin{aligned}
\begin{Bmatrix} l+h & l & 1\\ 1 & 1 & l\end{Bmatrix}=&\begin{Bmatrix} l & l & 1\\ 1 & 1 & l+h\end{Bmatrix}\\
=&\frac{(l+h)(l+h+1)-l(l+1)-2}{2\sqrt{6l(l+1)(2l+1)}}\\
=&\begin{cases}\sqrt{\dfrac{l}{6(l+1)(2l+1)}} & (h=+1)\\ -\sqrt{\dfrac{l+1}{6l(2l+1)}} & (h=-1)\end{cases},
\end{aligned}
\tag{I.113}
$$

and

$$
\begin{aligned}
\begin{Bmatrix} l+h & l & 1\\ 1 & 1 & l+h\end{Bmatrix}=&\begin{Bmatrix} l+h & l+h & 1\\ 1 & 1 & l\end{Bmatrix}\\
=&\frac{l(l+1)-(l+h)(l+h+1)-2}{2\sqrt{6(l+h)(l+h+1)(2l+2h+1)}}\\
=&\begin{cases}-\sqrt{\dfrac{l+2}{6(l+1)(2l+3)}} & (h=+1)\\ \sqrt{\dfrac{l-1}{6l(2l-1)}} & (h=-1)\end{cases}.
\end{aligned}
\tag{I.114}
$$

Thus,

$$
\begin{aligned}
&\sum_{l,m}\left(\nabla Y_l^m(\hat{r}_1)F_{l,l}(r_1,r_2)\right)\cdot\left(\boldsymbol{\sigma}(1)\times\boldsymbol{\sigma}(2)\right)Y_l^{m*}(\hat{r}_2)\\
=&i\sqrt{6}q_0\sum_l\sum_{h=\pm1}f_l^{(2)}(h)F_{l+h,l}^{q_0}(r_1,r_2)(-1)^1\sqrt{2l+1}\\
&\times\left(\begin{Bmatrix} l+h & l & 1\\ 1 & 1 & l\end{Bmatrix}\boldsymbol{T}_{l+h,1,l}(1)\cdot\boldsymbol{T}_{l,1,l}(2)+\begin{Bmatrix} l+h & l & 1\\ 1 & 1 & l+h\end{Bmatrix}\boldsymbol{T}_{l+h,1,l+h}(1)\cdot\boldsymbol{T}_{l,1,l+h}(2)\right)\\
=&iq_0\sum_l\sum_{h=\pm1}F_{l+h,l}^{q_0}(r_1,r_2)\left(f_l^{(3)}(h)\boldsymbol{T}_{l+h,1,l}(1)\cdot\boldsymbol{T}_{l,1,l}(2)+\tilde{f}_l^{(3)}(h)\boldsymbol{T}_{l+h,1,l+h}(1)\cdot\boldsymbol{T}_{l,1,l+h}(2)\right).
\end{aligned}
\tag{I.115}
$$

Here the coefficients are defined as

$$f_l^{(3)}(h) = \begin{cases} -\sqrt{\dfrac{l}{2l+1}} & (h=+1) \\ \sqrt{\dfrac{l+1}{2l+1}} & (h=-1) \end{cases}, \tag{I.116}$$

$$\tilde{f}_l^{(3)}(h) = \begin{cases} \sqrt{\dfrac{l+2}{2l+3}} & (h=+1) \\ -\sqrt{\dfrac{l-1}{2l-1}} & (h=-1) \end{cases}. \tag{I.117}$$

Now noticing that

$$f_l^{(3)}(h) = \tilde{f}_{l+h}^{(3)}(-h), \tag{I.118}$$

it reduces to

$$\begin{aligned} &\sum_{l,m} \left(\nabla Y_l^m(\hat{r}_1) F_{l,l}^{q_0}(r_1,r_2) \right) \cdot (\boldsymbol{\sigma}(1) \times \boldsymbol{\sigma}(2)) \, Y_l^{m*}(\hat{r}_2) \\ =& i q_0 \sum_l \sum_{h=\pm 1} f_l^{(3)}(h) \left(F_{l+h,l}^{q_0}(r_1,r_2) \boldsymbol{T}_{l+h,1,l}(1) \cdot \boldsymbol{T}_{l,1,l}(2) + F_{l,l+h}^{q_0}(r_1,r_2) \boldsymbol{T}_{l,1,l}(1) \cdot \boldsymbol{T}_{l+h,1,l}(2) \right) \\ =& i q_0 \sum_l \sum_{j=l\pm 1 \geq 0} f_j^{(3)}(l-j) \left(F_{l,j}^{q_0}(r_1,r_2) \boldsymbol{T}_{l,1,j}(1) \cdot \boldsymbol{T}_{j,1,j}(2) + F_{j,l}^{q_0}(r_1,r_2) \boldsymbol{T}_{j,1,j}(1) \cdot \boldsymbol{T}_{l,1,j}(2) \right), \end{aligned} \tag{I.119}$$

and we get

$$\begin{aligned} &\mathcal{O}_{ph;3}^{q_0}(\boldsymbol{r}_1, \boldsymbol{r}_2) \\ =& i q_0^2 \sum_l \sum_{j=l\pm 1 \geq 0} f_j^{(3)}(l-j) \left(F_{l,j}^{q_0}(r_1,r_2) \boldsymbol{T}_{l,1,j}(1) \cdot \boldsymbol{T}_{j,1,j}(2) + F_{j,l}^{q_0}(r_1,r_2) \boldsymbol{T}_{j,1,j}(1) \cdot \boldsymbol{T}_{l,1,j}(2) \right) \\ &\times \left[\begin{pmatrix} A_+ & A_- \\ A_- & A_+ \end{pmatrix} \right] \otimes \left[\begin{pmatrix} 0 & -1 \\ 1 & 0 \end{pmatrix} \right]. \end{aligned} \tag{I.120}$$

Now let us estimate the expectation value between initial and final states of the operators, Eqs. (I.99), (I.110), and (I.120). Using the expression of Eqs. (4.58) and (4.59), we obtain these three expectation values:

$$\begin{aligned} &\int d^3 r_1 d^3 r_2 \left\{ \overline{\psi}_{p_1}^{\kappa_1,\nu_1}(\boldsymbol{r}_1) \otimes \overline{\psi}_{p_2}^{\kappa_2,\nu_2}(\boldsymbol{r}_2) \right\} \mathcal{O}_{ph;1}^{q_0}(\boldsymbol{r}_1, \boldsymbol{r}_2) \left\{ \psi_\mu^{1S_{1/2},s_\mu}(\boldsymbol{r}_1) \otimes \psi_e^{\alpha_e,s_e}(\boldsymbol{r}_2) \right\} \\ =& q_0^2 \sum_l \sum_{j=|l-1|}^{l+1} (-1)^{l+1+j} \\ &\times \Big\{ A_+ \Big[I_r^{l,l}(g,f,g,f) I_\Omega^{l,l,1,j}(\kappa_1, -\kappa_\mu, \kappa_2, -\kappa_e) + I_r^{l,l}(f,g,g,f) I_\Omega^{l,l,1,j}(-\kappa_1, \kappa_\mu, \kappa_2, -\kappa_e) \\ &- I_r^{l,l}(g,f,f,g) I_\Omega^{l,l,1,j}(\kappa_1, -\kappa_\mu, -\kappa_2, \kappa_e) - I_r^{l,l}(f,g,f,g) I_\Omega^{l,l,1,j}(-\kappa_1, \kappa_\mu, -\kappa_2, \kappa_e) \Big] \\ &+ i A_- \Big[-I_r^{l,l}(g,g,g,f) I_\Omega^{l,l,1,j}(\kappa_1, \kappa_\mu, \kappa_2, -\kappa_e) + I_r^{l,l}(f,f,g,f) I_\Omega^{l,l,1,j}(-\kappa_1, -\kappa_\mu, \kappa_2, -\kappa_e) \\ &+ I_r^{l,l}(g,g,f,g) I_\Omega^{l,l,1,j}(\kappa_1, \kappa_\mu, -\kappa_2, \kappa_e) - I_r^{l,l}(f,f,f,g) I_\Omega^{l,l,1,j}(-\kappa_1, -\kappa_\mu, -\kappa_2, \kappa_e) \Big] \Big\}, \end{aligned} \tag{I.121}$$

$$
\begin{aligned}
&\int d^3r_1 d^3r_2 \left\{\overline{\psi}_{p_1}^{\kappa_1,\nu_1}(\boldsymbol{r}_1)\otimes\overline{\psi}_{p_2}^{\kappa_2,\nu_2}(\boldsymbol{r}_2)\right\}\mathcal{O}_{ph;2}^{q_0}(\boldsymbol{r}_1,\boldsymbol{r}_2)\left\{\psi_{\mu}^{^1S_{1/2},s_\mu}(\boldsymbol{r}_1)\otimes\psi_e^{\alpha_e,s_e}(\boldsymbol{r}_2)\right\}\\
=&q_0^2\sum_l\sum_{j=l\pm1\geq0}f_j^{(2)}(l-j)\\
&\times\Big\{-A_+\Big[I_r^{l,j}(g,f,g,g)I_\Omega^{l,j,0,j}(\kappa_1,-\kappa_\mu,\kappa_2,\kappa_e)+I_r^{l,j}(f,g,g,g)I_\Omega^{l,j,0,j}(-\kappa_1,\kappa_\mu,\kappa_2,\kappa_e)\\
&+I_r^{l,j}(g,f,f,f)I_\Omega^{l,j,0,j}(\kappa_1,-\kappa_\mu,-\kappa_2,-\kappa_e)+I_r^{l,j}(f,g,f,f)I_\Omega^{l,j,0,j}(-\kappa_1,\kappa_\mu,-\kappa_2,-\kappa_e)\Big]\\
&+iA_-\Big[I_r^{l,j}(g,g,g,g)I_\Omega^{l,j,0,j}(\kappa_1,\kappa_\mu,\kappa_2,\kappa_e)-I_r^{l,j}(f,f,g,g)I_\Omega^{l,j,0,j}(-\kappa_1,-\kappa_\mu,\kappa_2,\kappa_e)\\
&+I_r^{l,l}(g,g,f,f)I_\Omega^{l,j,0,j}(\kappa_1,\kappa_\mu,-\kappa_2,-\kappa_e)-I_r^{l,l}(f,f,f,f)I_\Omega^{l,j,0,j}(-\kappa_1,-\kappa_\mu,-\kappa_2,-\kappa_e)\Big]\Big\},
\end{aligned}
\tag{I.122}
$$

and

$$
\begin{aligned}
&\int d^3r_1 d^3r_2 \left\{\overline{\psi}_{p_1}^{\kappa_1,\nu_1}(\boldsymbol{r}_1)\otimes\overline{\psi}_{p_2}^{\kappa_2,\nu_2}(\boldsymbol{r}_2)\right\}\mathcal{O}_{ph;3}^{q_0}(\boldsymbol{r}_1,\boldsymbol{r}_2)\left\{\psi_{\mu}^{^1S_{1/2},s_\mu}(\boldsymbol{r}_1)\otimes\psi_e^{\alpha_e,s_e}(\boldsymbol{r}_2)\right\}\\
=&q_0^2\sum_l\sum_{j=l\pm1\geq0}f_j^{(3)}(l-j)\sum_{\{l_x,l_y\}=\{l,j\},\{j,l\}}\\
&\times\Big\{A_+\Big[I_r^{l_x,l_y}(g,g,g,f)I_\Omega^{l_x,l_y,1,j}(\kappa_1,\kappa_\mu,\kappa_2,-\kappa_e)-I_r^{l_x,l_y}(f,f,g,f)I_\Omega^{l_x,l_y,1,j}(-\kappa_1,-\kappa_\mu,\kappa_2,-\kappa_e)\\
&-I_r^{l_x,l_y}(g,g,f,g)I_\Omega^{l_x,l_y,1,j}(\kappa_1,\kappa_\mu,-\kappa_2,\kappa_e)+I_r^{l_x,l_y}(f,f,f,g)I_\Omega^{l_x,l_y,1,j}(-\kappa_1,-\kappa_\mu,-\kappa_2,\kappa_e)\Big]\\
&+iA_-\Big[I_r^{l_x,l_y}(g,f,g,f)I_\Omega^{l_x,l_y,1,j}(\kappa_1,-\kappa_\mu,\kappa_2,-\kappa_e)+I_r^{l_x,l_y}(f,g,g,f)I_\Omega^{l_x,l_y,1,j}(-\kappa_1,\kappa_\mu,\kappa_2,-\kappa_e)\\
&-I_r^{l_x,l_y}(g,f,f,g)I_\Omega^{l_x,l_y,1,j}(\kappa_1,-\kappa_\mu,-\kappa_2,\kappa_e)-I_r^{l_x,l_y}(f,g,f,g)I_\Omega^{l_x,l_y,1,j}(-\kappa_1,\kappa_\mu,-\kappa_2,\kappa_e)\Big]\Big\}.
\end{aligned}
\tag{I.123}
$$

Here, the radial and angular integral are defined as

$$
I_r^{l_1,l_2}(a,b,c,d)=\int_0^\infty dr_1 r_1^2 a_{p_1}^{\kappa_1}(r_1)b_{\mu,n_\mu}^{\kappa_\mu}(r_1)\int_0^\infty dr_2 r_2^2 F_{l_1,l_2}^{q_0}(r_1,r_2)c_{p_2}^{\kappa_2}(r_2)d_{e,n_e}^{\kappa_e}(r_2),
\tag{I.124}
$$

and

$$
\begin{aligned}
&I_\Omega^{l_1,l_2,s,j}(\kappa_1,\kappa_\mu,\kappa_2,\kappa_e)\\
=&\int d\Omega_1 d\Omega_2\left[\chi_{\kappa_1}^{\nu_1}(\hat{r}_1)\otimes\chi_{\kappa_2}^{\nu_2}(\hat{r}_2)\right]^\dagger\boldsymbol{T}_{l_1,1,j}(1)\cdot\boldsymbol{T}_{l_2,s,j}(2)\left[\chi_{\kappa_\mu}^{s_\mu}(\hat{r}_1)\otimes\chi_{\kappa_e}^{s_e}(\hat{r}_2)\right],
\end{aligned}
\tag{I.125}
$$

respectively. The angular integral is performed to be

$$
\begin{aligned}
&I_{\Omega}^{l_1,l_2,s,j}(\kappa_1,\kappa_\mu,\kappa_2,\kappa_e)\\
=&\sum_{J_f,M_f}\sum_{J_i,M_i}\left(j_{\kappa_1},\nu_1,j_{\kappa_2},\nu_2|J_f,M_f\right)\left(j_{\kappa_\mu},s_\mu,j_{\kappa_e},s_e|J_i,M_i\right)\\
&\times\int d\Omega_1 d\Omega_2\left[\chi_{\kappa_1}(\hat{r}_1)\otimes\chi_{\kappa_2}(\hat{r}_2)\right]_{J_f}^{M_f\dagger}\boldsymbol{T}_{l_1,1,j}(1)\cdot\boldsymbol{T}_{l_2,s,j}(2)\left[\chi_{\kappa_\mu}(\hat{r}_1)\otimes\chi_{\kappa_e}(\hat{r}_2)\right]_{J_i}^{M_i}\\
=&\sum_{J_f,M_f}\sum_{J_i,M_i}\left(j_{\kappa_1},\nu_1,j_{\kappa_2},\nu_2|J_f,M_f\right)\left(j_{\kappa_\mu},s_\mu,j_{\kappa_e},s_e|J_i,M_i\right)\\
&\times\langle\kappa_1,\kappa_2;J_f,M_f|\boldsymbol{T}_{l_1,1,j}(1)\cdot\boldsymbol{T}_{l_2,s,j}(2)|\kappa_\mu,\kappa_e;J_i,M_i\rangle\\
=&\sum_{J_f,M_f}\sum_{J_i,M_i}\left(j_{\kappa_1},\nu_1,j_{\kappa_2},\nu_2|J_f,M_f\right)\left(j_{\kappa_\mu},s_\mu,j_{\kappa_e},s_e|J_i,M_i\right)\\
&\times\frac{\delta_{J_f,J_i}\delta_{M_f,M_i}}{\sqrt{2J_f+1}}\langle\kappa_1,\kappa_2;J_f||\boldsymbol{T}_{l_1,1,j}(1)\cdot\boldsymbol{T}_{l_2,s,j}(2)||\kappa_\mu,\kappa_e;J_i\rangle\\
=&\sum_{J,M}\left(j_{\kappa_1},\nu_1,j_{\kappa_2},\nu_2|J,M\right)\left(j_{\kappa_\mu},s_\mu,j_{\kappa_e},s_e|J,M\right)\\
&\times(-1)^{j_{\kappa_2}+j_{\kappa_\mu}+J}\begin{Bmatrix}j_{\kappa_1}&j_{\kappa_2}&J\\j_{\kappa_e}&j_{\kappa_\mu}&j\end{Bmatrix}\langle\kappa_1||\boldsymbol{T}_{l_1,1,j}(1)||\kappa_\mu\rangle\langle\kappa_2||\boldsymbol{T}_{l_2,s,j}(2)||\kappa_e\rangle\,.
\end{aligned}
\tag{I.126}
$$

The reduced matrix elements which appear here are calculable by the formula

$$
\begin{aligned}
\langle\kappa_b||\boldsymbol{T}_{l,s,j}||\kappa_a\rangle=&\sqrt{\frac{(2j_{\kappa_b}+1)(2j_{\kappa_a}+1)}{4\pi}}(-1)^{l+1+\kappa_b}\\
&\times\left(j_{\kappa_b},1/2,j_{\kappa_a},-1/2|j,0\right)V_{l,s,j}^{\kappa_b,\kappa_a}\frac{1+(-1)^{l_{\kappa_b}+l_{\kappa_a}+l}}{2},
\end{aligned}
\tag{I.127}
$$

$$
V_{l,s,j}^{\kappa_b,\kappa_a}=\begin{cases}\delta_{l,j}&(s=0,j=l)\\(j-\kappa_a-\kappa_b)/\sqrt{j(2j+1)}&(s=1,j=l+1)\\(\kappa_a-\kappa_b)/\sqrt{j(j+1)}&(s=1,j=l)\\-(j+1+\kappa_a+\kappa_b)/\sqrt{(j+1)(2j+1)}&(s=1,j=l-1)\end{cases}.
\tag{I.128}
$$

Thus we obtain

$$
\begin{aligned}
&I_{\Omega}^{l_1,l_2,s,j}(\kappa_1,\kappa_\mu,\kappa_2,\kappa_e)\\
=&\frac{1}{4\pi}\sum_{J,M}\left(j_{\kappa_1},\mu_1,j_{\kappa_2},\mu_2|J,M\right)\left(j_{\kappa_\mu},s_\mu,j_{\kappa_e},s_e|J,M\right)\sqrt{\left[j_{\kappa_1}\cdot j_{\kappa_\mu}\cdot j_{\kappa_2}\cdot j_{\kappa_e}\right]}\\
&\times(-1)^{j_{\kappa_2}+j_{\kappa_\mu}+J+l_1+l_2+\kappa_1+\kappa_2}\begin{Bmatrix}j_{\kappa_1}&j_{\kappa_2}&J\\j_{\kappa_e}&j_{\kappa_\mu}&j\end{Bmatrix}\frac{1+(-1)^{l_{\kappa_1}+l_{\kappa_\mu}+l_1}}{2}\frac{1+(-1)^{l_{\kappa_2}+l_{\kappa_e}+l_2}}{2}\\
&\times\left(j_{\kappa_1},1/2,j_{\kappa_\mu},-1/2|j,0\right)\left(j_{\kappa_2},1/2,j_{\kappa_e},-1/2|j,0\right)V_{l_1,1,j}^{\kappa_1,\kappa_\mu}V_{l_2,s,j}^{\kappa_2,\kappa_e}.
\end{aligned}
\tag{I.129}
$$

In summary of this section, we show the explicit formula for $\tilde{\mathcal{M}}_{\text{photonic}}$,

$$
\begin{aligned}
\tilde{\mathcal{M}}_{\text{photonic}}=&2i\frac{4G_F}{\sqrt{2}}m_\mu q_e\frac{1}{4\pi}\sum_{J,M}\left(j_{\kappa_1},\mu_1,j_{\kappa_2},\mu_2|J,M\right)\left(j_{\kappa_\mu},s_\mu,j_{\kappa_e},s_e|J,M\right)\\
&\times\sqrt{\left[j_{\kappa_1}\cdot j_{\kappa_\mu}\cdot j_{\kappa_2}\cdot j_{\kappa_e}\right]}\sum_{c=\pm}A_c\sum_{l=0}^{\infty}\sum_{j=|l-1|}^{l+1}\sum_{n=1}^{3}X_n^c.
\end{aligned}
\tag{I.130}
$$

Therefore, compared to Eq. (4.63), it is found that

$$\mathcal{N}^{\beta_1,\beta_2}_{\text{photonic}}(J) = -2im_\mu q_e \sum_{c=\pm} A_c \sum_{l=0}^{\infty} \sum_{j=|l-1|}^{l+1} \sum_{n=1}^{3} X^c_n. \tag{4.88}$$

Here,

$$X^+_1(l,j,\kappa_1,\kappa_2,J) = (-1)^{l+j}\left\{Z^{l,l,1,j}_{gfgf}(J) + Z^{l,l,1,j}_{fggf}(J) - Z^{l,l,1,j}_{gffg}(J) - Z^{l,l,1,j}_{fgfg}(J)\right\}, \tag{4.89}$$

$$X^+_2(l,j,\kappa_1,\kappa_2,J) = f^{(2)}_j(l-j)\left\{Z^{l,j,0,j}_{gfgg}(J) + Z^{l,j,0,j}_{fggg}(J) + Z^{l,j,0,j}_{gfff}(J) + Z^{l,j,0,j}_{fgff}(J)\right\}, \tag{4.90}$$

$$\begin{aligned} X^+_3(l,j,\kappa_1,\kappa_2,J) =& f^{(3)}_j(l-j) \sum_{\{l_x,l_y\}=\{l,j\},\{j,l\}} \\ & \times \left\{Z^{l_x,l_y,1,j}_{gggf}(J) - Z^{l_x,l_y,1,j}_{ffgf}(J) - Z^{l_x,l_y,1,j}_{ggfg}(J) + Z^{l_x,l_y,1,j}_{fffg}(J)\right\}, \end{aligned} \tag{4.91}$$

$$X^-_1(l,j,\kappa_1,\kappa_2,J) = -i(-1)^{l+j}\left\{Z^{l,l,1,j}_{gggf}(J) - Z^{l,l,1,j}_{ffgf}(J) - Z^{l,l,1,j}_{ggfg}(J) + Z^{l,l,1,j}_{fffg}(J)\right\}, \tag{4.92}$$

$$X^-_2(l,j,\kappa_1,\kappa_2,J) = -if^{(2)}_j(l-j)\left\{Z^{l,j,0,j}_{gggg}(J) - Z^{l,j,0,j}_{ffgg}(J) + Z^{l,j,0,j}_{ggff}(J) - Z^{l,j,0,j}_{ffff}(J)\right\}, \tag{4.93}$$

$$\begin{aligned} X^-_3(l,j,\kappa_1,\kappa_2,J) =& if^{(3)}_j(l-j) \sum_{\{l_x,l_y\}=\{l,j\},\{j,l\}} \\ & \times \left\{Z^{l_x,l_y,1,j}_{gfgf}(J) + Z^{l_x,l_y,1,j}_{fggf}(J) - Z^{l_x,l_y,1,j}_{gffg}(J) - Z^{l_x,l_y,1,j}_{fgfg}(J)\right\}, \end{aligned} \tag{4.94}$$

where Z means

$$\begin{aligned} Z^{l_x,l_y,s,j}_{abcd}(J) =& q_0^2 \int_0^\infty dr_1 r_1^2 a^{\kappa_1}_{p_1}(r_1) b^{\kappa_\mu}_{\mu}(r_1) \int_0^\infty dr_2 r_2^2 F^{q_0}_{l_x,l_y}(r_1,r_2) c^{\kappa_2}_{p_2}(r_2) d^{\kappa_e}_{e}(r_2) \\ & \times (-1)^{\kappa_1+\kappa_\mu+J+l_x+l_y} \begin{Bmatrix} j_{\kappa_1} & j_{\kappa_2} & J \\ j_{\kappa_e} & j_{\kappa_\mu} & j \end{Bmatrix} \\ & \times \left(j_{\kappa_1}, 1/2, j_{\kappa_\mu}, -1/2 | j, 0\right) \left(j_{\kappa_2}, 1/2, j_{\kappa_e}, -1/2 | j, 0\right) V^{s_a\kappa_1, s_b\kappa_\mu}_{l_x,1,j} V^{s_c\kappa_2, s_d\kappa_e}_{l_y,s,j} \\ & \times \frac{1+(-1)^{l^a_{\kappa_1}+l^b_{\kappa_\mu}+l_x}}{2} \frac{1+(-1)^{l^c_{\kappa_2}+l^d_{\kappa_e}+l_y}}{2} - (-1)^{j_{\kappa_1}+j_{\kappa_2}-J}\left(\beta_1 \leftrightarrow \beta_2\right), \end{aligned} \tag{4.95}$$

where

$$s_h = \begin{cases} +1 & (h=g) \\ -1 & (h=f) \end{cases}. \tag{4.96}$$

I.4 Derivation for Eqs. (5.8)-(5.11)

Substituting Eq. (4.64) into Eq. (5.6), we obtain

$$\begin{aligned}\frac{d\Gamma}{dE_1 d\Omega_1 d\Omega_2} =& \sum_{\alpha_e} \frac{G_F^2}{2\pi^3} |\boldsymbol{p}_1| |\boldsymbol{p}_2| \sum_{s_1,s_2} \sum_{s_\mu,s'_\mu} \sum_{s_e} \sum_{\kappa_1,\nu_1,m_1} \sum_{\kappa_2,\nu_2,m_2} \sum_{\kappa'_1,\nu'_1,m'_1} \sum_{\kappa'_2,\nu'_2,m'_2} \\ & \times Y_{l_{\kappa'_1}}^{m'_1 *}(\hat{p}_1) Y_{l_{\kappa'_2}}^{m'_2 *}(\hat{p}_2) Y_{l_{\kappa_1}}^{m_1}(\hat{p}_1) Y_{l_{\kappa_2}}^{m_2}(\hat{p}_2) \\ & \times (l_{\kappa'_1}, m'_1, 1/2, s_1 | j_{\kappa'_1}, \nu'_1)(l_{\kappa'_2}, m'_2, 1/2, s_2 | j'_{\kappa_2}, \nu'_2) \\ & \times (l_{\kappa_1}, m_1, 1/2, s_1 | j_{\kappa_1}, \nu_1)(l_{\kappa_2}, m_2, 1/2, s_2 | j_{\kappa_2}, \nu_2) \\ & \times 2\left[j_{\kappa_e}\right] \sqrt{\left[j_{\kappa_1} \cdot j_{\kappa_2} \cdot j_{\kappa'_1} \cdot j_{\kappa'_2}\right]} \\ & \times \sum_{J',M'} (j_{\kappa'_1}, \nu'_1, j_{\kappa'_2}, \nu'_2 | J', M')(1/2, s'_\mu, j_{\kappa_e}, s_e | J', M') N^{\beta'_1,\beta'_2 *}(J') \\ & \times \langle s_\mu | \left(\mathbf{1} + \boldsymbol{\sigma} \cdot \boldsymbol{P}\right) | s'_\mu \rangle \\ & \times \sum_{J,M} (j_{\kappa_1}, \nu_1, j_{\kappa_2}, \nu_2 | J, M)(1/2, s_\mu, j_{\kappa_e}, s_e | J, M) N^{\beta_1,\beta_2}(J). \end{aligned} \tag{I.131}$$

Let us define

$$\begin{aligned} X =& \sum_{s_1,s_2} \sum_{s_\mu,s'_\mu} \sum_{s_e} \sum_{\kappa_1,\nu_1,m_1} \sum_{\kappa_2,\nu_2,m_2} \sum_{\kappa'_1,\nu'_1,m'_1} \sum_{\kappa'_2,\nu'_2,m'_2} \\ & \times Y_{l_{\kappa'_1}}^{m'_1 *}(\hat{p}_1) Y_{l_{\kappa'_2}}^{m'_2 *}(\hat{p}_2) Y_{l_{\kappa_1}}^{m_1}(\hat{p}_1) Y_{l_{\kappa_2}}^{m_2}(\hat{p}_2) \\ & \times (l_{\kappa'_1}, m'_1, 1/2, s_1 | j_{\kappa'_1}, \nu'_1)(l_{\kappa'_2}, m'_2, 1/2, s_2 | j'_{\kappa_2}, \nu'_2) \\ & \times (l_{\kappa_1}, m_1, 1/2, s_1 | j_{\kappa_1}, \nu_1)(l_{\kappa_2}, m_2, 1/2, s_2 | j_{\kappa_2}, \nu_2) \\ & \times \sqrt{\left[j_{\kappa_1} \cdot j_{\kappa_2} \cdot j_{\kappa'_1} \cdot j_{\kappa'_2}\right]} \\ & \times \sum_{J',M'} (j_{\kappa'_1}, \nu'_1, j_{\kappa'_2}, \nu'_2 | J', M')(1/2, s'_\mu, j_{\kappa_e}, s_e | J', M') N^{\beta'_1,\beta'_2 *}(J') \\ & \times \langle s_\mu | \boldsymbol{\sigma} \cdot \hat{P} | s'_\mu \rangle \\ & \times \sum_{J,M} (j_{\kappa_1}, \nu_1, j_{\kappa_2}, \nu_2 | J, M)(1/2, s_\mu, j_{\kappa_e}, s_e | J, M) N^{\beta_1,\beta_2}(J), \end{aligned} \tag{I.132}$$

which satisfies

$$\frac{d\Gamma}{dE_1 d\Omega_1 d\Omega_2} = \frac{1}{8\pi^2} \frac{d\Gamma_{unpol.}}{dE_1 d\cos\theta_{12}} + P \sum_{\alpha_e} \frac{G_F^2}{\pi^3} \left(2j_{\kappa_e} + 1\right) |\boldsymbol{p}_1| |\boldsymbol{p}_2| X. \tag{I.133}$$

Here, magnitude of polarization vector P is factored out from X.

The factor of $\langle s_\mu | \boldsymbol{\sigma} \cdot \hat{P} | s'_\mu \rangle$ is represented by a $3j$ symbol as

$$\begin{aligned} \langle s_\mu | \boldsymbol{\sigma} \cdot \hat{P} | s'_\mu \rangle =& \sum_n \hat{P}^{-n} (-1)^n \langle s_\mu | \sigma^n | s'_\mu \rangle \\ =& \sum_n \hat{P}^{-n} (-1)^{1/2 - s'_\mu} \begin{pmatrix} 1/2 & 1/2 & 1 \\ s'_\mu & -s_\mu & n \end{pmatrix} \sqrt{6}. \end{aligned} \tag{I.134}$$

Moreover, according to Eq. (G.49), we get

$$
\begin{aligned}
&\sum_{s_\mu,s'_\mu,s_e}(-1)^{1/2-s'_\mu}\begin{pmatrix}1/2 & 1/2 & 1\\ s'_\mu & -s_\mu & n\end{pmatrix}(1/2,s_\mu,j_{\kappa_e},s_e|J,M)(1/2,s'_\mu,j_{\kappa_e},s_e|J',M')\\
=&\sqrt{[J\cdot J']}\sum_{s_\mu,s'_\mu,s_e}(-1)^{1/2-s'_\mu+M+M'}\begin{pmatrix}1/2 & 1/2 & 1\\ s'_\mu & -s_\mu & n\end{pmatrix}\begin{pmatrix}1/2 & j_{\kappa_e} & J\\ s_\mu & s_e & -M\end{pmatrix}\begin{pmatrix}1/2 & j_{\kappa_e} & J'\\ s'_\mu & s_e & -M'\end{pmatrix}\\
=&\sqrt{[J\cdot J']}(-1)^{n+M-j_{\kappa_e}-1/2}\\
&\times\sum_{s_\mu,s'_\mu,s_e}(-1)^{1/2+1/2+j_{\kappa_e}+s_\mu+s'_\mu-s_e}\begin{pmatrix}1/2 & 1/2 & 1\\ s'_\mu & -s_\mu & n\end{pmatrix}\begin{pmatrix}1/2 & j_{\kappa_e} & J\\ s_\mu & s_e & -M\end{pmatrix}\begin{pmatrix}j_{\kappa_e} & 1/2 & J'\\ -s_e & -s'_\mu & M'\end{pmatrix}\\
=&\sqrt{[J\cdot J']}(-1)^{n+M-j_{\kappa_e}-1/2}\begin{pmatrix}J & J' & 1\\ -M & M' & n\end{pmatrix}\begin{Bmatrix}J & J' & 1\\ 1/2 & 1/2 & j_{\kappa_e}\end{Bmatrix}.
\end{aligned}
\tag{I.135}
$$

Therefore,

$$
\begin{aligned}
X=&\sqrt{6}\sum_{s_1,s_2}\sum_{\kappa_1,\nu_1,m_1}\sum_{\kappa_2,\nu_2,m_2}\sum_{\kappa'_1,\nu'_1,m'_1}\sum_{\kappa'_2,\nu'_2,m'_2}\sum_{J,M}\sum_{J',M'}\sum_{n}\hat{P}^{-n}(-1)^n\\
&\times Y^{m'_1*}_{l_{\kappa'_1}}(\hat{p}_1)Y^{m'_2*}_{l_{\kappa'_2}}(\hat{p}_2)Y^{m_1}_{l_{\kappa_1}}(\hat{p}_1)Y^{m_2}_{l_{\kappa_2}}(\hat{p}_2)\\
&\times(l_{\kappa'_1},m'_1,1/2,s_1|j_{\kappa'_1},\nu'_1)(l_{\kappa'_2},m'_2,1/2,s_2|j_{\kappa'_2},\nu'_2)\\
&\times(l_{\kappa_1},m_1,1/2,s_1|j_{\kappa_1},\nu_1)(l_{\kappa_2},m_2,1/2,s_2|j_{\kappa_2},\nu_2)\\
&\times(-1)^{M-j_{\kappa_e}-1/2}\sqrt{[J\cdot J'\cdot j_{\kappa_1}\cdot j_{\kappa_2}\cdot j_{\kappa'_1}\cdot j_{\kappa'_2}]}\\
&\times(j_{\kappa'_1},\nu'_1,j_{\kappa'_2},\nu'_2|J',M')(j_{\kappa_1},\nu_1,j_{\kappa_2},\nu_2|J,M)N^{\beta'_1,\beta'_2*}(J')N^{\beta_1,\beta_2}(J)\\
&\times\begin{pmatrix}J & J' & 1\\ -M & M' & n\end{pmatrix}\begin{Bmatrix}J & J' & 1\\ 1/2 & 1/2 & j_{\kappa_e}\end{Bmatrix}.
\end{aligned}
\tag{I.136}
$$

By converting Clebsch-Gordan coefficients into $3j$ symbols and coupling the spherical harmonics, let us rewrite it as

$$
\begin{aligned}
X=&\frac{\sqrt{6}}{4\pi}\sum_{s_1,s_2}\sum_{\kappa_1,\nu_1,m_1}\sum_{\kappa_2,\nu_2,m_2}\sum_{\kappa'_1,\nu'_1,m'_1}\sum_{\kappa'_2,\nu'_2,m'_2}\sum_{J,M}\sum_{J',M'}\sum_{l_1,n_1}\sum_{l_2,n_2}\sum_{n}\hat{P}^{-n}(-1)^n\\
&\times(-1)^{M-j_{\kappa_e}-1/2+l_{\kappa_1}+l_{\kappa'_1}+l_{\kappa_2}+l_{\kappa'_2}+j_{\kappa_1}-j_{\kappa_2}+j_{\kappa'_1}-j_{\kappa'_2}+m_1+m_2}\\
&\times\left[J\cdot J'\cdot j_{\kappa_1}\cdot j_{\kappa_2}\cdot j_{\kappa'_1}\cdot j_{\kappa'_2}\right]\sqrt{\left[l_{\kappa_1}\cdot l_{\kappa_2}\cdot l_{\kappa'_1}\cdot l_{\kappa'_2}\cdot l_1\cdot l_2\right]}\\
&\times Y^{n_1}_{l_1}(\hat{p}_1)Y^{n_2}_{l_2}(\hat{p}_2)N^{\beta'_1,\beta'_2*}(J')N^{\beta_1,\beta_2}(J)\\
&\times\begin{pmatrix}l_{\kappa_1} & l_{\kappa'_1} & l_1\\ 0 & 0 & 0\end{pmatrix}\begin{pmatrix}l_{\kappa_2} & l_{\kappa'_2} & l_2\\ 0 & 0 & 0\end{pmatrix}\begin{pmatrix}l_{\kappa_1} & l_{\kappa'_1} & l_1\\ m_1 & -m'_1 & -n_1\end{pmatrix}\begin{pmatrix}l_{\kappa_2} & l_{\kappa'_2} & l_2\\ m_2 & -m'_2 & -n_2\end{pmatrix}\\
&\times\begin{pmatrix}l_{\kappa_1} & 1/2 & j_{\kappa_1}\\ m_1 & s_1 & -\nu_1\end{pmatrix}\begin{pmatrix}l_{\kappa'_1} & 1/2 & j_{\kappa'_1}\\ m'_1 & s_1 & -\nu'_1\end{pmatrix}\begin{pmatrix}l_{\kappa_2} & 1/2 & j_{\kappa_2}\\ m_2 & s_2 & -\nu_2\end{pmatrix}\begin{pmatrix}l_{\kappa'_2} & 1/2 & j_{\kappa'_2}\\ m'_2 & s_2 & -\nu'_2\end{pmatrix}\\
&\times\begin{pmatrix}j_{\kappa_1} & j_{\kappa_2} & J\\ \nu_1 & \nu_2 & -M\end{pmatrix}\begin{pmatrix}j_{\kappa'_1} & j_{\kappa'_2} & J'\\ \nu'_1 & \nu'_2 & -M'\end{pmatrix}\begin{pmatrix}J & J' & 1\\ -M & M' & n\end{pmatrix}\begin{Bmatrix}J & J' & 1\\ 1/2 & 1/2 & j_{\kappa_e}\end{Bmatrix}.
\end{aligned}
\tag{I.137}
$$

The summation over s_i, m_i, and m_i' is performed to be

$$
\begin{aligned}
X =& \frac{\sqrt{6}}{4\pi} \sum_{\kappa_1,\nu_1} \sum_{\kappa_2,\nu_2} \sum_{\kappa_1',\nu_1'} \sum_{\kappa_2',\nu_2'} \sum_{J,M} \sum_{J',M'} \sum_{l_1,n_1} \sum_{l_2,n_2} \sum_{n} \hat{P}^{-n} (-1)^n \\
& \times (-1)^{n-j_{\kappa_e}+1/2+j_{\kappa_1}-j_{\kappa_2}+j_{\kappa_1'}-j_{\kappa_2'}} \\
& \times \left[J \cdot J' \cdot j_{\kappa_1} \cdot j_{\kappa_2} \cdot j_{\kappa_1'} \cdot j_{\kappa_2'}\right] \sqrt{\left[l_{\kappa_1} \cdot l_{\kappa_2} \cdot l_{\kappa_1'} \cdot l_{\kappa_2'} \cdot l_1 \cdot l_2\right]} \\
& \times Y_{l_1}^{n_1}(\hat{p}_1) Y_{l_2}^{n_2}(\hat{p}_2) N^{\beta_1',\beta_2'*}(J') N^{\beta_1,\beta_2}(J) \\
& \times \begin{pmatrix} l_{\kappa_1} & l_{\kappa_1'} & l_1 \\ 0 & 0 & 0 \end{pmatrix} \begin{pmatrix} l_{\kappa_2} & l_{\kappa_2'} & l_2 \\ 0 & 0 & 0 \end{pmatrix} \\
& \times \begin{pmatrix} j_{\kappa_1} & j_{\kappa_1'} & l_1 \\ -\nu_1 & \nu_1' & n_1 \end{pmatrix} \begin{Bmatrix} j_{\kappa_1} & j_{\kappa_1'} & l_1 \\ l_{\kappa_1'} & l_{\kappa_1} & 1/2 \end{Bmatrix} \begin{pmatrix} j_{\kappa_2} & j_{\kappa_2'} & l_2 \\ -\nu_2 & \nu_2' & n_2 \end{pmatrix} \begin{Bmatrix} j_{\kappa_2} & j_{\kappa_2'} & l_2 \\ l_{\kappa_2'} & l_{\kappa_2} & 1/2 \end{Bmatrix} \\
& \times \begin{pmatrix} j_{\kappa_1} & j_{\kappa_2} & J \\ \nu_1 & \nu_2 & -M \end{pmatrix} \begin{pmatrix} j_{\kappa_1'} & j_{\kappa_2'} & J' \\ \nu_1' & \nu_2' & -M' \end{pmatrix} \begin{pmatrix} J & J' & 1 \\ -M & M' & n \end{pmatrix} \begin{Bmatrix} J & J' & 1 \\ 1/2 & 1/2 & j_{\kappa_e} \end{Bmatrix},
\end{aligned} \tag{I.138}
$$

where Eq. (G.49) is used. Next the summation for six projection quantum numbers are performed by

$$
\begin{aligned}
& \sum_{\nu_1,\nu_2,\nu_1',\nu_2',M,M'} \begin{pmatrix} j_{\kappa_1} & j_{\kappa_2} & J \\ \nu_1 & \nu_2 & -M \end{pmatrix} \begin{pmatrix} j_{\kappa_1'} & j_{\kappa_2'} & J' \\ \nu_1' & \nu_2' & -M' \end{pmatrix} \begin{pmatrix} j_{\kappa_1} & j_{\kappa_1'} & l_1 \\ -\nu_1 & \nu_1' & n_1 \end{pmatrix} \\
& \times \begin{pmatrix} j_{\kappa_2} & j_{\kappa_2'} & l_2 \\ -\nu_2 & \nu_2' & n_2 \end{pmatrix} \begin{pmatrix} J & J' & 1 \\ -M & M' & n \end{pmatrix} \\
=& (-1)^{j_{\kappa_1}+j_{\kappa_2}+J'+1} \sum_{\nu_1,\nu_2,\nu_1',\nu_2',M,M'} \begin{pmatrix} j_{\kappa_1} & j_{\kappa_2} & J \\ -\nu_1 & -\nu_2 & M \end{pmatrix} \begin{pmatrix} j_{\kappa_1'} & j_{\kappa_2'} & J' \\ \nu_1' & \nu_2' & -M' \end{pmatrix} \begin{pmatrix} j_{\kappa_1} & j_{\kappa_1'} & l_1 \\ -\nu_1 & \nu_1' & n_1 \end{pmatrix} \\
& \times \begin{pmatrix} j_{\kappa_2} & j_{\kappa_2'} & l_2 \\ -\nu_2 & \nu_2' & n_2 \end{pmatrix} \begin{pmatrix} J & J' & 1 \\ M & -M' & -n \end{pmatrix} \\
=& (-1)^{j_{\kappa_1}+j_{\kappa_2}+J'+1} \begin{pmatrix} l_1 & l_2 & 1 \\ n_1 & n_2 & -n \end{pmatrix} \begin{Bmatrix} j_{\kappa_1} & j_{\kappa_2} & J \\ j_{\kappa_1'} & j_{\kappa_2'} & J' \\ l_1 & l_2 & 1 \end{Bmatrix}.
\end{aligned} \tag{I.139}
$$

After the summation, we get

$$
\begin{aligned}
X =& \frac{\sqrt{6}}{4\pi} \sum_{\kappa_1,\kappa_2} \sum_{\kappa_1',\kappa_2'} \sum_{J,J'} \sum_{l_1,n_1} \sum_{l_2,n_2} \sum_{n} \hat{P}^{-n} (-1)^n \\
& \times (-1)^{n+J'+j_{\kappa_1'}-j_{\kappa_2'}-j_{\kappa_e}+1/2} \\
& \times \left[J \cdot J' \cdot j_{\kappa_1} \cdot j_{\kappa_2} \cdot j_{\kappa_1'} \cdot j_{\kappa_2'}\right] \sqrt{\left[l_{\kappa_1} \cdot l_{\kappa_2} \cdot l_{\kappa_1'} \cdot l_{\kappa_2'} \cdot l_1 \cdot l_2\right]} \\
& \times Y_{l_1}^{n_1}(\hat{p}_1) Y_{l_2}^{n_2}(\hat{p}_2) N^{\beta_1',\beta_2'*}(J') N^{\beta_1,\beta_2}(J) \\
& \times \begin{pmatrix} l_{\kappa_1} & l_{\kappa_1'} & l_1 \\ 0 & 0 & 0 \end{pmatrix} \begin{pmatrix} l_{\kappa_2} & l_{\kappa_2'} & l_2 \\ 0 & 0 & 0 \end{pmatrix} \begin{pmatrix} l_1 & l_2 & 1 \\ n_1 & n_2 & -n \end{pmatrix} \\
& \times \begin{Bmatrix} j_{\kappa_1} & j_{\kappa_1'} & l_1 \\ l_{\kappa_1'} & l_{\kappa_1} & 1/2 \end{Bmatrix} \begin{Bmatrix} j_{\kappa_2} & j_{\kappa_2'} & l_2 \\ l_{\kappa_2'} & l_{\kappa_2} & 1/2 \end{Bmatrix} \begin{Bmatrix} J & J' & 1 \\ 1/2 & 1/2 & j_{\kappa_e} \end{Bmatrix} \begin{Bmatrix} j_{\kappa_1} & j_{\kappa_2} & J \\ j_{\kappa_1'} & j_{\kappa_2'} & J' \\ l_1 & l_2 & 1 \end{Bmatrix}.
\end{aligned} \tag{I.140}
$$

Now, we use

$$\begin{aligned}
&\sum_n \hat{P}^{-n}(-1)^n \sum_{n_1,n_2} \sqrt{3}(-1)^{l_1-l_2+n} \begin{pmatrix} l_1 & l_2 & 1 \\ n_1 & n_2 & -n \end{pmatrix} Y_{l_1}^{n_1}(\hat{p}_1) Y_{l_2}^{n_2}(\hat{p}_2) \\
=&\sum_n \hat{P}^{-n}(-1)^n \left[Y_{l_1}(\hat{p}_1) \otimes Y_{l_2}(\hat{p}_2)\right]_1^n \\
=&\hat{P} \cdot \left[Y_{l_1}(\hat{p}_1) \otimes Y_{l_2}(\hat{p}_2)\right]_1 ,
\end{aligned} \tag{I.141}$$

to reduce X into

$$\begin{aligned}
X =&\frac{\sqrt{2}}{4\pi} \sum_{\kappa_1,\kappa_2} \sum_{\kappa_1',\kappa_2'} \sum_{J,J'} \sum_{l_1,l_2} (-1)^{l_1-l_2+J'+j_{\kappa_1'}-j_{\kappa_2'}-j_{\kappa_e}+1/2} N^{\beta_1',\beta_2'*}(J') N^{\beta_1,\beta_2}(J) \\
&\times \left[J \cdot J' \cdot j_{\kappa_1} \cdot j_{\kappa_2} \cdot j_{\kappa_1'} \cdot j_{\kappa_2'}\right] \sqrt{\left[l_{\kappa_1} \cdot l_{\kappa_2} \cdot l_{\kappa_1'} \cdot l_{\kappa_2'} \cdot l_1 \cdot l_2\right]} \\
&\times \hat{P} \cdot \left[Y_{l_1}(\hat{p}_1) \otimes Y_{l_2}(\hat{p}_2)\right]_1 \begin{pmatrix} l_{\kappa_1} & l_{\kappa_1'} & l_1 \\ 0 & 0 & 0 \end{pmatrix} \begin{pmatrix} l_{\kappa_2} & l_{\kappa_2'} & l_2 \\ 0 & 0 & 0 \end{pmatrix} \\
&\times \begin{Bmatrix} j_{\kappa_1} & j_{\kappa_1'} & l_1 \\ l_{\kappa_1'} & l_{\kappa_1} & 1/2 \end{Bmatrix} \begin{Bmatrix} j_{\kappa_2} & j_{\kappa_2'} & l_2 \\ l_{\kappa_2'} & l_{\kappa_2} & 1/2 \end{Bmatrix} \begin{Bmatrix} J & J' & 1 \\ 1/2 & 1/2 & j_{\kappa_e} \end{Bmatrix} \begin{Bmatrix} j_{\kappa_1} & j_{\kappa_2} & J \\ j_{\kappa_1'} & j_{\kappa_2'} & J' \\ l_1 & l_2 & 1 \end{Bmatrix} .
\end{aligned} \tag{I.142}$$

Noting that l_2 is allowed to be only l_1-1, l_1, or l_1+1 due to the condition for geometric factors, we write it as

$$\begin{aligned}
X =&\frac{\sqrt{2}}{4\pi} \sum_{\kappa_1,\kappa_2} \sum_{\kappa_1',\kappa_2'} \sum_{J,J'} \sum_{l} (-1)^{J'+j_{\kappa_1'}-j_{\kappa_2'}-j_{\kappa_e}-1/2} N^{\beta_1',\beta_2'*}(J') N^{\beta_1,\beta_2}(J) \\
&\times \left[J \cdot J' \cdot j_{\kappa_1} \cdot j_{\kappa_2} \cdot j_{\kappa_1'} \cdot j_{\kappa_2'}\right] \sqrt{\left[l_{\kappa_1} \cdot l_{\kappa_2} \cdot l_{\kappa_1'} \cdot l_{\kappa_2'}\right]} \begin{Bmatrix} J & J' & 1 \\ 1/2 & 1/2 & j_{\kappa_e} \end{Bmatrix} \\
&\times \Bigg[\sqrt{[l \cdot (l+1)]} \hat{P} \cdot \left[Y_l(\hat{p}_1) \otimes Y_{l+1}(\hat{p}_2)\right]_1 \begin{pmatrix} l_{\kappa_1} & l_{\kappa_1'} & l \\ 0 & 0 & 0 \end{pmatrix} \begin{pmatrix} l_{\kappa_2} & l_{\kappa_2'} & l+1 \\ 0 & 0 & 0 \end{pmatrix} \\
&\times \begin{Bmatrix} j_{\kappa_1} & j_{\kappa_1'} & l \\ l_{\kappa_1'} & l_{\kappa_1} & 1/2 \end{Bmatrix} \begin{Bmatrix} j_{\kappa_2} & j_{\kappa_2'} & l+1 \\ l_{\kappa_2'} & l_{\kappa_2} & 1/2 \end{Bmatrix} \begin{Bmatrix} j_{\kappa_1} & j_{\kappa_2} & J \\ j_{\kappa_1'} & j_{\kappa_2'} & J' \\ l & l+1 & 1 \end{Bmatrix} \\
&- [l+1] \hat{P} \cdot \left[Y_{l+1}(\hat{p}_1) \otimes Y_{l+1}(\hat{p}_2)\right]_1 \begin{pmatrix} l_{\kappa_1} & l_{\kappa_1'} & l+1 \\ 0 & 0 & 0 \end{pmatrix} \begin{pmatrix} l_{\kappa_2} & l_{\kappa_2'} & l+1 \\ 0 & 0 & 0 \end{pmatrix} \\
&\times \begin{Bmatrix} j_{\kappa_1} & j_{\kappa_1'} & l+1 \\ l_{\kappa_1'} & l_{\kappa_1} & 1/2 \end{Bmatrix} \begin{Bmatrix} j_{\kappa_2} & j_{\kappa_2'} & l+1 \\ l_{\kappa_2'} & l_{\kappa_2} & 1/2 \end{Bmatrix} \begin{Bmatrix} j_{\kappa_1} & j_{\kappa_2} & J \\ j_{\kappa_1'} & j_{\kappa_2'} & J' \\ l+1 & l+1 & 1 \end{Bmatrix} \\
&+ \sqrt{[l \cdot (l+1)]} \hat{P} \cdot \left[Y_{l+1}(\hat{p}_1) \otimes Y_l(\hat{p}_2)\right]_1 \begin{pmatrix} l_{\kappa_1} & l_{\kappa_1'} & l+1 \\ 0 & 0 & 0 \end{pmatrix} \begin{pmatrix} l_{\kappa_2} & l_{\kappa_2'} & l \\ 0 & 0 & 0 \end{pmatrix} \\
&\times \begin{Bmatrix} j_{\kappa_1} & j_{\kappa_1'} & l+1 \\ l_{\kappa_1'} & l_{\kappa_1} & 1/2 \end{Bmatrix} \begin{Bmatrix} j_{\kappa_2} & j_{\kappa_2'} & l \\ l_{\kappa_2'} & l_{\kappa_2} & 1/2 \end{Bmatrix} \begin{Bmatrix} j_{\kappa_1} & j_{\kappa_2} & J \\ j_{\kappa_1'} & j_{\kappa_2'} & J' \\ l+1 & l & 1 \end{Bmatrix} \Bigg] .
\end{aligned} \tag{I.143}$$

By the formulae for the spherical harmonics (G.69)-(G.71), we obtain

$$
\begin{aligned}
X =& \frac{\sqrt{6}}{(4\pi)^2} \sum_{\kappa_1,\kappa_2} \sum_{\kappa_1',\kappa_2'} \sum_{J,J'} \sum_{l} (-1)^{J'+j_{\kappa_1'}-j_{\kappa_2'}-j_{\kappa_e}+l+1/2} N^{\beta_1',\beta_2'*}(J') N^{\beta_1,\beta_2}(J) \\
& \times \sqrt{\frac{2l+3}{l+1}} \left[J \cdot J' \cdot j_{\kappa_1} \cdot j_{\kappa_2} \cdot j_{\kappa_1'} \cdot j_{\kappa_2'}\right] \sqrt{\left[l_{\kappa_1} \cdot l_{\kappa_2} \cdot l_{\kappa_1'} \cdot l_{\kappa_2'}\right]} \begin{Bmatrix} J & J' & 1 \\ 1/2 & 1/2 & j_{\kappa_e} \end{Bmatrix} \\
& \times \left[\sqrt{2l+1} \left\{ \hat{P} \cdot \hat{p}_1 P_l'(\cos\theta_{12}) - \hat{P} \cdot \hat{p}_2 P_{l+1}'(\cos\theta_{12}) \right\} \begin{pmatrix} l_{\kappa_1} & l_{\kappa_1'} & l \\ 0 & 0 & 0 \end{pmatrix} \begin{pmatrix} l_{\kappa_2} & l_{\kappa_2'} & l+1 \\ 0 & 0 & 0 \end{pmatrix} \right. \\
& \times \begin{Bmatrix} j_{\kappa_1} & j_{\kappa_1'} & l \\ l_{\kappa_1'} & l_{\kappa_1} & 1/2 \end{Bmatrix} \begin{Bmatrix} j_{\kappa_2} & j_{\kappa_2'} & l+1 \\ l_{\kappa_2'} & l_{\kappa_2} & 1/2 \end{Bmatrix} \begin{Bmatrix} j_{\kappa_1} & j_{\kappa_2} & J \\ j_{\kappa_1'} & j_{\kappa_2'} & J' \\ l & l+1 & 1 \end{Bmatrix} \\
& + i \frac{2l+3}{\sqrt{l+2}} \hat{P} \cdot (\hat{p}_1 \times \hat{p}_2) P_{l+1}'(\cos\theta_{12}) \begin{pmatrix} l_{\kappa_1} & l_{\kappa_1'} & l+1 \\ 0 & 0 & 0 \end{pmatrix} \begin{pmatrix} l_{\kappa_2} & l_{\kappa_2'} & l+1 \\ 0 & 0 & 0 \end{pmatrix} \\
& \times \begin{Bmatrix} j_{\kappa_1} & j_{\kappa_1'} & l+1 \\ l_{\kappa_1'} & l_{\kappa_1} & 1/2 \end{Bmatrix} \begin{Bmatrix} j_{\kappa_2} & j_{\kappa_2'} & l+1 \\ l_{\kappa_2'} & l_{\kappa_2} & 1/2 \end{Bmatrix} \begin{Bmatrix} j_{\kappa_1} & j_{\kappa_2} & J \\ j_{\kappa_1'} & j_{\kappa_2'} & J' \\ l+1 & l+1 & 1 \end{Bmatrix} \\
& - \sqrt{2l+1} \left\{ \hat{P} \cdot \hat{p}_1 P_{l+1}'(\cos\theta_{12}) - \hat{P} \cdot \hat{p}_2 P_l'(\cos\theta_{12}) \right\} \begin{pmatrix} l_{\kappa_1} & l_{\kappa_1'} & l+1 \\ 0 & 0 & 0 \end{pmatrix} \begin{pmatrix} l_{\kappa_2} & l_{\kappa_2'} & l \\ 0 & 0 & 0 \end{pmatrix} \\
& \times \left. \begin{Bmatrix} j_{\kappa_1} & j_{\kappa_1'} & l+1 \\ l_{\kappa_1'} & l_{\kappa_1} & 1/2 \end{Bmatrix} \begin{Bmatrix} j_{\kappa_2} & j_{\kappa_2'} & l \\ l_{\kappa_2'} & l_{\kappa_2} & 1/2 \end{Bmatrix} \begin{Bmatrix} j_{\kappa_1} & j_{\kappa_2} & J \\ j_{\kappa_1'} & j_{\kappa_2'} & J' \\ l+1 & l & 1 \end{Bmatrix} \right]. \qquad \text{(I.144)}
\end{aligned}
$$

Rearranging it, we obtain the following compact form

$$
X = \frac{1}{(4\pi)^2} \left\{ f(E_1, E_2, \cos\theta_{12}) \hat{P} \cdot \hat{p}_1 + f'(E_1, E_2, \cos\theta_{12}) \hat{P} \cdot \hat{p}_2 + \tilde{f}(E_1, E_2, \cos\theta_{12}) \hat{P} \cdot (\hat{p}_1 \times \hat{p}_2) \right\}, \quad \text{(I.145)}
$$

where

$$
\begin{aligned}
f(E_1, E_2, \cos\theta_{12}) =& \sqrt{6} \sum_{\kappa_1,\kappa_2} \sum_{\kappa_1',\kappa_2'} \sum_{J,J'} \sum_{l} (-1)^{J'+j_{\kappa_1'}-j_{\kappa_2'}-j_{\kappa_e}+l+1/2} N^{\beta_1',\beta_2'*}(J') N^{\beta_1,\beta_2}(J) \\
& \times \left[J \cdot J' \cdot j_{\kappa_1} \cdot j_{\kappa_2} \cdot j_{\kappa_1'} \cdot j_{\kappa_2'}\right] \sqrt{\left[l_{\kappa_1} \cdot l_{\kappa_2} \cdot l_{\kappa_1'} \cdot l_{\kappa_2'}\right]} \\
& \times \sqrt{\frac{(2l+1)(2l+3)}{l+1}} \begin{Bmatrix} J & J' & 1 \\ 1/2 & 1/2 & j_{\kappa_e} \end{Bmatrix} \\
& \times \left[P_l'(\cos\theta_{12}) \begin{pmatrix} l_{\kappa_1} & l_{\kappa_1'} & l \\ 0 & 0 & 0 \end{pmatrix} \begin{pmatrix} l_{\kappa_2} & l_{\kappa_2'} & l+1 \\ 0 & 0 & 0 \end{pmatrix} \right. \\
& \times \begin{Bmatrix} j_{\kappa_1} & j_{\kappa_1'} & l \\ l_{\kappa_1'} & l_{\kappa_1} & 1/2 \end{Bmatrix} \begin{Bmatrix} j_{\kappa_2} & j_{\kappa_2'} & l+1 \\ l_{\kappa_2'} & l_{\kappa_2} & 1/2 \end{Bmatrix} \begin{Bmatrix} j_{\kappa_1} & j_{\kappa_2} & J \\ j_{\kappa_1'} & j_{\kappa_2'} & J' \\ l & l+1 & 1 \end{Bmatrix} \\
& - P_{l+1}'(\cos\theta_{12}) \begin{pmatrix} l_{\kappa_1} & l_{\kappa_1'} & l+1 \\ 0 & 0 & 0 \end{pmatrix} \begin{pmatrix} l_{\kappa_2} & l_{\kappa_2'} & l \\ 0 & 0 & 0 \end{pmatrix} \\
& \times \left. \begin{Bmatrix} j_{\kappa_1} & j_{\kappa_1'} & l+1 \\ l_{\kappa_1'} & l_{\kappa_1} & 1/2 \end{Bmatrix} \begin{Bmatrix} j_{\kappa_2} & j_{\kappa_2'} & l \\ l_{\kappa_2'} & l_{\kappa_2} & 1/2 \end{Bmatrix} \begin{Bmatrix} j_{\kappa_1} & j_{\kappa_2} & J \\ j_{\kappa_1'} & j_{\kappa_2'} & J' \\ l+1 & l & 1 \end{Bmatrix} \right], \qquad \text{(5.10)}
\end{aligned}
$$

$$
\begin{aligned}
f'\left(E_1,E_2,\cos\theta_{12}\right) =& \sqrt{6}\sum_{\kappa_1,\kappa_2}\sum_{\kappa_1',\kappa_2'}\sum_{J,J'}\sum_{l}(-1)^{J'+j_{\kappa_1'}-j_{\kappa_2'}-j_{\kappa_e}+l+1/2}N^{\beta_1',\beta_2'*}(J')N^{\beta_1,\beta_2}(J)\\
&\times\left[J\cdot J'\cdot j_{\kappa_1}\cdot j_{\kappa_2}\cdot j_{\kappa_1'}\cdot j_{\kappa_2'}\right]\sqrt{\left[l_{\kappa_1}\cdot l_{\kappa_2}\cdot l_{\kappa_1'}\cdot l_{\kappa_2'}\right]}\\
&\times\sqrt{\frac{(2l+1)(2l+3)}{l+1}}\begin{Bmatrix} J & J' & 1\\ 1/2 & 1/2 & j_{\kappa_e}\end{Bmatrix}\\
&\times\left[P_l'\left(\cos\theta_{12}\right)\begin{pmatrix} l_{\kappa_1} & l_{\kappa_1'} & l+1\\ 0 & 0 & 0\end{pmatrix}\begin{pmatrix} l_{\kappa_2} & l_{\kappa_2'} & l\\ 0 & 0 & 0\end{pmatrix}\right.\\
&\times\begin{Bmatrix} j_{\kappa_1} & j_{\kappa_1'} & l+1\\ l_{\kappa_1'} & l_{\kappa_1} & 1/2\end{Bmatrix}\begin{Bmatrix} j_{\kappa_2} & j_{\kappa_2'} & l\\ l_{\kappa_2'} & l_{\kappa_2} & 1/2\end{Bmatrix}\begin{Bmatrix} j_{\kappa_1} & j_{\kappa_2} & J\\ j_{\kappa_1'} & j_{\kappa_2'} & J'\\ l+1 & l & 1\end{Bmatrix}\\
&-P_{l+1}'\left(\cos\theta_{12}\right)\begin{pmatrix} l_{\kappa_1} & l_{\kappa_1'} & l\\ 0 & 0 & 0\end{pmatrix}\begin{pmatrix} l_{\kappa_2} & l_{\kappa_2'} & l+1\\ 0 & 0 & 0\end{pmatrix}\\
&\left.\times\begin{Bmatrix} j_{\kappa_1} & j_{\kappa_1'} & l\\ l_{\kappa_1'} & l_{\kappa_1} & 1/2\end{Bmatrix}\begin{Bmatrix} j_{\kappa_2} & j_{\kappa_2'} & l+1\\ l_{\kappa_2'} & l_{\kappa_2} & 1/2\end{Bmatrix}\begin{Bmatrix} j_{\kappa_1} & j_{\kappa_2} & J\\ j_{\kappa_1'} & j_{\kappa_2'} & J'\\ l & l+1 & 1\end{Bmatrix}\right],
\end{aligned}
\tag{I.146}
$$

and

$$
\begin{aligned}
\tilde{f}\left(E_1,E_2,\cos\theta_{12}\right) =& \sqrt{6}\sum_{\kappa_1,\kappa_2}\sum_{\kappa_1',\kappa_2'}\sum_{J,J'}\sum_{l}(-1)^{J'+j_{\kappa_1'}-j_{\kappa_2'}-j_{\kappa_e}+l+1/2}N^{\beta_1',\beta_2'*}(J')N^{\beta_1,\beta_2}(J)\\
&\times\left[J\cdot J'\cdot j_{\kappa_1}\cdot j_{\kappa_2}\cdot j_{\kappa_1'}\cdot j_{\kappa_2'}\right]\sqrt{\left[l_{\kappa_1}\cdot l_{\kappa_2}\cdot l_{\kappa_1'}\cdot l_{\kappa_2'}\right]}\\
&\times\frac{(2l+3)^{3/2}}{\sqrt{(l+1)(l+2)}}\begin{Bmatrix} J & J' & 1\\ 1/2 & 1/2 & j_{\kappa_e}\end{Bmatrix}\\
&\times iP_{l+1}'\left(\cos\theta_{12}\right)\begin{pmatrix} l_{\kappa_1} & l_{\kappa_1'} & l+1\\ 0 & 0 & 0\end{pmatrix}\begin{pmatrix} l_{\kappa_2} & l_{\kappa_2'} & l+1\\ 0 & 0 & 0\end{pmatrix}\\
&\times\begin{Bmatrix} j_{\kappa_1} & j_{\kappa_1'} & l+1\\ l_{\kappa_1'} & l_{\kappa_1} & 1/2\end{Bmatrix}\begin{Bmatrix} j_{\kappa_2} & j_{\kappa_2'} & l+1\\ l_{\kappa_2'} & l_{\kappa_2} & 1/2\end{Bmatrix}\begin{Bmatrix} j_{\kappa_1} & j_{\kappa_2} & J\\ j_{\kappa_1'} & j_{\kappa_2'} & J'\\ l+1 & l+1 & 1\end{Bmatrix}.
\end{aligned}
\tag{5.11}
$$

Using the relation for replacement of indices of $3nj$ symbols and

$$
N^{\beta_1,\beta_2}(J)=(-1)^{j_{\kappa_1}+j_{\kappa_2}-J}N^{\beta_2,\beta_1}(J),
\tag{I.147}
$$

you can confirm

$$
f'\left(E_1,E_2,\cos\theta_{12}\right)=f\left(E_2,E_1,\cos\theta_{12}\right),
\tag{I.148}
$$

and

$$
\tilde{f}\left(E_1,E_2,\cos\theta_{12}\right)=-\tilde{f}\left(E_2,E_1,\cos\theta_{12}\right),
\tag{I.149}
$$

which are consistent with Eqs. (5.1) and (5.2). Relations to $F\left(E_1,\cos\theta_{12}\right)$ and $\tilde{F}\left(E_1,\cos\theta_{12}\right)$ are given as

$$
F\left(E_1,\cos\theta_{12}\right)=\frac{G_F^2}{2\pi^3}\left(\frac{d\Gamma_{unpol.}}{dE_1 d\cos\theta_{12}}\right)^{-1}\sum_{\alpha_e}\left|\boldsymbol{p}_1\right|\left|\boldsymbol{p}_2\right|\left(2j_{\kappa_e}+1\right)f\left(E_1,E_2,\cos\theta_{12}\right),
\tag{5.8}
$$

$$
\tilde{F}\left(E_1,\cos\theta_{12}\right)=\frac{G_F^2}{2\pi^3}\left(\frac{d\Gamma_{unpol.}}{dE_1 d\cos\theta_{12}}\right)^{-1}\sum_{\alpha_e}\left|\boldsymbol{p}_1\right|\left|\boldsymbol{p}_2\right|\left(2j_{\kappa_e}+1\right)\tilde{f}\left(E_1,E_2,\cos\theta_{12}\right),
\tag{5.9}
$$

respectively.

References

[1] S. H. Neddermeyer and C. D. Anderson, Phys. Rev. **51**, 884 (1937).

[2] M. Conversi, E. Pancini, and O. Piccioni, Phys. Rev. **71**, 209 (1947).

[3] C. M. G. Lattes, H. Muirhead, G. P. S. Occhialini, and C. F. Powell, Nature **159**, 694 (1947).

[4] E. P. Hincks and B. Pontecorvo, Phys. Rev. **73**, 257 (1948).

[5] R. P. Feynman and M. Gell-Mann, Phys. Rev. **109**, 193 (1958).

[6] G. Feinberg, Phys. Rev. **110**, 1482 (1958).

[7] K. Nishijima, Phys. Rev. **108**, 907 (1957).

[8] J. Schwinger, Ann. Phys. **2**, 407 (1957).

[9] G. Danby *et al.*, Phys. Rev. Lett. **9**, 36 (1962).

[10] S. L. Glashow, Nucl. Phys. **22**, 579 (1961).

[11] P. W. Higgs, Phys. Lett. **12**, 132 (1964).

[12] P. W. Higgs, Phys. Rev. Lett. **13**, 508 (1964).

[13] F. Englert and R. Brout, Phys. Rev. Lett. **13**, 321 (1964).

[14] G. 't Hooft, Nucl. Phys. B **33**, 173 (1971).

[15] G. 't Hooft, Nucl. Phys. B **35**, 167 (1971).

[16] G. 't Hooft and M. Veltman, Nucl. Phys. B **44**, 189 (1972).

[17] W. J. Marciano and A. I. Sanda, Phys. Lett. B **67**, 303 (1977).

[18] S. Bilenky, S. Petcov, and B. Pontecorvo, Phys. Lett. B **67**, 309 (1977).

[19] B. W. Lee and R. E. Shrock, Phys. Rev. D **16**, 1444 (1977).

[20] F. Borzumati and A. Masiero, Phys. Rev. Lett. **57**, 961 (1986).

[21] J. Hisano, D. Nomura, and T. Yanagida, Phys. Lett. B **437**, 351 (1998).

[22] J. Hisano and D. Nomura, Phys. Rev. D **59**, 116005 (1999).

[23] M. Koike, Y. Kuno, J. Sato, and M. Yamanaka, Phys. Rev. Lett. **105**, 121601 (2010).

[24] R. Abramishvili *et al.*, "COMET Phase-I Technical Design Report", `http://comet.kek.jp/Documents_files/PAC-TDR-2016/COMET-TDR-2016_v2.pdf`

[25] A. Abada, V. De Romeri, and A. M. Teixeira, J. High Energy Phys. 02 (2016) 083.

[26] R. W. Huff, Ann. Phys. (N.Y.) **16**, 288 (1961).

[27] P. Hänggi, R. D. Viollier, U. Raff, and K. Alder, Phys. Lett. **51**B, 119 (1974).

[28] R. Watanabe, M. Fukui, H. Ohtsubo, and M. Morita, Prog. Theor. Phys. **78**, 114 (1987).

[29] R. Kitano, M. Koike, and Y. Okada, Phys. Rev. D **66**, 096002 (2002).

[30] O. Shanker, Phys. Rev. D **20**, 1608 (1979).

[31] A. Czarnecki, W. J. Marciano, and K. Melnikov, AIP Conf. Proc. **435**, 409 (1998).

[32] K. Koshigiri, N. Nishimura, H. Ohtsubo, and M. Morita, Nucl. Phys. A**319**, 301 (1979).

[33] Y. Uesaka, Y. Kuno, J. Sato, T. Sato, and M. Yamanaka, Phys. Rev. D **93**, 076006 (2016).

[34] Y. Uesaka, Y. Kuno, J. Sato, T. Sato, and M. Yamanaka, Phys. Rev. D **97**, 015017 (2018).

[35] Y. Kuno and Y. Okada, Rev. Mod. Phys. **73**, 151 (2001).

[36] W. J. Marciano, T. Mori, and J. M. Roney, Rev. Nucl. Part. Sci. **58**, 315 (2008).

[37] M. Raidal *et al.*, Eur. Phys. J. C **57**, 13 (2008).

[38] R. H. Bernstein and P. S. Cooper, Phys. Rep. **532**, 27 (2013).

[39] A. de Gouvêa and P. Vogel, Prog. Part. Nucl. Phys. **71**, 75 (2013).

[40] S. Mihara, J. P. Miller, P. Paradisi, and G. Piredda, Ann. Rev. Nucl. Part. Sci. **63**, 531 (2013).

[41] F. Cei and D. Nicol, Adv. High Energy Phys. **2014**, 282915 (2014).

[42] T. Mori and W. Ootani, Prog. Part. Nucl. Phys. **79**, 57 (2014).

[43] W. Ootani, J. Phys. Soc. Jap. **85**, 091002 (2016).

[44] L. Calibbi and G. Signorelli, Riv. Nuovo Cim. **41**, no. 2, 1 (2018).

[45] A. Baldini *et al.* (MEG Collaboration), Eur. Phys. J. C**76**, 434 (2016).

[46] U. Bellgardt *et al.*, Nucl. Phys. B **299**, 1 (1988).

[47] P. Wintz, "*Proceedings of the First International Symposium on Lepton and Baryon Number Violation*", H. V. Klapdor-Kleingrothaus and I. V. Krivosheina Editors, IOP Publishing, 534 (1998).

[48] W. Bertl *et al.*, Eur. Phys. J. C **47**, 337 (2006).

[49] W. Honecker *et al.*, Phys. Rev. Lett. **76**, 200 (1996).

[50] Y. Okada, K. I. Okumura, and Y. Shimizu, Phys. Rev. D **61**, 094001 (2000).

[51] C. Fronsdal and H. Überall, Phys. Rev. **113**, 654 (1959).

[52] S. G. Eckstein and R. H. Pratt, Ann. Phys. (N.Y.) **8**, 297 (1959).

[53] Y. Kuno and Y. Okada, Phys. Rev. Lett. **77**, 434 (1996).

[54] A. M. Baldini *et al.*, arXiv:1301.7225 [physics.ins-det].

[55] A. Blondel *et al.*, arXiv:1301.6113 [physics.ins-det].

[56] T. S. Kosmas, A. Faessler, and F. Šimkovic, Phys. Rev. C **56**, 526 (1997).

[57] T. Siiskonen, J. Suhonen, and T. S. Kosmas, Phys. Rev. C **62**, 035502 (2000).

[58] V. Cirigliano, S. Davidson, and Y. Kuno, Phys. Lett. B **771**, 242 (2017).

[59] O. Shanker, Phys. Rev. D **25**, 1847 (1982).

[60] R. Szafron and A. Czarnecki, Phys. Lett. B **753**, 61 (2016).

[61] L. Bartoszek *et al.*, arXiv:1501.05241 [physics.ins-det].

[62] T. M. Nguyen, PoS FPCP **2015**, 060 (2015).

[63] C. Patrignani *et al.* (Particl Data Group), Chin. Phys. C**40**, 100001 (2016).

[64] Sw. Banerjee *et al.*, "HFLAV-Tau Spring 2017 report", `http://www.slac.stanford.edu/xorg/hflav/tau/spring-2017/tau-report-web.pdf`

[65] B. Aubert *et al.*, Phys. Rev. Lett. **104**, 021802 (2010).

[66] K. Hayasaka *et al.*, Phys. Lett. B **687**, 139 (2010).

[67] Y. Miyazaki *et al.*, Phys. Lett. B **648**, 341 (2007).

[68] B. Aubert *et al.*, Phys. Rev. Lett. **98**, 061803 (2007).

[69] Y. Miyazaki *et al.*, Phys. Lett. B **699**, 251 (2011).

[70] C. Schwanda, Nucl. Phys. B (Proc. Suppl.) **248250**, 67 (2014).

[71] E. Abouzaid *et al.*, Phys. Rev. Lett. **100**, 131803 (2008).

[72] D. Ambrose *et al.*, Phys. Rev. Lett. **81**, 5734 (1998).

[73] A. Sher *et al.*, Phys. Rev. D **72**, 012005 (2005).

[74] M. Ablikim *et al.*, Phys. Rev. D **87**, 112007 (2013).

[75] M. Ablikim *et al.*, Phys. Lett. B **598**, 172 (2004).

[76] R. Aaij *et al.*, Phys. Rev. Lett. **111** 141801 (2013).

[77] B. Aubert *et al.*, Phys. Rev. D **77**, 091104 (2008).

[78] B. Aubert *et al.*, Phys. Rev. D **73**, 092001 (2006).

[79] J. P. Lees *et al.*, Phys. Rev. D **86**, 012004 (2012).

[80] W. Love *et al.*, Phys. Rev. Lett. **101**, 201601 (2008).

[81] D. Black, T. Han, H.-J. He, and M. Sher, Phys. Rev. D **66**, 053002 (2002).

[82] G. Aad *et al.*, Phys. Rev. D **90**, 072010 (2014).

[83] R. Akers *et al.*, Z. Phys. C **67**, 555 (1995).

[84] P. Abreu *et al.*, Z. Phys. C **73**, 243 (1997).

[85] V. Khachatryan *et al.*, Phys. Lett. B **763**, 472 (2016).

[86] CMS Collaboration, CMS-PAS-HIG-17-001.

[87] J. Heeck and W. Rodejohann, Phys. Lett. B **776**, 385 (2018).

[88] R. Bolton *et al.*, Phys. Rev. D **38**, 2077 (1988).

[89] R. Bayes *et al.*, Phys. Rev. D **91**, 052020 (2015).

[90] R. Eichler *et al.*, Phys. Lett. B **175** 101 (1986).

[91] H. Natori, PhD thesis, University of Tokyo, 2012.

[92] S. N. Gninenko, M. M. Kirsanov, N. V. Krasnikov, and V. A. Matveev, Mod. Phys. Lett. A **17**, 1407 (2002).

[93] M. Sher and I. Turan, Phys. Rev. D **69**, 017302 (2004).

[94] W. Liao and X.-H. Wu, Phys. Rev. D **93**, 016011 (2016).

[95] A. Abada, V. De Romeri, J. Orloff, and A. M. Teixeira, Eur. Phys. J. C **77**, 304 (2017).

[96] S. Kanemura, Y. Kuno, M. Kuze, and T. Ota, Phys. Lett. B **607**, 165 (2005).

[97] M. Takeuchi, Y. Uesaka, and M. Yamanaka, Phys. Lett. B **772**, 279 (2017).

[98] B. Murakami, T. M. P. Tait, Phys. Rev. D **91**, 015002 (2015).

[99] G. C. Cho and H. Shimo, Mod. Phys. A **32**, 1750127 (2017).

[100] J.-J. Cao, T. Han, X. Zhang, and G.-R. Lu, Phys. Rev. D **59**, 095001 (1999).

[101] Y. Muramatsu, T. Nomura, Y. Shimizu, and H. Yokoya, Phys. Rev. D **97**, 015003 (2018).

[102] G. Feinberg, P. Kabir, and S. Weinberg, Phys. Rev. Lett. **3**, 527 (1959).

[103] R. Watanabe, K. Muto, T. Oda, T. Niwa, H. Ohtsubo, R. Morita, and M. Morita, At. Data Nucl. Data Tables **54**, 165 (1993).

[104] M. Berglund and M. E. Wieser, Pure Appl. Chem. **83**, 397 (2011).

[105] C. W. De Jager, H. De Vries, and C. De Vries, At. Data Nucl. Data Tables **14**, 479 (1974).

[106] S. Ando, J. A. McGovern, and T. Sato, Phys. Lett. B **677**, 109 (2009).

[107] L. Michel, Proc. Phys. Soc. A **63**, 514 (1950).

[108] W. Greiner, *Relativistic Quantum Mechanics: Wave Equations* (Springer, 2000).

[109] A. Czarnecki, G. P. Lepage, and W. J. Marciano, Phys. Rev. D **61**, 073001 (2000).

[110] A. Czarnecki, X. G. i Tormo, and W. J. Marciano, Phys. Rev. D **84**, 013006 (2011).

[111] A. Czarnecki, M. Dowling, X. G. i Tormo, W. J. Marciano, and R. Szafron, Phys. Rev. D **90**, 093002 (2014).

[112] J. A. Wheeler, Rev. Mod. Phys. **21**, 133 (1949).

[113] K. W. Ford and J. G. Wills, Nucl. Phys. **35**, 295 (1962).

[114] H. Primakoff, Rev. Mod. Phys. **31**, 802 (1959).

[115] T. Suzuki, D. F. Measday, and J. Roalsvig, Phys. Rev. C **35**, 2212 (1987).

[116] M. E. Rose, *Relativistic electron theory*, (John Wiley & Sons, New York, 1961).

[117] C. J. Joachain, *Quantum collision theory* (North-Holland Pub. Co., 1975).

[118] M. E. Rose, *Elementary Theory of Angular Momentum* (John Wiley & Sons, New York, 1957).